

**University College London**  
**UCL**

*The Development of Novel Thiomaleimide Photochemical Transformations and Their Application to the Manipulation of Proteins.*

Daniel Ashley Richards

A thesis submitted to University College London in accordance with the requirements of the degree of Doctor of Philosophy

Supervisor: Dr James. R. Baker

February 2016

## *Declaration*

I, Daniel Richards, confirm that the work presented in this thesis is my own. Where information has been derived from other sources, I confirm that this has been indicated in the thesis.

-----

## Abstract

The unique spatiotemporal control provided by photochemical transformations allows for exquisite power over biochemical processes. Despite this, relatively little research involving novel biocompatible photochemical transformations has been described. This is due in part to the difficulty in discovering photochemical reactions which fulfil the strict criteria required for biocompatibility, and also a lack of available methods for the reliable site-selective modification of proteins. Thus, a method for achieving site selective attachment of novel photoactive chemical moieties to biomolecules would represent a significant contribution to the field.

Recently published work has highlighted the photochemical reactivity of thiomaleimides, which can be easily and site-selectively installed on protein cysteine residues. This thesis describes the discovery and investigation of novel thiomaleimide based photochemical reactions, with special focus on utilising these reactions as phototriggers for peptide and protein manipulation. The initial work expands on a previously reported thiomaleimide [2+2] photocycloaddition to develop a method for photochemically rebridging peptides and proteins at the site of a disulfide bond. This method was employed for the photochemical activation of the therapeutic peptide Octreotide, and as a tool for generating highly thiol stable *bis*-modified antibody fragment conjugates.

During the course of this study two novel thiomaleimide-mediated photochemical decarboxylation reactions were discovered and their utility as photolabile linkers for bioconjugation was explored. This led to the development of a cysteine selective photolabile linker based around the thiomaleimide scaffold, which was subsequently employed to release an analogue of the cytotoxic drug Doxorubicin from an anti-CEA scFv antibody fragment. This work highlights the previously unreported ability of thiomaleimides to act as electron acceptors in photoinduced electron transfer reactions, greatly expanding the reactivity profile of this chemical motif.

The excellent photochemical reactivity of thiomaleimides, coupled with the relative ease of their installation on proteins, suggests that these reagents could play an important part in the future of photochemical protein and peptide manipulation.

*In memory of Debra Jane Falcon*

*02.09.1962 - 04.10.2015*

## Acknowledgements

The work presented in this thesis has been made possible through the guidance, technical expertise, knowledge, and psychological respite provided by an excellent network of mentors, colleagues, and friends. I am confident that without the people listed below this thesis would not have been completed, and for that I am forever grateful.

In the first instance I would like to thank Dr James “Jamie” Baker for providing me with such a challenging project and remaining optimistic throughout, despite my frequent unnecessary despair. Though at times frustrating, the work has allowed me to develop as a researcher and introduced me to a field which I have since grown to love. I am also grateful to Jamie for teaching me the power of perspective and that knowledge can be gained even through apparent failures.

I would like to thank the academic staff within the Kathleen Lonsdale Building, especially Dr Tom Sheppard, Dr Jon Wilden, and Dr Mark Smith, for their academic guidance and role in creating such a pleasant working atmosphere. A special mention goes to Dr Vijay Chudasama, for his constant reassurances, support, and inspiration. This gratitude extends to all members of labs 230 and 237, past and present, particularly Dr Sally Fletcher, Dr Elizabeth Love, Dr Rosemary Huckvale, Dr João Nunes, Dr Cristina Marculescu, Dr Favad Iqbal, Nafsika Forte, Alexandra King, Dr Antoine Maruani, Dr Rachel Lanigan, Roomi Chowdhury, Dr Matt Pennell, Samantha Gibson and Valerija Karaluka. Of these Dr Sally Fletcher and Samantha Gibson deserve special mention, as their uncanny ability to both lighten the mood and lower the tone has provided immeasurable enjoyment.

For their technical help I would like to thank Dr Abil Aliev for his excellent NMR advice, and Dr Kersti Karu and Dr Lisa Harris for their invaluable mass spectrometry knowledge. I would extend this to Dr Carolyn Hyde for her help with HPLC, Dr Enrique Miranda Rota for his help with ELISA and cell kill assays and Dr Muriel Nobles for her help with patch clamping.

Outside of the lab I would like to sincerely thank my closest friends, Collette Chaney and Diggory Dunn, for helping me more than they may ever realise. They have provided a necessary balance, helped me stay (relatively) sane, and kept me motivated throughout. I'd like to extend this to Holley Morris, for putting up with me and supporting me as best she could.

Finally, I would like to thank my parents Debra Falcon and Jeremy Richards, and my grandparents Deirdre Styles-Thompson and Harold Thompson, for a lifetime of support and encouragement. I can never thank them enough for what they have done to get me to this point, though I hope they will in some way share in my sense of achievement upon completion of this work.

## Abbreviations

<b>A</b>	absorbance
<b>ADC</b>	antibody drug conjugate
<b>AIBN</b>	azobisisobutyronitrile
<b>ATP</b>	adenosine triphosphate
<b>BBS</b>	borate buffered saline
<b>BDMAP</b>	1,6-bis(di-methylamino)pyrene
<b>BME</b>	b-mercaptoethanol
<b>Boc</b>	<i>tert</i> -Butyloxycarbonyl
<b>BSA</b>	bovine serum albumin
<b>CA-4</b>	combretastatin A-4
<b>cAMP</b>	cyclic adenosinemonophosphate
<b>CEA</b>	carcinoembryonic antigen
<b>CNS</b>	central nervous system
<b>Da</b>	Dalton
<b>DCC</b>	N,N'-Dicyclohexylcarbodiimide
<b>DIPEA</b>	N,N-Diisopropylethylamine
<b>DMAP</b>	4-Dimethylaminopyridine
<b>DMF</b>	dimethylformamide
<b>DMNB</b>	4,5-dimethoxy-2-nitrobenzyl
<b>DNA</b>	deoxyribonucleic acid
<b>Dox</b>	Doxorubicin
<b>ds-scFv</b>	disulfide stabilised single chain variable fragment
<b>DTT</b>	dithiothreitol
<b>EDC</b>	1-Ethyl-3-(3-dimethylaminopropyl)carbodiimide
<b>EDT</b>	ethanedithiol
<b>EDTA</b>	ethylenediaminetetraacetic acid
<b>EGTA</b>	ethylene glycol tetraacetic acid
<b>ELISA</b>	enzyme linked immunosorbent assay
<b>ES</b>	electrospray
<b>ESI</b>	electrospray ionisation
<b>ET</b>	electron transfer
<b>Fab</b>	fragment antigen binding
<b>Fc</b>	fragment crystallisable
<b>FDA</b>	Food and Drug Administration
<b>Fmoc</b>	fluorenylmethyloxycarbonyl
<b>GABA</b>	gamma-Aminobutyric acid
<b>GFP</b>	green fluorescent protein
<b>GIRK</b>	G protein-coupled inwardly-rectifying potassium
<b>GSH</b>	glutathione
<b>GTP</b>	guanosine triphosphate
<b>HATU</b>	(1-[Bis(dimethylamino)methylene]-1H-1,2,3-triazolo- [4,5-b]pyridinium-3-oxid hexafluorophosphate)
<b>HBTU</b>	(2-(1H-benzotriazol-1-yl)-1,1,3,3-tetramethyluronium -hexafluorophosphate)
<b>HEK</b>	human embryonic kidney
<b>HEPES</b>	4-(2-hydroxyethyl)-1-piperazineethanesulfonic acid

<b>HMBC</b>	heteronuclear multiple bond correlation
<b>HOMO</b>	highest occupied molecular orbital
<b>HPLC</b>	high performance liquid chromatography
<b>HSA</b>	human serum albumin
<b>IC</b>	internal conversion
<b>ICT</b>	intramolecular charge transfer
<b>Ig</b>	immunoglobulin
<b>IR</b>	Infrared
<b>ISC</b>	intersystem crossing
<b>kDa</b>	kilodalton
<b>Kir</b>	Inward-rectifier potassium ion channel
<b>LCMS</b>	liquid chromatography - mass spectrometry
<b>LED</b>	light-emitting diode
<b>LUMO</b>	lowest unoccupied molecular orbital
<b>M</b>	molar
<b>MALDI</b>	matrix -assisted laser desorption/ionisation
<b>MAPK</b>	mitogen-activated protein kinase
<b>mg</b>	milligram
<b>MgATP</b>	adenosine triphosphate, magnesium salt.
<b>μl</b>	microliter
<b>ml</b>	millilitre
<b>μM</b>	micromolar
<b>mM</b>	millimolar
<b>MMAE</b>	monomethyl auristatin E
<b>mmol</b>	millimole
<b>MO</b>	molecular orbital
<b>MS</b>	mass spectrometry
<b><i>m</i>-THPC</b>	<i>meso</i> -tetra-hydroxyphenyl-chlorin
<b>Na<sub>2</sub>GTP</b>	guanosine triphosphate, sodium salt
<b>nAChR</b>	nicotinic acetylcholine receptor
<b>nbC</b>	nitrobenzyl caged caspase 3
<b>NHS</b>	N-Hydroxysuccinimide
<b>NMR</b>	nuclear magnetic resonance
<b>OEG</b>	oligoethylene glycol
<b>OPD</b>	<i>o</i> -phenylenediamine dihydrochloride
<b>p-ADC</b>	photoactivatable antibody drug conjugate
<b>PAP-S</b>	pokeweed antiviral protein S
<b>PBS</b>	phosphate buffered saline
<b>PDT</b>	photodynamic therapy
<b>PEG</b>	polyethylene glycol
<b>PET</b>	photoinduced electron transfer
<b>PIT</b>	photoimmunotherapy
<b>ppm</b>	parts per million
<b>PTM</b>	post-translational modification
<b>PTP</b>	phosphotyrosine phosphatase
<b>PTSA</b>	para-toluenesulfonic acid
<b>RNA</b>	ribonucleic acid

<b>RSH</b>	thiol
<b>S</b>	singlet
<b>S*</b>	singlet excited state
<b>scFv</b>	single chain variable fragment
<b>SDS-PAGE</b>	sodium dodecyl sulfate polyacrylamide gel electrophoresis
<b>SOMO</b>	singly occupied molecular orbital
<b>SST</b>	somatostatin
<b>T</b>	triplet
<b>T*</b>	triplet excited state
<b>TCEP</b>	(tris(2-carboxyethyl)phosphine)
<b>tert</b>	tertiary
<b>TFA</b>	trifluoroacetic acid
<b>THF</b>	tetrahydrofuran
<b>TLC</b>	thin layer chromatography
<b>TOF</b>	time of flight
<b>Trt</b>	trityl
<b>UPLC</b>	ultra performance liquid chromatography
<b>UV</b>	ultraviolet

<b>Abstract .....</b>	<b>3</b>
<b>Acknowledgements .....</b>	<b>5</b>
<b>Abbreviations .....</b>	<b>6</b>
<b>1: INTRODUCTION .....</b>	<b>13</b>
<b>1.1: Photochemistry.....</b>	<b>13</b>
1.1.1: Fundamentals of Photochemistry .....	13
1.1.2: [2+2] photocycloadditions .....	15
1.1.2.1: [2+2] photocycloadditions of maleimides .....	19
1.1.2.2: [2+2] photocycloaddition reactions of thiomaleimides .....	20
1.1.3: Photochemical decarboxylation reactions .....	21
1.1.3.1: Photochemical decarboxylation reactions of phthalimides .....	23
1.1.4: Photocleavable protecting groups.....	25
1.1.4.1: Photocleavable protecting groups in chemical biology .....	26
<b>1.2: Chemical modification of proteins and peptides .....</b>	<b>27</b>
1.2.1: Background .....	27
1.2.2: Amino acid modification .....	28
1.2.3: Cysteine modification .....	29
1.2.3.1: Next generation maleimides as tools for cysteine modification .....	31
1.2.4: Antibody modification .....	32
1.2.4.1: Antibody structure.....	32
1.2.4.2: Antibody conjugates .....	33
1.2.5: Peptide based therapeutics .....	36
1.2.5.1: Somatostatin and its analogues .....	36
<b>1.3: Photochemistry and Chemical Biology .....</b>	<b>38</b>
1.3.1: Photochemical protein uncaging.....	40
1.3.2: Photochemical release from proteins .....	43
1.3.2.1: Photocleavable antibody drug conjugates (pADCs) .....	43
1.3.2.2: Antibody-directed photodynamic therapy.....	45
1.3.3: Photochemical manipulation of peptides .....	46
1.3.3.1: Photochemical switches .....	46
1.3.3.2: Phototriggers .....	48
<b>1.4: Research overview .....</b>	<b>49</b>
<b>2: RESULTS AND DISCUSSION .....</b>	<b>50</b>
<b>2.1: Photochemical peptide activation .....</b>	<b>50</b>
2.1.1: Aims and introduction.....	50
2.1.2: Modification and irradiation of Octreotide .....	51
2.1.2.1: HPLC data .....	53
2.1.2.2: Tandem-MS data.....	57
2.1.2.3: NMR data.....	59
2.1.3: Determining the binding affinity of Octreotide conjugates .....	60
2.1.3.1: Dose-Response curve .....	60

2.1.3.2: Measuring maximum current activation .....	63
2.1.4: Conclusions and future work.....	65
<b>2.2: Thiomaleimide [2+2] cyclisations on antibody fragments .....</b>	<b>67</b>
2.2.1: Aims and introduction.....	67
2.2.2: Modification of an anti-CEA scFv.....	68
2.2.2.1: Thiol stability of a rebridged anti-CEA scFv conjugate .....	71
2.2.3: Modification of Rituxan Fab .....	71
2.2.3.1: Preparation of Rituxan Fab .....	71
2.2.3.2: Modification of Rituxan Fab.....	72
2.2.3.3: Thiol stability of Rituxan Fab conjugates .....	74
2.2.3.4: Synthesis of functionalised bromomaleimides .....	75
2.2.3.5: Generating functionalised Rituxan Fab fragments.....	77
2.2.4: Modification of Rituxan.....	79
2.2.5: Modification of Herceptin Fab .....	81
2.2.5.1: Preparation of Herceptin Fab fragments.....	81
2.2.5.2: Modification of Herceptin Fab .....	82
2.2.6: C-terminal decarboxylation of Fab Fragments .....	84
2.2.7: ELISA data for Herceptin Fab conjugates .....	86
2.2.8: Conclusions and future work.....	87
<b>2.3: C-terminal cysteine thiomaleimide decarboxylations .....</b>	<b>90</b>
2.3.1: Aims and introduction.....	90
2.3.2: Small molecule models of C-terminal cysteine decarboxylation .....	91
2.3.2.1: Synthesis and irradiation of a single cysteine model .....	91
2.3.2.2: C-terminal decarboxylation of a dipeptide model.....	93
2.3.3: Attempts to determine the fate of the maleimide .....	95
2.3.3.1: Synthesis and irradiation of an N-methyl maleimide model.....	95
2.3.3.2: Synthesis and irradiation of an N-dansyl maleimide model.....	99
2.3.4: Postulated mechanism for C-terminal thiomaleimide decarboxylation.....	101
2.3.6: Conclusions and future work.....	103
<b>2.4: Dithiomaleimide based photocleavable linkers .....</b>	<b>104</b>
2.4.1: Aims and introduction.....	104
2.4.2: Synthesis of a simple cysteine-maleimide model .....	105
2.4.2.1: Synthesis of dibromomaleimide-N-L-serine .....	105
2.4.2.2: Irradiation of a simple cysteine model.....	108
2.4.3: A postulated mechanism for thiomaleimide decarboxylation-elimination.....	108
2.4.4: Photochemical cleavage from a peptide model .....	110
2.4.4.1: Preparing and irradiating a suitable Octreotide model.....	110
2.4.5: Altering the scaffold of the thiomaleimide photocleavable linker.....	114
2.4.5.1: Synthesis of structurally varied dibromomaleimide linkers .....	114
2.4.5.2: Comparing the effects of structural modifications.....	118
2.5.6: Developing a photocleavable antibody-drug-conjugate .....	124

2.4.6.1: Synthesis of a photocleavable click handle .....	124
2.4.6.2: Synthesis of a doxorubicin-azide analogue .....	125
2.4.6.3: Generation of a photocleavable scFv-Doxorubicin ADC .....	125
2.4.6.4: Cell kill assay for the photocleaved Doxorubicin analogue.....	129
2.4.6.5: Cell kill assay for Doxorubicin-amine .....	130
2.4.7: Conclusions.....	132
2.4.8: Future Work.....	134
2.4.8.1: Perfecting the photochemical-scFv-Doxorubicin conjugate.....	134
2.4.8.2: Determining the quantum yield .....	135
2.4.8.3: Long term outlook.....	136
<b>3: EXPERIMENTAL.....</b>	<b>138</b>
<b>3.1: Synthetic organic chemistry.....</b>	<b>138</b>
3.1.1: General experimental.....	138
3.1.2: Synthesis.....	139
3.1.2.1: Synthesis of monobromomaleimide reagents.....	139
3.1.2.2: Synthesis of C-terminal cysteine models .....	144
3.1.2.3: HPLC analysis of the Irradiation of C-terminal cysteine models.....	153
3.1.2.4: Synthesis of photocleavable linkers .....	154
<b>3.2: Chemical Biology Experimental .....</b>	<b>174</b>
3.2.1: General experimental.....	174
3.2.1.1: HPLC methods .....	175
3.2.1.2: MALDI-TOF methods .....	175
3.2.1.3: Tandem-MS methods.....	175
3.2.1.4: LCMS methods.....	176
3.2.2: Octreotide photoactivation .....	177
3.2.2.1: Modification of Octreotide.....	177
3.2.2.2: Thiol reactivity of Octreotide conjugates .....	180
3.2.2.4: Electrophysiology data .....	181
3.2.3: Anti-CEA scFv fragment.....	183
3.2.3.1: Anti-scFv fragment modification.....	183
3.2.3.2: Thiol stability of a bridged anti-CEA scFv conjugate .....	184
3.2.4: Rituxan .....	184
3.2.4.1: Preparation of Rituxan Fab .....	184
3.2.4.2: Modification of Rituxan Fab.....	185
3.2.4.3: Thiol stability of bridged Rituxan Fab conjugates .....	193
3.2.4.4: Modification of Rituxan .....	195
3.2.5: Herceptin .....	195
3.2.5.1: Preparation of Herceptin Fab .....	195
3.2.5.2: Modification of Herceptin Fab .....	196
3.2.5.3: ELISA data for Herceptin conjugates.....	201
3.2.7: Dithiomaleimide photocleavable linkers.....	202

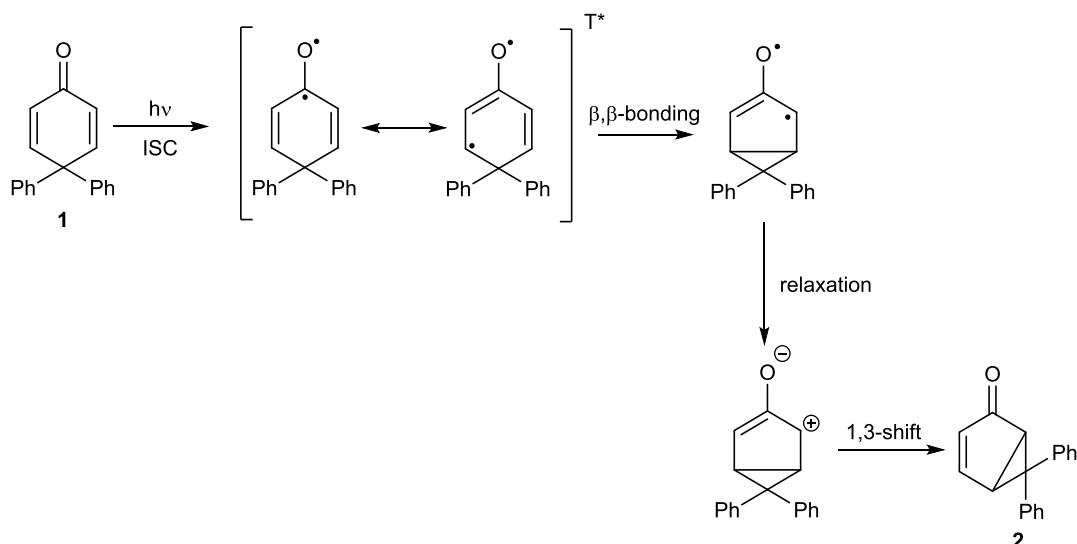
3.2.7.1: Modification of Octreotide.....	202
3.2.7.2: Anti-CEA scFv-Dox photocleavable ADC. ....	211
3.2.8: Cell kill assays for Doxorubicin analogues.....	212
<b>4: REFERENCES .....</b>	<b>213</b>
<b>5: APPENDIX .....</b>	<b>228</b>

# 1: Introduction

## 1.1: Photochemistry

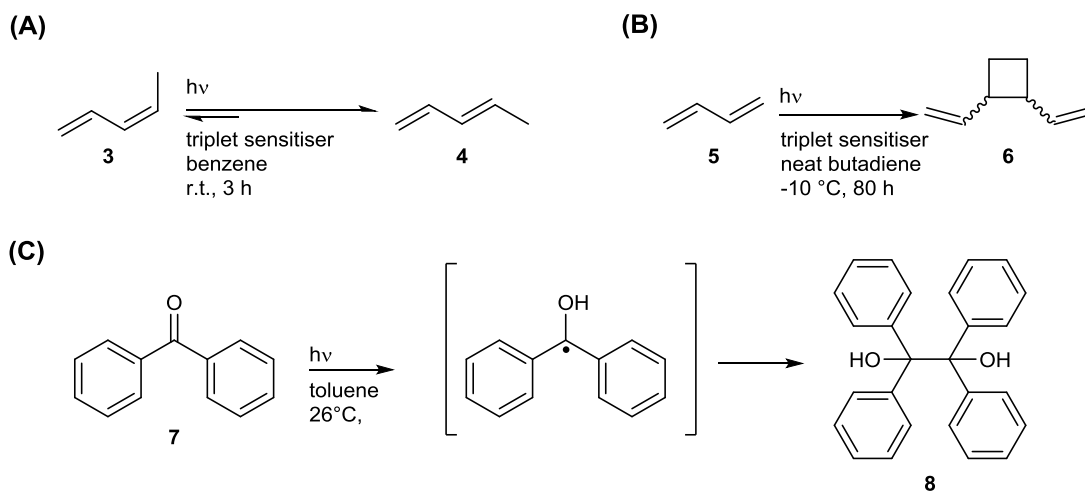
### 1.1.1: Fundamentals of Photochemistry

Accurately defining the genesis of modern organic photochemistry is a non-trivial task, complicated by a historical lack of understanding at a fundamental level. Despite the identification of many photochemical processes throughout history, research into their mechanisms only began in earnest in the mid to late 20<sup>th</sup> century. Advancements in quantum mechanics, along with more sophisticated spectroscopic techniques, gave researchers unprecedented insight into the underlying processes involved in these unique transformations.<sup>1</sup> Key work by Zimmerman in the early 1960s used this insight to offer a mechanistic explanation for the photochemical rearrangement of 4,4-diphenylhexadienone **1** to 3,3-diphenylpentenone product **2**, providing one of the earliest examples of a truly mechanistically reasoned photochemical reaction (Scheme 1).<sup>2</sup> Subsequent studies within the group expanded on this work and explored the mechanisms of a variety of photochemical rearrangements.<sup>3-6</sup>



**Scheme 1**  
The photochemical rearrangement of 4,4-diphenylhexadienone **1**.

Similarly, parallel work by Hammond explored the role of the excited triplet state in organic photochemical transformations.<sup>7-9</sup> This work provided mechanistic explanations for a variety of photochemical processes which are now common place, such as photochemically induced *cis-trans* isomerisations,<sup>10,11</sup> [2+2] cycloadditions,<sup>12</sup> and photoreductions<sup>13,14</sup> (Scheme 2).



### Scheme 2

Some early photochemical reactions studied by Hammond *et al.*: (A) Photochemical *cis-trans* isomerisation of piperylene 3.<sup>10</sup> (B) Photochemical [2+2] cycloaddition of butadiene 5.<sup>12</sup> (C) Photochemical reduction of benzophenone 7.<sup>13,14</sup>

The pioneering work by these groups, and many others, highlighted the importance of the excited state and laid the foundation of modern mechanistic organic photochemistry. Chemists now have a more complete understanding of the structure and bonding of molecules in the excited state, and are thus better equipped to harness the power of photochemistry. The culmination of this research is perhaps best represented schematically in a Jablonski diagram (Figure 1). Jablonski diagrams were first introduced by their namesake in 1933 to explain the fluorescence observed in organic dyes,<sup>15</sup> but have since been adopted to describe a multitude of photochemical processes. The diagram depicts the fate of a molecule after absorbing a photon to generate an electronically excited state. The decay of this excited state can be categorised into two general processes: radiative and non-radiative. Non-radiative processes involve decay without emission of light, and are depicted on a Jablonski diagram as wavy lines. Non-radiative processes can be further divided by the change (or lack of) in spin multiplicity during the decay. If no change occurs the process is deemed “spin allowed” and is called an internal conversion (IC). This process allows higher energy singlet/triplet states to decay to lower energy singlet/triplet states. When a change in spin multiplicity accompanies a non-radiative decay the process is deemed “spin forbidden” and is called an intersystem crossing (ISC). This process allows for either the lowest energy singlet state to convert into the lowest energy triplet state or the lowest energy triplet state to decay to the ground state. Conversion between singlet and triplet states *via* ISC is important as it is the primary route through which triplet states are accessed. Chemical transformations can theoretically take place from each of these excited states, though it is worth noting that the lifetimes of excited states are often short and competition exists from other processes such as radiative decay. Radiative decay processes, depicted by straight lines on a Jablonski diagram, involve decay of an excited state accompanied by emission of a photon. Decay of a photon from

an excited singlet state ( $S_x$   $X \neq 0$ ) to the singlet ground state (spin allowed) is termed fluorescent emission, and decay from an excited triplet state ( $T_x$   $X \neq 0$ ) to the singlet ground state (spin forbidden) is termed phosphorescence.

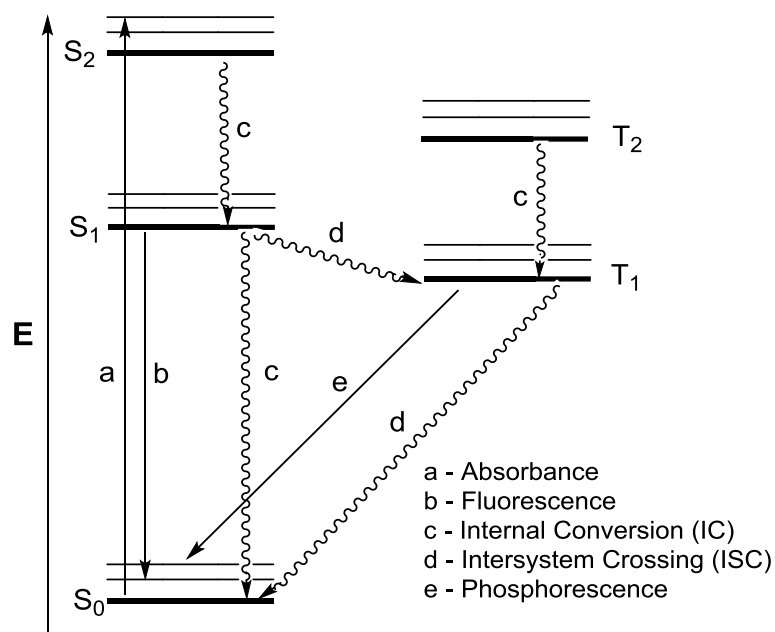


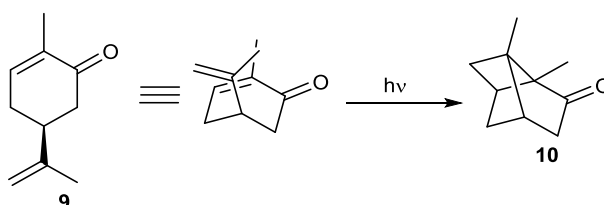
**Figure 1**  
A Jablonski diagram depicting the possible fates of an electronically excited compound.

The complexity of the Jablonski diagram in Figure 1 demonstrates the highly competitive nature of photochemical processes. For a chemical transformation to occur the reaction of the excited state must out-compete the various decay processes. It is worth noting that chemical transformation is not always the desirable outcome and radiative decay processes can be advantageous, as in the case with fluorescent probes.<sup>16</sup>

Despite these complexities photochemical reactions provide routes to previously inaccessible chemical transformations. This unique ability has allowed for the rapid evolution of photochemistry from a lab based curiosity to a highly developed field of research. Today photochemical reactions are routinely employed for laboratory syntheses<sup>17</sup> and have been exploited for commercial purposes, particularly in the printing,<sup>18</sup> renewable energy,<sup>19,20</sup> polymeric materials,<sup>21</sup> and biomedical sectors.<sup>22–25</sup>

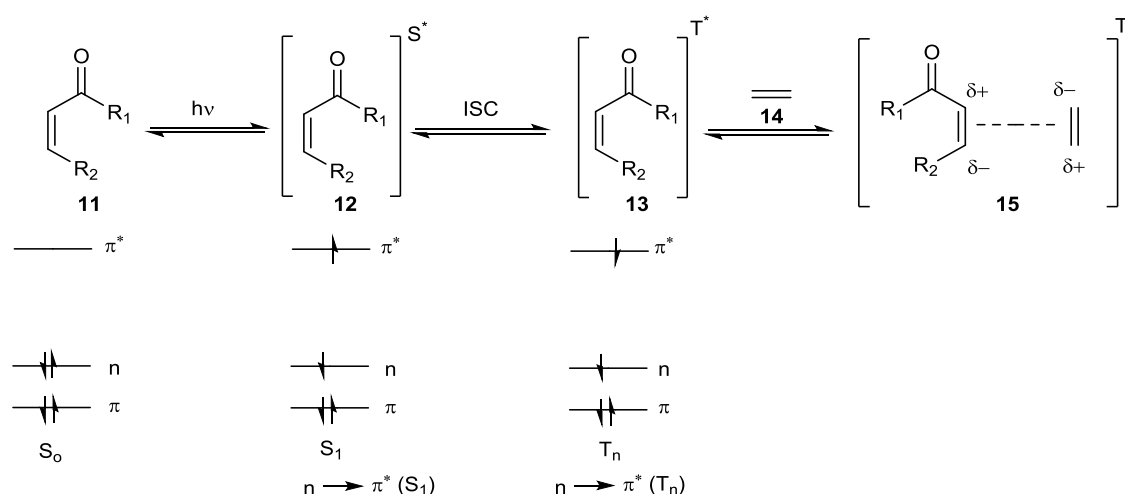
### 1.1.2: [2+2] photocycloadditions

Of the photochemical reactions initially studied in the early 20<sup>th</sup> century photocycloadditions have remained relatively well utilised. Perhaps the most intensely studied photocycloaddition is the enone-olefin [2+2] photocycloaddition, first observed through the conversion of carvone **9** to carvone-camphor **10** in 1908<sup>26</sup> and studied extensively in the 1950s and 1960s (Scheme 3).<sup>27–33</sup>



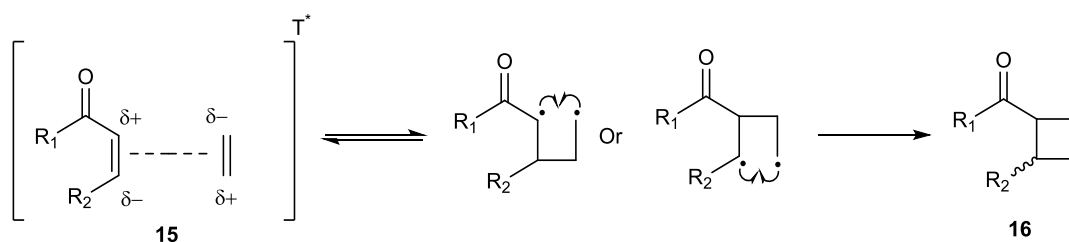
**Scheme 3**  
The photochemical conversion of S-carvone **9** to carvone-camphor **10**.

The general mechanism of this reaction is best demonstrated schematically as outlined in Scheme 4. Excitation of the enone **11** to the singlet state ( $S_1$ ) **12**, made possible by the n-bonding electrons of the oxygen atom, is followed by intersystem crossing (ISC) to the n –  $\pi^*$  triplet state ( $T_1$ ) **13**.<sup>34</sup> The excited triplet state **13** is subsequently able to form an excited state complex (exciplex) **15** with the ground state olefin **14**.<sup>35–37</sup> In this exciplex the molecules align in a way that maximises the new bonding interactions which are made possible through excitation. Though an exciplex cannot be observed directly, it can be inferred from the regioselectivity of certain intermolecular photocycloadditions and helps to explain the increased reactivity of photocycloadditions when compared to non-photochemical radical additions.<sup>36</sup>



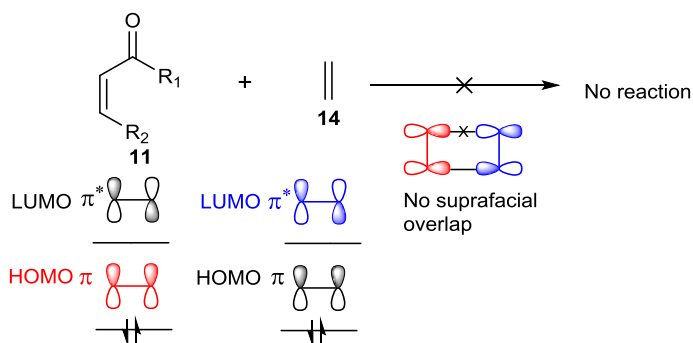
**Scheme 4**  
Photoexcitation of an enone **11** followed by formation of the required enone-olefin exciplex **15**.

The formed exciplex can then collapse to a 1,4-diradical through bond formation at the  $\alpha$  or  $\beta$  carbons of the enone and subsequently form cyclobutane **16** (Scheme 5). Relaxation back to the ground state enone can occur at several points during the process, though the overall process is irreversible due to the formation of the cyclobutane ring. A major route for this relaxation is *via* the *cis-trans* isomerisation of the enone in the excited state,<sup>38</sup> though this can be minimised through the use of cyclic enones.<sup>35,39</sup>



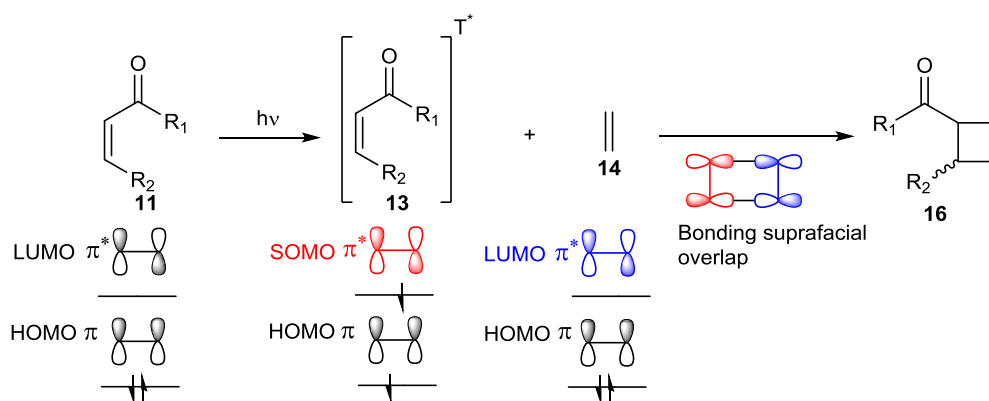
**Scheme 5**  
**Formation of a cyclobutane ring 16 through collapse of the exciplex 15.**

A clearer explanation of this process can be gained by considering the molecular orbitals (MOs) of the reacting species. Molecular orbital theory (in the form of frontier molecular orbital theory), was first described by Fukui in 1952,<sup>40</sup> and predicts reactivity based on the symmetry of interacting molecular orbitals. This theory was developed and expanded by Woodward and Hoffman and became the Woodward-Hoffman rules for electrocyclic processes.<sup>41-44</sup> The theory states that the fate of a reaction can be predicted by considering the interaction between the highest occupied molecular orbital (HOMO) of one reactant and the lowest unoccupied molecular orbital (LUMO) of another. Applying this theory to the enone-olefin cycloaddition explains why the reaction does not proceed from the ground state, but occurs rapidly upon photo-excitation. By considering the reacting molecular orbitals of the enone **11** and the olefin **14** in the ground state it becomes apparent that suprafacial (head on) overlap of the orbitals cannot form a bonding interaction (Scheme 6).



**Scheme 6**  
**A HOMO-LUMO interaction between a ground state enone 11 and olefin 14.**

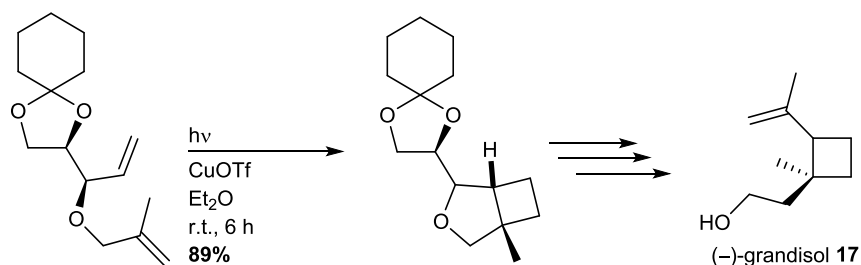
Upon excitation an electron from the HOMO of the enone gets promoted into a higher energy molecular orbital, termed the singly occupied molecular orbital (SOMO). The symmetry of the excited state SOMO **13** is complementary to that of the LUMO on the olefin **14**, enabling a symmetry allowed suprafacial bonding interaction.



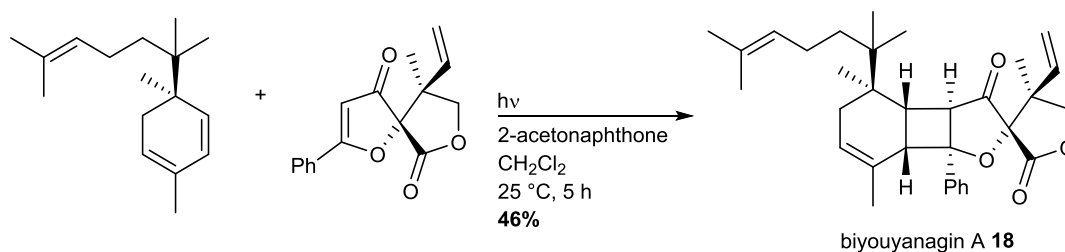
**Scheme 7**  
**The reaction between enone excited state 13 and olefin ground state 14.**

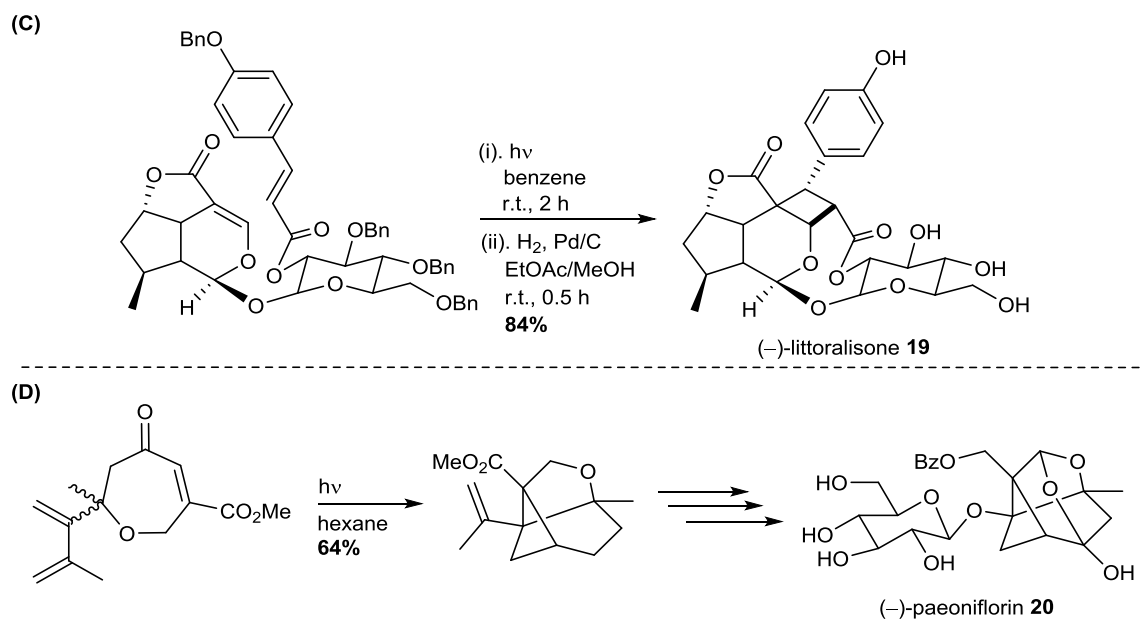
The knowledge gained from this early work has helped to establish the [2+2] photocycloaddition as a viable method for the laboratory synthesis of cyclobutane rings. Although the enone-olefin [2+2] cycloaddition is the most well studied of these reactions it is important to note that enone-alkyne,<sup>45–48</sup> arene-olefin,<sup>49</sup> enone-enone,<sup>11,50,51</sup> and even olefin-olefin [2+2] photocycloadditions have been reported, and the reaction is implicit in named reactions such as the de Mayo<sup>52</sup> and Paternò–Büchi<sup>53</sup> reactions. More recently the development of enantioselective variants has ensured the inclusion of the reaction in the field of asymmetric synthesis. Scheme 8 highlights some examples of photochemical [2+2] cycloaddition reactions towards the synthesis of natural products.

(A)



(B)



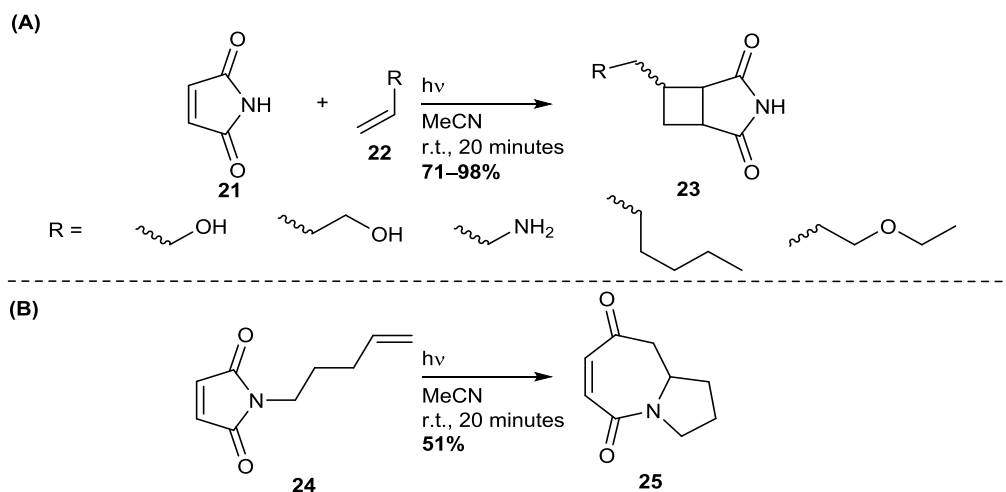


### Scheme 8

An intramolecular [2+2] photocycloaddition employed: (A) during the synthesis of grandisol **17**, an important natural product and synthetic precursor.<sup>54,55</sup> (B) as a final step towards biyouyanagin **A 18**, a potent HIV replication inhibitor.<sup>56</sup> (C) in the final step towards (-)-littoralisone **19**,<sup>57</sup> a compound which shows promise in the treatment of neurodegenerative disorders. (D) during the synthesis of (-)-paeoniflorin **20**, a compound with antiandrogenic properties.<sup>58</sup>

#### 1.1.2.1: [2+2] photocycloadditions of maleimides

In the context of this thesis the [2+2] photocycloaddition reactions of maleimides deserve special mention. Unsurprisingly, due to the conjugation of the double bond with two carbonyl systems, maleimides are readily able to act as enones in highly efficient enone-olefin [2+2] photocycloaddition reactions (Scheme 9).<sup>59–62</sup>

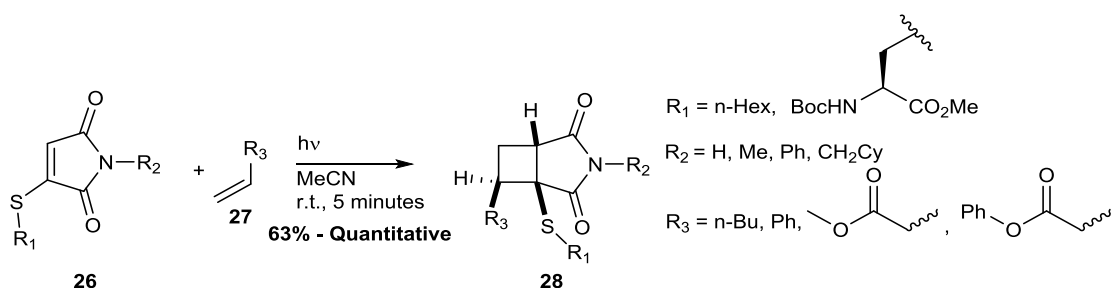


### Scheme 9

Photochemical cycloadditions involving maleimides: (A) The photochemical [2+2] cycloaddition between maleimide **21** and various olefins **22**. (B) The intramolecular photochemical [2+2] cycloaddition of N-alkene maleimide **24**. Subsequent rearrangement leads to cyclic product **25**.

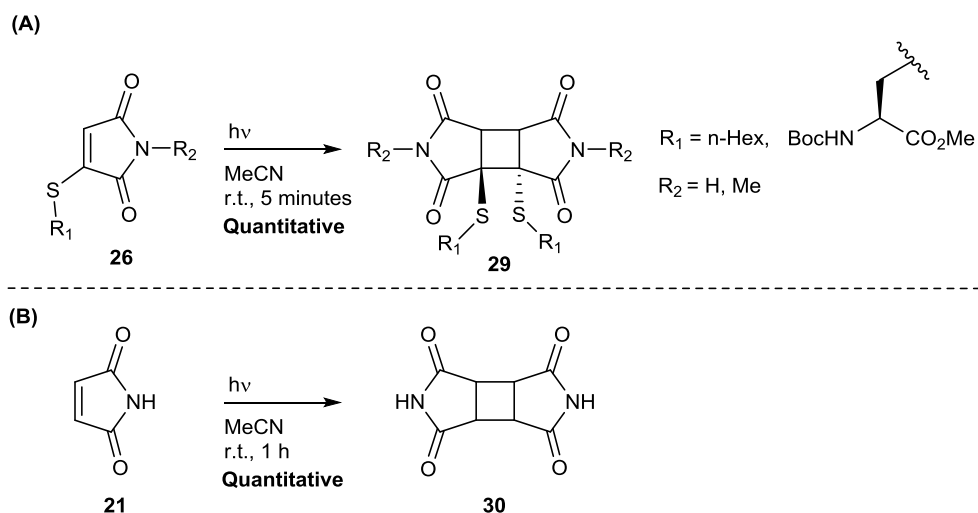
### 1.1.2.2: [2+2] photocycloaddition reactions of thiomaleimides

More recently, work within the Baker group has expanded on maleimide photochemistry by exploring the photochemical reactivity of thiomaleimides. It was discovered that thiomaleimides have much larger extinction coefficients than unsubstituted maleimides,  $9500 \text{ cm}^{-1}\cdot\text{M}^{-1}$  compared to  $720 \text{ cm}^{-1}\cdot\text{M}^{-1}$  at  $\lambda_{\text{max}}$ , presumably due to the increased conjugation provided by the sulfur lone pair. Studies into the photochemical reactions of thiomaleimides showed a substantial increase in reactivity when compared to unsubstituted maleimide, with [2+2] photocycloadditions reaching completion within five minutes. A reaction between various thiomaleimide analogues **26** and styrene **27** was used to test the scope of this reaction (Scheme 10).<sup>63</sup>



**Scheme 10**  
**Photochemical reactions of thiomaleimide(s) 26 with styrene 27.**

Though these reactions proceeded in a quantitative yield, a large excess of alkene was required to prevent competition from a thiomaleimide-thiomaleimide [2+2] photodimerisation to produce succinimide dimer **29** (Scheme 11). In the absence of an alkene this dimerisation reaction was found to proceed quantitatively within five minutes of irradiation. Maleimide **21** irradiated under the same conditions required one hour of irradiation to form the product in a quantitative yield, highlighting the increased photochemical reactivity of thiomaleimides. The application of this reaction forms part of the research described in this text.



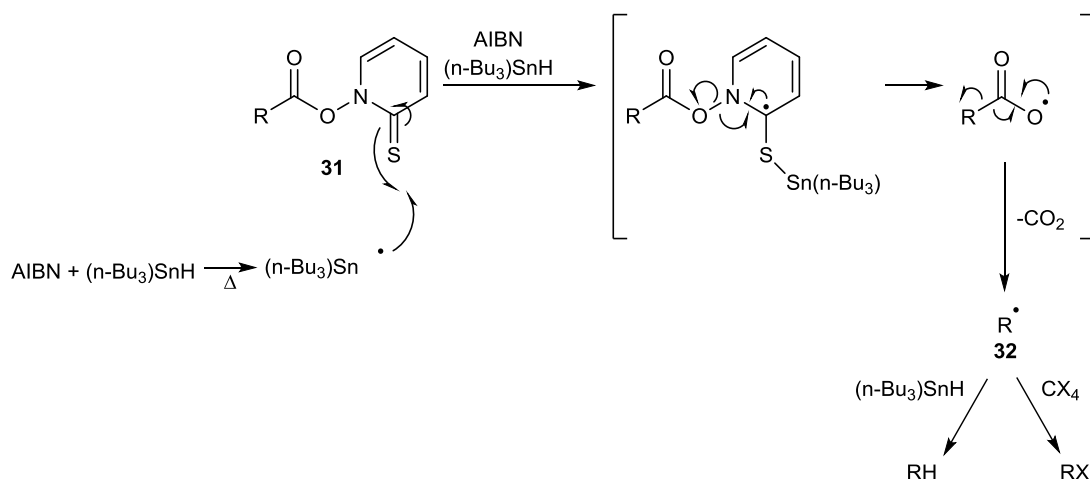
### Scheme 11

(A) Photochemical dimerisation reactions of thiomaleimide(s) 26. (B) A comparative photochemical dimerisation reaction of maleimide 21.

The efficiency of the thiomaleimide [2+2] photocycloaddition reactions, coupled with the remarkable lack of side reactions, demonstrate a significant step forwards in the field. At the time of writing these reactions are arguably the most efficient [2+2] photocyclic additions reported in the scientific literature. This impressive photochemical reactivity identifies thiomaleimides as a class of reagents deserving further study.

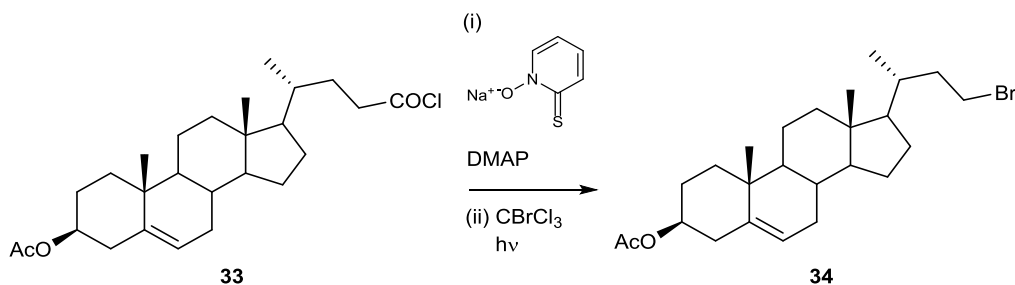
### 1.1.3: Photochemical decarboxylation reactions

A decarboxylation reaction is defined as a reaction which proceeds with concurrent loss of carbon dioxide. This process is most commonly initiated by the production of a carboxyl radical which is subsequently able to undergo radical fragmentation. The most famous of these reactions is the Barton decarboxylation, in which a pre-formed thiohydroxamate (Barton) ester (**31**) is treated with azobisisobutyronitrile (AIBN) and tributyltin hydride to initiate carboxylate radical formation. The resulting alkyl radical (**32**) is subsequently trapped with a suitably reactive compound, often a halogen or hydrogen source (Scheme 12).<sup>64–66</sup>



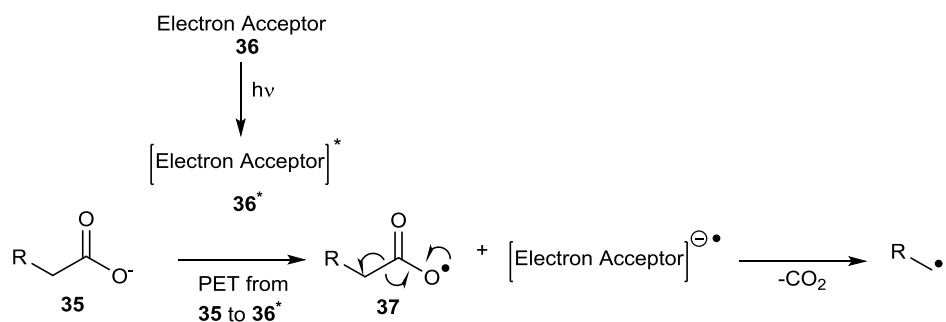
**Scheme 12**  
**A Barton decarboxylation initiated by AIBN and tributyltin hydride.**

Though radical initiators (such as AIBN and tributyltin hydride) are most commonly employed to produce the key carboxylate radical, photochemical methods have also been explored. As early as the 1960s and 1970s groups were observing room temperature decarboxylations of aliphatic carboxylic acids upon UV irradiation, suggesting a photochemical pathway to carboxylate radicals.<sup>67–69</sup> More recently photochemical variants of the aforementioned Barton decarboxylation have been developed which eliminate the need for radical initiators (Scheme 13).<sup>70–72</sup>



**Scheme 13**  
**A photochemical Barton decarboxylation utilised towards the synthesis of cholanic acid analogue 34.**

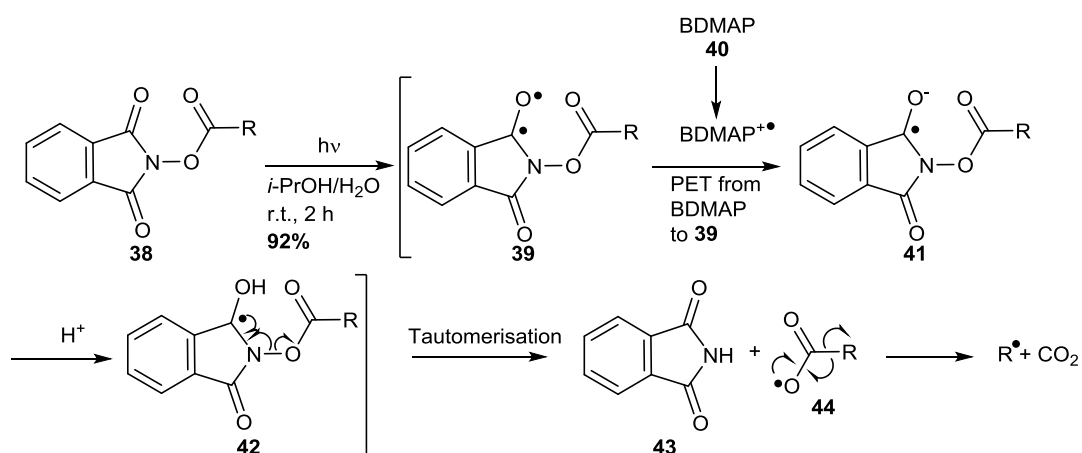
In the case of the photochemical Barton decarboxylation the radical is provided through homolytic cleavage of the N-O bond in the thiohydroxamate ester, though this need not be the case. Many reactions exploit photoinduced single electron transfer (PET), where an electron from the carboxylate **35** is transferred to a photochemically excited electron acceptor **36\***, to form the necessary carboxylate radical. Various electron acceptors have been employed for this purpose, including 1-cyanonaphthalene,<sup>73</sup> various heterocyclic dyes,<sup>74</sup> iminium salts,<sup>75</sup> and tetracyanobenzene.<sup>76</sup> A general scheme for photochemical decarboxylation *via* PET is shown below (Scheme 14).



**Scheme 14**  
A general scheme demonstrating PET from a carboxylate (35) to an electron acceptor (36).

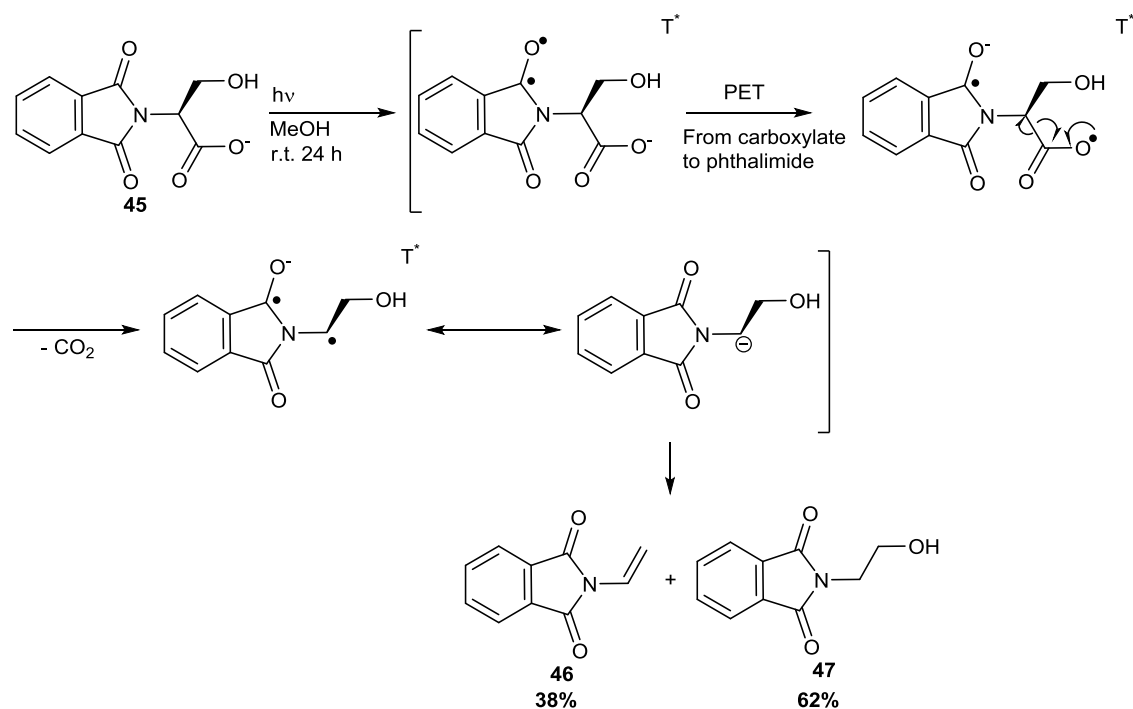
### 1.1.3.1: Photochemical decarboxylation reactions of phthalimides

Due to structural similarities with maleimides the photochemical decarboxylation reactions of phthalimides are of particular relevance to the work presented in this thesis. Reports of phthalimides engaging in decarboxylation reactions exist from as early as 1973,<sup>77</sup> though the reaction was not properly explored until the late 1980s.<sup>78</sup> Okada *et al.* demonstrated the photochemical decarboxylation of *o*-phthaloyl esters (38) by irradiation in the presence of the electron donating 1,6-bis(di-methylamino)pyrene (BDMAP) 40. The authors proposed donation of an electron from BDMAP 40 to the excited state phthalimide 39 followed by N-O bond cleavage and decarboxylation (Scheme 15).



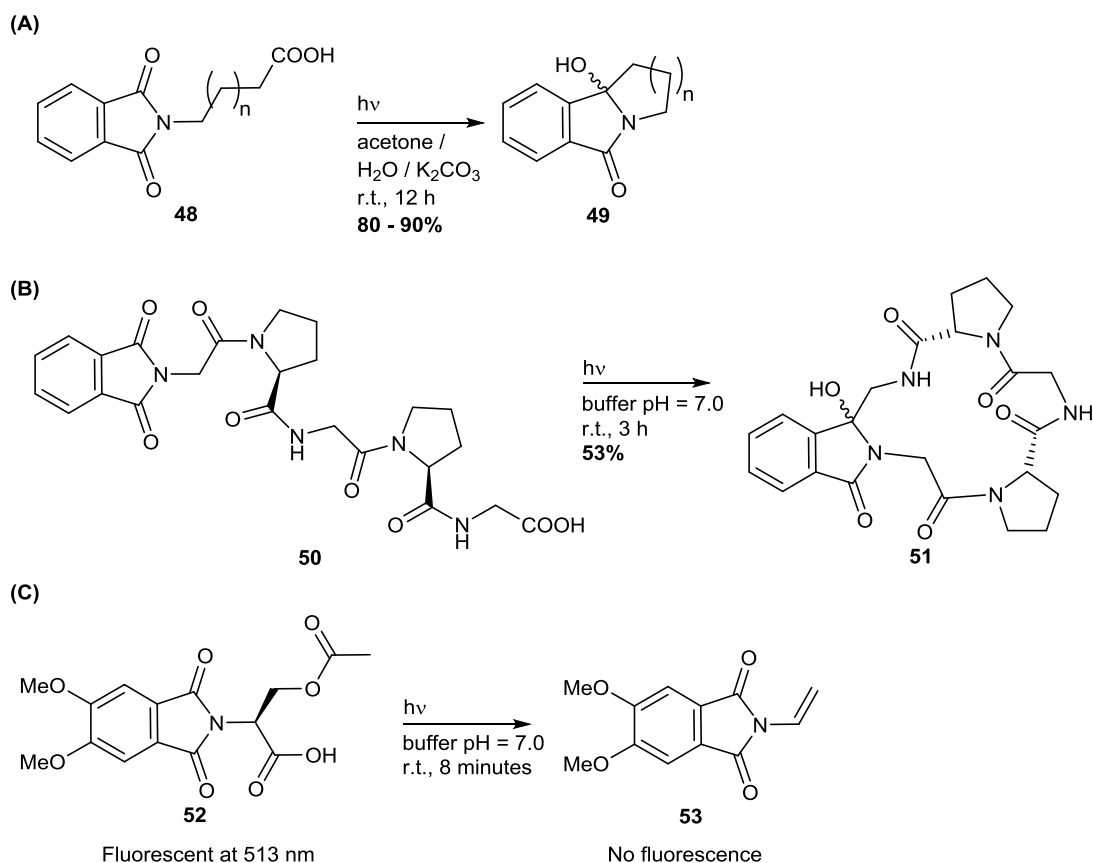
**Scheme 15**  
The mechanism proposed by Okada *et al.*<sup>78</sup> for the photochemical decarboxylation of *o*-phthaloyl esters (38).

In the early 1990's Griesbeck *et al.* expanded on this work by demonstrating an intramolecular PET process from an *N*-pendant carboxylic acid to the phthalimide.<sup>79,80</sup> In this scenario the carboxylate is the electron donor and the phthalimide the electron acceptor. This removes the need for the additional electron donor and expands the utility of the reaction (Scheme 16).



**Scheme 16**  
**The photochemical decarboxylation of *N*-phthaloyl-serine 45.**

Though in this early example the resulting carbon centred radical was not reacted further, this work demonstrated the capability of phthalimides to act as electron acceptors in PET reactions. Since their initial discovery phthalimide mediated decarboxylation reactions have been thoroughly explored and utilised for a variety of purposes. Though the vast majority of the work has been done by Griesbeck *et al.*, the reaction has been successfully adopted by other groups. At the time of writing the reaction has been employed towards the synthesis of phthalimide containing cyclic compounds and cyclic peptides,<sup>81,82</sup> and also as a photocage for the timed activation of fluorescent probes.<sup>83</sup> A small summary of some of the reported uses of phthalimide photodecarboxylations is shown below (Scheme 17).

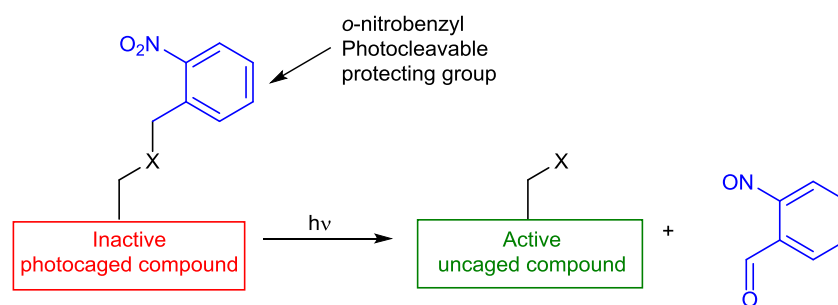


#### Scheme 17

A small summary of the photochemical decarboxylation reactions of phthalimides. (A) Photochemical macrocyclisation. (B) Photochemical peptide cyclisation. (C) A photochemical fluorescent probe.

### 1.1.4: Photocleavable protecting groups

Although photochemical reactions which form covalent bonds are often given more attention, photolytic bond cleaving processes should be treated with equal importance. Early research into photolytic bond breaking reactions was restricted to synthetic organic chemistry and was utilised in the photochemical deprotection of amines,<sup>84,85</sup> esters,<sup>86</sup> and carboxylic acids.<sup>85,87</sup> The early adoption of these reactions for protecting reactive chemical functionality led to them being termed “photocleavable” protecting groups. The general scheme below uses the *o*-nitrobenzyl photocleavable protecting group to demonstrate the premise (Scheme 18).



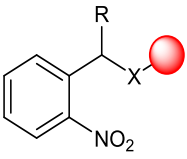
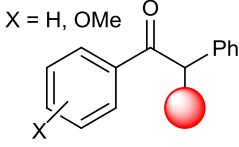
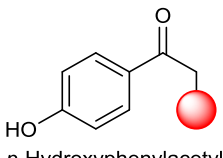
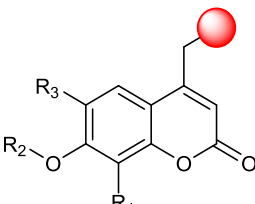
**Scheme 18**  
**The general premise of photocleavable protecting groups.**

Over the last few decades a plethora of photochemical protecting groups based around a variety of chemical structures have been discovered and several excellent reviews have been written on the subject.<sup>88–90</sup> Though the application of photocleavable protecting groups to chemical biology and biochemistry is most pertinent to this work, it is worth noting that these important reactions have had a huge influence on several areas of research including organic synthesis,<sup>17,49,91</sup> polymerisation,<sup>92,93</sup> peptide synthesis,<sup>94</sup> and surface modification.<sup>95</sup>

#### 1.1.4.1: Photocleavable protecting groups in chemical biology

The spatio-temporal release of functional compounds has proven particularly useful to the study of biological systems. Commonly employed photocleavable protecting groups, and their applications, are outlined in Table 1 below. This list is by no means exhaustive and more comprehensive summaries of this area can be found in the literature.<sup>89,96–98</sup>

**Table 1**  
**The applications of commonly employed photochemical protecting groups**

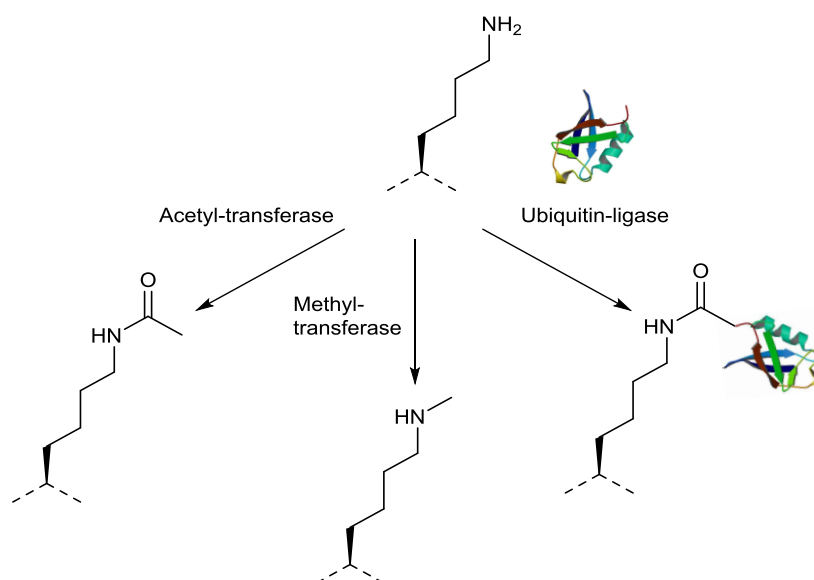
Photocage	Applications
 <p><i>o</i>-Nitrobenzyl</p>	<p>Photochemical release of ATP,<sup>99,100</sup> DNA activation,<sup>101</sup> RNA synthesis,<sup>102</sup> natural product synthesis,<sup>103</sup> drug delivery,<sup>104,105</sup> photochemically labile nanoparticles.<sup>106</sup></p>
 <p>Benzoin</p>	<p>Drug delivery,<sup>107</sup> protein folding,<sup>108,109</sup> photochemical release of cAMP, glutamate, and GABA.<sup>110,111</sup></p>
 <p><i>p</i>-Hydroxyphenylacetyl</p>	<p>Enzyme catalysis,<sup>98</sup> photochemical release of ATP,<sup>112</sup> GTP,<sup>113</sup> and GABA.<sup>114,115</sup></p>
 <p>Coumarinyl</p>	<p>Drug delivery,<sup>116</sup> photochemically labile nanoparticles.<sup>117</sup></p>

The extensive list of applications in which photocleavable protecting groups are implicit perfectly highlights the power of photochemistry and the importance of research into this area. This will be discussed in more detail later in this chapter.

## 1.2: Chemical modification of proteins and peptides

### 1.2.1: Background

Proteins and peptides are implicated in virtually every biological process within the body, and discovering ways to accurately study and probe the form and function of these macrostructures is essential to our ongoing understanding. Over the last century the importance of natural chemical modification, through post-translational modifications, has been extensively researched. These post-translational modifications serve to alter the chemistry of the protein or peptide and play essential roles in modulating their function inside the body.<sup>118</sup> Examples of post-translational modifications include acetylation, methylation, and ubiquitination. These are demonstrated below (Scheme 19).



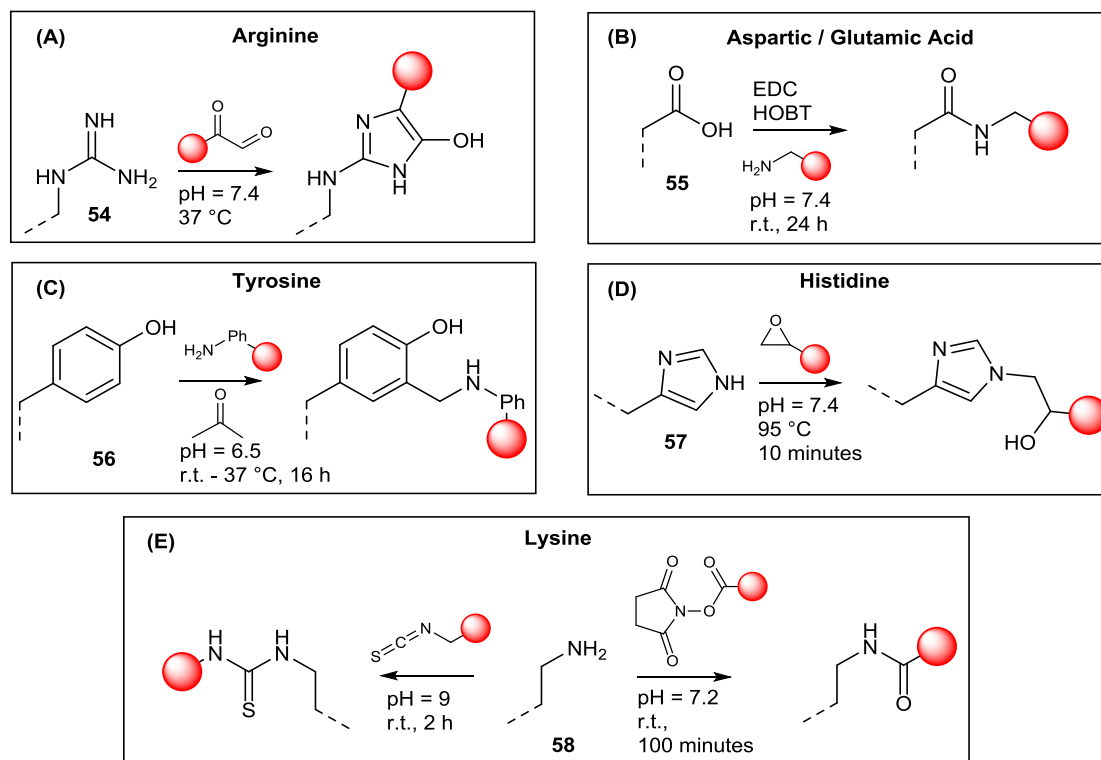
**Scheme 19**  
**A small selection of lysine post-translational modifications.**

Understanding the true potential of chemical protein modification has led to great efforts being made to extend beyond the limits of native post-translation modification. Over the last 50 years great efforts have been made to discover new methods to modify proteins with novel chemical functionality both *in vitro* and *in vivo*.<sup>119,120</sup> This has been a huge area of research within the rapidly expanding field of chemical biology and forms part of the work presented in this thesis. Since their conception chemically modified proteins have been used for a variety of purposes, with a particular focus placed on the development of novel protein based therapeutics.<sup>121,122</sup> To this end chemical protein modifications have been used to improve the pharmacokinetic and pharmacodynamic properties of known peptidic drugs<sup>123,124</sup> and to deliver therapeutic payloads to biological targets of interest.<sup>121,122,125</sup> Additionally, chemical protein modification has been employed to attach imaging agents,<sup>126</sup> diagnostic tools<sup>127</sup> and radionuclides,<sup>128</sup> for both research and therapeutic purposes.

### 1.2.2: Amino acid modification

In order to chemically modify a protein it is necessary to target a suitably reactive chemical moiety on the protein's surface. It is desirable to target the protein with a reagent which displays fast reaction kinetics, is site-selective, stable under physiological conditions and ultimately non-damaging to the protein or organism being studied. Fortunately, the amino acid side chains present a wide range of functionalities which can be targeted by an ever expanding tool box of chemical reactions that fulfil these criteria. Protocols for the selective modification of arginine **54**,<sup>129</sup> aspartic/glutamic acid **55**,<sup>130</sup> cysteine **59**,<sup>131</sup> histidine **57**,<sup>132</sup> lysine **58**,<sup>120,133</sup> and tyrosine **56**<sup>134</sup> have been discovered and are routinely employed (Scheme 20). Of these methods lysine modification has historically dominated the field, though cysteine modification (which will be covered in detail in the next section) has recently seen increased attention.

 = Chemical payload

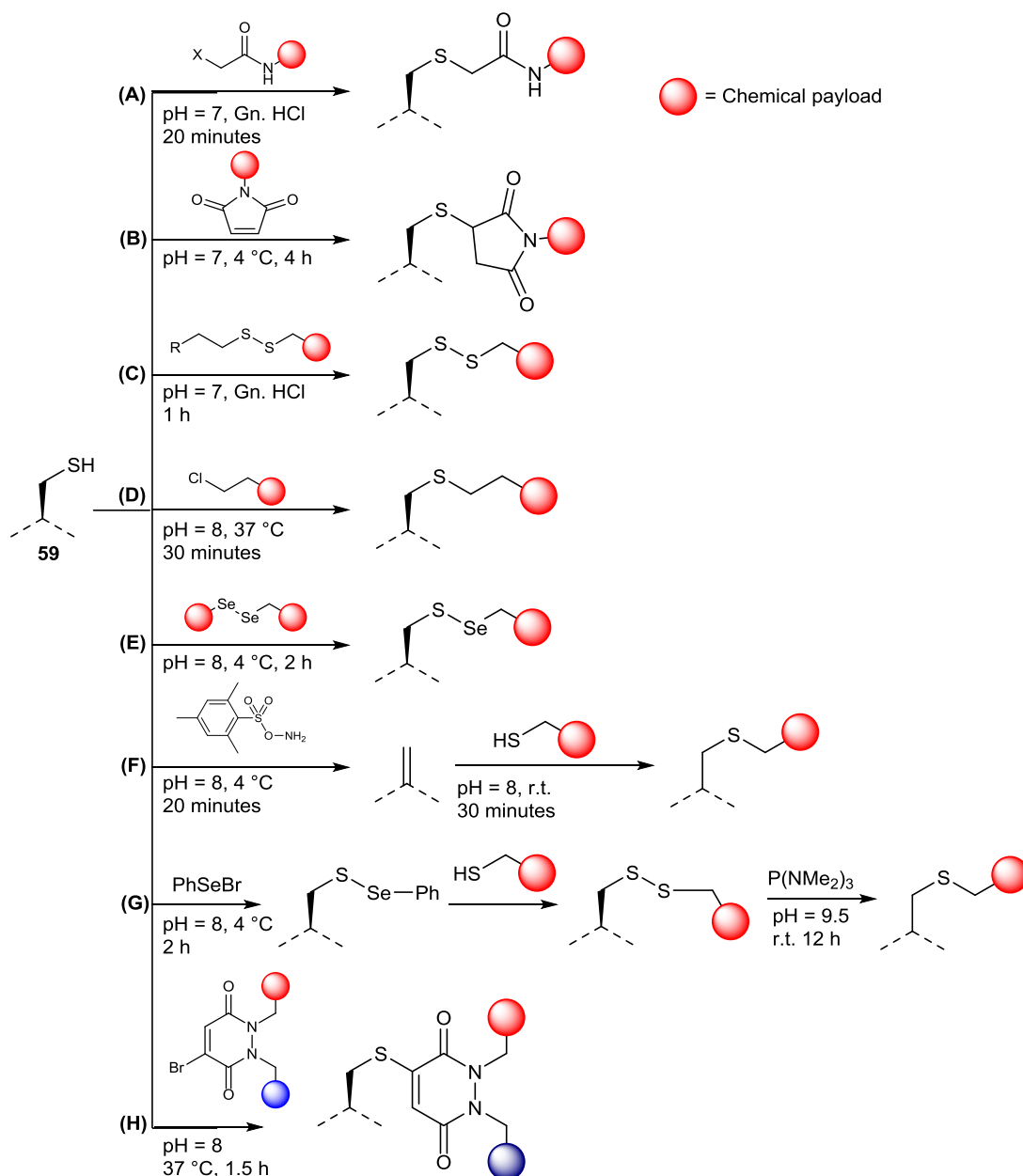


### Scheme 20

A selection of chemical modifications for specific amino acid side chains: (A) The reaction of arginine 54 with substituted glyoxal.<sup>129</sup> (B) The EDC coupling reaction of carboxylic acid side chains.<sup>130</sup> (C) Tyrosine 56 modification through a three component Mannich reaction.<sup>134</sup> (D) Histidine 57 modification through a functionalised epoxide.<sup>132</sup> (E) Lysine 58 modification via activated NHS esters<sup>133</sup> or isothiocyanates.<sup>120</sup>

## 1.2.3: Cysteine modification

Though each of the amino acid targets has particular advantages the bulk of this work will focus on selective cysteine modification. Cysteine residues offer two major benefits over the more commonly targeted lysine residues: they display a greater nucleophilicity at low pH and are present in a lower natural abundance.<sup>120,135</sup> These are desirable qualities when selectivity is required.<sup>119,136</sup> The second point is particularly relevant for clinical applications as it is becoming increasingly apparent that the heterogeneous mixtures resulting from lysine modification display less than ideal therapeutic qualities.<sup>137</sup> Lysine residues are abundant on the surface of proteins, decreasing the site-selectivity of any technique which targets them.<sup>120</sup> Conversely, cysteine residues have a natural abundance of just 2.26%.<sup>135</sup> This leads to a greater degree of selectivity and homogeneity, especially when combined with site directed mutagenesis. For these reasons methods that target cysteine residues have seen an enormous amount of interest, especially over the last 20 years. Scheme 21 displays a selection of some of the more prevalent methods.<sup>119,120,122,131,136,137</sup>

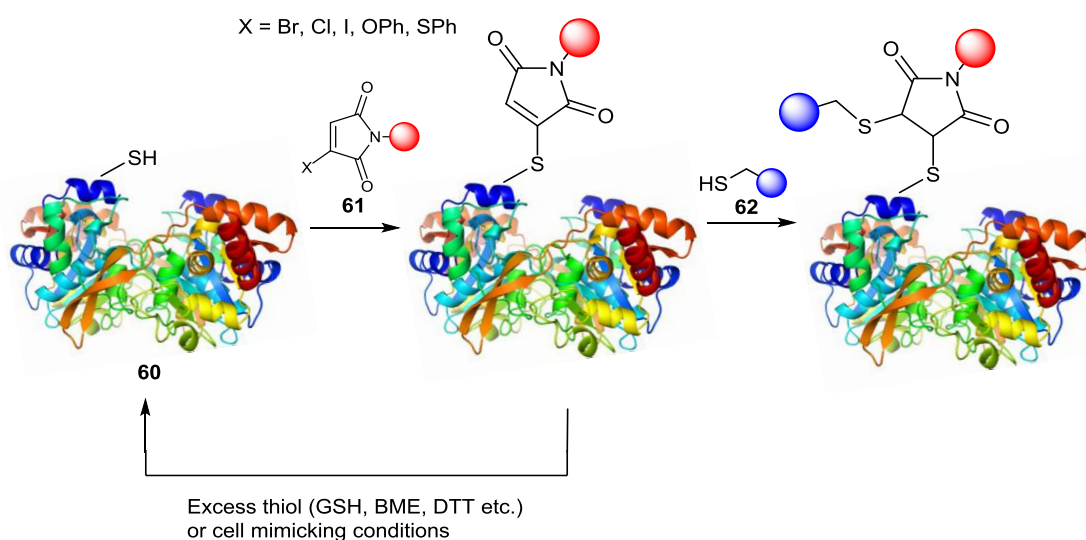


**Scheme 21**

**Cysteine-selective chemical modifications:** (A) Modification using haloacetamides.<sup>138</sup> (B) Modification using maleimide.<sup>139</sup> (C) Modification using oxidative disulfide exchange.<sup>138</sup> (D) Modification using an alkyl halide.<sup>140</sup> (E) Modification using diselenide exchange.<sup>141</sup> (F) DHA formation using *o*-mesitylenesulfonylhydroxylamine (MSH) and subsequent modification using a thiol-ene reaction.<sup>142</sup> (G) Sulfur-selenide exchange followed by desulfurisation.<sup>143</sup> (H) Modification using a *bis*-modified pyridazinedione.<sup>144,145</sup>

### 1.2.3.1: Next generation maleimides as tools for cysteine modification

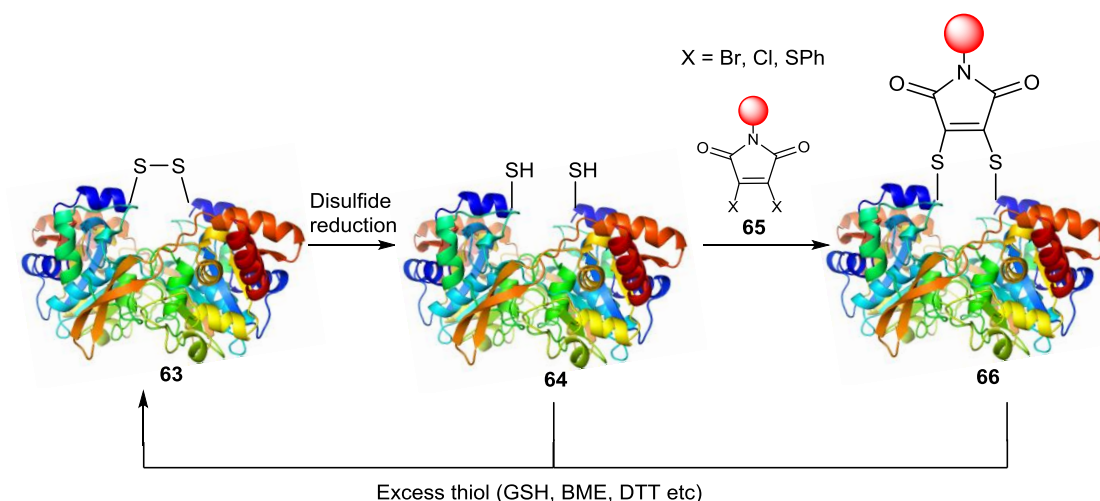
Work in the Baker and Caddick groups at UCL has focused on the development of next generation cysteine-selective reagents based around the maleimide scaffold.<sup>145–153</sup> The addition of a leaving group to the alkene of the maleimide greatly expands the reactivity of these reagents. Next generation maleimides (**61**) react with cysteine residues (**60**) *via* addition-elimination and thus retain the maleimide double bond, further expanding the reactivity profile of these reagents and allowing for the incorporation of a second chemical or peptidic moiety **62**.<sup>146,154</sup> Early work with the resulting cysteine-maleimide linkers discovered that the modification is reversible under high thiol concentration, opening up the possibility that these linkers could be used to develop thiol-cleavable protein-drug conjugates which release the chemical payload in the thiol rich intracellular environment.<sup>146,148,151,155</sup> A summary of the reactivity of next generation maleimides is shown below (Scheme 22).



#### Scheme 22

**The reaction between cysteine and a substituted maleimide **61**. Cleavage of the maleimide is observed under high thiol concentrations or cell mimicking conditions.**

A further extension of these maleimides are the disubstituted maleimides.<sup>147,149,152,153,156</sup> These reagents contain two suitable leaving groups and are thus able to react with two cysteine residues, making them ideal for insertion into a disulfide bond. Cysteine residues are often “tied up” in disulfide bonds, making them unavailable for chemical ligation. Chemical tagging of these cysteine residues is dependent on reduction of the disulfide bond, which can often lead to structural changes to the quaternary structure of the protein and give rise to undesirable issues with stability or functionality. Disubstituted maleimides can react with both of the liberated cysteines from a disulfide bridge, reforming the covalent link and retaining the three-dimensional structure of the protein. An overview of the reactivity of disubstituted maleimides is shown below (Scheme 23).



**Scheme 23**  
**Inserting disubstituted maleimide reagents (65) into native disulfide bonds.**

Though the importance of disulfide bonds is dependent on a wide range of factors, including the size of the protein and the position of the bridge within the protein's structure, it is clear that maintaining their presence is hugely beneficial. In smaller proteins such as insulin and somatostatin, used for the treatment of diabetes and neuroendocrine tumours respectively, the disulfide is known to be essential for the function of the peptide.<sup>157</sup> Often, especially in larger proteins such as immunoglobulins, the accessible disulfide bonds are not essential for function but do provide a significant degree of thermal stability.<sup>158</sup> Maintaining this stability is valuable for any therapeutic application.

## 1.2.4: Antibody modification

The power of chemical protein modification is perhaps best exemplified by the rapidly expanding field of antibody conjugation. Antibodies have an innate specificity for the antigen against which they are expressed, which makes them an attractive vehicle for the targeted delivery of small molecules. Over the last three decades a considerable amount of research has been dedicated to developing methods for reliably modifying antibodies and their associated fragments.<sup>125,128,159–163</sup>

### 1.2.4.1: Antibody structure

Antibodies are large glycoproteins which are responsible for identifying and eliminating foreign bodies. Consequently, their evolution has been directly linked to their ability to recognise particular disease markers, which has in turn led to a high degree of target specificity. So far five classes of antibodies have been identified in vertebrates; IgA, IgD, IgE, IgG and IgM.<sup>164–166</sup> IgG antibodies represent the predominant class of human immunoglobulins and can be further categorised into four sub-families; IgG1, IgG2, IgG3 and IgG4.<sup>167</sup> IgG1 antibodies are the most abundant of the four and are consequently the most commonly employed therapeutic antibodies.<sup>168</sup> An IgG1 consists of four smaller protein chains; two identical ~25 KDa “light” chains and two identical ~50 KDa “heavy”

chains. The N-termini of these chains converge to make up the antigen binding region of the protein and as a result considerable structural variation is seen in this region. This has led to the N-terminus being named the variable region, with the associated regions on the light and heavy chains designated  $V_L$  and  $V_H$  respectively. Further from the antigen binding region the amino acid sequence becomes more conserved on both the heavy and the light chain, leading to the area being designated the constant region. Each light chain contains a single constant region  $C_L$  whereas the heavy chain is made up of three distinct constant regions  $C_{H1}$ ,  $C_{H2}$  and  $C_{H3}$ . The individual chains are connected by disulfide bonds and considerable non-covalent interactions to form the characteristic symmetrical “Y” structure. The whole structure can be roughly divided into two distinct structures; antigen binding fragment (Fab) and the constant fragment (Fc, “Fragment crystallisable”). Further division of the Fab fragment can produce the variable fragment Fv (Figure 2).<sup>164</sup>

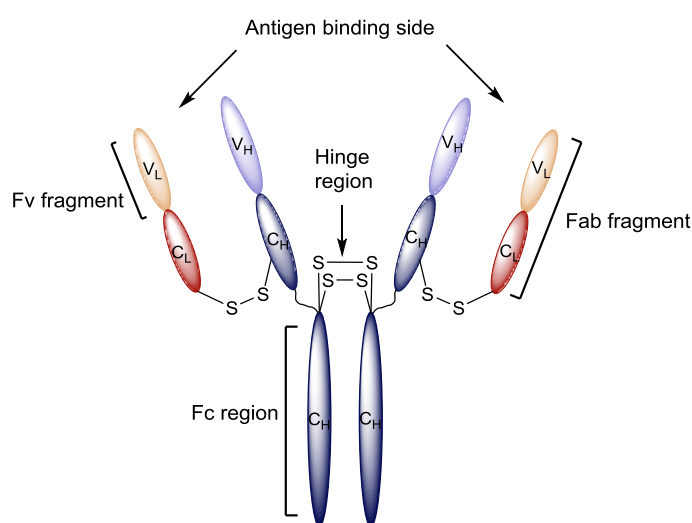


**Figure 2**  
**A schematic representation of an IgG1 immunoglobulin.**

Both Fab fragments and Fv fragments are able to successfully bind to antigens and have been used as therapeutics.<sup>169</sup> The Fc region, though unable to bind to the antigen, is responsible for the immunological effect of antibodies and is essential for antibody-dependent cellular cytotoxicity and complement-dependent cytotoxicity.<sup>166,170</sup>

### 1.2.4.2: Antibody conjugates

#### Full antibody conjugates

By far the most well accepted antibody directed therapies are based around the full antibody scaffold.<sup>160,162,171</sup> In fact, due to the immunogenic nature of the Fc region some success has been had in treating disease with native antibodies containing no additional chemical modification.<sup>172,173</sup> Early examples of antibody based therapeutics were based entirely on murine monoclonal antibodies and problems of immunogenicity, efficacy and serum half life were frequently encountered.<sup>171</sup> The advent of chimeric antibodies, in which the Fc region of a foreign antibody is replaced with that of a human antibody, has helped to

overcome these issues.<sup>174,175</sup> In 1997 Rituxan, used for the treatment of B-cell non-Hodgkin's lymphoma,<sup>171,172,176</sup> became the first chimeric antibody to be awarded FDA approval. Since this milestone the number of monoclonal antibodies with clinical approval in both the USA and the EU has rapidly increased.<sup>121,177</sup> Though this impact is significant there are several drawbacks to using native antibodies for therapeutic purposes. The large size of the proteins leads to poor tumour penetration and long *in vivo* half-lives, which can lead to non-selective cell toxicity.<sup>178</sup> These issues decrease the efficacy of the treatments and make native antibodies a non-ideal therapeutic choice.<sup>179</sup>

Fortunately, these issues can be remedied through the covalent attachment of small chemical moieties. These attachments can be used to modulate the properties of the antibody or, as in the case of Antibody Drug Conjugates (ADCs), to attach a cytotoxic payload to improve potency.<sup>123,124,160</sup> This latter approach has gained significant attention and led to the development of the area of ADC research. In designing an effective ADC several chemical problems must be addressed. The attached drug must be extremely potent to compensate for low delivery levels. The linker between the drug and the antibody must be stable within the blood but labile within the cell to ensure efficient release of the drug occurs only at the target. In addition to this all of the components (antibody, drug, and linker) must have been individually assessed to eliminate any safety concerns (Figure 3).<sup>160</sup>

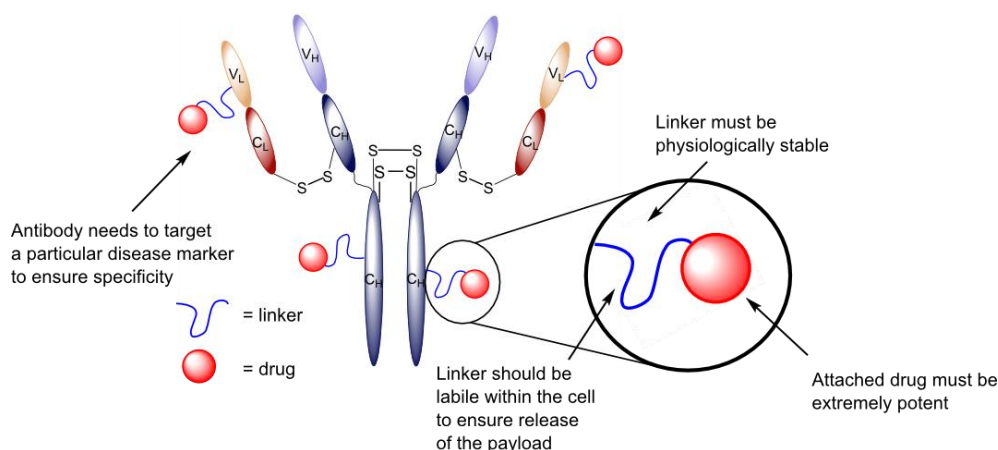


**Figure 3**  
**A schematic highlighting some of the criteria for a successful antibody drug conjugate.**

Within the last few years the FDA have approved two ADC based therapeutics; Kadcyla for the treatment of HER2-positive breast cancer and Adcetris for the treatment of Hodgkin and systemic anaplastic large cell lymphomas. Kadcyla consists of the cytotoxic agent DM1 conjugated to the monoclonal antibody trastuzumab and targets the HER2 receptor which is over expressed in cancer cells.<sup>180</sup> Adcetris consists of the antimetabolic agent monomethyl auristatin E (MMAE) conjugated to the chimeric monoclonal antibody brentuximab which targets the CD30 antigen.<sup>181</sup>

Several methods for attaching drugs to antibodies have been developed, the vast majority relying on conjugation to native amino acids. Historically, lysine modification has prevailed but in recent years cysteine modification, due to the many advantageous outlined previously, has become the industry standard.

### Fab fragment conjugates

Fab fragments (antigen binding fragment) are made up of the  $V_H$  and  $V_{CH1}$  regions of the heavy chain attached by a single inter-chain disulfide bond to the light chain (Figure 4). These fragments are able to bind to the antigen, though the absence of the immunological effector function-mediating region, which exists on the Fc fragment, precludes any immunogenic effects.<sup>164,182</sup> Though this can be a disadvantage the added benefit of increased tumour penetration and shorter half-life make Fab fragments an attractive target for conjugation.<sup>183,184</sup> Despite being less studied several successful therapeutic examples have reached the market.<sup>169</sup> The unique properties of Fab fragments (fast clearance and improved tumour penetration) make them ideal for the delivery of imaging agents for diagnostic purposes (Figure 4). Considerably better resolution between the target site and the background can be achieved with Fab fragments when compared to full antibodies.<sup>185,186</sup>

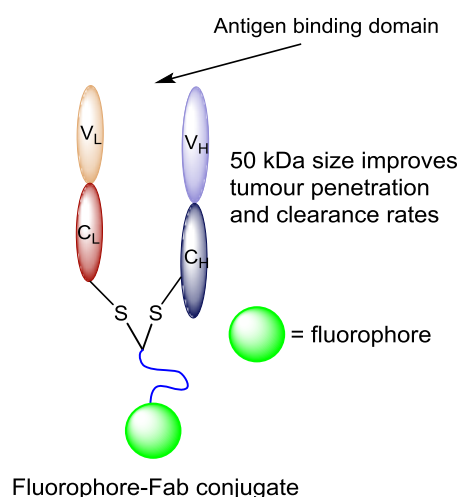


**Figure 4**  
A schematic representation of a Fab fragment imaging agent.

### scFv conjugates

Single chain variable fragments (scFvs) contain only the variable region of the antibody and represent one of the smallest classes of clinically employed antibody fragments. These fragments are termed “single chain” due to the introduction of a link between the  $V_L$  and  $V_H$  regions of the Fv fragment, covalently binding the two regions into a single fragment. This covalent link is necessary to improve the *in vivo* stability of the Fv region, which has been found to be too unstable for clinical use in the native form.<sup>187</sup> Typically a peptide chain is introduced for this purpose, though interchain disulfide bonds have also been engineered

into the structure for the same effect.<sup>188,189</sup> More recently hybrid approaches in which both a peptide chain and a disulfide bond have been utilised to create scFv fragments that are readily expressed and display excellent stability.<sup>190</sup> An overview of the different types of scFv are shown below (Figure 5).

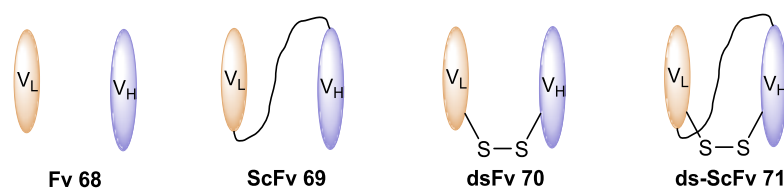


**Figure 5**  
**Schematic representations of a variable fragment (Fv) 68, a single chain variable fragment (scFv) 69, a disulfide stabilised variable fragment (dsFv) 70 and a disulfide stabilised single chain variable fragment (ds-scFv) 71.**

scFvs display improved tumour penetration and clearance rates, surpassing those demonstrated by Fab fragments.<sup>183,191–193</sup> This makes them ideal for many of the same applications, and indeed scFv fragments are regularly employed as imaging agents.<sup>179,185,194</sup>

## 1.2.5: Peptide based therapeutics

Peptides are well studied biomolecules which generally show excellent selectivity for their specific cell surface receptors.<sup>195</sup> Over 7000 naturally occurring peptides have been identified and implicated in crucial roles, acting as hormones,<sup>196</sup> ion channel regulators,<sup>197</sup> growth factors,<sup>196</sup> and anti-infectives,<sup>198</sup> amongst others.<sup>195,199,200</sup> Poor pharmacological properties plagued early peptide based drugs, primarily due to rapid enzymatic digestion, and led to a poor adoption of these therapeutics in the mid 20<sup>th</sup> century.<sup>199</sup> A notable exception can be found with the polypeptide insulin, which remains one of the most utilised clinically available peptidic drugs. Despite these disadvantages the use of peptides in therapy continues to grow as formulation methods are developed to help minimise their negative attributes. At the time of writing over 130 peptidic therapeutics are in the clinical pipeline, with a further 600 in pre-clinical development.<sup>199</sup>

### 1.2.5.1: Somatostatin and its analogues

Somatostatin is a cyclic peptide expressed in both the central nervous system (CNS) and gastrointestinal tract. In the former the peptide acts as a neurotransmitter, and in the latter it is a potent inhibitor of the release of growth hormone, glucagon, insulin and gastrin.<sup>201–205</sup> Two forms of natural somatostatin are known, somatostatin-14 (SST-14) **72** and somatostatin-28 (SST-28) **73**; the number relating to the length of the amino acid backbone. SST-28 **73** contains the same core 14 amino acids as SST-14 **72** with a further 14 added on to the N-terminus (Figure 6). Both forms of the protein activate the same signalling pathways, though SST-28 **73** displays higher potency.<sup>204</sup>

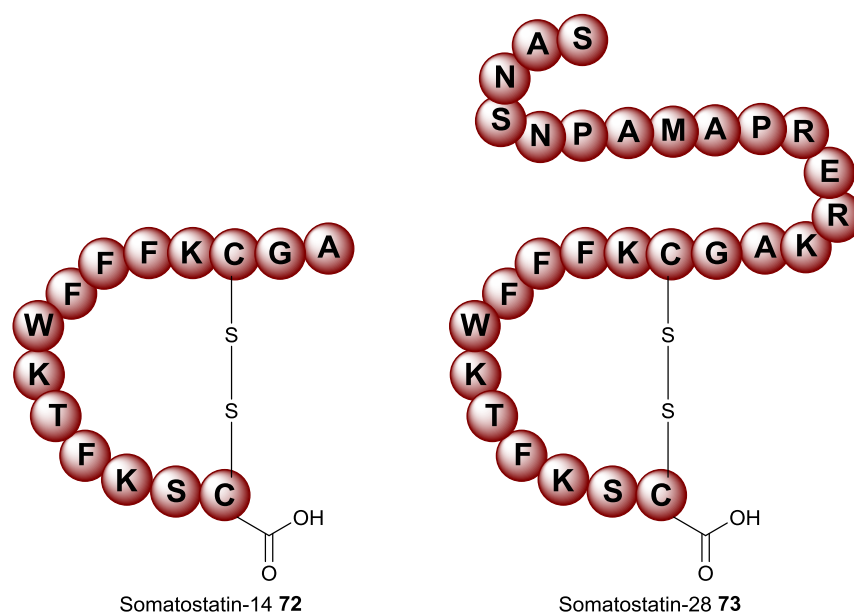


**Figure 6**  
**Schematic representations of somatostatin-14 **72** and somatostatin-28 **73**.**

Somatostatin receptors, of which there are currently five known human subtypes (SST1-5), are over-expressed in various diseases, particularly cancers related to growth hormone.<sup>203</sup> The relative expression of these five subtypes has been found to vary significantly depending on location within the body, but they all bind both forms of somatostatin with low nanomolar affinity.<sup>205</sup> Binding of somatostatin to the receptor initiates signalling pathways which activate protein tyrosine phosphatase (PTP), inhibit adenylyl cyclase, activate  $K^+/Ca^{2+}$  channels and modulate mitogen-activated protein kinase (MAPK). The combination of these pathways results in the characteristic effects of the peptide.<sup>203,205</sup> The potent effects on cancer targets, and low nanomolar concentrations required to realise them, make somatostatin an ideal candidate for therapeutic investigation. Unfortunately both forms of the peptide suffer from a short *in vivo* half life of just 2-3 minutes, making them unsuitable for therapeutic applications in their native form.<sup>201</sup>

### **Octreotide**

Significant effort has been made to overcome the poor pharmacokinetics of somatostatin and has resulted in the generation of several analogues. Structure-activity relationship studies discovered that several changes to the structure of somatostatin-14 **72** were well tolerated and helped to improve its pharmacokinetic properties. Reversing the chirality of the tryptophan residue from L to D significantly improved the half life without reducing the potency.<sup>206</sup> It was found that the binding of the peptide to the receptor was predominantly through a  $\beta$ -turn at amino acid residues 7-10 (Phe-Trp-Lys-Thr) and modifications to this region resulted in a significant loss in potency.<sup>206,207</sup> With this in mind the amino acids distal to the pharmacophore were substituted or removed (though the disulfide bridge was conserved out of necessity) resulting in several analogues.<sup>206</sup> This work culminated in the

generation of several highly potent somatostatin analogues that displayed greater *in vivo* half life and selectivity for one SST receptor over the others. Of these Octreotide **74** (SST2 selective),<sup>208</sup> Lanreotide **75** (SST2/SST5 selective)<sup>209</sup> and Vapreotide **76** (SST5 selective)<sup>202</sup> have obtained FDA approval (Figure 7).

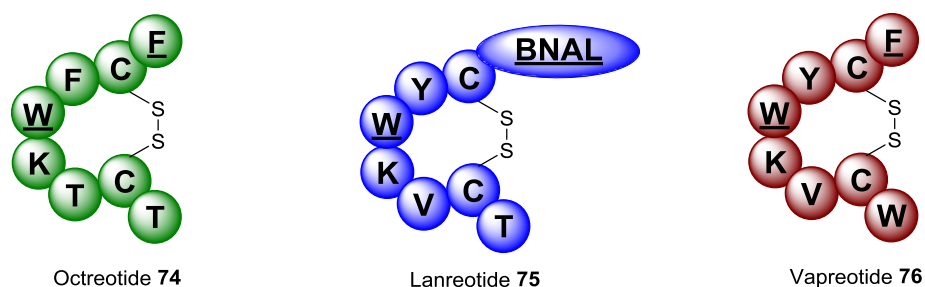


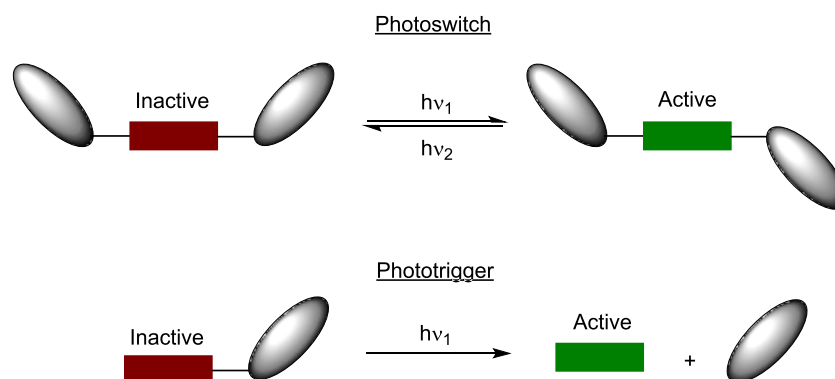
**Figure 7**  
Somatostatin analogues currently on the market. Underlined = D enantiomer.

Of these analogues Octreotide **74** is perhaps the most well utilised. This analogue was originally reported by Wilfried Bauer<sup>208</sup> and is today marketed under the trade name Sandostatin by Novartis Pharmaceuticals.<sup>200</sup> The peptide has FDA approval for the treatment of neuroendocrine tumours, which have been found to over-express the SST2 receptor.<sup>203</sup> Octreotide **74** has been found to be nearly 20 times more potent than native somatostatin and displays exquisite selectivity for the SST2 receptor, making it an ideal therapeutic for the treatment of neuroendocrine tumours. Additionally, the *in vivo* stability was found to be significantly improved compared to somatostatin.<sup>208</sup> Octreotide **74** is still receiving significant research interest, with recent work focused on increasing the half-life of the drug through formulation within a biodegradable polymer.<sup>210</sup> The excellent potency and improved pharmacokinetic properties of Octreotide **74** make it a highly desirable therapeutic drug and an excellent candidate for further study.

### 1.3: Photochemistry and Chemical Biology

The marriage of photochemistry and protein modification perfectly exemplifies the power of interdisciplinary research. Advances in both fields over the last 20 years have led to the rapid rise of photochemical probes being used to observe, influence or exploit biological processes.<sup>211–217</sup> These photochemical probes can be broadly split into two categories; photoswitches and phototriggers. Whilst both have the power to initiate dynamic biological processes, photoswitches refer to reversible photochemical processes whereas phototriggers generally refer to irreversible systems.<sup>212</sup> Reversible photochemical control over biological mechanisms has proven to be a valuable tool for studying time sensitive cellular processes<sup>218,219</sup> and protein interactions.<sup>220,221</sup> Sadly photoswitches often display slow reaction kinetics, and incomplete conversions are common. Additionally, thermal reversion from one form to the other can occur. The combination of these problems often leads to poor contrast between the “on” and “off” forms of the switch, limiting their utility.

For situations where reversibility is not required it is often more prudent to employ phototriggers, which typically display more favourable reaction kinetics and greater conversions. The two are compared in the schematic representation below (Scheme 24).



**Scheme 24**  
A comparison of photoswitches and phototriggers.

A large body of work exists on both photoswitches and phototriggers being employed to release biologically active organic molecules and thus gain spatio-temporal control over biological processes. This is especially prevalent in neuroscience where these techniques have been employed to gain exquisite control over the concentrations of neurologically important chemicals such as glutamate, nitrous oxide, and calcium. Indeed photouncaging of glutamate has become so popular that compounds for this purpose are now commercially available (Figure 8).<sup>96,212,222</sup>

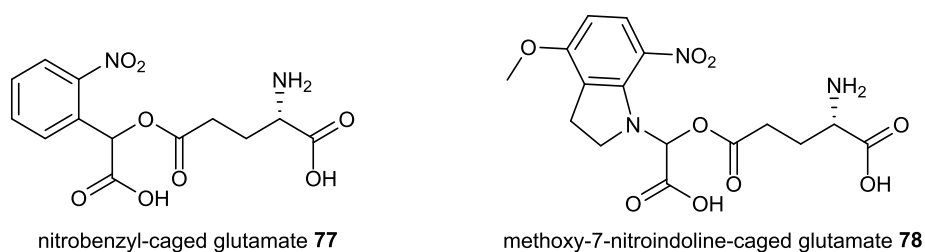
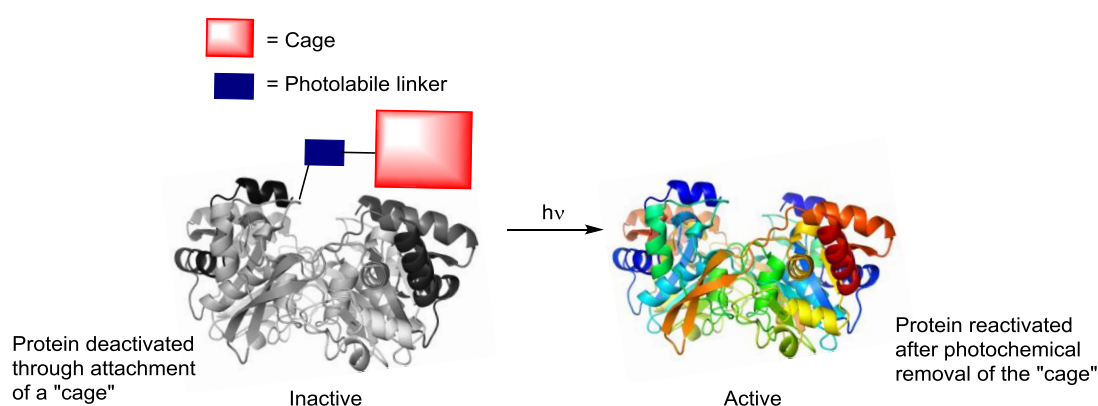


**Figure 8**  
Commercially available photocaged glutamate analogues.

Whilst this approach of releasing an organic substrate to elicit a desired effect on a protein is common, less work has been reported on directly initiating phototriggered reactions on proteins.<sup>96,215–217,223</sup> This is unsurprising as the increased size and complexity of proteins complicates this approach. Part of the work described in this thesis falls into this category, thus the remainder of this section will be spent introducing this area.

### 1.3.1: Photochemical protein uncaging

The applications of photoactivatable peptides and proteins fall generally into two categories: photochemical protein uncaging and photochemical targeted small molecule delivery. Photochemical protein uncaging describes a system in which a protein is deactivated through the covalent attachment of a suitable photolabile chemical “cage”. Subsequent irradiation releases the protein or peptide from the cage and restores the biological activity. Typically a cage is installed at a topologically sensitive location to cause the greatest detrimental effect to the activity, leading to a greater contrast before and after irradiation. The choice of cage can be tailored to the protein or peptide under study and numerous photocleavable protecting groups have been found to be suitable for these applications.<sup>215,216</sup> This approach has gained significant interest over the last few decades for research purposes, though clinical applications are only now being fully realised.<sup>215,216</sup> A general scheme demonstrating this approach is shown below (Scheme 25).

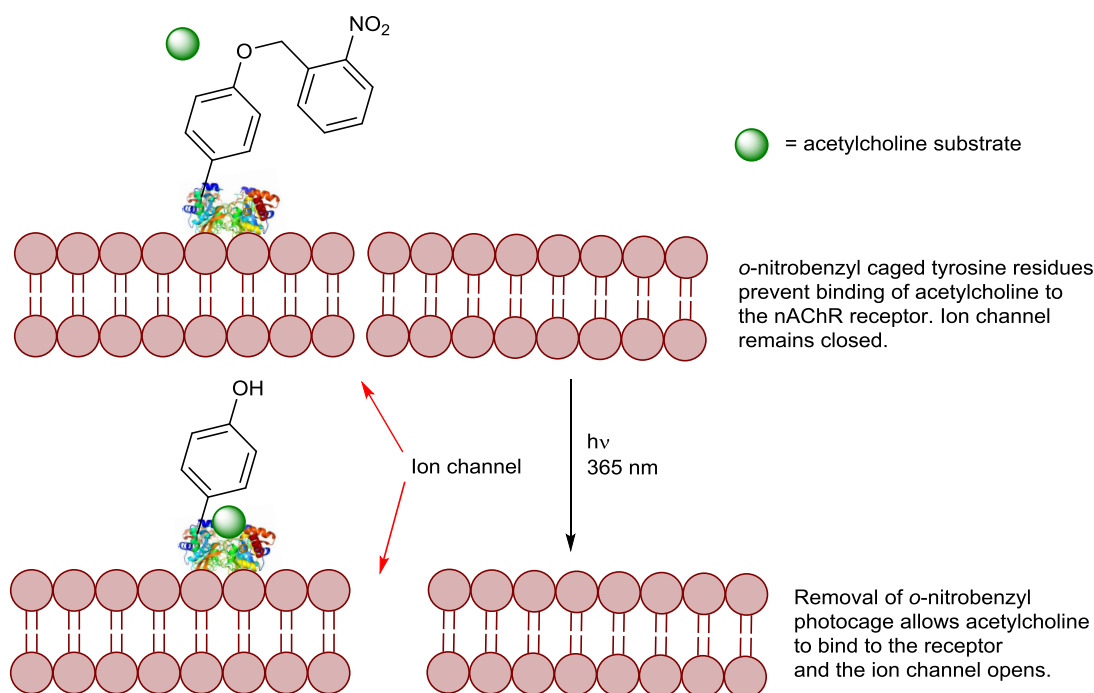


**Scheme 25**

**A schematic demonstrating the concept of photochemical protein uncaging.**

#### Photochemical Ion Channel Control

An excellent early example of photochemical protein uncaging was reported by Lester *et al.* on the “optochemical” control of a nicotinic acetylcholine receptor (nAChR) ion channel. By introducing an *o*-nitrobenzyl photocage to essential tyrosine residues at the extra-cellular N-terminus of the protein, the potential difference across the cell was eliminated. Irradiation at 365 nm resulted in cleavage of the photocages and reintroduction of the desired cross-membrane current (Scheme 26).<sup>224</sup>



**Scheme 26**  
Using an *o*-nitrobenzyl photocleavable protecting group to gain control over an ion channel.<sup>224</sup>

More recently a similar approach using a dimethoxynitrobenzyl caged cysteine residue to gain photochemical control of a potassium ion channel both *in vitro* and *in vivo* was reported.<sup>225</sup> Some excellent reviews have been written on this area.<sup>219,226,227</sup>

### Photochemical Enzyme Control

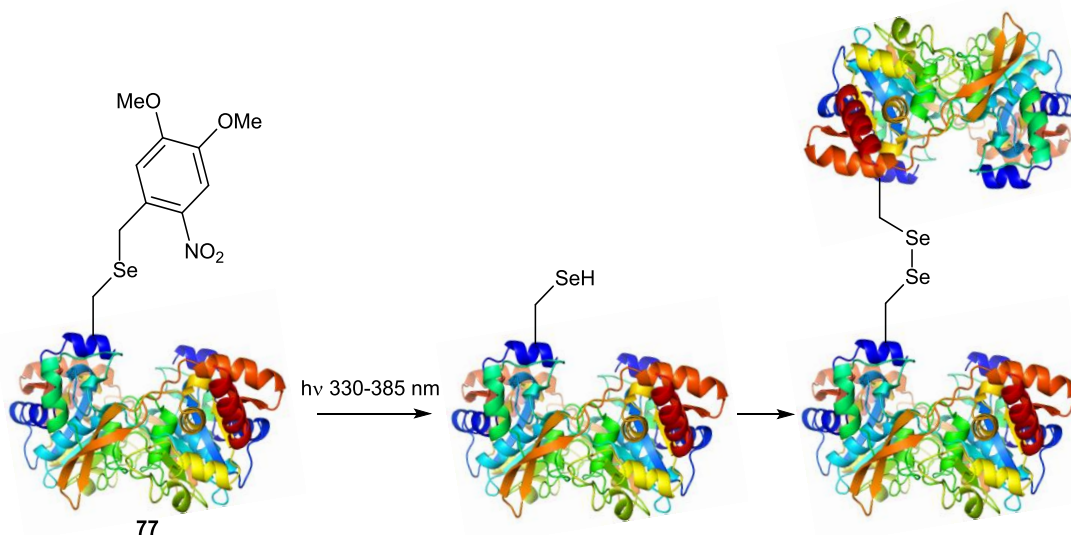
Gaining photochemical control over enzymatic reactions has greatly expanded our understanding of the processes in which they are implicated. An early example of using photocaging to activate an enzyme was provided by Schultz *et al.* The team engineered an *o*-nitrobenzyl protected cysteine residue into the human proapoptotic protein caspase 3, preventing conversion to the active enzyme and thus inhibiting catalytic activity. Irradiation at 365 nm to remove the photocage resulted in the generation of the active enzyme and a subsequent reformation of catalytic activity was observed.<sup>228</sup>

Though the photochemically uncaged enzyme did not achieve the same catalytic activity as the native enzyme, significant contrast between the caged and uncaged enzymes was observed. The same team employed a similar approach to gain photochemical control over the enzyme  $\beta$ -galactosidase both *in vitro* and *in vivo*.<sup>229</sup> More recently photocaging has been applied to photoregulate a variety of enzymes, including proteases,<sup>230</sup> luciferase<sup>231</sup> and DNA polymerase.<sup>232</sup>

### Light activated protein dimerisation

Selenocysteine is a highly reactive cysteine analogue which has been shown to impart unusual chemical reactivity to engineered proteins. Though the expanded chemical

reactivity is advantageous installing selenocysteine residues is non-trivial due to the amplified chemical reactivity of the group under aerobic and physiological conditions. A method for incorporating 4,5-dimethoxy-2-nitrobenzyl (DMNB) photocaged selenocysteine into a green fluorescent protein (GFP) mutant **77** to alleviate these installation problems was recently reported. Klimašauskas *et al.* exploited the photolabile nature of DMNB to gain photochemical control over protein dimerisation (Scheme 27).<sup>233</sup>



**Scheme 27**  
Using photocaged selenocysteine to gain control over protein dimerisation.<sup>233</sup>

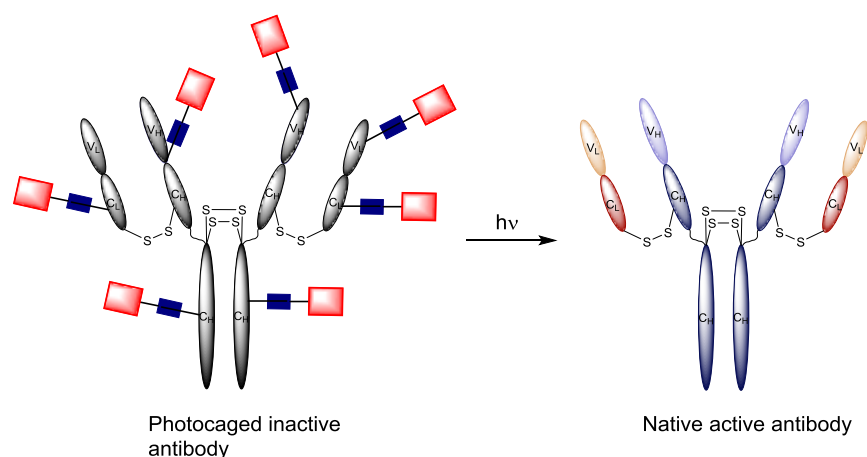
This work could be used to control the assembly of multi-domain proteins by combining the unique reactivity of selenocysteine and spatiotemporal control of phototriggers.

In addition to the applications highlighted above photochemical protein uncaging has also been utilised to modulate kinases,<sup>234</sup> recombinases<sup>235</sup> and nucleases,<sup>236</sup> and exploited to achieve spatiotemporal control over protein phosphorylation sites<sup>237</sup> and cellular protein translocation.<sup>238</sup> These applications demonstrate the power of combining photochemistry with chemical biology and highlight the importance of developing chemical reactions to further explore this area. It is worth noting in each of the cases above the unnatural amino acid phototrigger was introduced using sited directed mutagenesis. This is necessitated by a lack of reliable means for introducing photocages site selectively to the natural amino acid backbone.<sup>216</sup> Site directed mutagenesis complicates the preparation of these biomolecules and is a significant drawback. Methods to site selectively introduce a photocage to a natural amino acid without the need for mutagenesis would represent a significant contribution to the field.

### Protein photocages in antibody photoimmunotherapy

Protein photocages have been employed successfully in antibody based photoimmunotherapy (PIT). In this approach a therapeutic immunoglobulin is deactivated

through the covalent attachment of photolabile cages and subsequently activated by irradiation (Scheme 28).



**Scheme 28**  
A scheme depicting the premise behind photochemical uncaging in antibody photoimmunotherapy.

This process was described as early as 1996<sup>239</sup> though has been exploited with greater success more recently.<sup>240,241</sup> Work by Self *et al.* describes how attachment of *o*-nitrobenzyl photocleavable cages to anti-CD3 antibodies reduces the binding affinity of the antibody to the antigen. Subsequent irradiation with UV-A removes the photocages and restores the activity of the antibody.<sup>241</sup>

### 1.3.2: Photochemical release from proteins

An alternative use for the combination of photocages and protein conjugation is to utilise the protein as a vehicle to deliver a chemical payload to a particular target, and subsequently release the compound photochemically. This approach differs in the sense that in general the activity of the protein must be retained upon attachment of the “cage” to observe the desired effect. For this reason the site of attachment is often chosen to be distal from any functionally important regions on the protein. Considerably less research has been done in this area when compared to photochemical protein uncaging, though several excellent pieces of work (highlighted below) demonstrate the potential of this approach.

#### 1.3.2.1: Photocleavable antibody drug conjugates (pADCs)

One of the first examples of targeted drug delivery using a photolabile protein-drug conjugate was provided by Senter *et al.* The group conjugated the toxin PAP-S (pokeweed antiviral protein S) to a murine monoclonal antibody (J5) *via* an *o*-nitrobenzyl based photolabile linker (Figure 9).<sup>242</sup> Subsequent irradiation released the active drug in yields of up to 90%. Though the toxic effect of the antibody drug conjugate was significantly less than the native PAP-S this work provided the earliest known example of a photocleavable ADC.

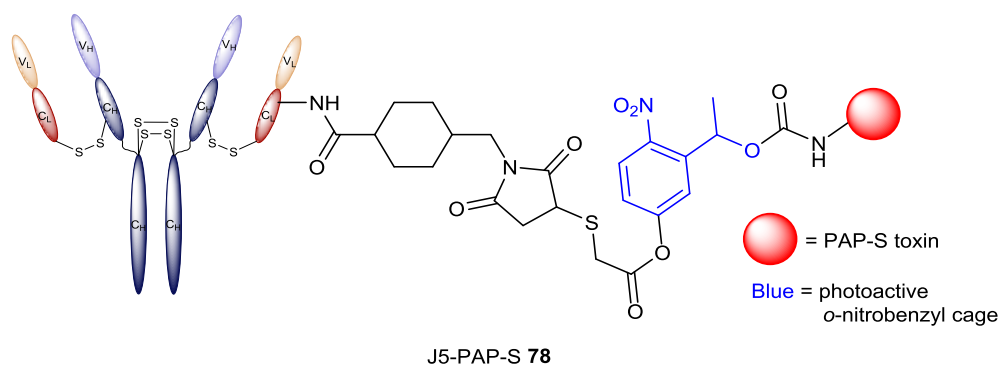


**Figure 9**  
**The earliest reported photocleavable ADC J5-PAP-S 78.**

The next example of a photocleavable ADC found within the literature was provided by Pegram *et al.* in 2003.<sup>243</sup> The group used Paclitaxel linked to the therapeutic antibody Herceptin *via* a proprietary photocleavable linker (Figure 10). Though the group did not release details of the linker the results suggest that non-photochemical release of the drug was occurring. Despite this a significant increase in toxicity was observed after irradiation when compared to the non-irradiated control.<sup>243</sup> Whilst the non-specific release of drug decreases the appeal of this work it does exemplify the premise and provide further validation for this technique.

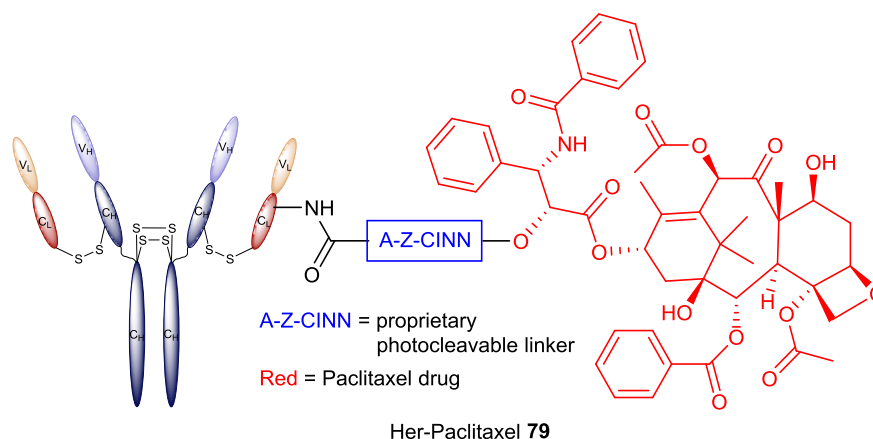


**Figure 10**  
**The photocleavable ADC Her-Paclitaxel 79.**

The most robust photocleavable ADC reported thus far was by Schnermann *et al.* who used a novel cyanine based photocage<sup>244</sup> to release a highly potent microtubule polymerisation inhibitor combretastatin A-4 (CA4) from the clinical monoclonal antibody panitumumab.<sup>245</sup> Photoexcitation of the cyanine cage results in photooxidative cleavage of the C-N bond between the cage and the linker. Subsequent intramolecular cyclisation of the amine onto the carbamate bond results in cleavage of the toxic CA4. The work describes both the *in vitro* and *in vivo* application of this photocleavable ADC which displays excellent contrast in toxicity before and after irradiation (Figure 11). However, the

approach does have several drawbacks, particularly the long winded synthesis of the linker and the time taken for the drug to reach maximum concentration after irradiation (18 hours). This work provides the first true *in vivo* demonstration of the power of photocleavable-ADCs and provides a benchmark for future work in the area.

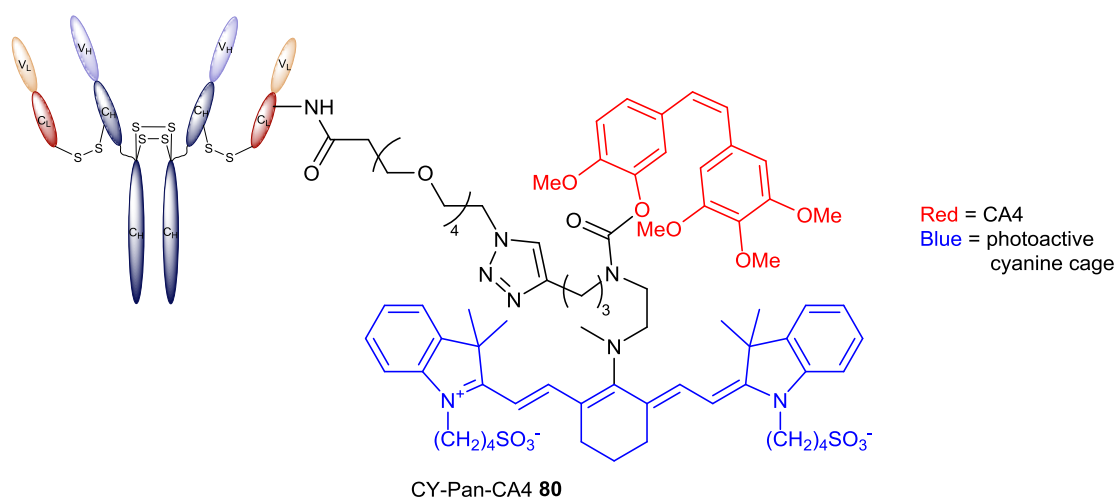


**Figure 11**  
The recently reported photocleavable ADC CY-Pan-CA4 **80**.

### 1.3.2.2: Antibody-directed photodynamic therapy

Photodynamic therapy (PDT) utilises photosensitising drugs typically made up of extended porphyrin ring systems. Upon absorption of light the drug is able to undergo an intersystem crossing with triplet oxygen to produce singlet oxygen which can cause significant damage to surrounding tissue (Figure 12).<sup>246,247</sup>

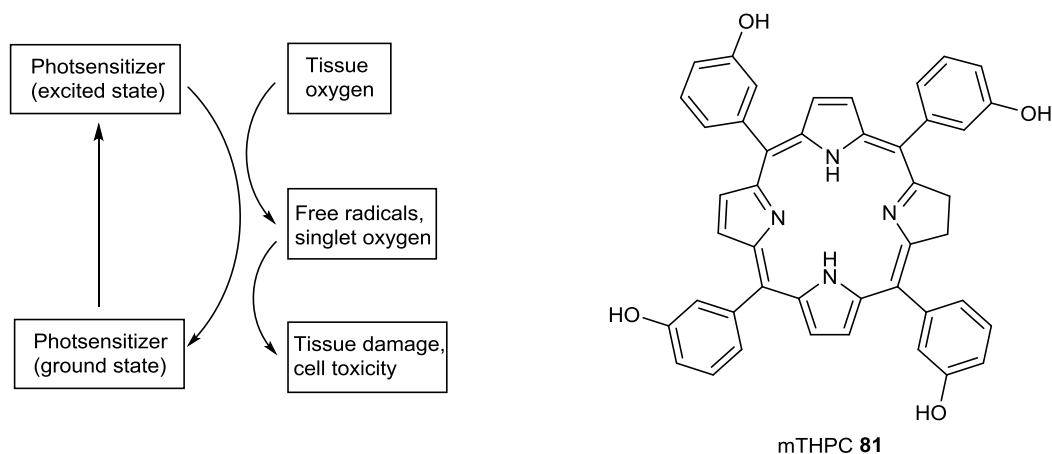


**Figure 12**  
A schematic representation of photodynamic therapy (PDT) and the porphyrin based PDT agent *meso*-tetra-hydroxyphenyl-chlorin (mTHPC) **81**.

In traditional PDT selectivity for the disease target is achieved through targeted irradiation of the disease location using lasers, though off-target side effects are still common. Antibody directed PDT is a subset of photoinduced immunotherapy (PIT) which adds an extra layer of defence against side effects by exploiting the targeted nature of immunoglobulins to deliver the photosensitiser specifically to the disease target. Though early attempts at this ideal system produced only minor therapeutic advantages, more recent work has produced antibody-photosensitiser conjugates which display selective toxicity *in vivo*.<sup>248</sup> A particularly promising example is provided by the work of Kobayashi *et al.* The group utilise a hydrophilic phthalocyanine photosensitiser (IR700) attached to the monoclonal antibody panitumumab (Figure 13). Irradiation with deep penetrating near-IR light results in selective destruction of the target tumour cells and a significant reduction in total tumour volume when compared to the non-irradiated control.<sup>249</sup>

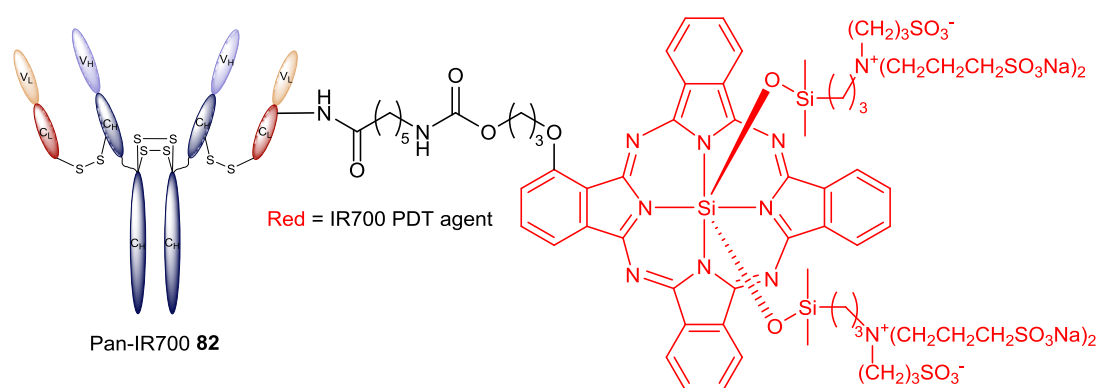


**Figure 13**  
The antibody directed photodynamic therapy agent Pan-IR700 82.

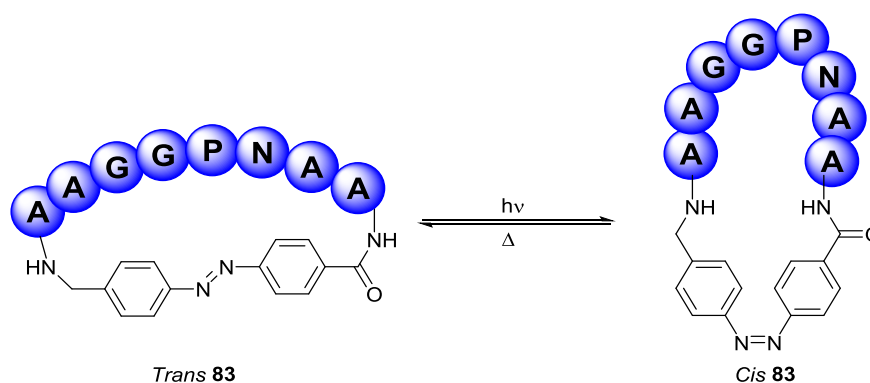
### 1.3.3: Photochemical manipulation of peptides

As with larger proteins, the photochemical manipulation of peptides has gained significant research interest over the last two decades. The smaller size of peptides makes them more sensitive to topological changes and thus easier to deactivate through installation of photoremoval protecting groups.<sup>250</sup> This makes them ideal candidates for photochemical manipulation.

#### 1.3.3.1: Photochemical switches

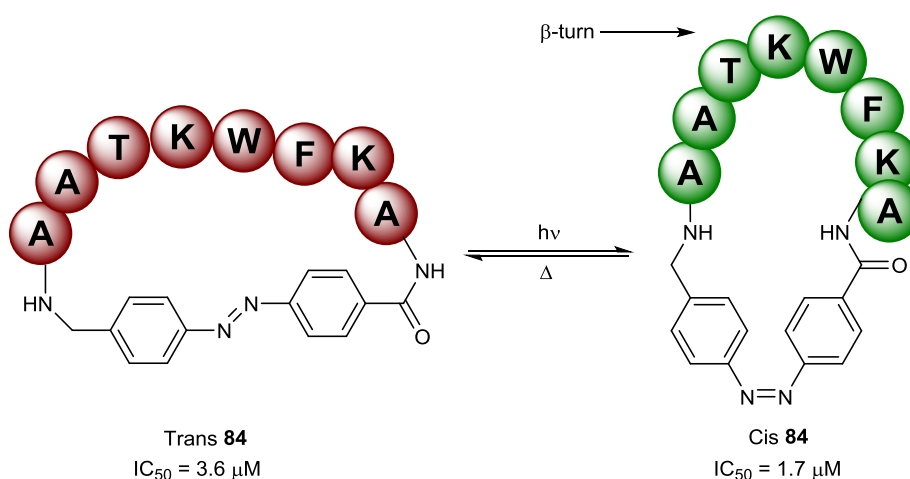
##### Azobenzene photoswitches

The majority of photochemical peptide manipulation has revolved around the use of photoswitches to gain reversible control over peptide conformation and function.<sup>250,251</sup> An early example of this approach was reported by Chmielewski *et al.* who incorporated an azobenzene photoisomerisable switch into the backbone of a short cyclic peptide (**83**). Irradiation of the peptide resulted in isomerisation of the azobenzene from *trans* to *cis* and consequently a change in the peptides conformation was observed (Scheme 29).<sup>252</sup>



**Scheme 29**  
**Photochemical control over peptide conformation using an azobenzene switch.**

In this first instance the group did not employ this technique towards any particular application, though they have since gone on to adapt this work for other peptides. A particularly relevant application of this work is the photomodulation of the conformation of a modified somatostatin analogue **84**. Knowing the importance of the  $\beta$ -turn centred around the Phe-Trp-Lys-Thr region the group installed an azobenzene switch on either side of the pharmacophore. Using elegant NMR experiments the group concluded that the trans form of the peptide contained no  $\beta$ -turn conformation. Irradiation to the cis isomer formed a type II'  $\beta$ -turn, demonstrating considerable contrast in peptide conformation between the two isomers. A consequent decrease in  $IC_{50}$  was also observed upon irradiation; 1.7  $\mu$ M for the cis form compared to 3.6  $\mu$ M for the trans form (Scheme 30).<sup>253</sup> Whilst this change is very minimal it highlights the potential of photochemical switches for the modulation of peptide conformation.

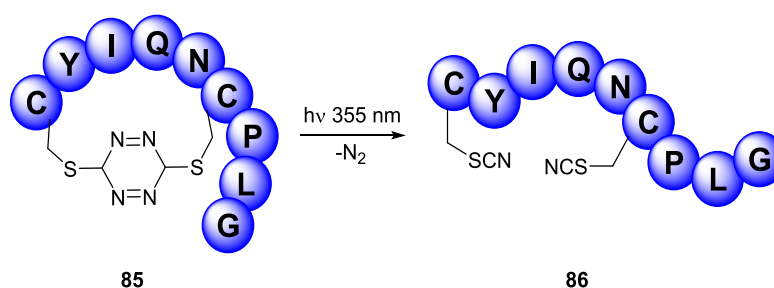


**Scheme 30**  
**The photoisomerisation of somatostatin analogue 84.**

Since this study photoswitches have been applied to peptides for a variety of applications, including photomodulation of redox active peptides,<sup>254,255</sup> membrane-binding peptides,<sup>256</sup> and peptides involved in muscle contraction.<sup>257</sup> An excellent review on this subject has been written by Feringa *et al.*<sup>250</sup>

### S,S-Tetrazine phototriggers

Another photochemical reaction which has been explored for the photochemical manipulation of peptides is the photolytic degradation of S,S-Tetrazine analogues. In this approach the peptide is bound into a cyclic conformation through the introduction of a cysteine selective tetrazine moiety (**85**). Irradiation at 355 nm results in rapid photolysis of the N-N bonds of the S,S-Tetrazine and formation of an acyclic peptide (**86**). This reforms the non-cyclic native structure of the peptide and in this way could theoretically be used to photochemically control function (Scheme 31).<sup>258,259</sup>

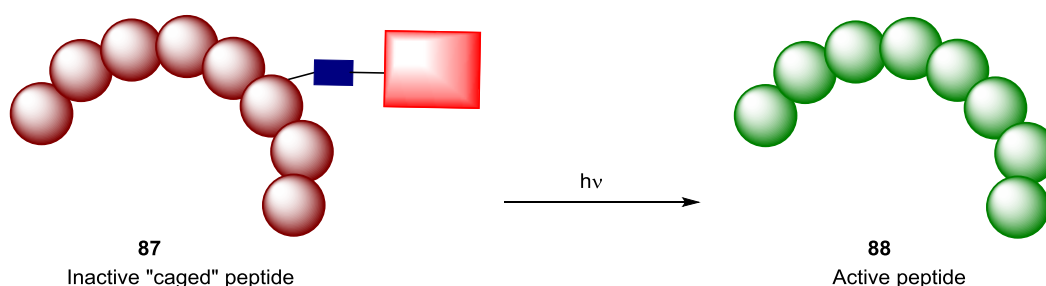


**Scheme 31**  
Irradiation of a S,S-Tetrazine bridged peptide **85** to form open chain peptide **86**.<sup>258</sup>

This reaction displays unprecedented kinetics, with photolysis times in the picosecond range.<sup>259</sup> To the best of our knowledge this technique has not yet been employed towards any therapeutic purpose though speculative applications for studying protein folding/unfolding dynamics have been put forward.<sup>258,260</sup>

### 1.3.3.2: Phototriggers

Photolabile protecting groups have been employed to cage peptides in much the same way as caging proteins. A photocleavable chemical moiety is attached to the peptide at a structurally important position to block the function (**87**). Upon photolysis of the cage the activity of the peptide (**88**) is reinstated (Scheme 32).



**Scheme 32**  
A schematic representation of photochemical peptide uncaging.

Though caged peptides have not been as widely adopted as caged proteins several excellent studies have been reported. This technique has been employed to gain control over cell-binding peptides,<sup>261,262</sup> peptidic vasoconstrictors,<sup>263,264</sup> and a peptide involved in neurotransmission.<sup>265</sup> A small review on this subject has been written by David Lawrence.<sup>213</sup>

## **1.4: Research overview**

The research discussed in this chapter clearly highlights photochemical transformations as powerful tools for studying and manipulating biological systems. This thesis explores the use of novel thiomaleimide based photochemical transformations as tools for photochemical protein and peptide modification. Through this work we hoped to make a contribution to the ever expanding toolbox of chemical reactions which can be employed for the manipulation of biological processes.

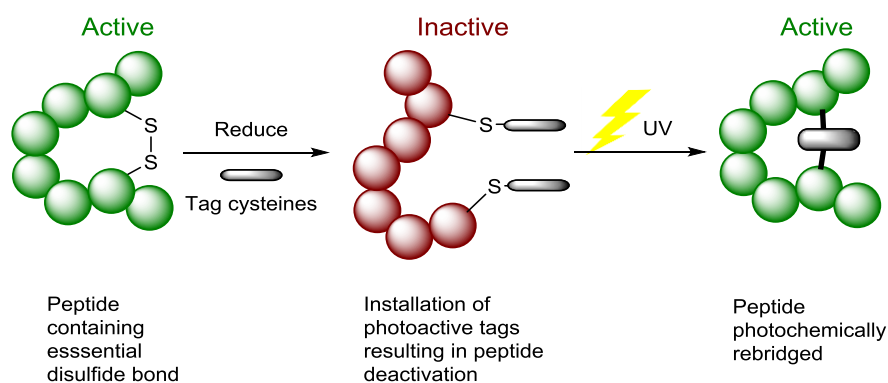
Chapters 2.1 and 2.2 explore the use of a recently reported thiomaleimide [2+2] photocycloaddition as a novel “photoswitch”. The application of this reaction towards peptide photoactivation and photochemical disulfide rebridging is described. Chapters 2.3 and 2.4 describe the discovery of novel photochemical decarboxylation reactions and their application towards novel cysteine selective photocleavable linkers. Each individual section is accompanied by research aims, conclusions and future directions.

## 2: Results and Discussion

### 2.1: Photochemical peptide activation

#### 2.1.1: Aims and introduction

The first aim of this work was to expand on the recently discovered thiomaleimide photochemistry to develop a method for photochemically activating peptides. We originally envisioned a system in which a small therapeutic peptide could be deactivated through the installation of cysteine selective photoactive tags, and subsequently reactivated through reformation of the cysteine bridge *via* irradiation at a specific wavelength (Scheme 33). This method could exploit the unique spatial and temporal control offered by photochemistry to develop a new type of targeted chemical tool.



**Scheme 33**  
**Photochemical peptide activation *via* the installation of cysteine selective photoactive tags.**

Though conceptually simple this approach does require a specific set of conditions to reach full potential. The peptide must contain a disulfide bond which is easily modified and functionally important. This will allow for simple installation of the photoactive tags and also ensure installation is accompanied by a decrease, or preferably complete nullification, of activity. A greater conformational change between “open” and “bridged” forms of the peptide would lend more power to this technique. Additionally, the photoactive tag must be able to target cysteine residues efficiently, selectively, and without causing unnecessary steric perturbation. This last point is particularly important, as upon irradiation the peptide must be able to reform its active conformation. Finally, the photochemical reaction itself must be rapid, highly efficient, and selective for the photoactive tags *i.e.* unreactive with naturally occurring amino acids. With these criteria in mind we set towards finding a suitable peptide and photoactive tag to explore this method.

#### **Octreotide**

Octreotide **74** (Figure 14) is a synthetic octapeptide based on the natural hormone Somatostatin used for the treatment of neuroendocrine tumours.<sup>266</sup> The therapeutic use of Octreotide was previously covered (Section 1.2.5.1, page 36) and an excellent review on

the use of Somatostatin analogues, including Octreotide **74**, in neuroendocrine tumour therapy has been written by Modlin *et al.*,<sup>202</sup> so this subject will not be covered further here. Octreotide **74** contains a single essential disulfide bond, which has been shown as essential to the activity of Somatostatin analogues,<sup>157</sup> and previous work has demonstrated the ease in which the cysteine residues can be modified.<sup>152</sup>

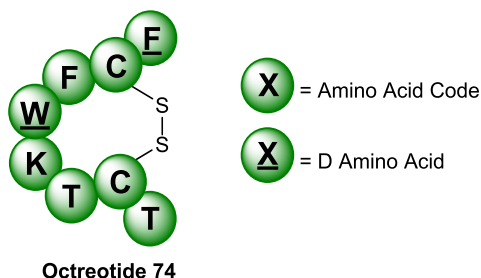
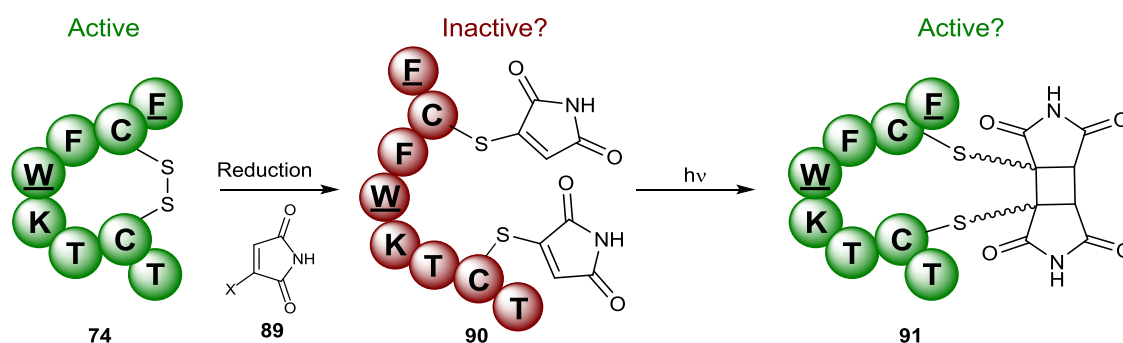


**Figure 14**  
A schematic representation of Octreotide **74**.

### Maleimides as Photoactive Tags

As previously described (Section 1.2.3.1, page 31), monobromomaleimides (**89**) react in a highly efficient and selective manner with cysteine residues to produce cysteine-maleimide conjugates. More recent work has highlighted the ability of cysteine-maleimides to undergo highly efficient [2+2] photodimerisations (Section 1.1.2.1, page 21).<sup>63</sup> This dimerisation proceeds quantitatively within five minutes of irradiation and is able to out-compete [2+2] cycloadditions between the maleimide and other olefins. Thus in substituted maleimides we have discovered a reagent which fulfils the criteria listed previously. We hypothesised that Octreotide **74** could be successfully deactivated through the installation of two maleimide moieties to generate *bis*-modified Octreotide **90**, and then subsequently reactivated *via* the highly efficient [2+2] dimerisation to generate bridged Octreotide **91** (Scheme 34).

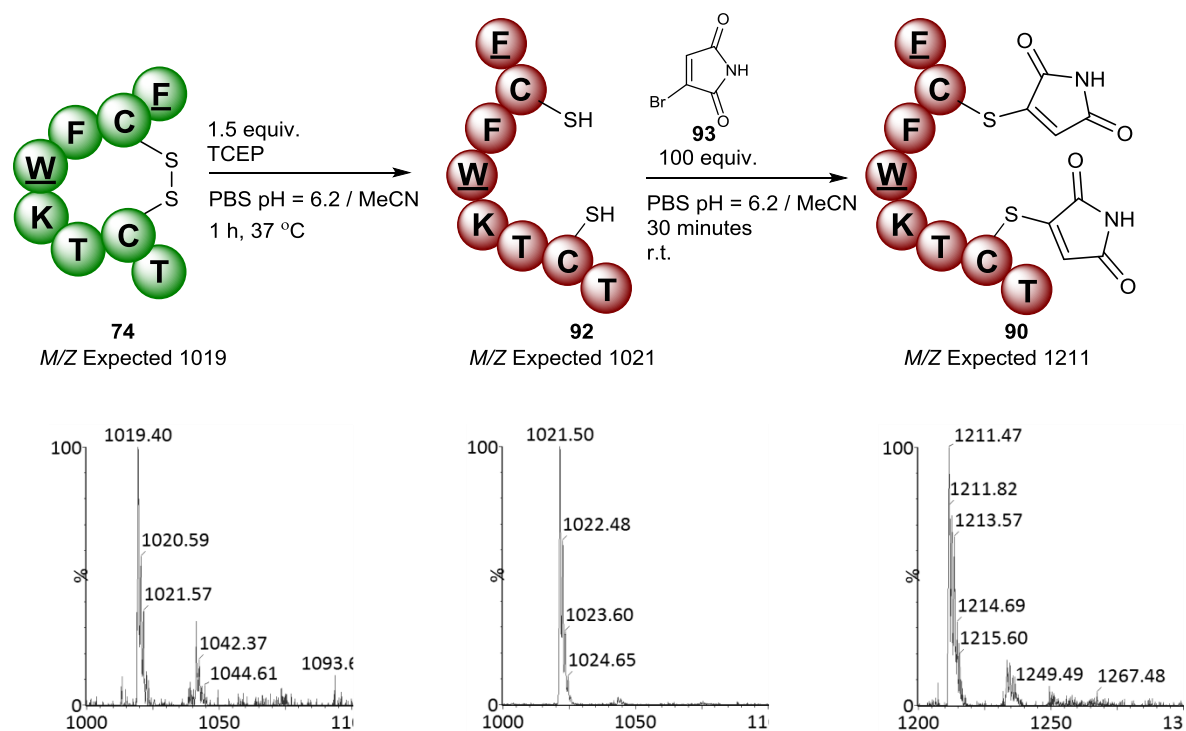


**Scheme 34**  
A proposed strategy to photochemical rebridge cysteine residues using thiomaleimide photochemistry.

### 2.1.2: Modification and irradiation of Octreotide

Octreotide was reduced and modified according to a previously optimised protocol (Scheme 35). Tris(2-carboxyethyl)phosphine (TCEP) was chosen as a reducing agent due to its limited cross reactivity with substituted maleimides. It is more common to use thiol

containing reducing agents, such as dithiothreitol (DTT),  $\beta$ -mercaptoethanol (BME) and glutathione (GSH). However, these readily react with substituted maleimides so must be removed before the modification step of any protocol, a time consuming process with small peptides. *Bis*-modification of the peptide with monobromomaleimide **93**, which was synthesised using a known protocol,<sup>267</sup> proceeded smoothly. A large excess of monobromomaleimide **93** was used to prevent unwanted succinimide formation that results from attack of both cysteine residues onto a single maleimide.<sup>267</sup> Success at each step was evidenced using LCMS (Figure 15).



#### Scheme 35

The reduction and modification of Octreotide **74**.

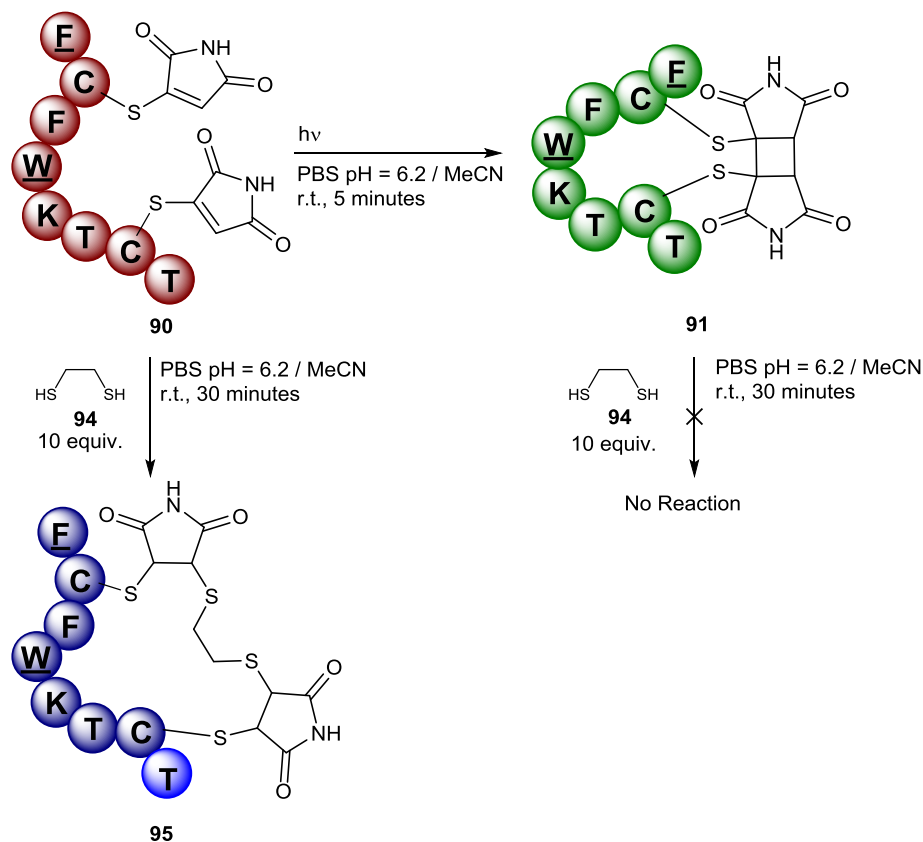
Figure 15

LCMS spectra of Octreotide **74**, reduced Octreotide **92** and modified Octreotide **90**.

See experimental section for full spectra (Section 3.2.2.1, page 178, Figure 62 & Figure 64).

Irradiation of *bis*-modified conjugate **90** was carried out to attempt [2+2] cyclisation of the peptide (Scheme 36). However, as no mass change accompanies this reaction confirmation by LCMS was not possible. To compensate for this a chemical test was devised which exploited the maleimide conjugate acceptors. Before irradiation the double bond of the maleimide is susceptible to thiol attack,<sup>146,151</sup> so conjugate **90** yields a positive reaction with ethanedithiol **94** (EDT). Interestingly only mono-addition of EDT **94** was observed, suggesting that a single molecule of EDT bridges the two thiomaleimides to form Octreotide conjugate **95**. This was unexpected as an excess of EDT was employed thus some di-addition, i.e. addition of EDT to both thiomaleimides, was anticipated. Upon irradiation to form bridged conjugate **91** the conjugate acceptors are removed and EDT **94**

can no longer react *via* addition-elimination. After five minutes of irradiation no reaction with EDT **94** was observed by LCMS, providing evidence for successful [2+2] cycloaddition and rebridging of the peptide to form bridged Octreotide conjugate **91**.

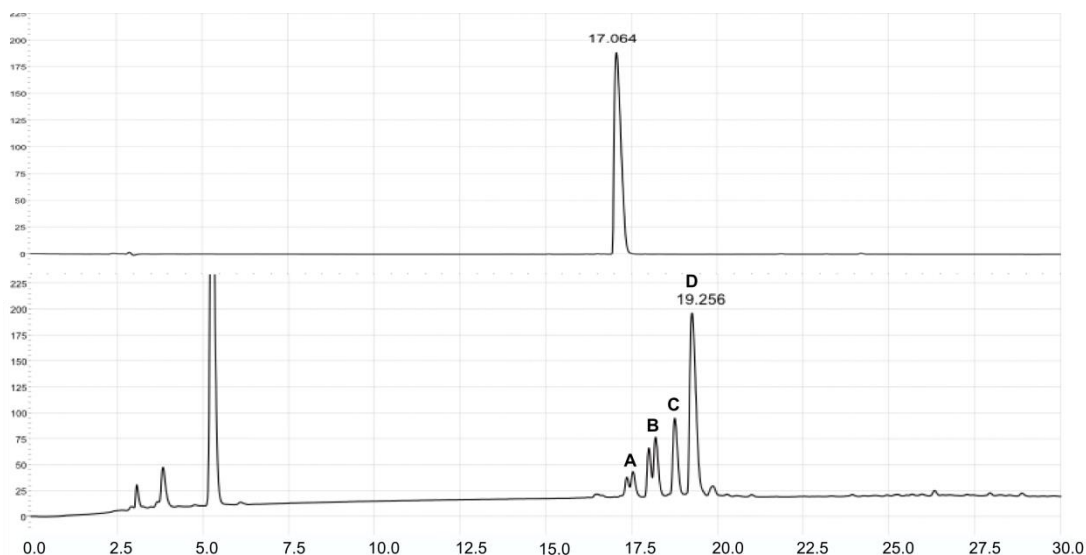
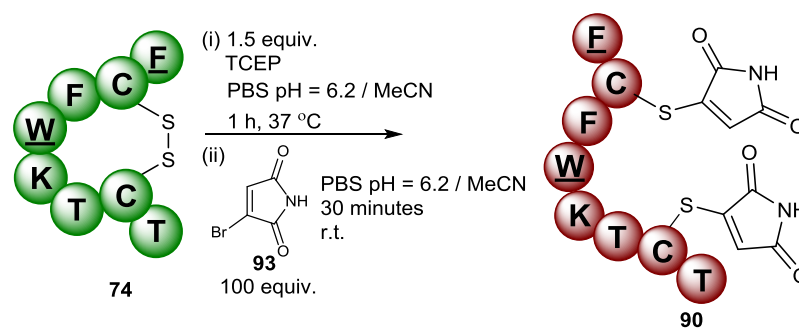


**Scheme 36**

**A chemical test to demonstrate the success of the photochemical [2+2] cycloaddition. See experimental section for mass spectra (Section 3.2.2.2, page 181, Figure 65 & Figure 66).**

### 2.1.2.1: HPLC data

Though the chemical test with EDT **94** (Scheme 36) provided evidence for the success of the photochemical [2+2] dimerisation, further data was sought for corroboration. We also wished to obtain as much structural information as possible, since any conformational changes occurring upon irradiation would undoubtedly affect binding affinity and potency of the peptide. High performance liquid chromatography (HPLC) is well established as a tool for studying peptide modification and can also reveal important changes in polarity. Each step of the newly optimised reaction sequence was repeated and studied using analytical HPLC. Analysis of the *bis*-modification step is shown below (Scheme 37) (Figure 16).



### Scheme 37

The modification of Octreotide 74 using an optimised protocol.

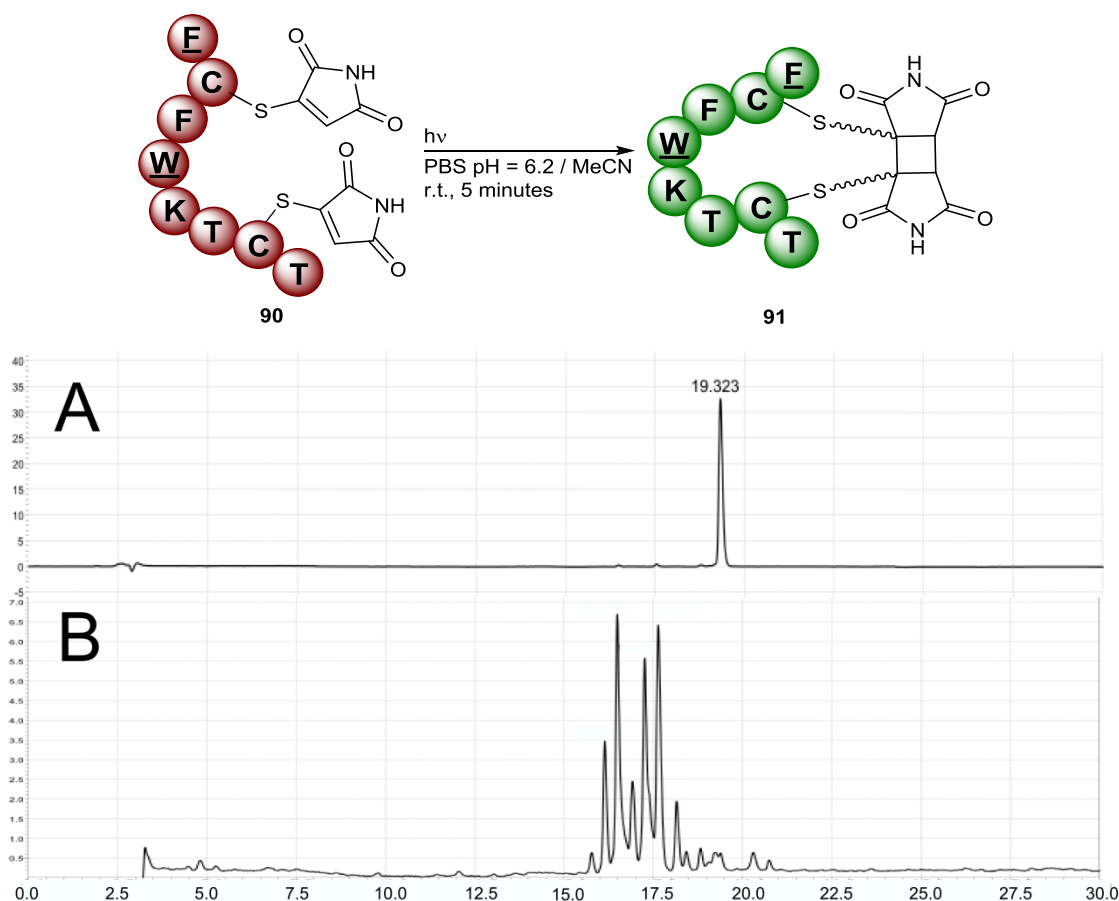
### Figure 16

HPLC of Octreotide 74 and the crude mixture of conjugate 90. For HPLC conditions see experimental (section 3.2.1.1, p 175)

Analysis of the crude solution of *bis*-modified conjugate 90 revealed that the conjugation step results in a major product and several minor products. Analysis of the individual peaks by MALDI-TOF revealed them to have identical masses of 1211 Da, corroborating the previously obtained LCMS data. This suggests that the peaks correspond to different isomers of the desired peptide. This was unexpected and, due to limited data, identification of the peaks was not possible. It seems unlikely that the peaks correspond to conformational isomers of the desired product as any non-covalent interactions would be removed under the acidic HPLC conditions. Another possibility is that isomers are forming upon intramolecular reaction of the Octreotide lysine with the generated thiomaleimides. However, the fact that the lysine residue appears to be inert towards the large excess of the more reactive monobromomaleimide **93** discourages this hypothesis. Evidence against both of these theories was obtained upon isolation and incubation of the major product (peak D) under the reaction conditions, which upon reanalysis by HPLC showed no change. If the minor products result from isomerisation of the major product it is reasonable to assume incubation and reanalysis by HPLC would reveal multiple peaks. Further exploration of these results was not deemed pertinent to the overall aim. Isolation and

irradiation of the most prominent by-product (peak C) resulted in no change to the HPLC trace upon analysis, indicating the unidentified species was not photoactive.

The major product was isolated and subsequently irradiated under the optimised irradiation conditions (Scheme 38). HPLC of the resulting crude solution revealed a complex mixture of products with at least four dominant species (Figure 17). Analysis of each of the major peaks, as well as a collection of the eluent between 15.0 and 20.0 minutes, by MALDI-TOF revealed the desired mass of 1211 Da (see experimental section 3.2.2.1, page 179, Figure 63). This suggests that the mixture consists of several isomeric species.

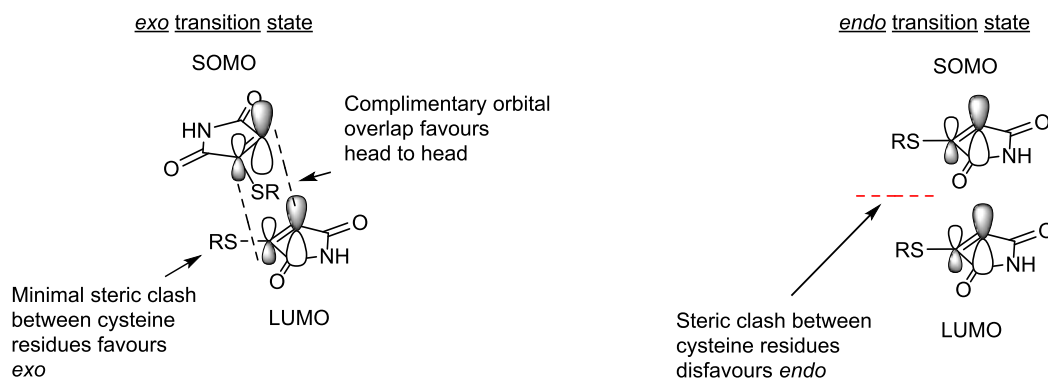


**Scheme 38**  
The optimised irradiation of *bis*-modified Octreotide 90.

**Figure 17**  
HPLC data of the mixture resulting from the irradiation of Octreotide conjugate 90. (A) Pure Octreotide conjugate 90; (B) Pure Octreotide conjugate 90 irradiated for five minutes.

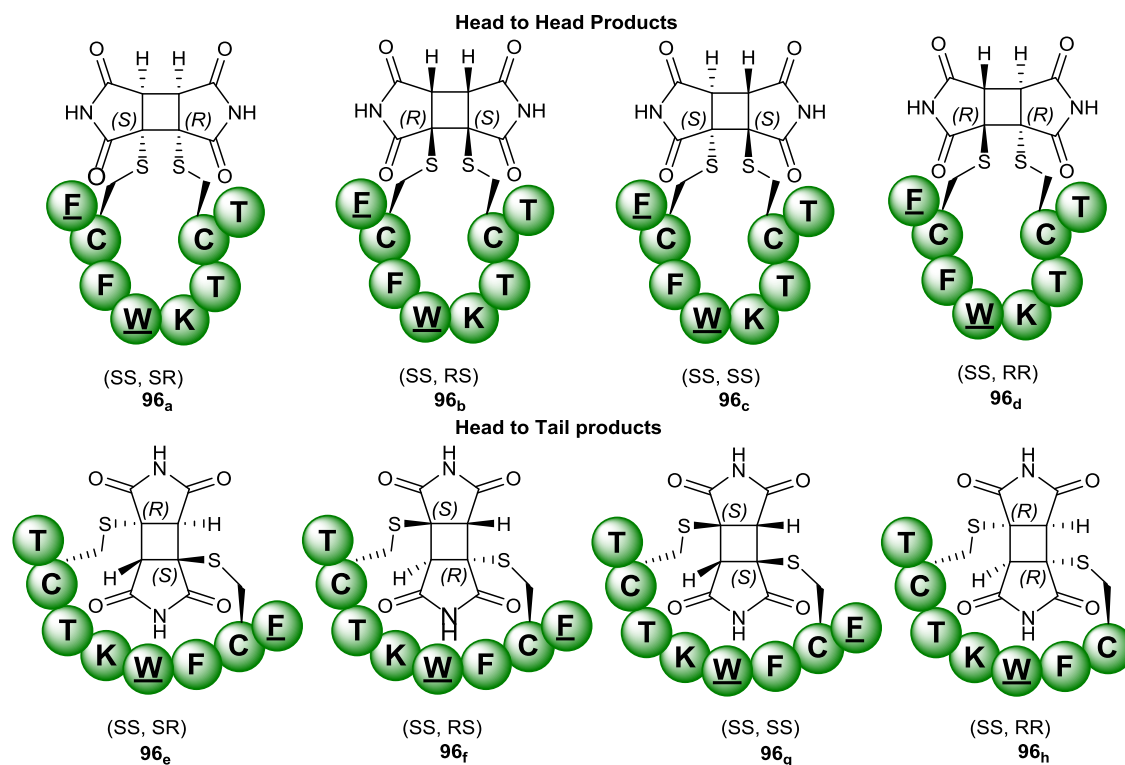
In this instance this was somewhat expected, as [2+2] cycloadditions are known to produce several isomers; *endo* head-to-head, *endo* head-to-tail, *exo* head-to-head and *exo* head-to-tail. This is further complicated by the diastereoisomers of these forms caused by the chirality of the amino acid backbone. However, the generation of such a complex mixture was not anticipated due to the stereoselective nature of the previously studied cysteine-maleimide photochemical [2+2] dimerisation which produced only the *exo* head-to-head products (section 1.1.2.2, page 20).<sup>63</sup> This selectivity was reasoned using both

Frontier Molecular Orbital theory and steric arguments. For a favourable orbital interaction the thiomaleimide moieties must approach each other in a suprafacial manner. In addition to this, a head-to-head configuration is favoured due to the complimentary overlap between SOMO and LUMO, as is often the case with [2+2] cycloadditions, and an *exo* transition state minimises steric clash between cysteine residues (Scheme 39).



**Scheme 39**  
**Electronic and steric arguments for the stereoselectivity of the thiomaleimide [2+2] cyclisation.**

This level of stereoselectivity is clearly not occurring with the photochemical [2+2] cycloaddition of *bis*-modified Octreotide conjugate **90**. The HPLC data reveals at least four major products and several minor products, highlighting a decrease in the stereoselectivity of this reaction when applied to Octreotide. This decrease can be rationalised by taking into account the inherent structure of the peptide. Though only eight amino acids in length Octreotide **90** still holds tertiary structure that could affect the orientation of the two thiomaleimides during the cyclisation. The propensity of the peptide to obtain a particular conformation, perhaps to maximise its intramolecular forces or avoid steric clashes elsewhere, could be competing with the orbital or steric considerations of the photochemical [2+2] cycloaddition. The possible outcomes from the photochemical [2+2] dimerisation are shown below (Scheme 40).



In order to rationalise the probability of each of the isomers it is necessary to have some idea of the three-dimensional structure of Octreotide conjugate **90**. Knowledge of the relative position of the two maleimides in the transition state could provide important information regarding the structure of the product. Unfortunately, this requires detailed knowledge of the exciplex, particularly the intermolecular distance between the bonding carbons, which we do not possess. Thus any attempt to draw structural information from the current evidence would be mostly conjecture and any conclusions inherently flawed. A lack of preparative scale HPLC inhibited large scale isolation of the products and it was decided that isolation and identification of each individual peak was not a priority.

### 2.1.2.2: Tandem-MS data

Though the HPLC data provided valuable information regarding the stereoselectivity of the reaction it did not conclusively confirm the reformation of the bridge between the two cysteine residues. It was envisaged that this information could be obtained by studying the fragmentation patterns of *bis*-modified Octreotide conjugate **90** before and after irradiation using tandem mass spectrometry. A bridge between the cysteine residues should inhibit fragmentation, giving rise to several unique peaks when compared to the acyclic form. The results of the fragment analysis of both conjugates **90** and **91** are shown below (Figure 18) (Figure 19).

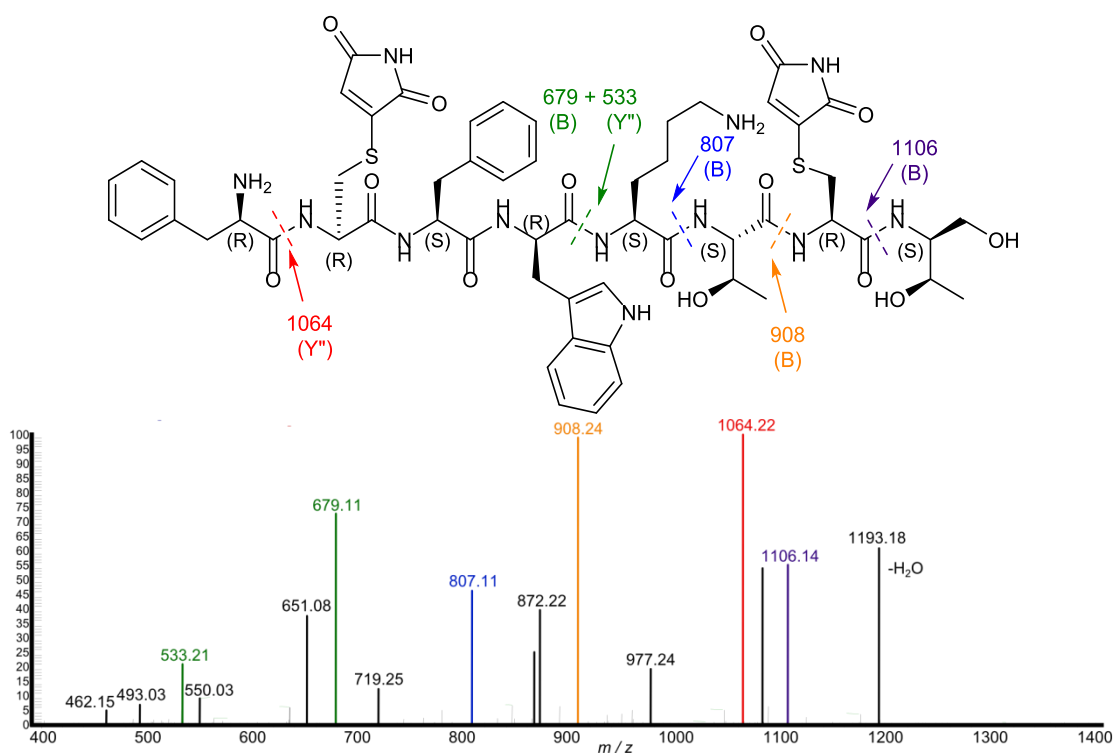


**Figure 18**  
A fragment assigned tandem mass spectrum of conjugate 90.

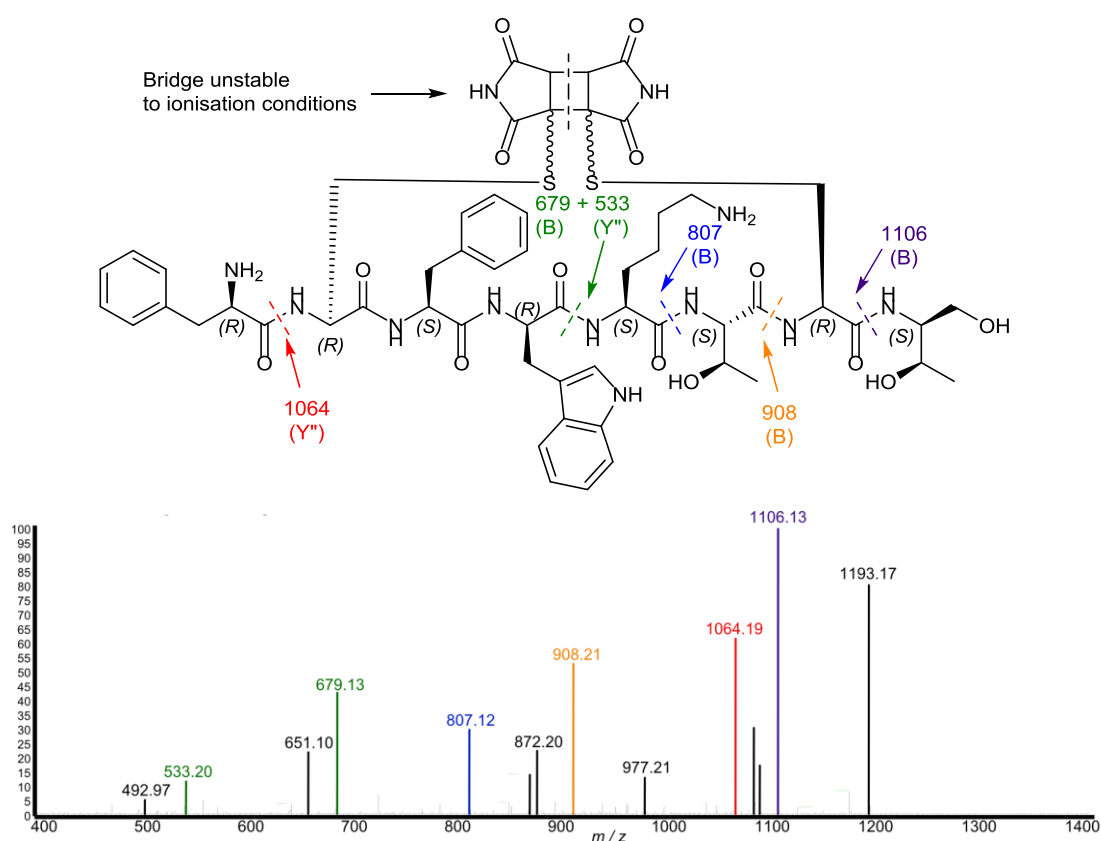


**Figure 19**  
A fragment assigned mass spectrum of conjugate 91.

Unfortunately, the results proved inconclusive. Analysis of the B and Y'' fragments ( $\text{CO}^+$  and  $\text{NH}_3^+$ , respectively) of conjugate 90 before irradiation confirmed the lack of bridge

between cysteine residues. Fragments of 679.11 and 533.21 Da evidenced cleavage between the tryptophan and lysine residues, whilst a fragment of 807.12 Da was indicative of cleavage between lysine and threonine. If the cysteine residues were bridged cleavage at these positions would not cause fragmentation. However, analysis of the bioconjugate after irradiation showed that fragmentation at these positions was still occurring. Fragments at 908, 807, 679 and 533 Da suggest extended fragmentation which would not be possible in the presence of a stable bridge between cysteine residues. Ideally only the 1106 and 1064 Da fragments would be observed after formation of the cyclobutane bridge. Though these peaks have increased relative to the other fragment ions, the results are not conclusive enough to confirm the success of the reaction. These results initially suggest that the photochemical [2+2] dimerisation did not proceed as expected, though it is possible the cyclobutane bridge is simply unstable under the conditions of the electrospray ionisation. Cleavage of the c-c bonds in the ring would destroy the bridge between the cysteine residues and nullify the results. There is a literature precedent for the cleavage of cyclobutane rings under ionising conditions with c-c cleavage on opposing sides of the ring a common occurrence.<sup>268</sup> Cleavage at this position would not be entirely unexpected given the significant ring strain of cyclobutane systems, a problem potentially exacerbated by the neighbouring succinimide ring systems and sulfur atoms. If ring cleavage is occurring this represents a significant drawback in using MS-MS for studying these constructs.

### **2.1.2.3: NMR data**

To try and provide conclusive evidence for the formation of bridged Octreotide **91** it was decided to analyse Octreotide conjugates **90** and **91** using NMR. Unfortunately attempts to purify the mixtures obtained from modification and irradiation by preparative scale HPLC were unsuccessful due to the difficult separation caused by the isomeric nature of the products. However, additional information was found by analysing the crude NMR of Octreotide conjugate **90** before and after irradiation (Figure 20). Though the NMR of conjugate **90** was crude the addition of the maleimides was clear, evidenced by the appearance of two alkene singlets. The disappearance of these peaks upon irradiation and the formation of characteristic cyclobutane singlets between 3.40 and 3.55 ppm<sup>63</sup> indicate successful [2+2] cycloaddition. Two unknown non-peptidic impurities were also observed (2.20 + 2.51 ppm and 3.65 +3.75 ppm) but could not be removed from the peptide product. The spectrum after irradiation was further complicated by the number of stereoisomers produced during the reaction, a feature which will be discussed in detail later in this section.

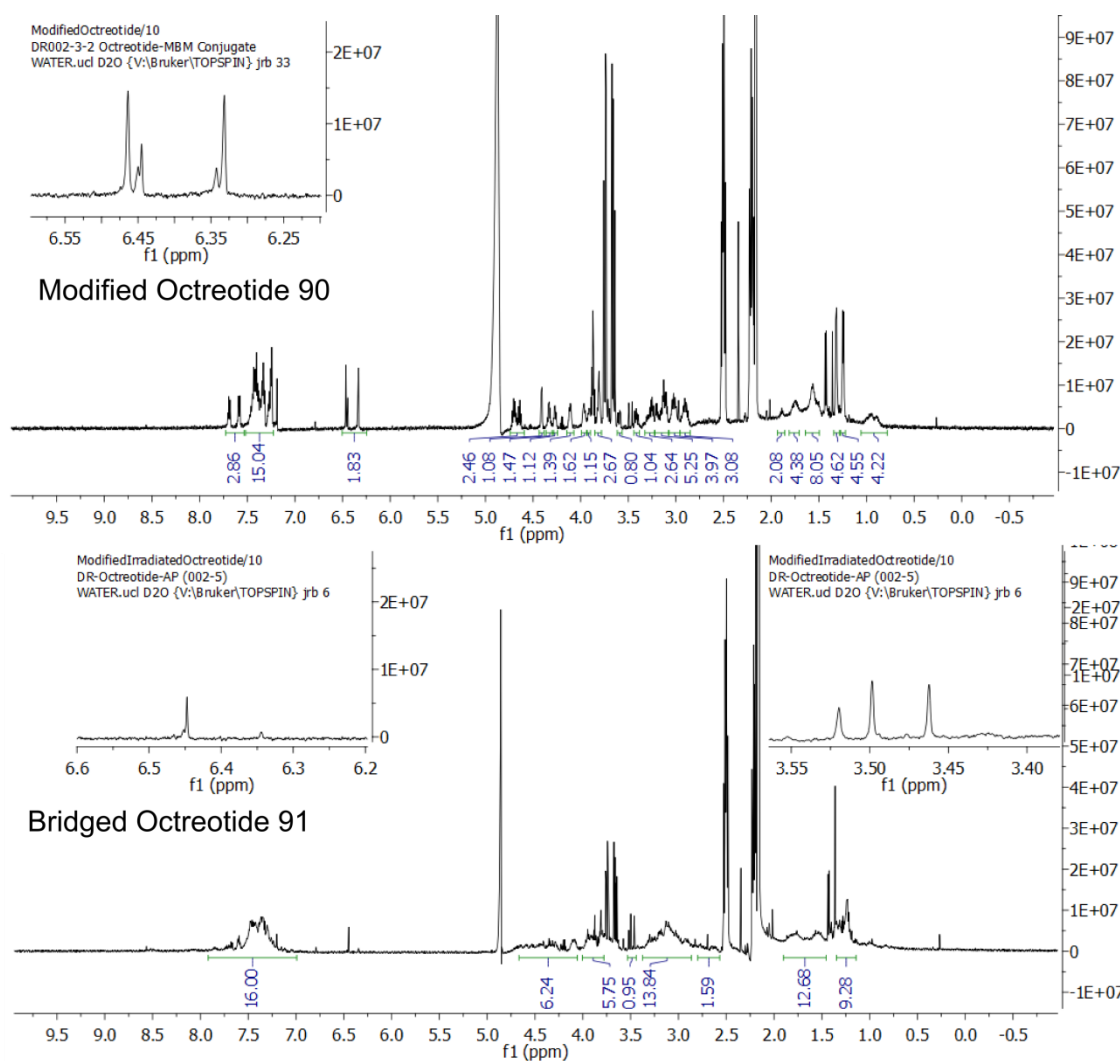


**Figure 20**  
**NMR data showing the appearance of characteristic maleimide alkene singlets upon modification of Octreotide 74, and the disappearance of these peaks upon irradiation of modified Octreotide 90. The appearance of cyclobutane singlets is also observed.**

Though these spectra are crude they do provide additional evidence for the formation of a cyclobutane ring, and when coupled with the HPLC data, previously published small molecule study,<sup>63</sup> and chemical test with EDT, suggest the thiomaleimide [2+2] photocycloaddition was successful.

## 2.1.3: Determining the binding affinity of Octreotide conjugates

### 2.1.3.1: Dose-Response curve

\*The cell work and patch clamping described in this section was completed by Dr Sally Fletcher and Dr Muriel Nobles, with my intellectual input and guidance. All peptide conjugation and irradiation was completed by me.\*

As the balance of evidence suggested the photochemical [2+2] cycloaddition was successful, it was decided to proceed to test the hypothesis that the dimerisation could be used to activate a small therapeutic peptide. This required a reliable method for measuring

the binding affinity of conjugates **90** and **91** to the SST2 receptor. Previous work with collaborators at Queen Mary University of London had already utilised whole cell patch clamping for this purpose.<sup>152</sup> Whole cell patch clamping is a technique used to measure the voltage across a cell membrane, working on the premise that ligand binding opens up an ion channel, consequently increasing the potential across the membrane. The greater the affinity and potency of the ligand the larger the current across the cell membrane. Detailed descriptions of the patch clamping method are abundant in the literature so this technique will not be discussed here.<sup>269</sup>

In order to study the binding of Octreotide **74**, and analogues **90** and **91**, to the SST2 receptor it was necessary to acquire a suitable cell line with an appropriate ion channel. Analogues of Somatostatin, such as Octreotide **74**, have been reported to activate G protein-coupled inwardly-rectifying potassium (GIRK) channels causing hyperpolarisation of cell membranes.<sup>270</sup> Consequently cells which express GIRK channels can be transfected with the SST2 receptor and utilised for patch clamping. The SST2 receptor is coupled to the GIRK channel by G-protein, therefore activation of the SST2 receptor leads to activation of the GIRK channel and an influx of potassium ions.<sup>270</sup> Fortunately a HEK293 cell line transfected with SST2 and stably expressing the GIRK1/2a channel had already been engineered by our collaborators for a related project. Octreotide **74**, *bis*-modified conjugate **90** and *bis*-modified Octreotide **91** irradiated for five minutes to produce bridged conjugate **91** were prepared in a series of dilutions ( $10^{-12}$  -  $10^{-6}$  M) and tested for current activation against SST2. Because potential applications would rely on *in situ* generation of the bridged conjugate, Conjugate **91** was not purified further before being applied to the cells (Figure 21).

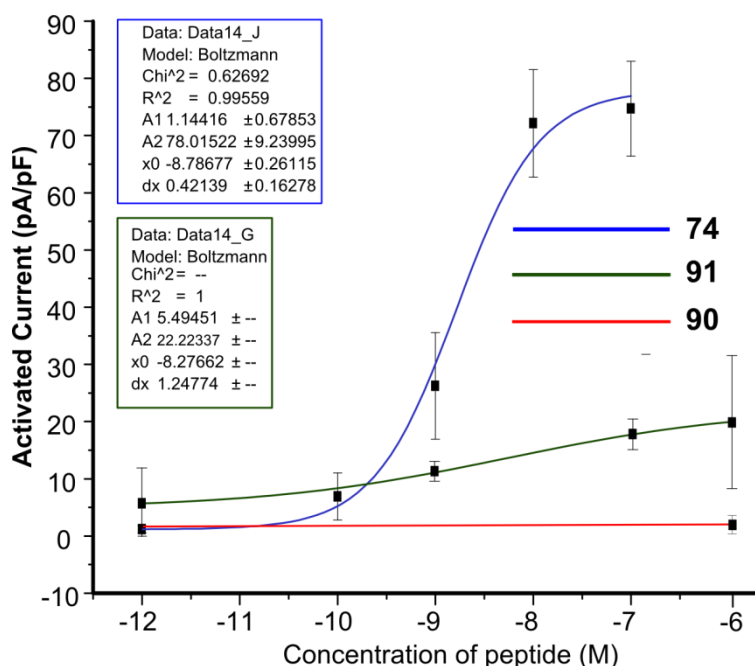


**Figure 21**  
**Dose response curves for Octreotide 74, and conjugates 90 and 91. Curve parameters for native Octreotide 74 are in the blue box, and for modified Octreotide 90 in the green box. Due to the large error bars R<sup>2</sup> and Chi<sup>2</sup> tests for bridged Octreotide 91 could not be determined. Five readings were taken at each concentration.**

Native Octreotide **74** behaved as expected and produced a sigmoidal dose response curve with a high R<sup>2</sup> value, demonstrating a good data fit. It is apparent that at high concentrations the current activation reaches a plateau as maximum current activation is reached. From this curve we obtain an EC<sub>50</sub> value, the concentration at half maximum current, of 1.58 nM. This is slightly higher than the previously obtained literature value of 0.66 nM<sup>152</sup> though still remains in the nM range. Open conjugate **90** was tested several times at the highest concentration (1 μM) and found to elicit only negligible current activation, demonstrative of a lack of binding to the SST2 receptor. For this reason, and due to time restraints, a full range of dilutions were not tested for this conjugate. This confirmed that installation of the maleimide tags deactivated the peptide towards the SST2 receptor. Bridged conjugate **91**, though eliciting a current response upon application to the cell, produced erratic data. Repeated application of the construct to the cell at identical concentrations produced a wide range of current response, e.g. a concentration of 10<sup>-12</sup> M could elicit the same response as 10<sup>-6</sup> M and *vice versa* (see error bars). In addition to this increasing the dose of the peptide did not produce the expected response in current activation leading to a very shallow non-sigmoidal dose response curve. The shallow curve, coupled with the large margins of error, made calculating an accurate EC<sub>50</sub> for the bridged construct impossible.

### 2.1.3.2: Measuring maximum current activation

An alternative measure of the ability of the peptide to bind to the receptor is to measure the peptide concentration at which maximum activation is achieved. Cells identical to those previously described (section 2.1.3.1, page 60) were exposed to solutions of native Octreotide **74**, and conjugates **90** and **91** of varying concentrations ( $10^{-12}$  -  $10^{-6}$  M) until maximum current activation was achieved. Native Octreotide **74** demonstrated a large maximum current at a concentration of only  $0.01 \mu\text{M}$  ( $\text{pA/pF} = -73.7 \pm 5.9$ ), open conjugate **90** showed negligible current activation as high as  $1 \mu\text{M}$  ( $\text{pA/pF} = -2.1 \pm 1.0$ ), and bridged conjugate **91** showed significant restoration of activity at  $0.1 \mu\text{M}$  ( $\text{pA/pF} = -16.1 \pm 4.7$ ) (Figure 22).

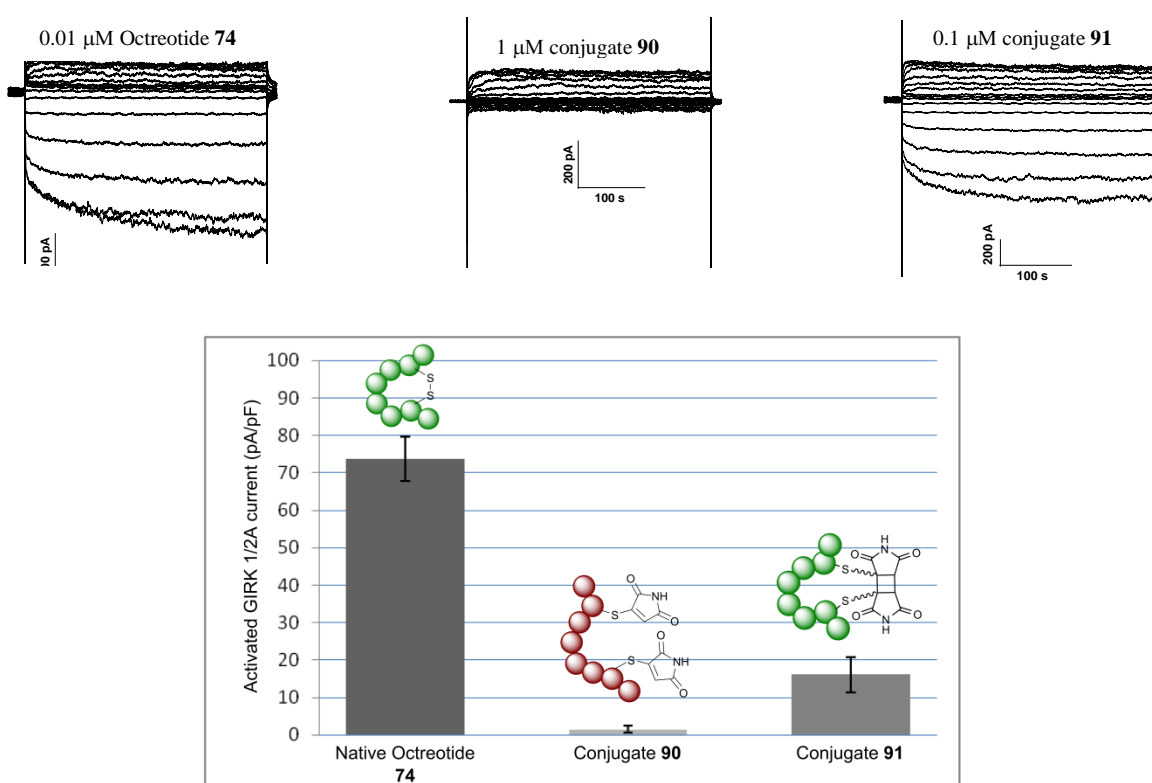


**Figure 22**  
Maximum current activation for Octreotide **74** ( $0.01 \mu\text{M}$ ), conjugate **90** ( $1 \mu\text{M}$ ) and conjugate **91** ( $0.1 \mu\text{M}$ ). Values shown are an average of 10 readings at each concentration (9 for conjugate **90**).

This data highlights the complete loss of activity upon installation of the maleimide tags, and then restoration of activity after irradiation. Significant attenuation in both binding affinity and agonist efficacy is observed compared to the native peptide, evidenced by the required increase in concentration to reach a lower maximum current activation. This was expected due to the small size of Octreotide **74** and the proximity of the modification to the peptides pharmacophore (Phe-Trp-Lys-Thr).<sup>271</sup> Previous work has highlighted that addition of a maleimide bridge into to the disulfide bond of Octreotide **74** can elicit a dramatic change in both affinity and efficacy.<sup>152</sup> It is also likely that only a small number of the

possible diastereo and regioisomers obtained from the photochemical [2+2] cyclisation result in active conformations, leading to a relative decrease in the concentration of the active peptide (Figure 23).

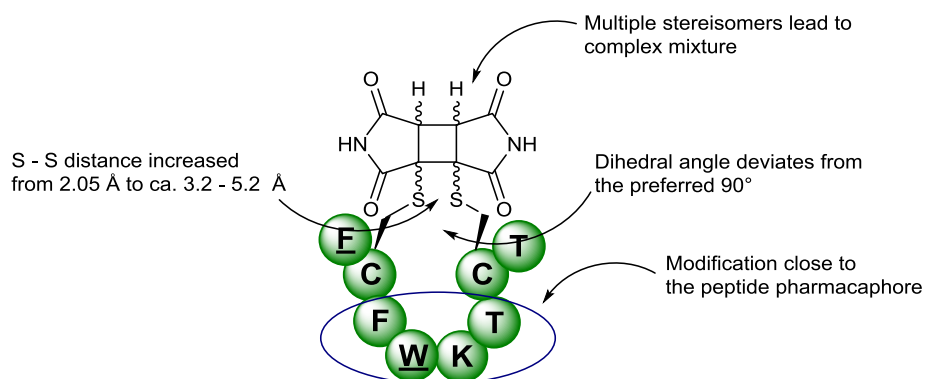


**Figure 23**  
**Explanations for the attenuation in activity after photochemical rebridging. Bond distances were calculated in ChemBio3D after energy minimisation using the MM2 algorithm with an RMS gradient of 0.01.**

The presence of multiple isomers in the solution poses the question as to which is most active. Regrettably no crystal structure of the SST2 receptor exists, precluding our ability to undertake computational docking studies. Nevertheless, it is worth noting that the conformation favoured in the small molecule study, *exo* head-to-head, would seemingly cause a larger perturbation in structure than the disfavoured *endo* head-to-head product. *Exo* structures place the sulfur atoms *trans* to each other at a distance of approximately 4.1 Å, potentially causing a large perturbation in the structure. *Endo* structures place the sulfur atoms *cis* to each other at a distance of approximately 3.1 Å, creating a structure in which the sulfur atoms are placed a less perturbed conformation (Figure 24).

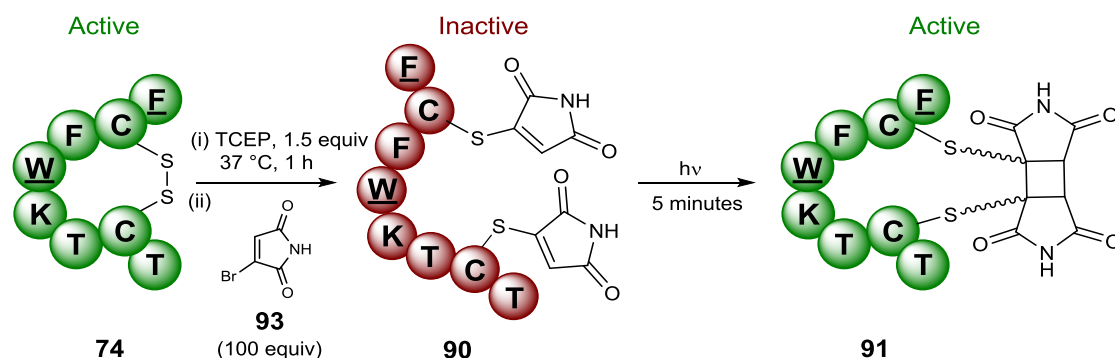


**Figure 24**  
**Ball and stick 3D models showing the difference between *exo* and *endo* conformations of bridged Octreotide 91. Lowest energy conformations were fitted using the MM2 algorithm in ChemBio3D with an RMS gradient of 0.01.**

Regardless of this, we are presently unable to influence the stereochemistry of the photochemical [2+2] cyclisation, which appears to be directed by the conformational considerations of the protein. It is entirely possible that this reaction will exhibit protein dependent stereoselectivity, with larger proteins undergoing less overall perturbation and thus suffering only a minimal loss in affinity and efficacy.

#### 2.1.4: Conclusions and future work

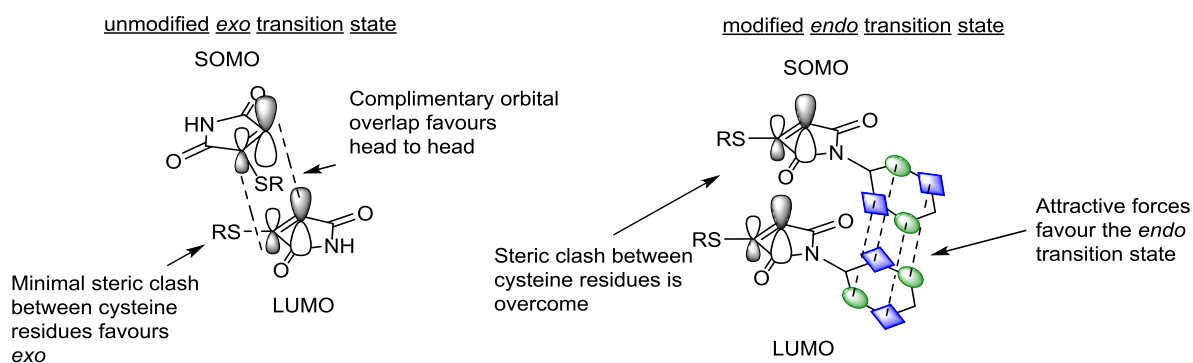
The initial aim of this work was to test the applicability of the thiomaleimide photochemical [2+2] cycloaddition towards the photoactivation of a small therapeutic peptide. By using the SST2 receptor agonist Octreotide **74** as a model system we successfully demonstrated this concept. HPLC, MS-MS, MALDI, LCMS and chemical tests were utilised to optimise the modification and irradiation of the peptide. Previously unknown information regarding the influence of peptide conformation on the key photochemical reaction was obtained through this careful analysis. Finally, binding affinity and peptide efficacy data obtained through whole cell patch clamping demonstrated the capability of the reaction for reforming the active conformation of the peptide. Though a significant drop in both binding affinity and efficacy is observed the overall aim was achieved, providing the first example of peptide photoactivation through photochemical manipulation at the site of a disulfide bond (Scheme 41).



**Scheme 41**  
The optimised protocol for photochemically activating Octreotide **74**.

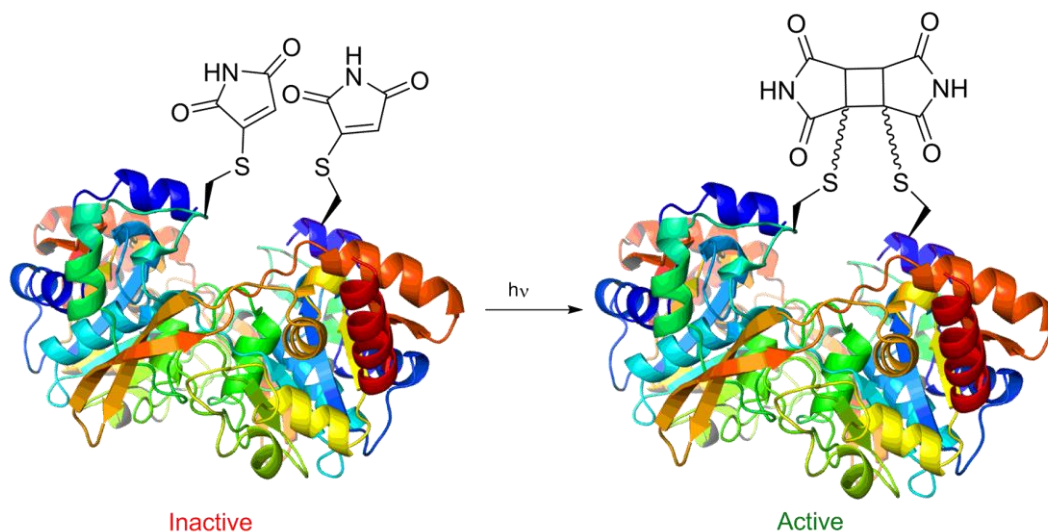
Future work could focus on developing stereoselective variants of this reaction. With sufficient knowledge of the target receptor a stereospecific cycloaddition could be incredibly powerful, as the desired peptide conformation for the active site could be selected for and achieved in a higher yield than currently possible. Presently the preference for *exo* products is attributed to the desire to avoid a steric clash between cysteine residues in the transition state. If a modification could be found which provides sufficient reason to overcome these steric factors this preference could be flipped and *endo* would be preferred. A possible route towards this would be to functionalise the imide nitrogen with groups which stack efficiently through extensive intermolecular forces and steric attraction

(Scheme 42). Similar methods have been employed with some success for asymmetric [2+2] cycloadditions.<sup>272–274</sup>



**Scheme 42**  
A potential method for asymmetric thiomaleimide photochemical [2+2] cyclisation reactions.

It would also be worthwhile to demonstrate the general applicability of this method by testing it on a variety of peptides or proteins with essential disulfide bonds. Of particular interest would be the photochemical activation of enzymatic processes. By targeting disulfide bonds near the active site of an enzyme photochemical control of enzymatic processes could be achieved.

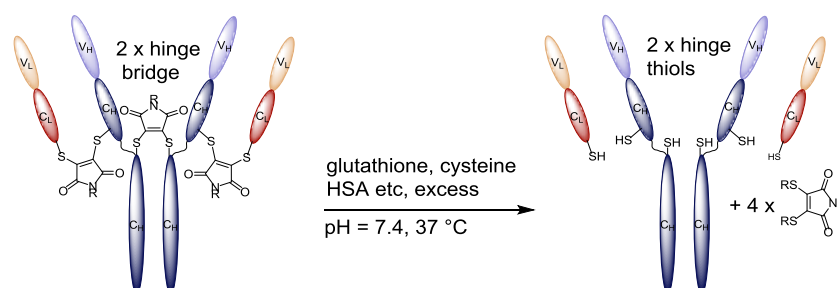


**Scheme 43**  
Photochemically activating enzymes using the thiomaleimide photochemical [2+2] cyclisation.

## 2.2: Thiomaleimide [2+2] cyclisations on antibody fragments

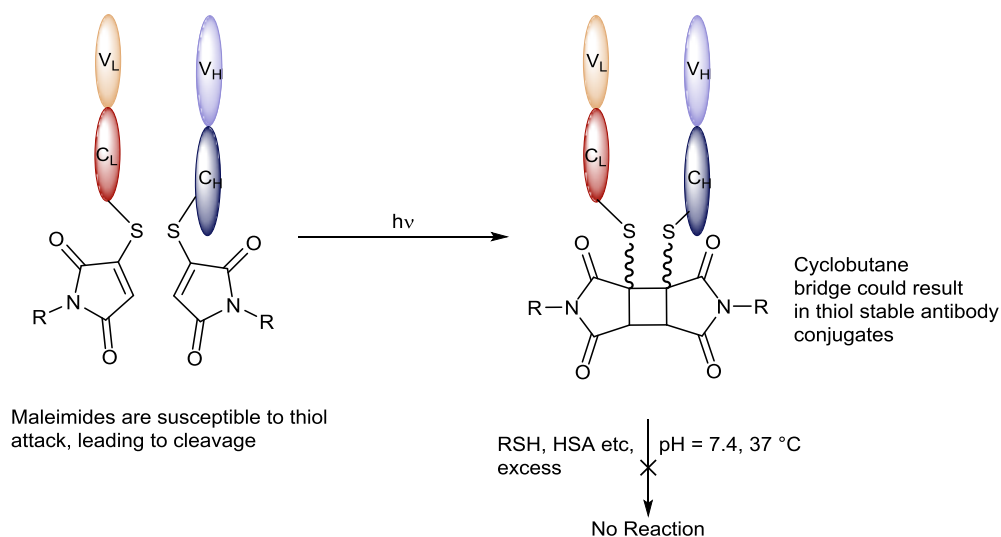
### 2.2.1: Aims and introduction

After the success of the thiomaleimide [2+2] cyclisation on a small peptide we wanted to test the scope of the reaction through its application to more complex proteins. Recent work in the field of protein modification has utilised next generation maleimides to insert chemical functionality into the disulfide bonds of antibodies to generate functional antibody conjugates.<sup>146,149,153,156</sup> Most recently this technology has been used to develop a functional Antibody Drug Conjugate (ADC) by targeting disulfide bonds with a monomethyl auristatin E (MMAE) functionalised disubstituted maleimide.<sup>153</sup> By retaining the bridge between the heavy and light chain the conjugates are able to maintain the thermal stability of the native antibody, which is lost upon removal of the interchain covalent bond.<sup>158</sup> Though highly selective and efficient the modification suffers from thiol instability. The installed maleimide bridge is susceptible to thiol attack which can lead to premature cleavage of the payload, decreasing the efficacy and potentially leading to off-target side effects (Scheme 44).<sup>146</sup> More recently issues of thiol mediated maleimide transfer between the ADC and Human Serum Albumin (HSA) within the blood have reinforced this problem.<sup>153</sup>



**Scheme 44**  
**The thiol instability of maleimide-bridged ADCs.**

Methods to address this unwanted reactivity by hydrolysing the maleimide to the unreactive maleimic acid have been very successful.<sup>153</sup> We hypothesised that the thiomaleimide photochemical [2+2] cycloaddition could also be employed for this purpose. Upon successful cycloaddition the maleimide conjugate acceptor is removed and the susceptibility to thiol attack eliminated, as evidenced by lack of reactivity towards EDT described in the previous chapter. By applying the thiomaleimide [2+2] cyclisation we could demonstrate the scope of this reaction on larger proteins whilst simultaneously addressing the issues related to thiol instability (Scheme 45).



**Scheme 45**  
**The proposed photochemical thiomaleimide [2+2] cyclisation to stabilise maleimide antibody conjugates towards thiols.**

We aimed to apply the photochemical thiomaleimide [2+2] cycloaddition to an immunoglobulin and a selection of associated antibody fragments. Through this the scope of the reaction on a range of proteins of various sizes could be tested, whilst simultaneously generating a small library of thiol stable functional antibody conjugates. Towards this aim the reaction would be tested on scFv and Fab antibody fragments, as well as a full antibody (Figure 25).

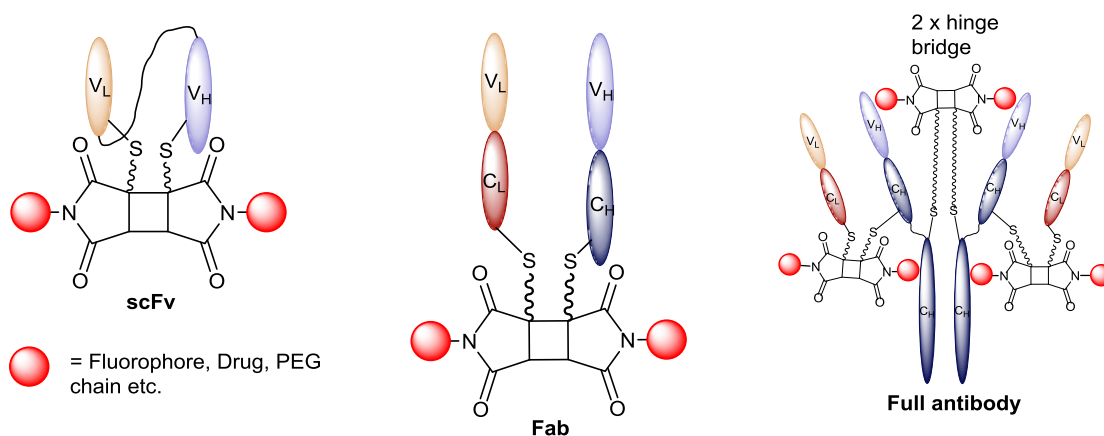


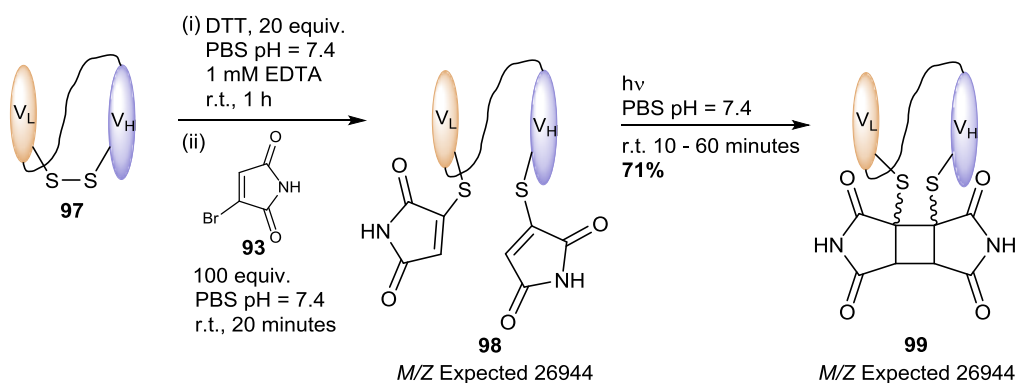
**Figure 25**  
**The proposed protein models; full antibody, Fab fragment and scFv fragment.**

### 2.2.2: Modification of an anti-CEA scFv

As discussed earlier (Section 1.2.4.1, page 32) an scFv is an antibody fragment comprising of the antigen binding region (Fv) stabilised through the addition of covalent interchain  $V_L - V_H$  peptide linkages and disulfide bonds.<sup>188,189</sup> Previous work has shown a mutant form of the anti-carcinoembryonic antigen (Anti-CEA) scFv **97**, engineered by the Chester group at UCL Cancer Research, is a good candidate for conjugation with maleimide.<sup>150</sup> Protocols for

the reduction and modification of the disulfide bond are well established<sup>150</sup> and as a relatively small antibody fragment scFv **97** presented the sensible next step in establishing the scope of the photochemical thiomaleimide [2+2] cycloaddition. Reduction and *bis*-modification of the fragment was performed using DTT and a large excess of monobromomaleimide **93**. In this instance TCEP proved ineffective as a reducing agent, possibly due to the more buried nature of the disulfide bond within the protein structure. Due to the aforementioned cross reactivity DTT was removed by size exclusion filtration before *bis*-modification with monobromomaleimide **93**. The addition of EDTA to the buffer systems minimises disulfide reoxidation by chelating redox active metal impurities. Under these conditions *bis*-modification proceeded smoothly and no further optimisation was required. scFv conjugate **98** was subsequently irradiated using a single 5W LED system for ten, thirty and sixty minutes (Scheme 46) (Figure 26) (Figure 27).

As with irradiating Octreotide conjugate **90** no mass change can be seen upon successful photochemical [2+2] cyclisation. However, previous work has shown that changes in the protein structure between the bridged (**99**) and unbridged (**98**) forms of this scFv are sufficiently large to be resolved by SDS-PAGE (Figure 27).<sup>150,275</sup> SDS-PAGE analysis shows destruction of the bridge upon reduction and modification (lanes 2 and 4), and subsequent reformation upon irradiation (lanes 6 - 8). Though the change is small there is a clear transformation taking place which results in the protein moving further down the gel, consistent with a structure more similar to native scFv **97** with the disulfide bridge intact.<sup>275</sup> The results suggest that maximum bridging was obtained within ten minutes of irradiation, with extended irradiation providing no further benefit. Quantification by densitometry gives a yield of 71% for the photochemical bridging of the cysteine residues.



**Scheme 46**  
**The modification and irradiation of scFv fragment 97.**

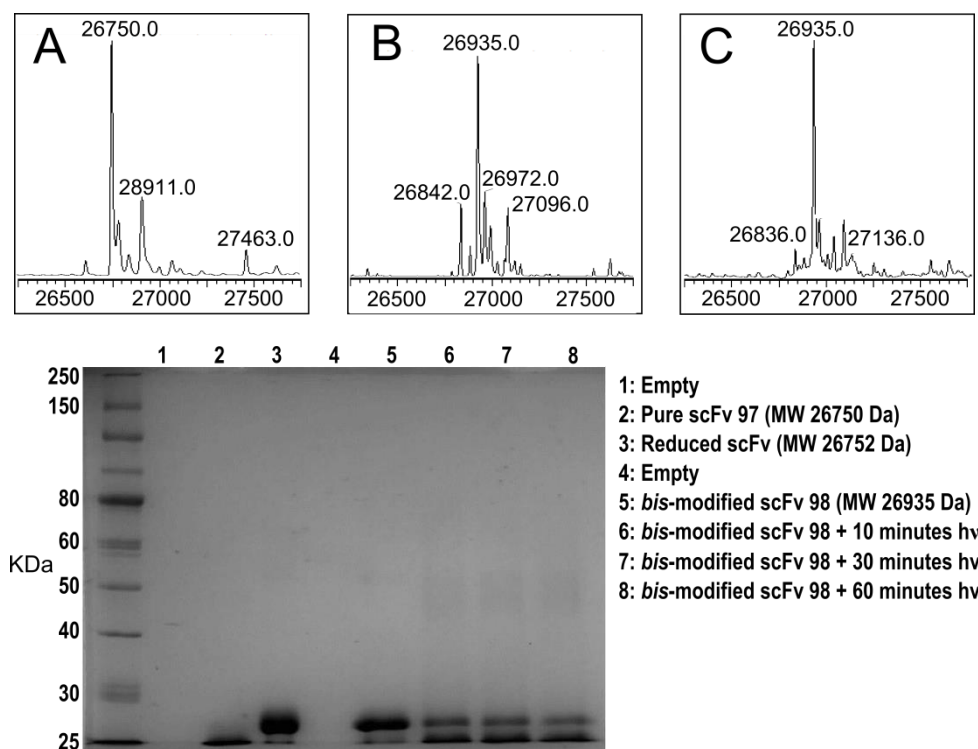


**Figure 26**  
**MS data: (A) Pure scFv 97, (B) bis-modified scFv 98, (C) Rebridged scFv 99. See experimental section for full spectra (Section 3.2.3.1, page 183, Figure 68).**  
**Figure 27**  
**SDS-PAGE (12%) analysis of the modification and irradiation of scFv 97.**

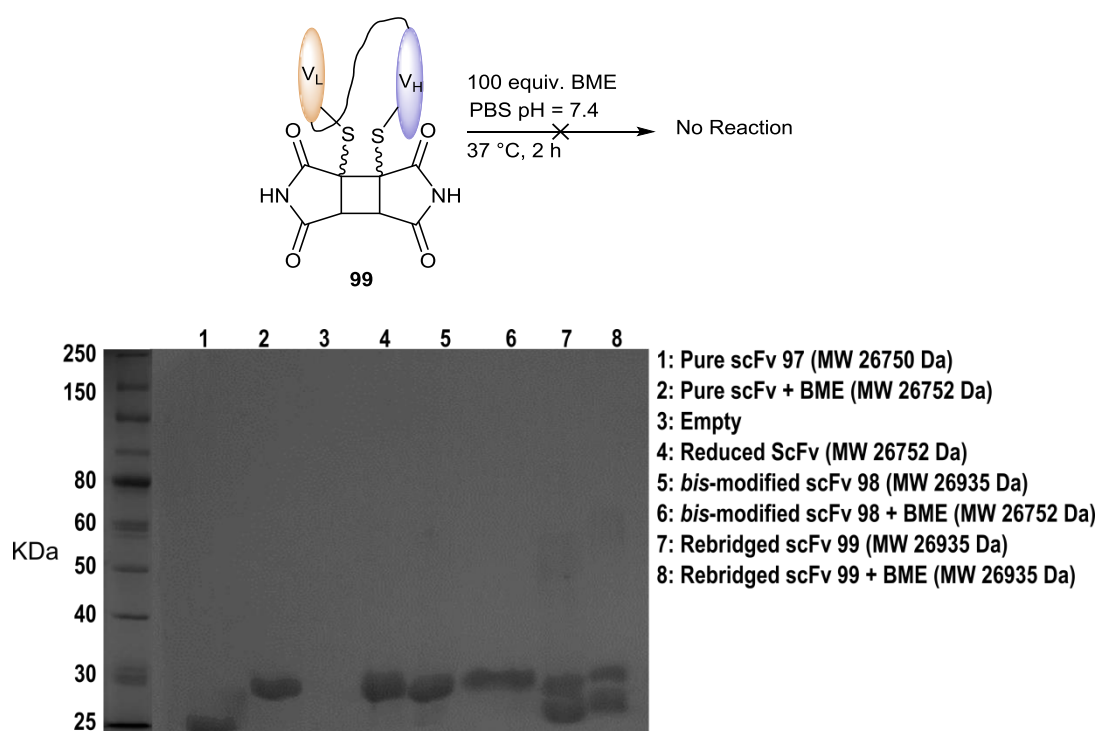
It is postulated that the retention difference observed with SDS-PAGE results from the bridged protein forming a more tightly packed three dimensional-structure. This provides a smaller surface area for the SDS to bind, generating a lower overall charge and lowering the retention factor of the protein on the gel. Analysis by LCMS highlighted purity issues of the native protein, which are a result of the post-expression purification protocol employed during expression of the protein. Enzymatic cleavage of the leader sequence after expression gives rise to multiple species with pendant N-terminal amino acids in addition to the desired protein. Though complicating the LCMS spectra these modifications cause no adverse effects with regards to the behaviour of the protein.

Whilst SDS-PAGE seems to indicate that consumption of the starting material is incomplete we must assume this is not the case, as extended irradiation times do not increase the bridging yield. LCMS does not indicate any additional mass fragments, though the previously mentioned issues with quality prevent confident interpretation of the spectra. Analysis of the amino acid sequence of the peptide reveals the amino acids proximal to the cysteine residues as glycine, threonine, phenylalanine, alanine, and histidine. There is no obvious explanation as to how these residues could adversely affect the photochemical [2+2] cyclisation between the cysteine-maleimides. Of course considering only neighbouring residues is insufficient, and it is entirely possible that an aspect of the quaternary structure of the protein is interfering with the reaction. Without detailed structural

information further reasoning behind the reduction in efficiency of the photochemical thiomaleimide [2+2] cyclisation is not possible.

### 2.2.2.1: Thiol stability of a rebridged anti-CEA scFv conjugate

To test the hypothesis that the cyclobutane bridge would be resistant to thiol attack bridged scFv conjugate **99** was incubated with an excess of  $\beta$ -mercaptoethanol (BME) (Scheme 47). SDS-PAGE analysis showed no change, indicating the bridge was retained (Figure 28). LCMS data also showed no change, supporting this result. *Bis*-modified scFv **98** was subjected to the same conditions and cleavage of the maleimides was observed by LCMS, though as expected no change could be seen by SDS-PAGE. As a control reaction native scFv **97** was subjected to the same conditions to demonstrate that BME was capable of reducing this particular scFv.



Scheme 47

Testing the thiol stability of rebridged scFv conjugate **99**.

Figure 28

SDS-PAGE (12%) showing the thiol stability of scFv conjugate **99** (lane 8).

As a model system anti-CEA scFv **97** demonstrated the potential of this reaction for bridging cysteine residues on larger proteins and also validated the hypothesis regarding thiol stability.

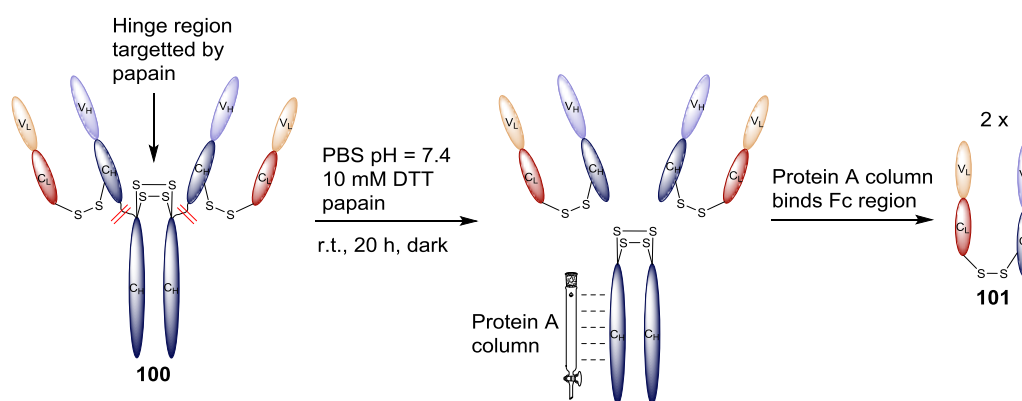
### 2.2.3: Modification of Rituxan Fab

#### 2.2.3.1: Preparation of Rituxan Fab

Given the success of the thiomaleimide [2+2] photocycloaddition on anti-CEA scFv **97** it was decided to attempt the reaction on a larger antibody fragment. Fab fragments consist of the heavy and light chains of the antibody connected by a single disulfide bond, thus

offer a unique chance to test the scope of the photochemical thiomaleimide [2+2] cycloaddition. Upon removal of the disulfide bridge the two chains are no longer covalently connected, though intramolecular forces keep them tightly associated, so in the strictest sense rebridging *via* a [2+2] cycloaddition could be considered an intermolecular reaction.

As discussed in the introduction, Rituxan is a clinically relevant chimeric monoclonal antibody which has attracted significant interest in the ADC field.<sup>172,176</sup> Rituxan Fab **101** was produced through an enzymatic digest of the full antibody **100**. The hinge region of the antibody is selectively targeted by the thiol-endopeptidase enzyme papain to cleave the two Fab fragments **101** from the Fc region. The Fc and Fab fragments are then separated using a protein A column, which selectively binds the Fc region and allows for efficient purification. Using this protocol Rituxan Fab **101** was prepared in an overall yield of 43% (Scheme 48). Characterisation by SDS-PAGE and LCMS showed the protein was obtained in excellent purity (Figure 29) (Figure 30).

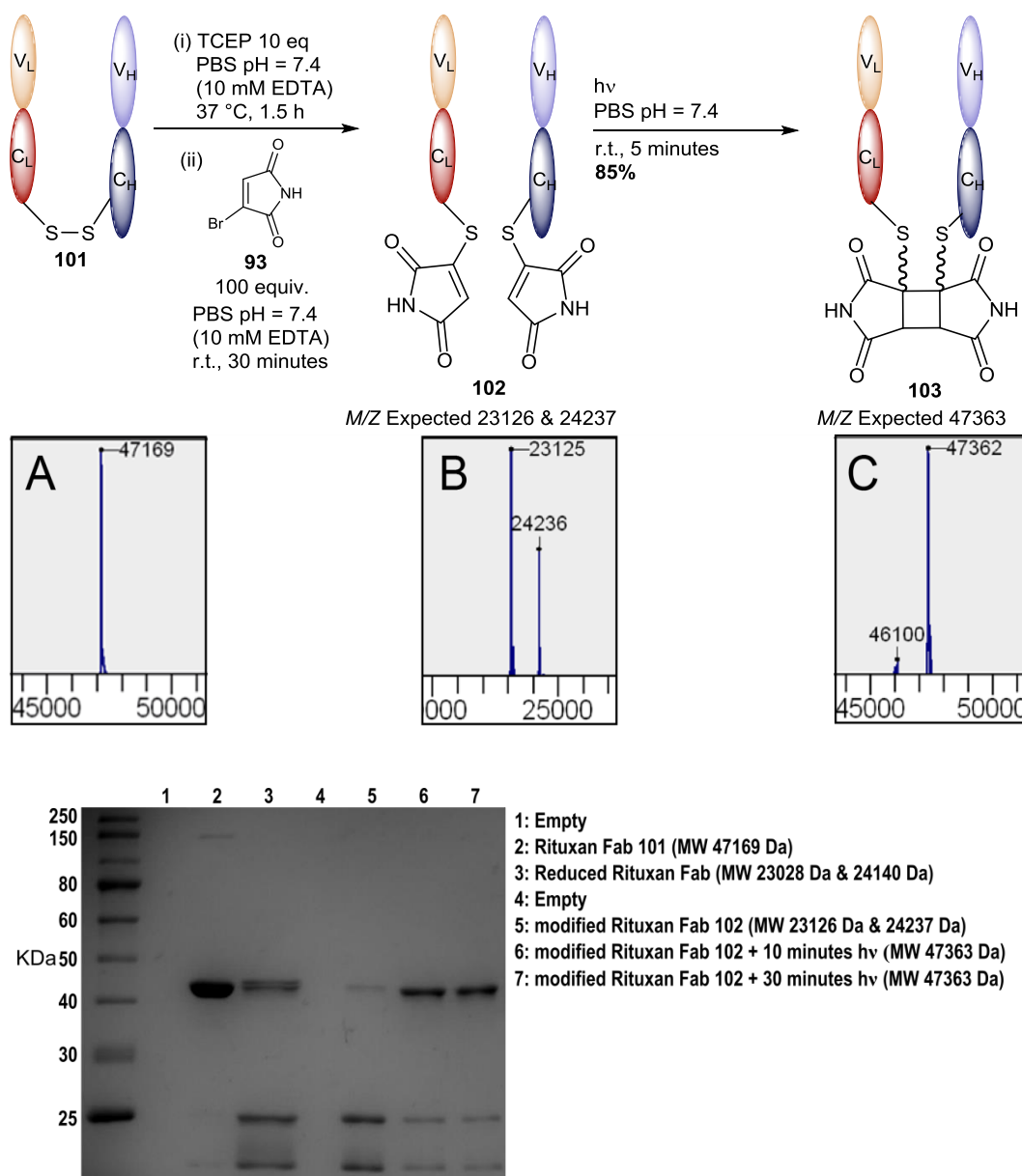


**Scheme 48**  
**Preparation of Rituxan Fab 101.**

### 2.2.3.2: Modification of Rituxan Fab

Reduction of Rituxan Fab **101** using TCEP in EDTA containing buffer proceeded smoothly and subsequent *bis*-modification using monobromomaleimide **97** produced *bis*-modified Rituxan Fab **102**. Attempts to reduce the equivalents of maleimide showed some promise, with both thirty equivalents and fifty equivalents producing *bis*-modified Rituxan Fab **102** as the major product. However, evidence of trace succinimide formation was found in both LCMS and SDS-PAGE data, demonstrating the negative effect of lowering the equivalents of monobromomaleimide **93**. Irradiation of *bis*-modified Rituxan Fab **102** affected successful bridging to rebridged Rituxan Fab **103** within ten minutes (Scheme 49). It is worth noting that the lack of a covalent link between the two fragments in *bis*-modified Rituxan Fab **101** can be seen in the mass spectrum (Figure 29B) and in the SDS-PAGE (Figure 30, lane 6+7), providing unambiguous evidence for the success of the photochemical thiomaleimide [2+2] cycloaddition on a protein. As with the photochemical thiomaleimide [2+2] cycloaddition on the scFv the reaction does not produce complete

rebridging, with gel densitometry giving a bridging yield of 85%; this will be discussed later in this chapter.



#### Scheme 49

The reduction, modification and irradiation of Rituxan Fab 101.

#### Figure 29

LCMS data: (A) Rituxan Fab 101, (B) *bis*-modified Rituxan Fab 102, (C) Bridged Rituxan Fab 103. See experimental section for full spectra (Section 3.2.4, page 186, Figure 71 & page 190, Figure 76).

#### Figure 30

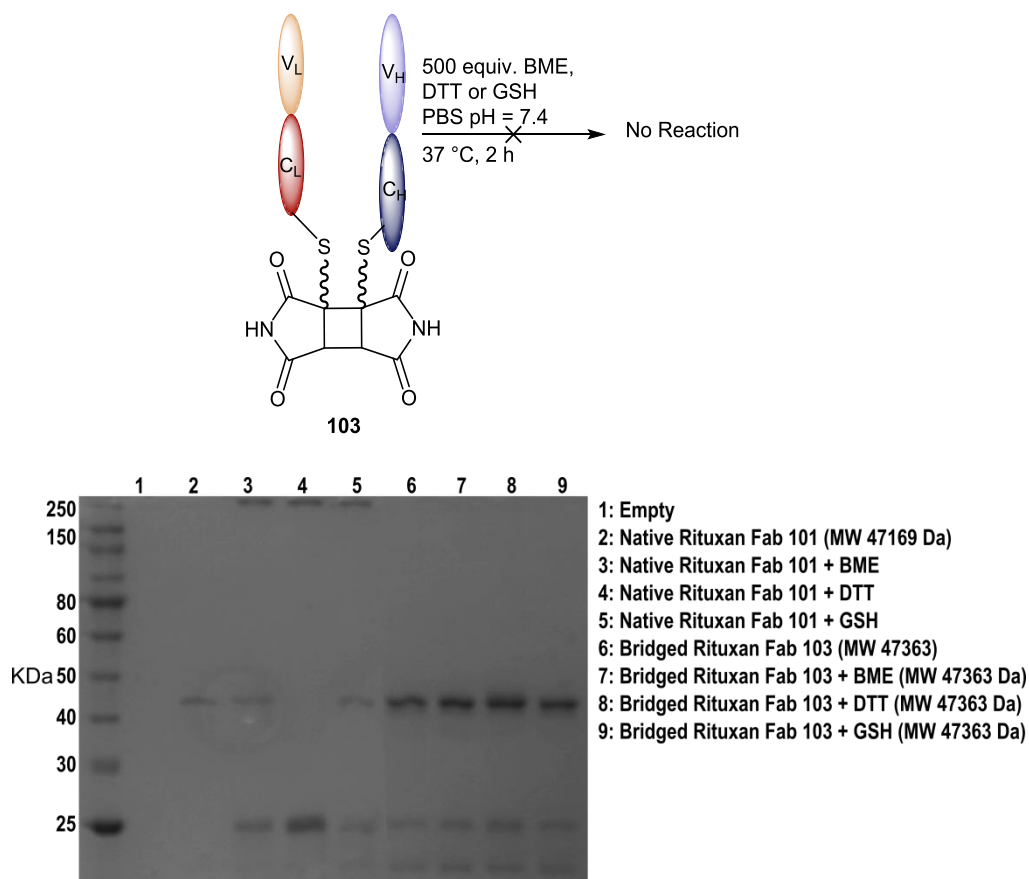
SDS-PAGE (12%) analysis of the modification and irradiation of Rituxan Fab 102.

The novel nature of this work necessitates careful control reactions to rule out secondary reactions which could contribute to the observed rebridging. In the case of the Rituxan Fab work we primarily wanted to rule out non-photochemical rebridging of the two chains. *Bis*-modified Rituxan Fab **102** was incubated both at room temperature and 37 °C for one hour. Analysis by SDS-PAGE (see experimental section 3.2.4.2, page 193, Figure 81) and LCMS

showed no change, suggesting that the observed reactivity upon irradiation is purely photochemical.

### 2.2.3.3: Thiol stability of Rituxan Fab conjugates

As with the scFv conjugate **98** we wanted to demonstrate the thiol stability of the cyclobutane bridge of Rituxan Fab conjugate **103**. To test for stability against a wide range of thiols we incubated bridged Rituxan conjugate **103** with up to 500 equivalents of BME, DTT and GSH (Scheme 50). As a control pure Rituxan Fab **101** was subjected to the same conditions. As expected the SDS-PAGE shows the cyclobutane bridge was unaffected by the excess thiol. No difference can be seen between the negative control (Figure 31, lane 6) and the lanes containing bridged Rituxan Fab **103** incubated with excess thiol (Figure 31, lanes 7-9). LCMS data once again supports this conclusion as no change can be seen in the spectra after incubation. Interestingly pure Rituxan Fab **101** proved much less robust, with high molecular weight bands appearing at the top of the gel, suggesting significant aggregation (Figure 31, lanes 3-5).



**Scheme 50**

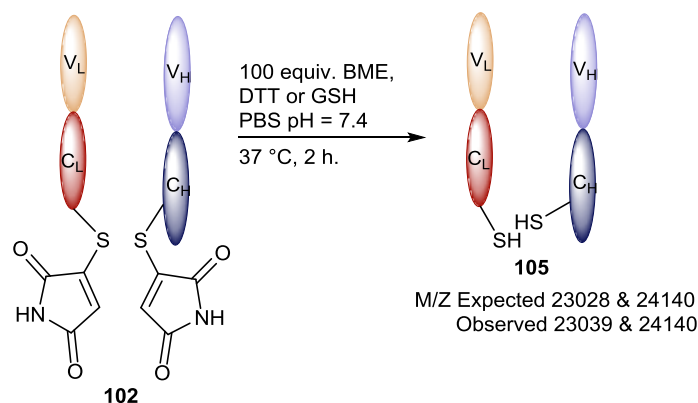
**Testing the thiol stability of bridged Rituxan Fab 103.**

**Figure 31**

**SDS-PAGE demonstrating the thiol stability of the bridged Rituxan Fab fragments.**

This work provided the most conclusive evidence yet for both the success of the photochemical thiomaleimide [2+2] cycloaddition on larger proteins and also the thiol

stability of the resulting cyclobutane bridge. To demonstrate that the conjugates before irradiation are unstable under the same conditions *bis*-modified Rituxan Fab conjugate **102** was subjected to the same conditions. Complete cleavage of the maleimide from both the heavy and light chain with only 100 equivalents of thiol demonstrates the thiol instability of the maleimide structure and highlights the importance of forming the cyclobutane ring (Scheme 51).



#### Scheme 51

Reacting *bis*-modified Rituxan Fab conjugate **102** with thiol leads to complete cleavage of the maleimide. Evidence of this transformation was shown using LCMS. See experimental section for full spectra (Section 3.2.4.3, page 194, Figure 82).

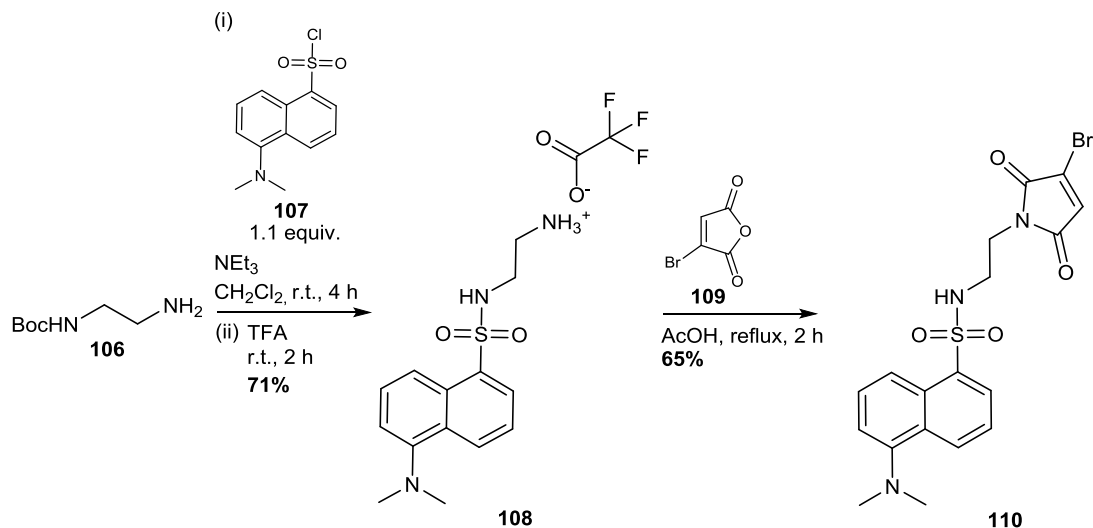
#### 2.2.3.4: Synthesis of functionalised bromomaleimides

Whilst chemically interesting the photochemical thiomaleimide [2+2] cyclisation reaction of unfunctionalised maleimides on antibody fragments serves a limited purpose. Though a covalent link between heavy and light chains is beneficial for stability, binding to the antigen is not affected upon removal of the bridge. Thus, unlike with Octreotide **74**, the photochemical thiomaleimide [2+2] cyclisation cannot be used for photochemical activation of the protein. It was decided that the best way to exploit the stabilising nature of this reaction would be to generate functionalised thiol-stable Rituxan Fab fragments. By placing functional groups such as PEG, Biotin, fluorophores, or cytotoxic drugs onto the imide nitrogen of the maleimide a small library of thiol stable *bis*-modified Fab fragments could be generated. Through this work valuable information regarding the scope of the reaction could also be ascertained.

#### Synthesis of N-dansyl-bromomaleimide

Dansyl analogues are well established fluorescence probes for protein modification, often attached directly to lysine residues *via* reaction with dansyl chloride.<sup>276–278</sup> More recent work has highlighted the ability of maleimide to quench this fluorescence through photo-induced charge transfer (PET) or intramolecular charge transfer (ICT), leading to the development of thiol-mediated “switch on” fluorescent probes.<sup>151</sup> For these reasons it was decided that a dansyl analogue would be synthesised for the functionalisation of Rituxan

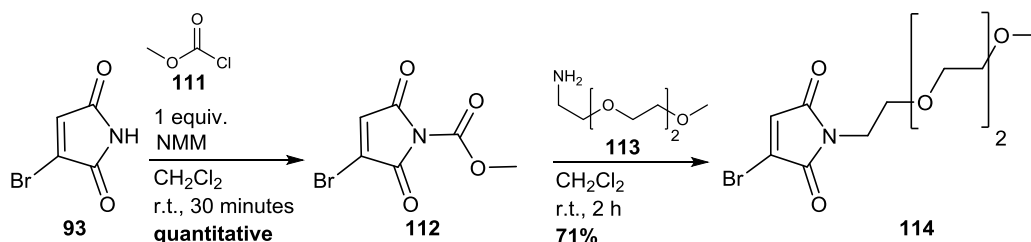
Fab **101**. N-dansyl-bromomaleimide **110** was synthesised simply over three steps. Reaction of mono-Boc protected amine **106** with dansyl chloride **107** followed by Boc deprotection afforded intermediate **108**. Subsequent condensation with bromomaleic anhydride **109** produced the desired compound in a 46% yield over two steps (Scheme 52).



**Scheme 52**  
The synthesis of N-dansyl-bromomaleimide **110**.

#### Synthesis of N-OEG-bromomaleimide **114**

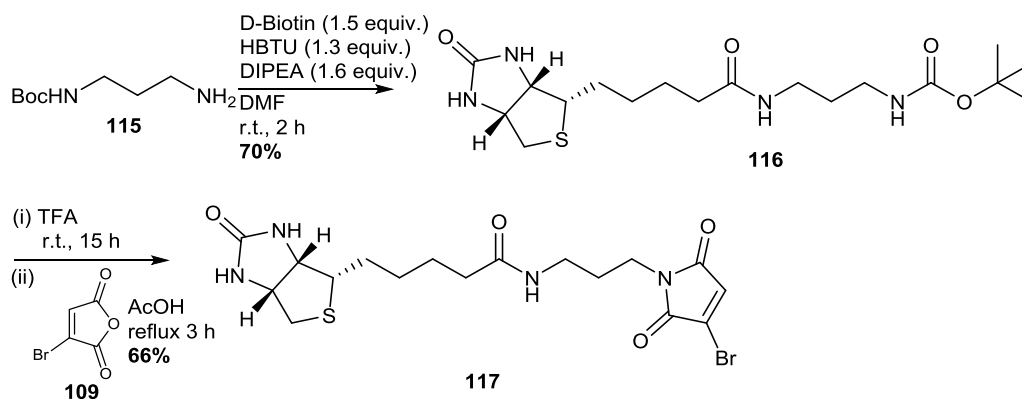
Though the low molecular weight of Fab fragments can be advantageous for tumour penetration, the lower half life is often problematic for clinical applications.<sup>279</sup> This can be overcome by PEGylation i.e. the covalent attachment of high molecular weight PEG chains.<sup>280</sup> Compatibility of PEG-maleimides with the photochemical thiomaleimide [2+2] cycloadditions is desirable as it will provide a method for thiol-stable antibody PEGylation. A small OEG “mini PEG” bromomaleimide **114** was synthesised for this purpose. The smaller three unit polymer was chosen for ease of synthesis and availability. Activated carbamate **112**, quantitatively synthesised from bromomaleimide **93**, was reacted with OEG-amine **113** to produce the desired OEG-bromomaleimide **114** in a 71% yield (Scheme 53).



**Scheme 53**  
The synthesis of N-OEG-bromomaleimide **114**.

### Synthesis of N-biotin-bromomaleimide 117

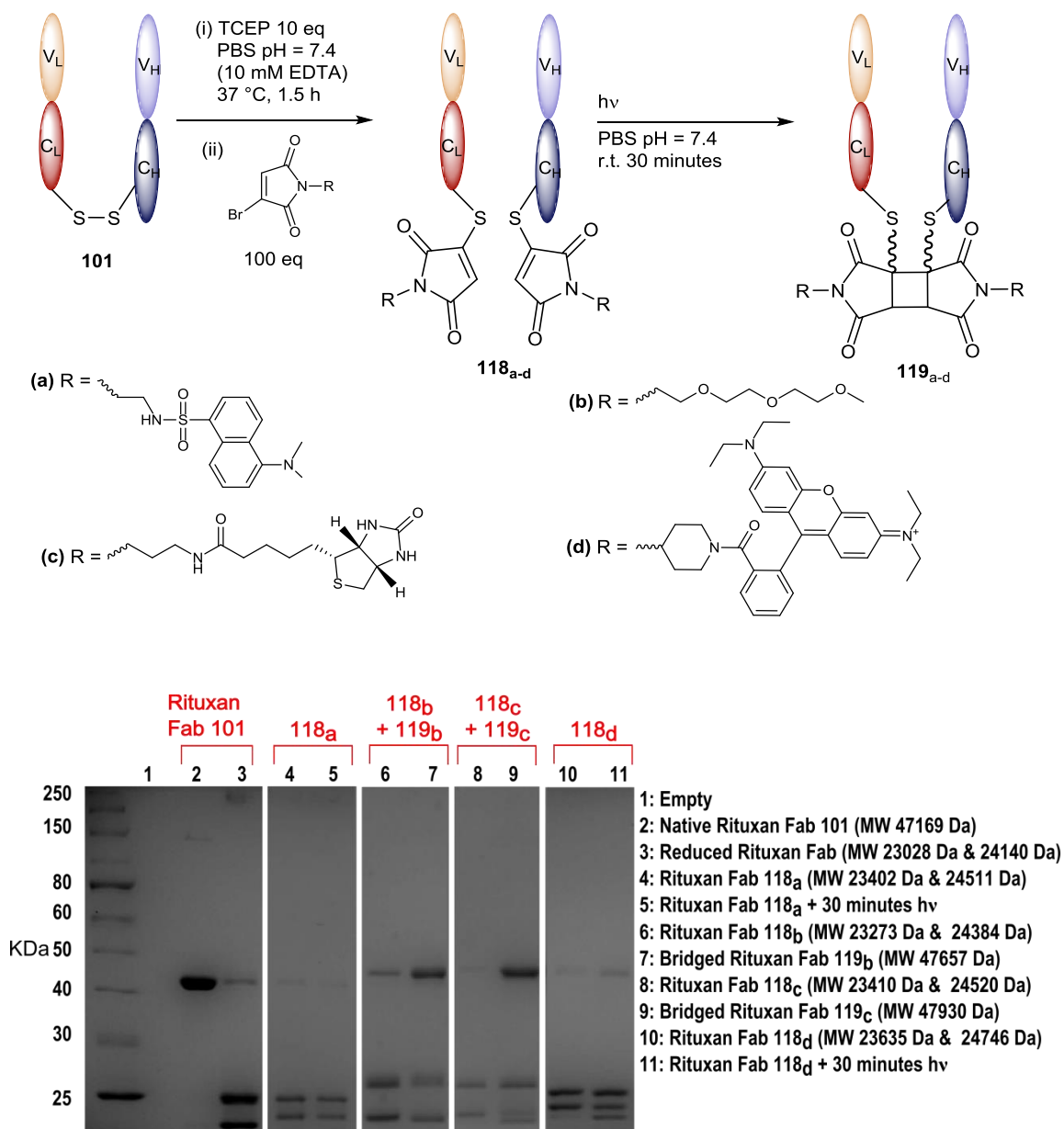
D-Biotin, or vitamin B<sub>7</sub>, is a coenzyme complicit in a number of biological processes.<sup>281</sup> However, its utility as a tool for covalent protein modification results from the ability to bind strongly to the protein avidin.<sup>282</sup> This affinity is regularly exploited for immobilising proteins onto solid resins for diagnostic or purification purposes. Incorporation of a biotin functionalised Fab fragment into the Rituxan Fab library could expand this work into these areas. Biotin-Boc-amine **116** was synthesised *via* HBTU mediated amide coupling. Deprotection of the amine and subsequent condensation with bromomaleic anhydride produced N-biotin-bromomaleimide **117** in an overall yield of 47% (Scheme 54).



**Scheme 54**  
The synthesis of N-Biotin-bromomaleimide **117**.

### 2.2.3.5: Generating functionalised Rituxan Fab fragments

The successful synthesis of N-dansyl-bromomaleimide **110**, N-OEG-bromomaleimide **114** and N-biotin-bromomaleimide **117** paved the way for the generation of the desired library of functionalised Rituxan Fab fragments. In addition to the synthesised bromomaleimides an N-rhodamine bromomaleimide was provided by Cristina Marculescu<sup>283</sup> to test under these reaction conditions. The previously employed protocol for reduction, modification and irradiation of the Rituxan Fab was utilised to generate the desired conjugates (Scheme 55). Reduction and modification of Rituxan Fab **101** with the N-functionalised bromomaleimides went smoothly and LCMS confirmed successful *bis*-modification in each case (Figure 33, A-D). Upon irradiation successful photochemical thiomaleimide [2+2] cycloaddition was seen with the N-OEG and N-Biotin functionalised Fab fragments **188<sub>b</sub>** and **188<sub>c</sub>** (Figure 33, B, C), though irradiation times were increased to 30 minutes to achieve maximum conversion. As with the non-functionalised Rituxan Fab conjugate **102** complete conversion to the bridged form was not seen, and extended irradiation times did not improve this. Irradiation of the N-dansyl and N-rhodamine functionalised Fab fragments **118<sub>a</sub>** and **118<sub>d</sub>** did not proceed as anticipated. Upon extended irradiation no conversion to the bridged product was observed by either SDS-PAGE (Figure 32) or LCMS (Figure 33, A, D), though a loss of mass from the light chain of the Fab fragment was noted. This will be discussed later in this chapter.



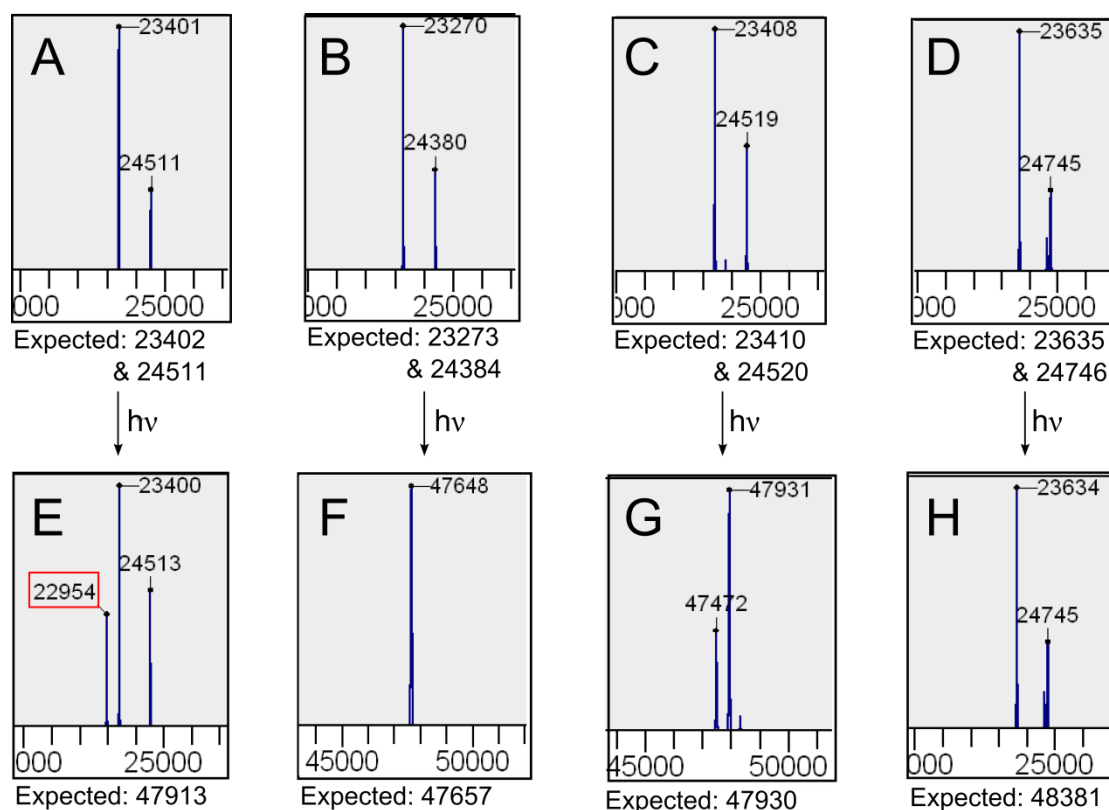


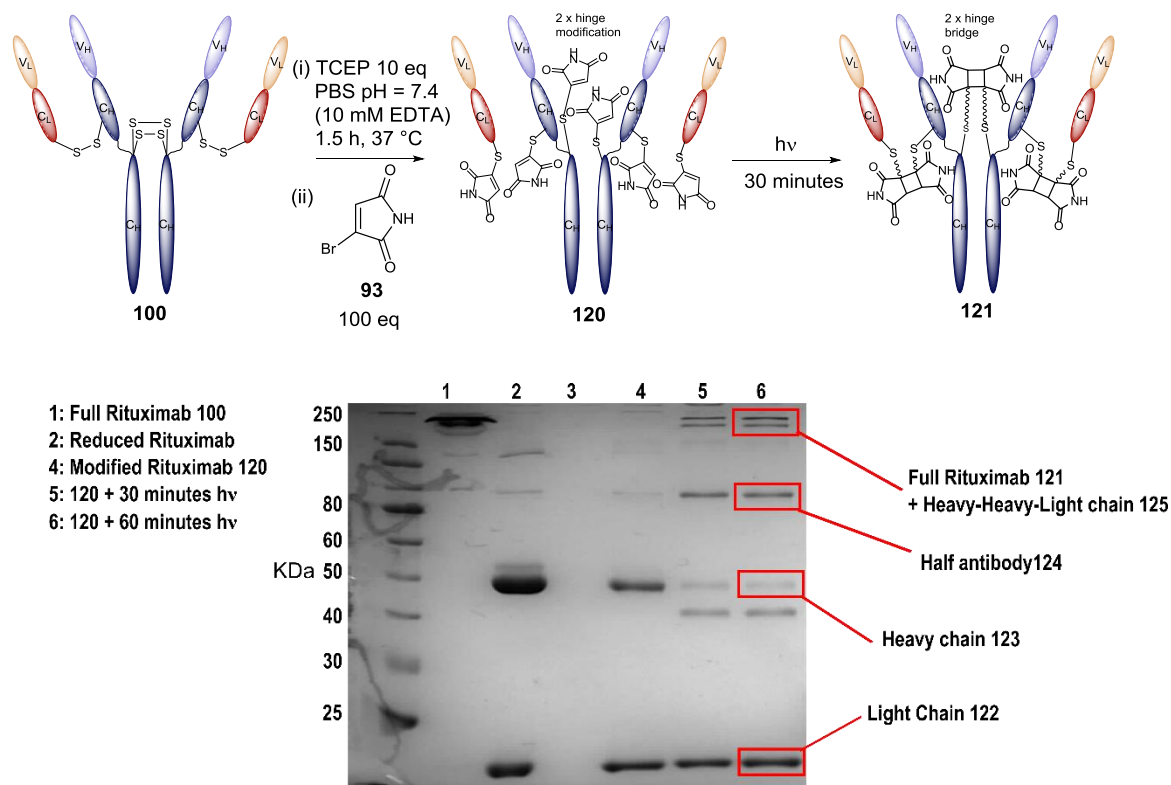
**Figure 33**  
**LCMS data for the modification and irradiation of Rituxan Fab with functionalised maleimides; (A) *bis*-modified conjugate 118<sub>a</sub>, (B) *bis*-modified conjugate 118<sub>b</sub>, (C) *bis*-modified conjugate 118<sub>c</sub>, (D) *bis*-modified conjugate 118<sub>d</sub>, (E) *bis*-modified conjugate 118<sub>a</sub> irradiated for 30 minutes, (F) bridged conjugate 119<sub>b</sub>, (G) bridged conjugate 119<sub>c</sub>, (H) *bis*-modified conjugate 118<sub>d</sub> irradiated for 30 minutes. See experimental section for full spectra (Section 3.2.4.2, page 185).**

Possible explanations for the lack of reactivity of fluorophore conjugates **118<sub>a</sub>** and **118<sub>d</sub>** are that the steric bulk caused by the large fluorophores so close to the maleimide discourages the [2+2] cyclisation. It is also possible that the excitation of the maleimide is quenched by the presence of the fluorophore through a charge transfer mechanism. However, small molecule studies of thiomaleimides have shown that [2+2] photocycloadditions of dansyl-linked thiomaleimides proceed efficiently, so this hypothesis is discouraged.<sup>151</sup> Nevertheless, these results provide valuable information regarding the limitations of this approach.

## 2.2.4: Modification of Rituxan

Following the success on smaller antibody fragments it was decided to test the applicability of the thiomaleimide [2+2] photocycloaddition on the full antibody. This was an ambitious task considering the additional complexity of the full antibody when compared to the smaller scFv and Fab fragments. Complete rebridging of the antibody is contingent on the success of four thiomaleimide [2+2] photocycloadditions, which is made possible only after successful modification of the eight cysteine residues liberated from the solvent accessible

interchain disulfide bonds. Rituxan **100** was reduced according to a known protocol and reacted with an excess of monobromomaleimide **93** to tag each resulting cysteine residue and produce modified Rituxan **120**, which was subsequently irradiated for sixty minutes, with a sample taken at thirty minutes (Scheme 56). Analysis by SDS-PAGE revealed a complex mixture corresponding to incomplete bridging upon irradiation (Figure 34). Single light chain **122**, single heavy chain **123**, half antibody **124** and a heavy-heavy-light fragment **125** could be identified in addition to the fully rebridged antibody **121** (Figure 35). A previously unobserved species was also apparent on the SDS-PAGE, appearing just beneath the heavy chain, though could not be identified.



**Scheme 56**

**The modification and irradiation of Rituxan 100.**

**Figure 34**

**SDS-PAGE (12%) analysis of the modification and irradiation of Rituxan 100.**

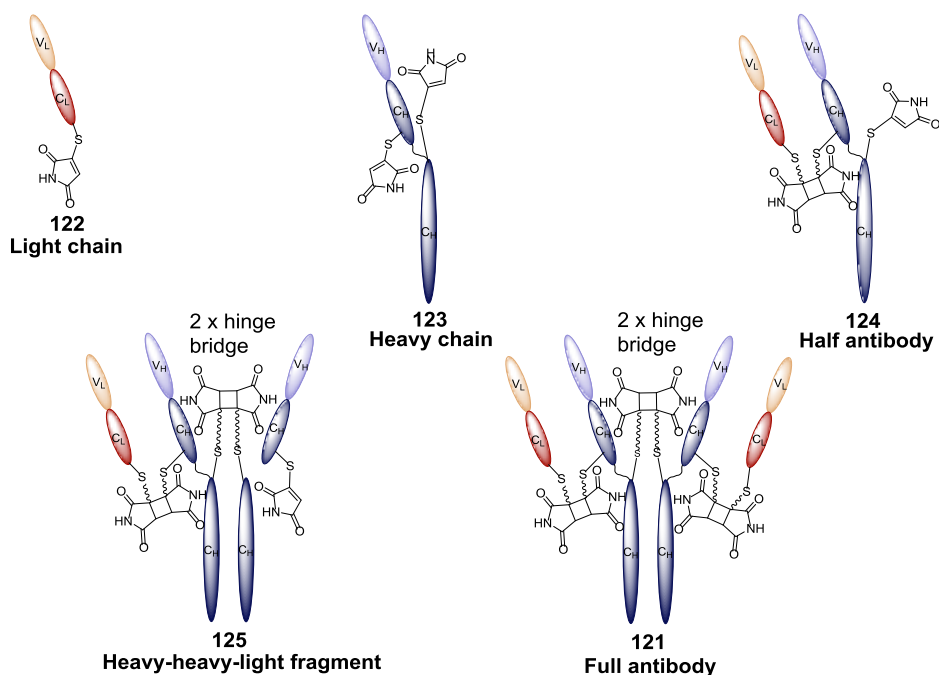


**Figure 35**  
The different fragments produced from the attempted photochemical thiomaleimide [2+2] cyclisation on the modified full Rituxan antibody 120.

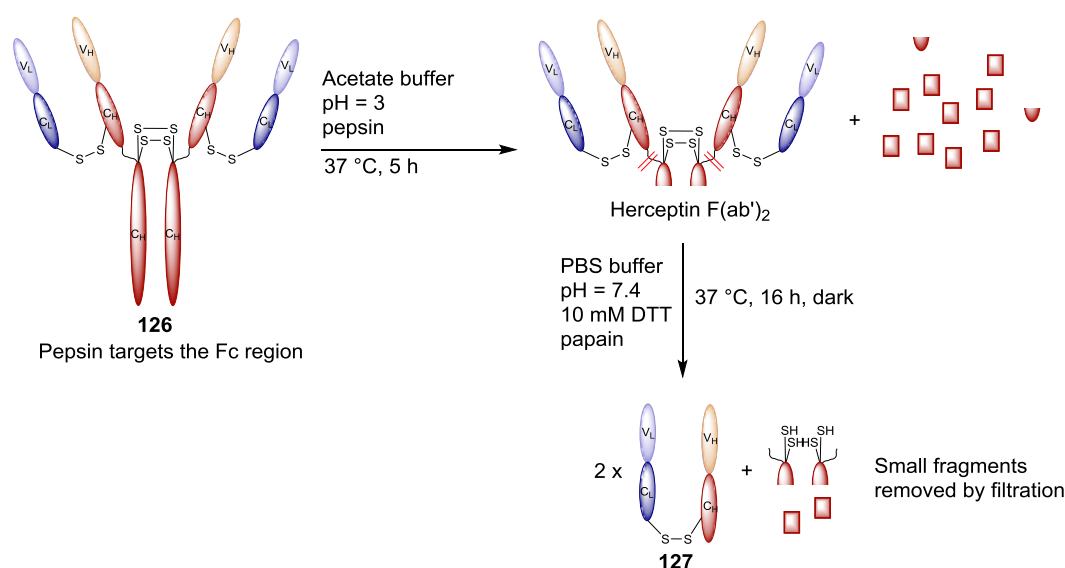
The prevalence of these peaks after irradiation indicates that the photochemical thiomaleimide [2+2] cyclisation is considerably lower yielding on the full antibody than it is on the smaller fragments. Reasons for this decreased reactivity could be secondary interactions within the larger quaternary structure of the protein or “intramolecular” bridging between cysteines in the hinge region i.e. cysteine bridging between residues on the same heavy chain. Incomplete bridging is a common occurrence even with next generation maleimide reagents,<sup>156</sup> which avoid the additional photochemical step, so the complex mixture obtained from this reaction was not entirely unanticipated. Due to these problems work with the full Rituxan antibody was not taken further.

## 2.2.5: Modification of Herceptin Fab

### 2.2.5.1: Preparation of Herceptin Fab fragments

In addition to testing the scope of the reaction with regards to the maleimide functionalisation it was also desirable to test its applicability to the antibody fragments of a different parent immunoglobulin. Herceptin is a humanised monoclonal antibody commonly utilised in antibody therapy,<sup>173,284,285</sup> and thus a desirable candidate for the photochemical thiomaleimide [2+2] cyclisation. Due to the problems associated with the reaction on the larger full Rituxan antibody 100, and the success of the reaction on Rituxan Fab 101, it was decided the Herceptin Fab fragment 127 would be used. Preparation of Herceptin Fab 127 from a sequential enzymatic digestion of full Herceptin 126 proceeded in a high yield. Herceptin 126 was digested first with the enzyme pepsin, which targets sites on the Fc region below the “hinge”, producing a Herceptin F(ab)<sub>2</sub> fragment and multiple smaller

protein fragments. Subsequent digestion with papain cleaves the hinge region, yielding pure Herceptin Fab **127** after size exclusion filtration (Scheme 57).



**Scheme 57**  
Production of the Herceptin Fab **127** through sequential enzymatic digest.

### 2.2.5.2: Modification of Herceptin Fab

Using the optimised protocol developed during the work with Rituxan Fab **101**, Herceptin Fab **127** was reduced, *bis*-modified and irradiated. Borate buffered saline (BBS) at pH = 8 was used in place of PBS as this was found to improve reduction efficiency. The decision to perform irradiation at pH = 6 will be discussed later in this chapter. Bromomaleimides **93**, **114**, and **117** (N-H, N-OEG and N-Biotin respectively) were chosen for conjugation based on the previous success of their photochemical thiomaleimide [2+2] reactions. Irradiation in this case was performed using the more powerful UVG-2 torch resulting in decreased irradiation times (Scheme 58). Successful photochemical [2+2] cyclisation and rebridging in each case was shown using SDS-PAGE (Scheme 58) and LCMS (Figure 37). The results mirrored those obtained with Rituxan Fab **101** demonstrating the applicability of this reaction towards different antibodies. Analysis of the SDS-PAGE gel by densitometry gave a bridging conversion of 85% for Herceptin Fab conjugate **129<sub>a</sub>**, and 80% for conjugates **129<sub>b</sub>** and **129<sub>c</sub>**. LCMS analysis of bridged conjugate **129<sub>b</sub>** and **129<sub>c</sub>** revealed additional peaks which could not be identified, though did contain an intact bridge between cysteine residues. The relative intensity of these peaks was found to vary considerably between repeated injections onto the LCMS, suggesting they resulted from fragmentation or addition during ionisation.



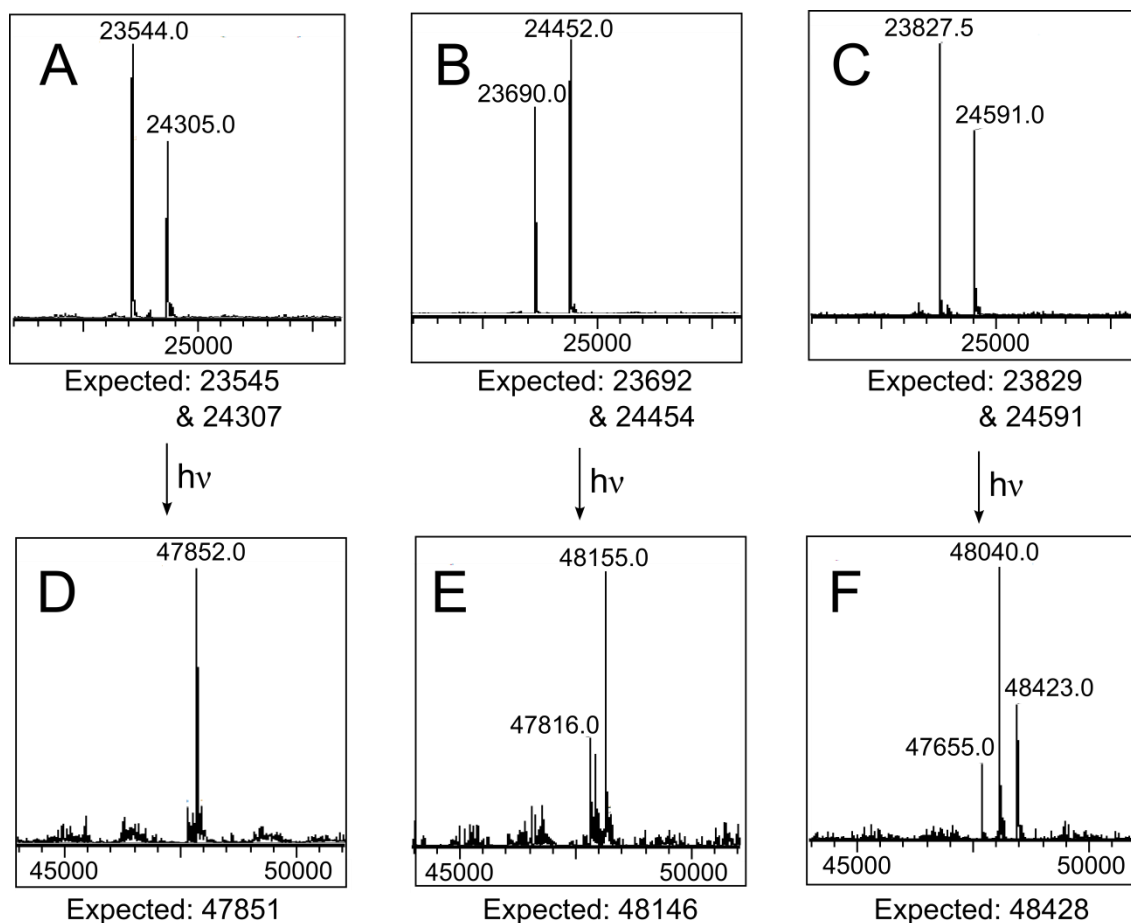


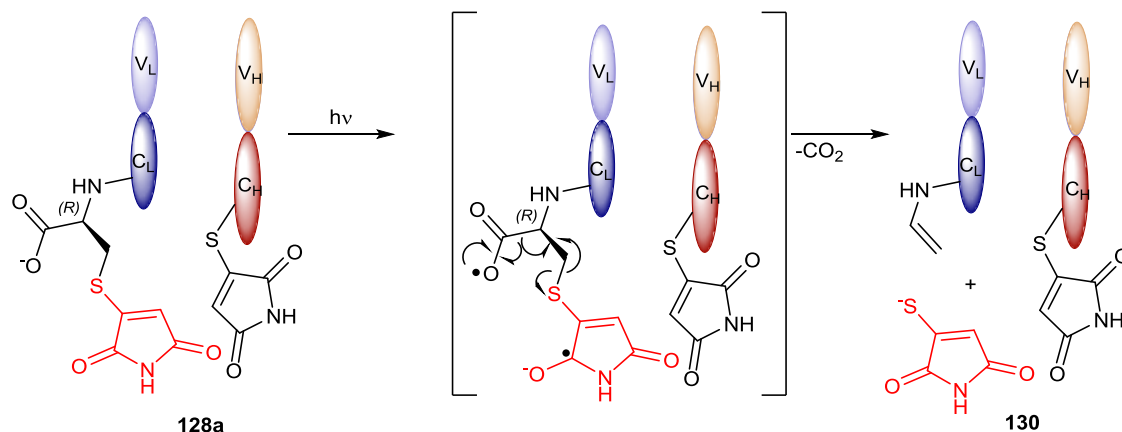
**Figure 37**  
**LCMS data for the modification and irradiation of Herceptin Fab 127 with functionalised maleimides; (A) *bis*-modified conjugate 128<sub>a</sub>, (B) *bis*-modified conjugate 128<sub>b</sub>, (C) *bis*-modified conjugate 128<sub>c</sub>, (D) bridged conjugate 129<sub>a</sub>, (E) bridged conjugate 129<sub>b</sub>, (F) bridged conjugate 129<sub>c</sub>. For full spectra see experimental section (Section 3.2.5.2, page 196).**

The success of these reactions on the Herceptin Fab fragment was expected, given the structural similarities between Rituxan and Herceptin. Bridged Herceptin-Fab fragment **129<sub>a</sub>** was tested in the same thiol stability assay employed for Rituxan Fab **103** (Scheme 50, Figure 31) and showed complete thiol stability. As a result, the general applicability of this method for generating thiol stable *bis*-modified Fab fragments has been demonstrated.

## 2.2.6: C-terminal decarboxylation of Fab Fragments

Throughout the work with Fab fragments incomplete bridging was observed in all cases, particularly with *bis*-modified Rituxan Fab conjugates **118<sub>a</sub>** and **118<sub>d</sub>**. Extended irradiation did not increase the bridging yield, hinting at a competing side reaction. Appearance of a common peak, independent of the functionalisation on the maleimide, in the LCMS spectra after irradiation suggested this side reaction resulted in loss of the maleimide. In each case the mass of the peak corresponded to a loss of the maleimide and a further 76 Da from the light chain of the maleimide. This was particularly obvious in the case of Rituxan Fab **118<sub>a</sub>**, as a change in mass of the light chain could be seen on the SDS-PAGE (Figure 32) and

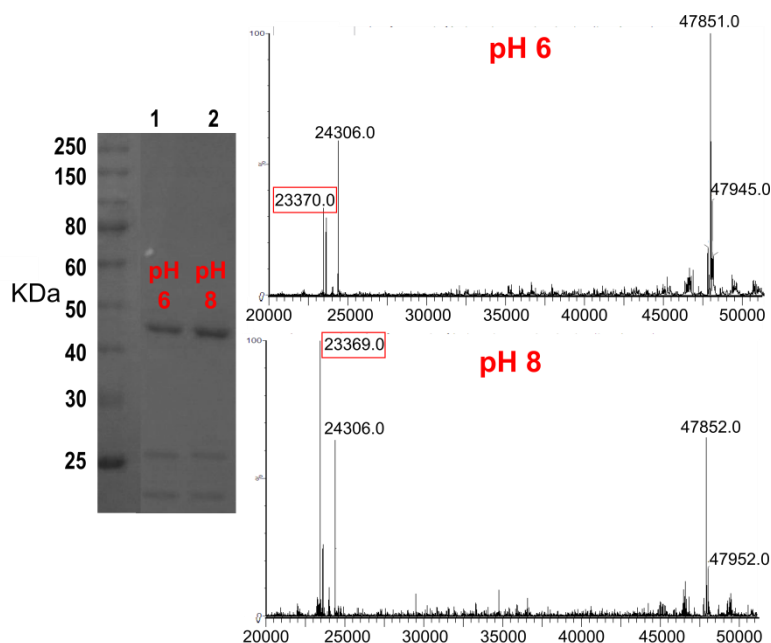
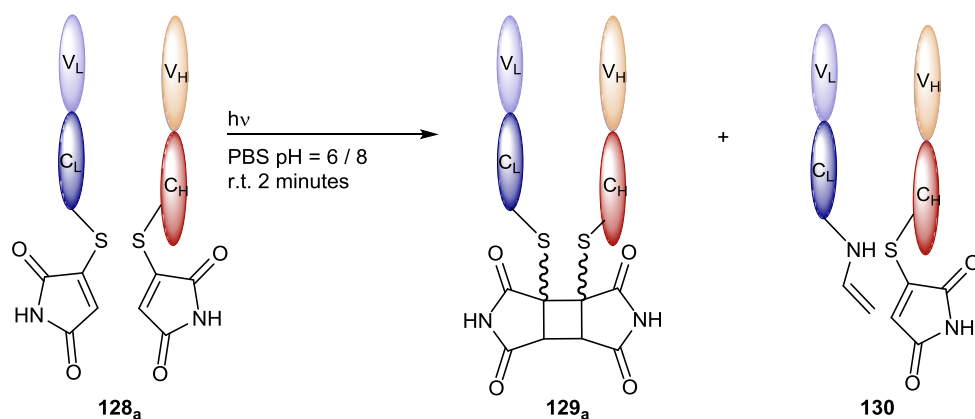
the LCMS (Figure 33E). Both Rituxan Fab **101** and Herceptin Fab **127** form disulfide bonds between the C-terminus of the light chain and an internal cysteine on the heavy chain; a feature shared amongst all Kappa type immunoglobulins. Thus the light chains on the Fab conjugates all contain C-terminal cysteine-maleimides, opening up decarboxylative reaction pathways. Based on the LCMS and SDS-PAGE data a photochemical decarboxylation was proposed (Scheme 59).



**Scheme 59**

**A proposed mechanism for the loss of mass from the light chain and formation of a decarboxylated Fab fragment, demonstrated using Herceptin Fab conjugate **128<sub>a</sub>**.**

Similar photochemical processes have been extensively studied on carboxyl containing phthalimides (Section 1.1.3.1, page 23).<sup>81,286–289</sup> Based on this hypothesis it was decided to test the effect of pH on the irradiation of *bis*-modified Herceptin Fab conjugate **128<sub>a</sub>**. Solutions of Herceptin Fab conjugate **128<sub>a</sub>** at pH 6 and pH 8 were irradiated for two minutes and compared (Scheme 60). LCMS analysis suggests that increasing the pH increases the formation of the side product, evidenced by an increase in the relative height of the peak corresponding to the proposed decarboxylative side product **130**. However, it is important to note that quantification by mass spectrometry is not possible due to the differences in ionisation of the two products. This problem is particularly highlighted in the LCMS of *bis*-modified Herceptin Fab **128<sub>a</sub>** irradiated at pH = 8, which suggests that decarboxylated Herceptin Fab **130** is the major product (Figure 38). Analysis by SDS-PAGE clearly contradicts this and in fact suggests that the difference between irradiation at pH = 6 and pH = 8 is minimal (Figure 38). Due to the simplified LCMS spectra irradiation of *bis*-modified Herceptin fragments **128<sub>a-c</sub>** in the optimised protocol was performed at pH = 6.



#### Scheme 60

Testing the affect of pH on the formation of proposed side product 130.

#### Figure 38

Analysis by SDS-PAGE and MS showing the difference in the photochemical [2+2] cycloaddition of *bis*-modified Herceptin Fab 128<sub>a</sub> at pH = 6 and pH = 8. The red box highlights decarboxylated Herceptin Fab 130.

In order to rule out non-photochemical pathways for the reaction *bis*-modified conjugate 128<sub>a</sub> was incubated both at room temperature and 37 °C for one hour. No change in LCMS trace was seen, suggesting the side reaction was purely photochemical in nature. That being said a peak corresponding to the same loss of mass from the light chain has been observed with dibromomaleimide bridging reagents under non-photochemical conditions.<sup>275</sup> This suggests there may also be a considerably slower thermal route to the product. Further exploration of this reaction is described in the following section (Section 2.3, page 90).

### 2.2.7: ELISA data for Herceptin Fab conjugates

After demonstrating the success of the photochemical thiomaleimide [2+2] cycloaddition on antibody fragments it was necessary to demonstrate that the reaction does not have a

negative impact on the antigen binding ability. ELISAs (Enzyme Linked Immunosorbent Assays) are regularly employed for detection and quantification of antibody binding.<sup>290</sup> The antigen against the antibody of interest is typically immobilised on the surface of a polystyrene plate before being incubated with a solution containing the antibody to be studied. Binding of the antibody to the antigen is then quantified by addition of a secondary antibody which is linked to an enzyme that catalyses a colourimetric reaction. Due to the specificity between the enzyme and the antibody the intensity of the colour is proportional to the amount of antibody bound to the plate. Protocols for ELISA affinity testing for Herceptin have been previously described,<sup>144</sup> thus Herceptin was chosen over Rituxan for affinity testing. Both Herceptin conjugates, *bis*-modified **128<sub>a</sub>** and bridged **129<sub>a</sub>**, showed a strong affinity for the HER2 antigen, as did the native Herceptin Fab **127**. A slight drop in binding affinity is seen in bridged Herceptin Fab **129<sub>a</sub>** though this was not large enough to cause major concern (Figure 39).

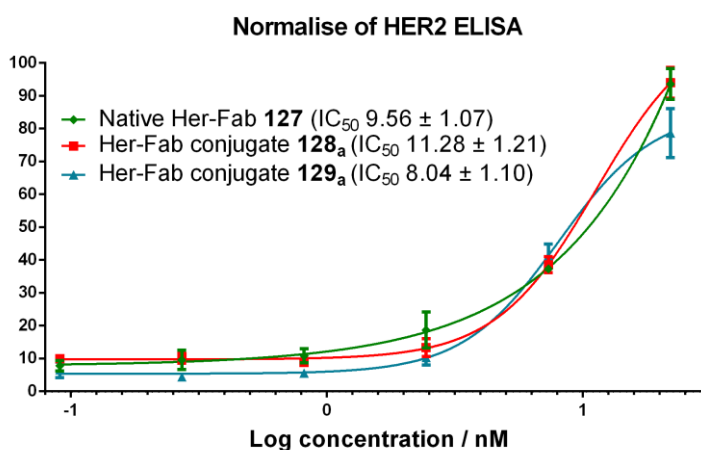


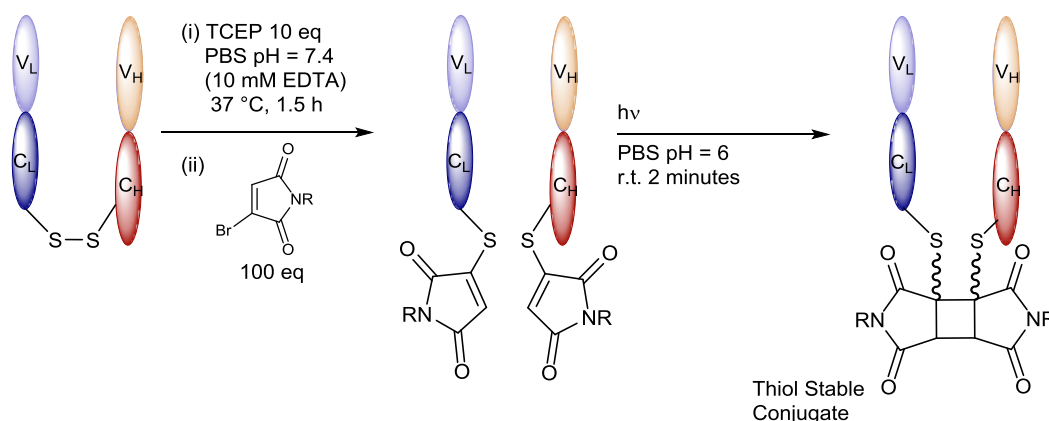
**Figure 39**  
An ELISA against HER2 antigen for native Herceptin Fab **127** and Herceptin Fab conjugates **128<sub>a</sub>** and **129<sub>a</sub>**. See section 3.2.5.3, page 201 for details.

Retention of the binding capability of Herceptin Fab conjugates **128<sub>a</sub>** and **129<sub>a</sub>** was expected as the modification occurs distal to the binding site of the protein. Any topological changes to the protein at the modification site have a negligible effect on the structure of the antigen binding region. These positive results further demonstrate the suitability of this reaction for antibody conjugation.

## 2.2.8: Conclusions and future work

The thiomaleimide photochemical [2+2] cyclisation was successfully applied to an scFv fragment and the Fab fragments of two clinically relevant antibodies, Rituxan and Herceptin. A small library of functionalised thiol-stable Fab conjugates was generated through a three step protocol which includes a highly efficient thiomaleimide [2+2] photocycloaddition (Scheme 61). The reaction was also attempted on the full antibody

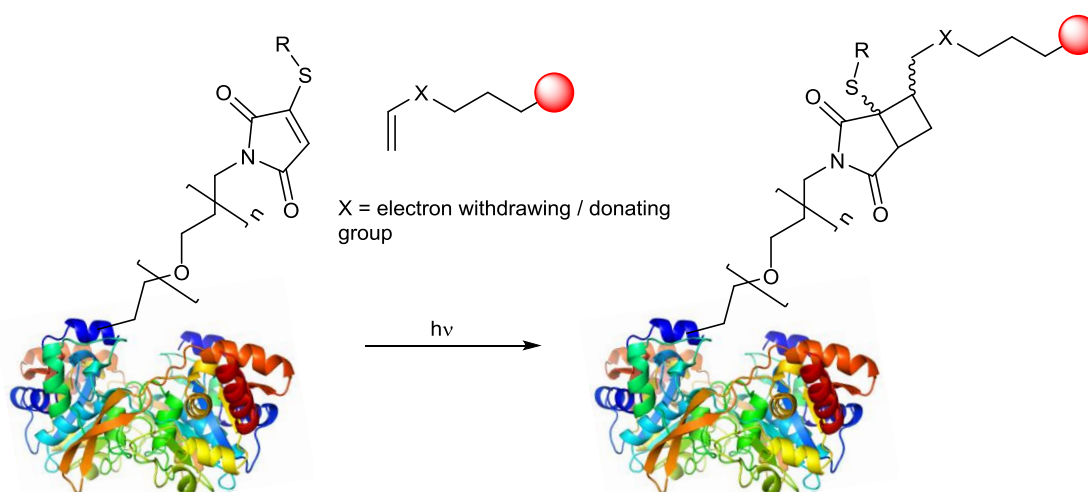
Rituxan, though the additional complexity of the protein reduced the rebridging efficiency of the reaction.



**Scheme 61**  
An optimised protocol for the generation of thiol stable Fab fragments.

The next logical step in this work would be to attach a drug to the imide nitrogen and generate a thiol-stable Fab ADC. This construct could then be compared to both traditional maleimide ADCs and also bridged maleimide ADCs for *in vivo* stability and efficacy against a target disease.

A different use for the photochemical thiomaleimide [2+2] cyclisation could be in the development of a novel bioorthogonal “photo click” reaction. By finding a suitable olefin to act as an electron acceptor the reaction could be used as a reagent free method for clicking chemical payloads to proteins of interest (Scheme 62).

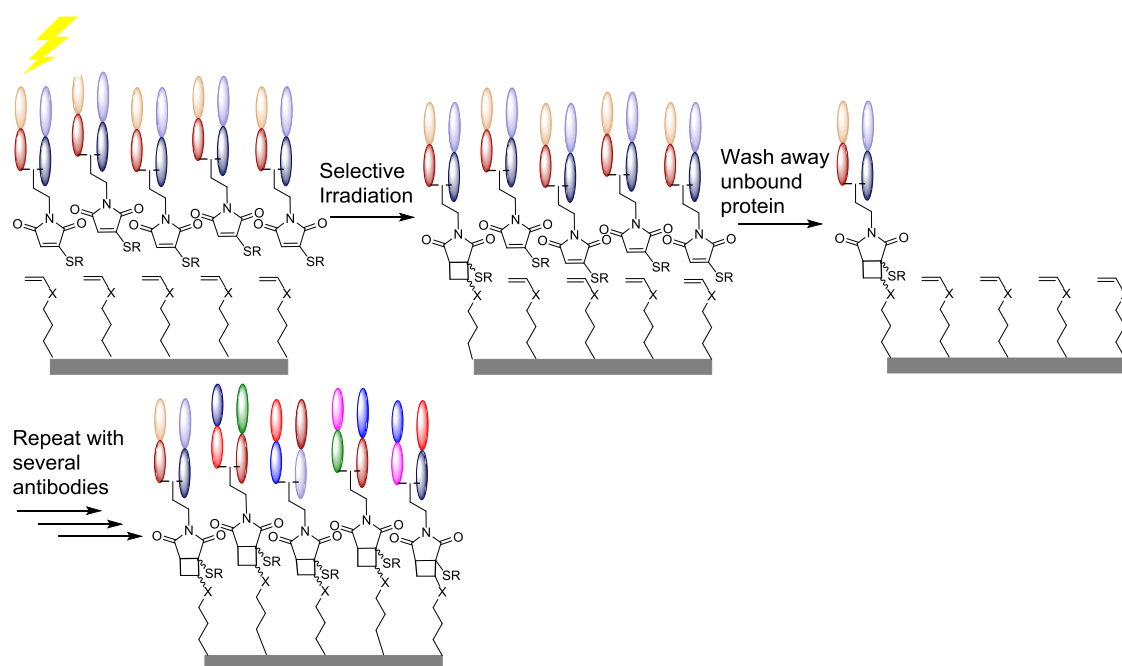


**Scheme 62**  
A proposed photochemical “click” reaction utilising the photochemical thiomaleimide [2+2] cyclisation.

The success of this reaction depends entirely on the efficiency of the intermolecular photochemical [2+2] cyclisation. Typically, very high concentrations are required for intermolecular photochemical transformations due to the short lived nature of the excited

state. At low concentrations a successful collision between an excited state molecule and its reactive partner is statistically unlikely. For these reasons historical methods for photochemical “click” reactions have relied on using photoactive cages to mask reactive species which can become active upon irradiation.<sup>291,292</sup> Excellent work based on tetrazole constructs utilises this approach to great effect.<sup>293–295</sup> However, typical yields of less than 60% limit the utility of this approach. Other methods such as the thiol-ene photoclick are limited by the necessity of a photosensitiser.<sup>296</sup> Highly efficient intermolecular photochemical cyclisations, such as the photochemical thiomaleimide [2+2] cyclisation, could prove a valuable addition to this field.

The photochemical thiomaleimide [2+2] reaction could also be employed for photochemical surface patterning. We envisage a system in which a solid support is modified with a suitable olefin to act as an electron acceptor for the maleimide. The support could then be incubated in a solution containing a thiomaleimide-modified structure of interest. Selective irradiation at a particular location on the support would form a covalent cyclobutane bridge between the structure and the support, while the remaining non-bound structure could be easily removed. Of particular interest would be the site selective immobilisation of antibodies onto surfaces. By repeating the process above with multiple antibodies against different antigens a multi-functional patterned surface could be generated for diagnostic purposes (Scheme 63).



**Scheme 63**  
**A conceptual method for photochemically modifying surfaces with antibody fragments.**

The success of this technique depends upon the same parameters as the photochemical click technique mentioned above. Photochemical surface derivatisation has been

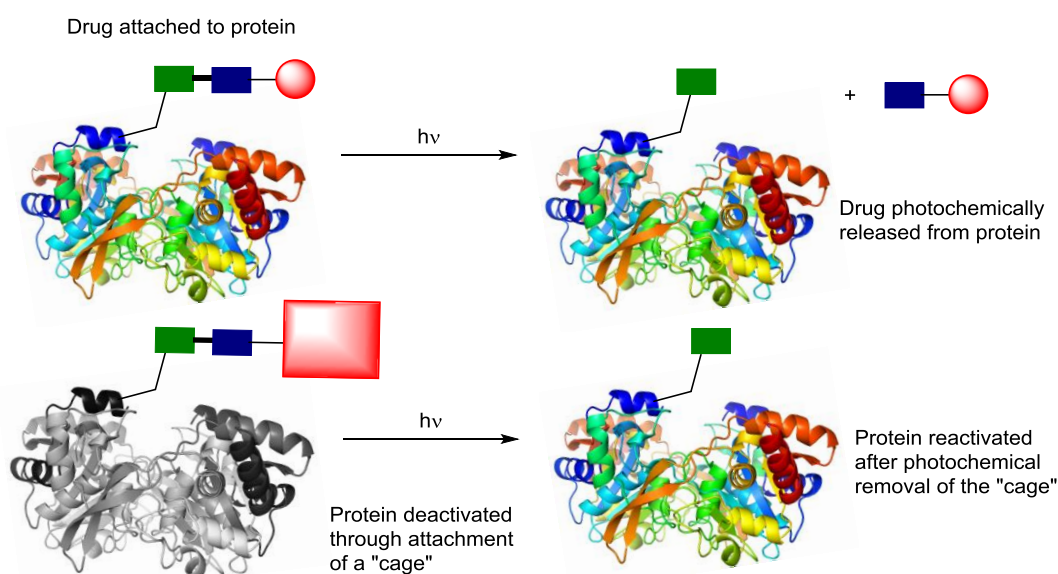
extensively researched and several excellent methods exist based on the photoclick reactions listed above. That being said, the high efficiency, biocompatibility and simplicity of the photochemical thiomaleimide [2+2] cyclisation could arguably make a useful contribution to the field.

## 2.3: C-terminal cysteine thiomaleimide decarboxylations

### 2.3.1: Aims and introduction

Whilst studying the photochemical thiomaleimide [2+2] cyclisation on antibody Fab fragments an interesting side reaction was observed. This reaction led to cleavage of the maleimide from the light chain of the protein and was tentatively assigned as a decarboxylation process initiated by photoexcitation of the maleimide (page 85, Scheme 59). Due to the size and complexity of the protein complete structural assignment of the proposed side-product was not possible.

The ability of the reaction to cleave the maleimide from the protein could provide a useful tool to photochemically cleave small molecule payloads from proteins, a powerful method for targeted therapeutics. The same reaction could also be employed for photochemical protein "uncaging" (Scheme 64).

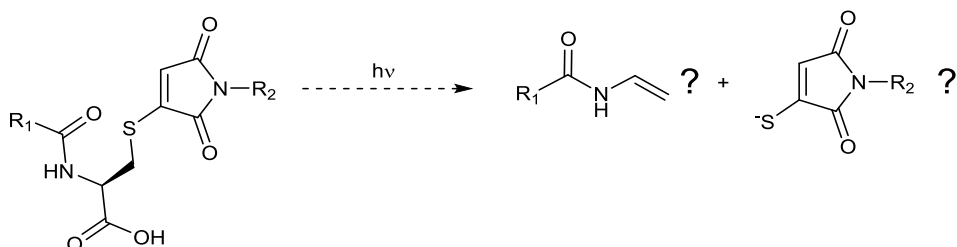


**Scheme 64**  
**Applications of photocleavable linkers.**

Current methods for photochemical uncaging are dominated by nitrobenzyl based photocleavable linkers which suffer from low yields, long reaction times, and potentially toxic by-products.<sup>89</sup> By studying this side reaction further we hoped to make a contribution to the field of photocleavable linkers and provide an alternative means of photochemical drug delivery and photochemical uncaging.

## Aims

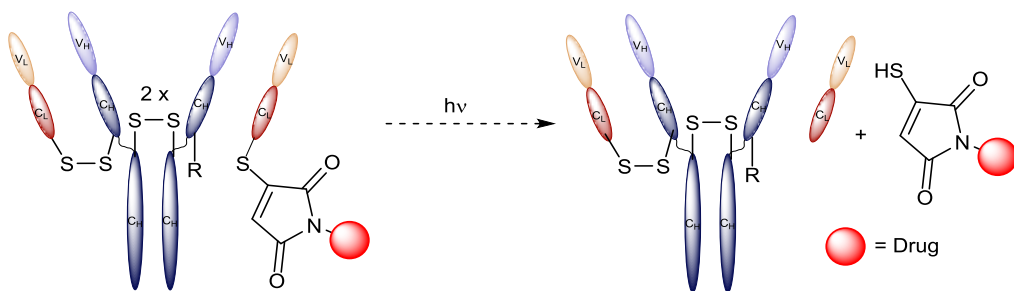
The first aim of this work was to use traditional synthetic and spectroscopic techniques to explore the proposed decarboxylative reaction observed with Kappa IgG1 Fab fragments. Though similar reactions have been studied on phthalimides<sup>81,286–288,297,298</sup> no such transformation has been reported with maleimides. Successful confirmation of the reaction would mean the discovery of a novel photochemical transformation and expand the photochemical reactivity of substituted maleimides (Scheme 65).



**Scheme 65**

**A proposed small molecule study to confirm the theorised photochemical decarboxylation.**

The second aim of this work was to use the knowledge gained to design a novel photocleavable linker based around the maleimide scaffold for use in protein uncaging or photochemical drug delivery, with particular focus on the development of photocleavable antibody drug conjugates (Scheme 66). At the time of writing very few examples of photocleavable ADCs exists in the literature<sup>245</sup> and any developments would represent a considerable contribution to the field of targeted therapeutics.



**Scheme 66**

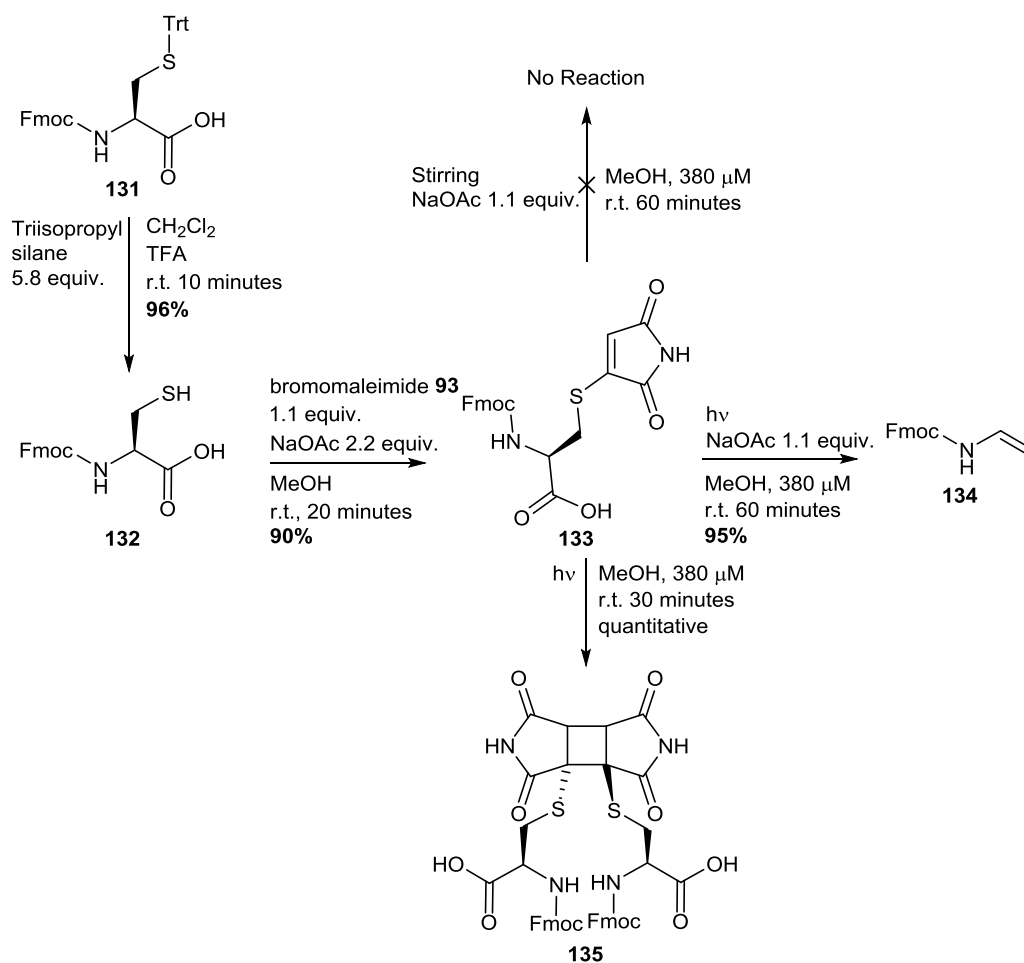
**A proposed photocleavable antibody drug conjugate utilising a maleimide based photocleavable linker.**

## 2.3.2: Small molecule models of C-terminal cysteine decarboxylation

### 2.3.2.1: Synthesis and irradiation of a single cysteine model

C-terminal Fmoc-L-cys-maleimide **133** was synthesised from readily available starting materials. Trityl deprotection of Fmoc-L-cys(Trt) **131** gave Fmoc-L-cys **132**, which was subsequently reacted with bromomaleimide **93** to furnish the desired compound **133** in an excellent yield. The bulky Fmoc group was employed to discourage competing

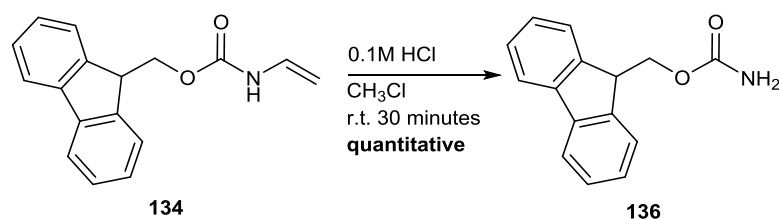
photochemical [2+2] cyclisation. Irradiation of **133** at low concentration (380  $\mu\text{M}$ ) using a UVG-2 365 nm torch in the presence of base resulted in complete consumption of the starting material and produced the suspected enecarbamate **134** in an isolated yield of 95% within one hour. Irradiation with a medium pressure mercury lamp reduced the reaction time to 20 minutes with no detrimental effect on the yield (93%). As a control Fmoc-L-cys-maleimide **133** was irradiated in the absence of base and showed no decarboxylation, producing only [2+2] cyclisation product **135**. This demonstrates the necessity of the carboxylate for this reaction and provides mechanistic insight. Stirring a solution of Fmoc-L-cys-maleimide **133** with base for one hour showed no reaction, ruling out potential non-photochemical routes to the product under these conditions (Scheme 67).



**Scheme 67**  
The synthesis and irradiation of Fmoc-L-cys-maleimide **133**.

Initially isolation of enecarbamate **134** was problematic. However, this was discovered to be the result of degradation of the enecarbamate product to the carbamate. Attempts to purify the irradiated mixture by silica gel chromatography produced confusing results as the mildly acidic nature of the silica is sufficient to promote this conversion. By changing the purification protocol to a simple extraction procedure isolation of the enecarbamate was possible. It is of interest to note that enecarbamate **134** appears to be unstable in

deuterated  $\text{CHCl}_3$  with significant conversion to the carbamate observed in samples left overnight. To test for acid catalysed degradation isolated enecarbamate **134** was subjected to a mildly acidic environment. Quantitative conversion to carbamate **136** was observed, providing evidence for the suspected degradation pathway (Scheme 68). The most logical mechanism for this process is tautomerisation of the enamide to the Schiff base, followed by acid catalysed hydrolysis to the carbamate.



**Scheme 68**  
The acid catalysed hydrolysis of enecarbamate **134** to carbamate **136**.

At the time of writing there appears to be no examples of enecarbamate hydrolysis in the literature, though some hydrolysis studies of structurally similar enamides can be found.<sup>299</sup> This is surprising as enecarbamates have been employed as synthetic building blocks.<sup>300–302</sup>

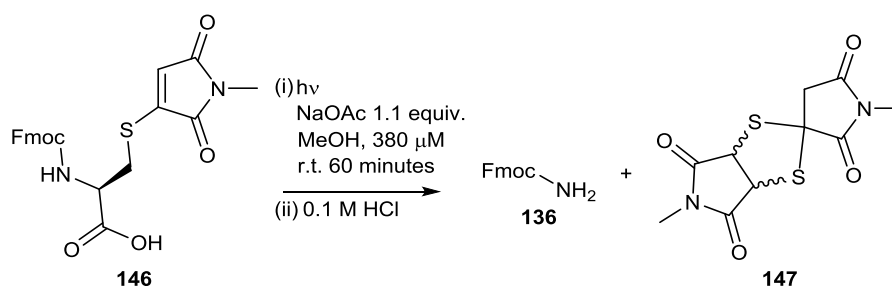
### 2.3.2.2: C-terminal decarboxylation of a dipeptide model

To provide a second model of this reaction dipeptide-maleimide **143** was synthesised via a simple convergent route. This model more closely resembles the reaction on a protein due to the adjacent amide bond, as opposed to the carbamate bond present in Fmoc-L-cys-maleimide **133**. Thus upon irradiation an enamide, rather than an enecarbamate, would be produced. NHS-Ester **138** was readily synthesised in excellent yield from Fmoc-L-phenylalanine **137** using EDC and DMAP. Subsequent coupling with L-cysteine(Trt) **140** proceeded smoothly to furnish dipeptide **141**. Removal of the trityl group followed by conjugate addition to bromomaleimide **93** furnished dipeptide-maleimide **143** in an overall yield of 33%. Irradiation of **143** in the presence of base produced enamide **144** in an 81% yield (Scheme 69).





Repeating the experiment with immediate quenching of the reaction using HCl after irradiation resulted in the rapid disappearance of the yellow colour (Scheme 71). NMR analysis of this crude mixture revealed the suspected carbamate **136** and small amounts of a proposed succinimide dimer **147**.



**Scheme 71**  
Irradiation of Fmoc-L-cys-N-methylmaleimide **146** with immediate quenching.

Though the complexity of the crude mixture made NMR analysis difficult, DEPT, HMBC (Figure 40) and HSQC techniques suggested the major impurity was dimer **147**. Correlations between the N-methyl groups and the carbonyls show one symmetrical succinimide and one asymmetrical succinimide. This is supported by the HMBC correlations between the CH<sub>2</sub> protons on each ring system. A quaternary carbon at  $\delta = 61.5$  is indicative of an aliphatic carbon adjacent to two hetero atoms. These assignments are supported by similar structures reported in the literature.<sup>148</sup> Unfortunately no further structures could be identified and full characterisation of the impurity was not possible.

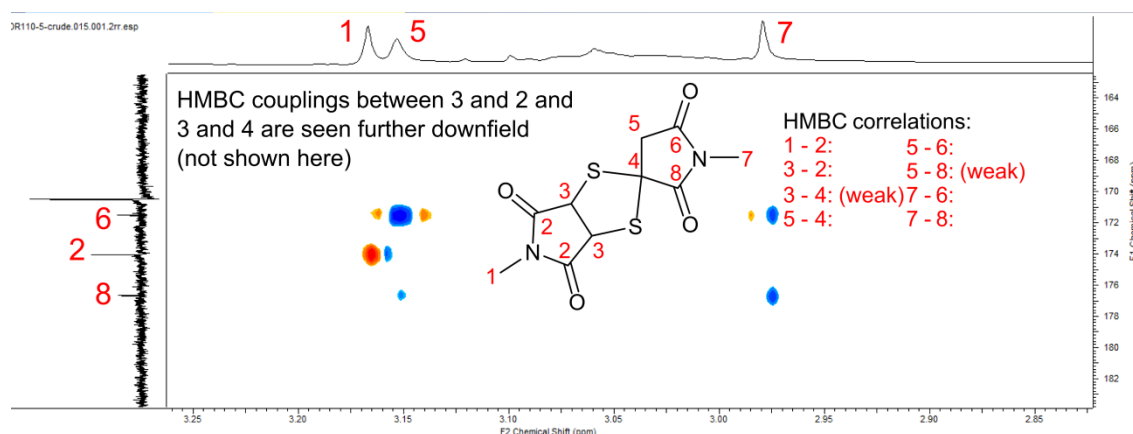
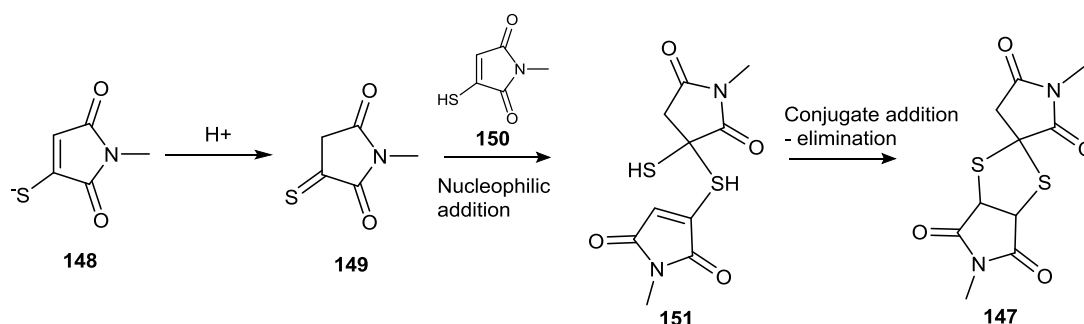


**Figure 40**  
A HMBC spectrum showing long distance couplings in support of dimer **147**.  
HMBC couplings between 3 and 2 and 3 and 4 are seen further downfield.

This analysis confirmed that the released maleimide is able to react with itself and supports the polymerisation theory. Possible mechanistic explanations for the formation of dimer **147** are provided below. Upon acidification thiolate **148** could convert to thioketone **149**. Subsequent nucleophilic addition from thiol **150**, which results from tautomerisation of

thioketone **149**, results in intermediate **151**. Intramolecular conjugate addition onto the remaining maleimide would then result in formation of dimer **147** (Scheme 72).



**Scheme 72**  
Potential mechanisms for the formation of dimer **147**.

This mechanism does not fully explain why dimer **147** is only observed if the reaction is quenched with HCl. It is possible that under basic conditions the maleimide exists as thiolate **148** which could be more likely to undergo extended polymerisation rather than form dimer **147**. At the present time any proposed mechanism is purely speculative and further study is required to truly understand this process.

#### UPLC-MS studies

With evidence suggesting that polymerisation was responsible for the loss of the released maleimide it was decided to analyse the reaction using UPLC-MS. The more sensitive technique allows reactions to be monitored at a low concentration, potentially alleviating issues of polymerisation. Fmoc-L-cys-N-methylmaleimide **147** was irradiated for 50 minutes with samples taken every 10 minutes. UPLC-MS analysis scanning at 254 nm clearly showed the disappearance of the starting material **147** (7.78 minutes) and the appearance of enecarbamate **134** (8.42 minutes). Upon addition of HCl enecarbamate **134** can be seen degrading to carbamate **136** (6.27 minutes). Standard solutions of enecarbamate **134** and carbamate **136** were injected to confirm the identity of these peaks (Figure 41). ES<sup>+</sup> and ES<sup>-</sup> ionisation analysis of the peaks provided additional evidence.

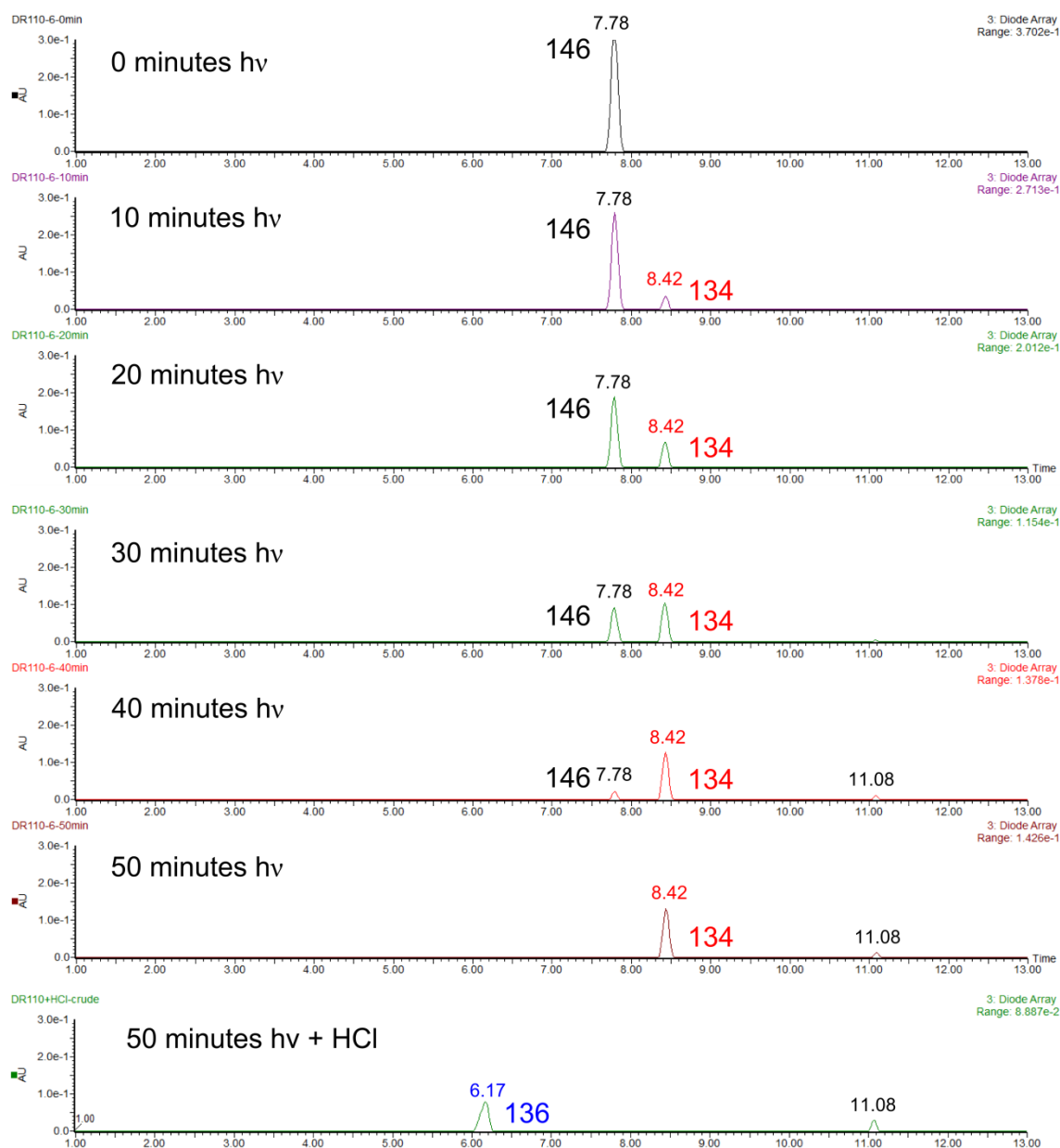


**Figure 41**  
**UPLC analysis of the irradiation of Fmoc-L-cys-N-methylmaleimide 146. Starting material 146 is observed at 7.78 minutes, with encarbamate 134 appearing at 8.42 minutes. Carbamate 136 appears at 6.17 minutes after addition of HCl. LC traces of standard solutions of 146, 134 and 136 can be found in the experimental section (section 3.1.2.3, page 154).**

After forty minutes of irradiation an additional peak at 11.08 minutes is observed. Analysis of this side product using ES+ ionisation identified several discrete mass peaks, though none correspond to a suspected polymerisation product. Ionisation using ES- mode produced equally inconclusive results (Figure 42).

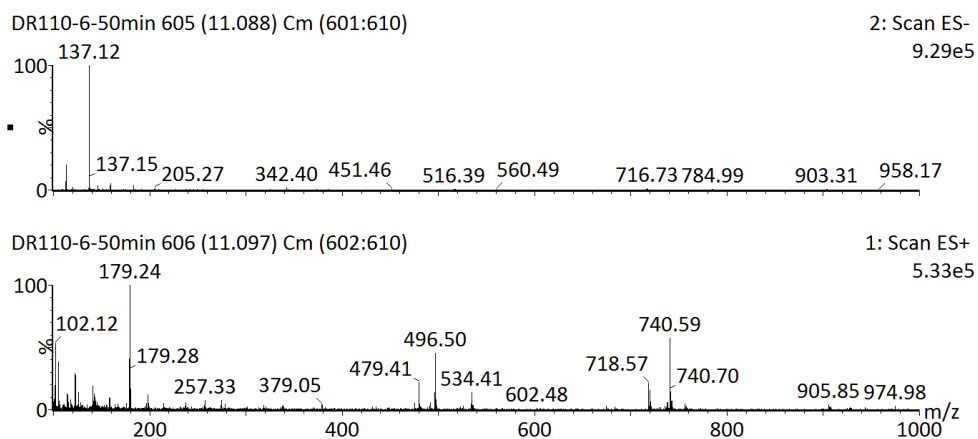
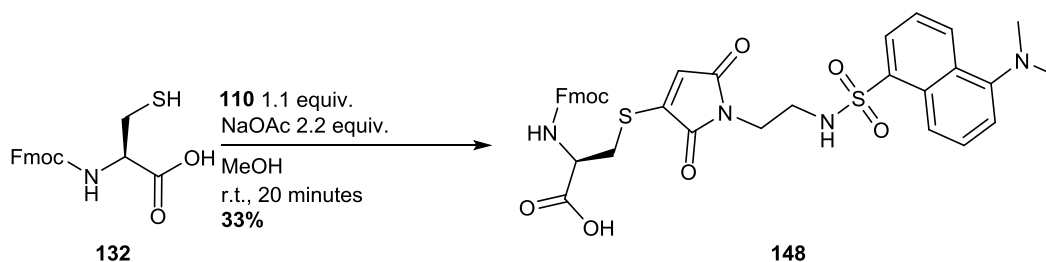


**Figure 42**  
ES- and ES+ ionisation patterns from the peak at 11.08 minutes (Figure 41).

Unfortunately, no additional peaks could be seen either by the LC trace or the mass trace. Scanning the ionisation trace for suspected polymer fragments, including dimer **147**, was equally unfruitful. Several LC solvent systems were assessed, in case the polymer was being retained on the column, but returned no positive results. These results were perplexing as there is a clear formation of a yellow colour during the reaction, so it stands to reason that the responsible compound should be observable. In order to rule out the possibility that interaction with the column was affecting the results a solution of **147** irradiated for one hour was analysed directly by ESI. Encarbamate **134** was observed though no other products could be identified.

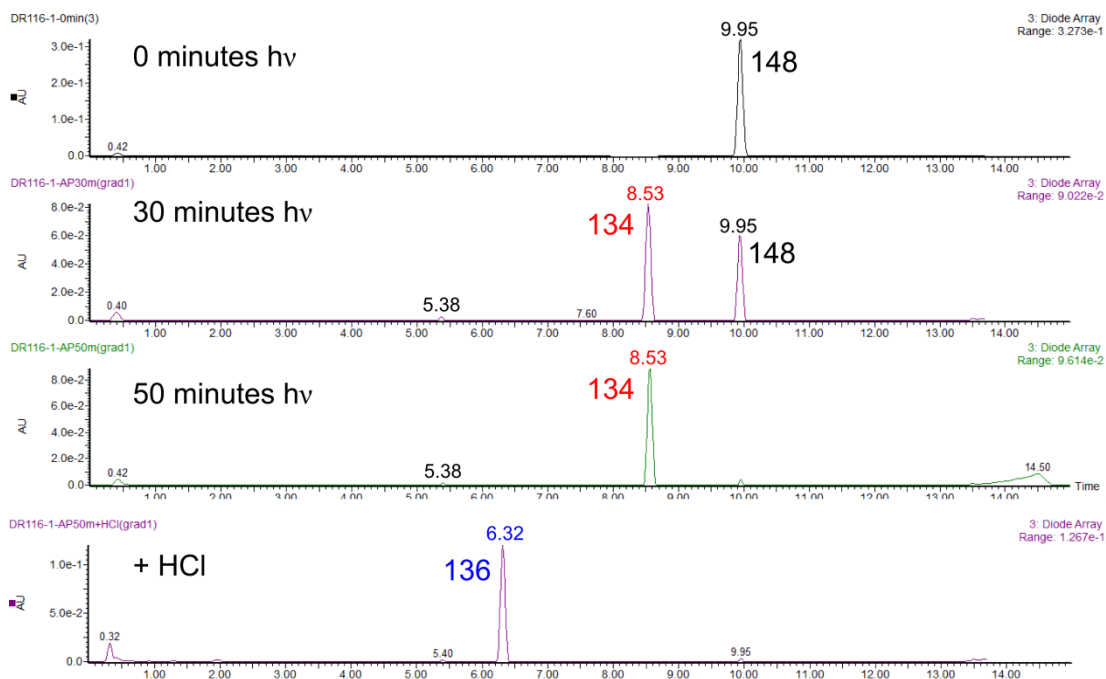
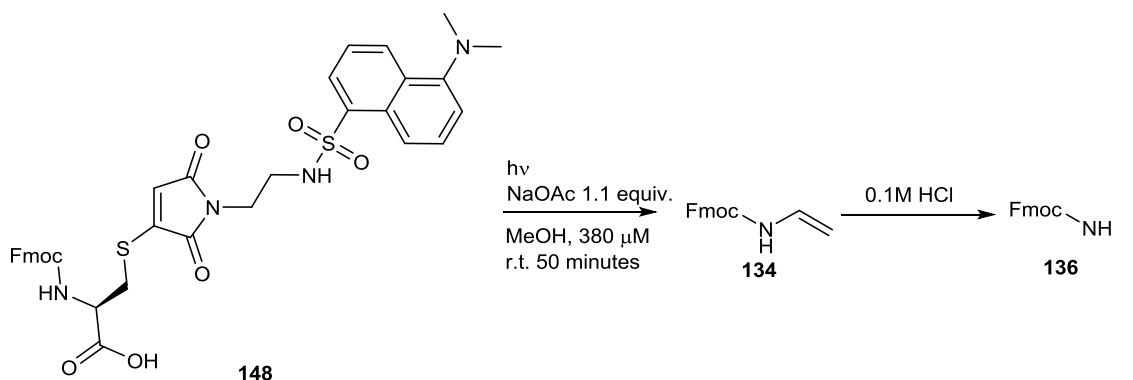
### 2.3.3.2: Synthesis and irradiation of an N-dansyl maleimide model

To attempt to ascertain further information regarding the fate of the released maleimide in the C-terminal photochemical decarboxylation Fmoc-L-cys-N-dansylmaleimide **148** was synthesised and irradiated. It was hoped that attachment of a strongly absorbing and fluorescing group to the imide nitrogen would help to locate the maleimide after photochemical cleavage. Fmoc-cysteine was reacted with previously synthesised N-dansylbromomaleimide **110** to produce Fmoc-L-cys-N-dansylmaleimide **148** (Scheme 73).



**Scheme 73**  
The synthesis of Fmoc-L-cys-N-dansylmaleimide **148**.

Irradiation of this construct was followed using UPLC-MS for a total of 50 minutes (Scheme 74) (Figure 43). Once again disappearance of the starting material **148** and appearance of enecarbamate **134** was clearly observed, though no peaks corresponding to the released maleimide could be detected at either 254 or 330 nm (dansyl absorbance<sup>305</sup>). Visible fluorescence over the course of irradiation was noticed, and TLC analysis revealed a complex mixture of fluorescent spots.



#### Scheme 74

The irradiation of Fmoc-L-cys-N-dansylmaleimide **148**.

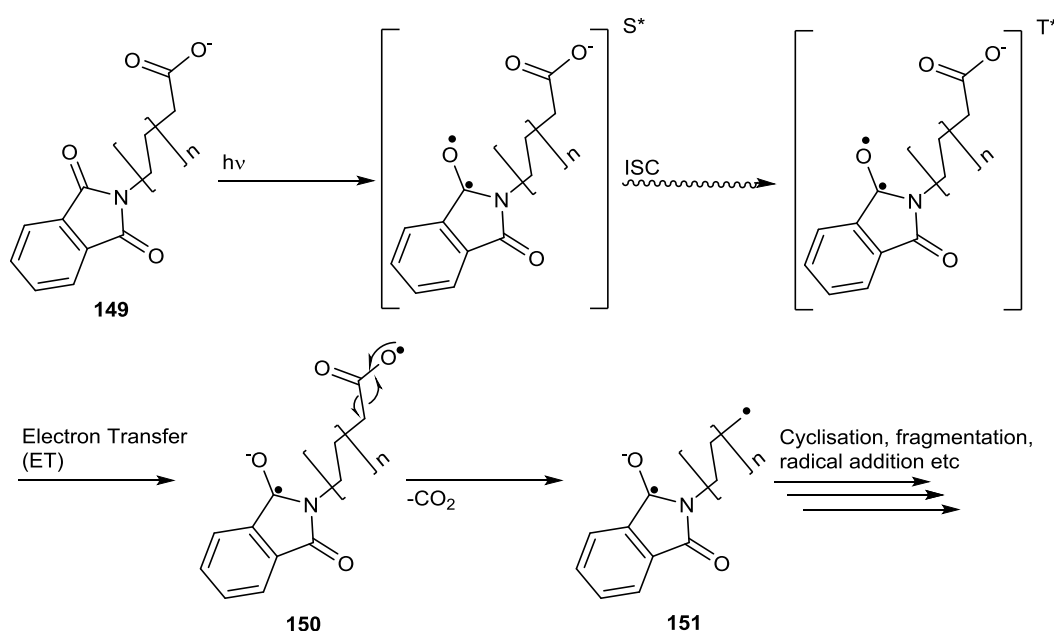
#### Figure 43

UPLC analysis of the irradiation of **148**. Starting material **148** is observed at 9.95 minutes, with enecarbamate **134** appearing at 8.53 minutes. Carbamate **136** appears at 6.32 minutes after addition of HCl. LC traces of standard solutions of **148**, **134** and **136** can be found in the experimental section (section 3.1.2.3, page 154).

The inability to confidently observe and identify the fate of the released maleimide in this reaction casts serious doubt on its application to photochemical drug delivery. Nevertheless, the reaction still represents a novel reactivity for maleimides and a high yielding photochemical method for producing enecarbamates and enamides.

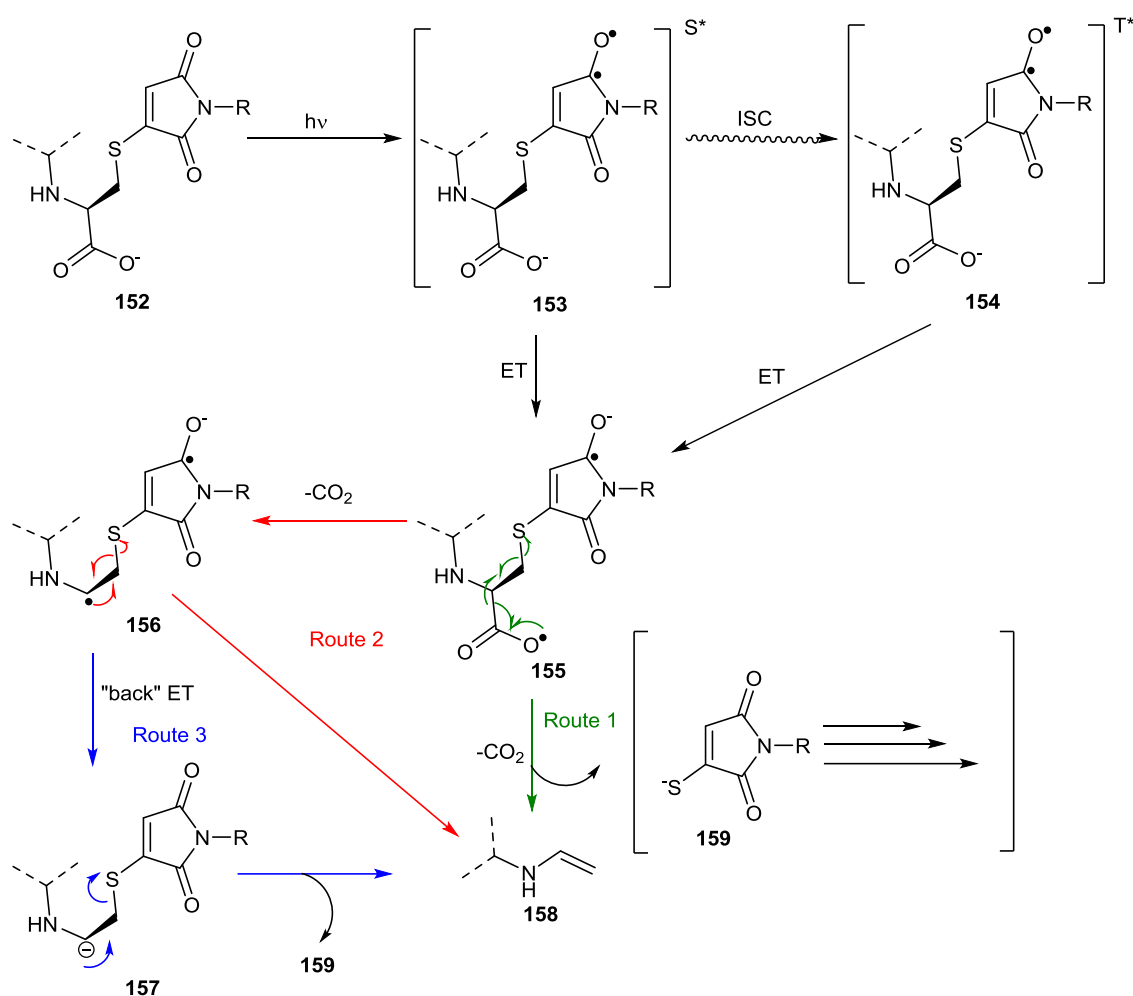
### 2.3.4: Postulated mechanism for C-terminal thiomaleimide decarboxylation

Given the novelty of this reaction it is interesting to postulate a mechanism. A considerable body of research exist on the decarboxylation reactions of phthalimides and mechanisms for this reaction have been proposed. In the generally accepted mechanism phthalimide **149** acts as an electron acceptor and the carboxylate as the electron donor in a photo-induced electron transfer (PET). The resultant carboxyl radical (**150**) decarboxylates to form carbon based radical **151** which can engage in further radical processes (Scheme 75).<sup>81</sup>



**Scheme 75**  
The mechanism of phthalimide photochemical decarboxylation proposed by Griesbeck *et al.*<sup>81</sup>

Translating this work to the maleimide-mediated decarboxylation reaction allows us to put forward several mechanisms (Scheme 76). In these proposed mechanisms the electron transfer takes place from either the singlet (**153**) or triplet (**154**) excited state. Formation of decarboxylated product **158** from the excited state could proceed as a single concerted radical elimination (route 1), or *via* intermediate **156** in a two-step process (route 2). It is also possible that intermediate **156** could engage in a “back” electron transfer from the maleimide to form a carbon centred anion (**157**), and enecarbamate **158** could subsequently form through an anionic elimination (route 3). In each case the maleimide would be released as thiolate **159** which could undergo further transformations.



**Scheme 76**  
Possible mechanisms for the photochemical decarboxylation of C-terminal cysteine-maleimides.

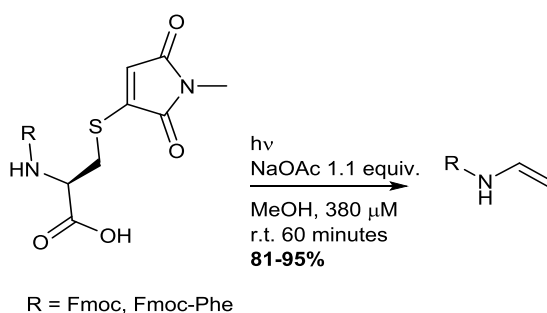
Without more detailed studies it is impossible to assign a mechanism with complete confidence, but given the similarities in photochemistry and structure between phthalimides and maleimides it is reasonable to assume parallels between the two. Laser flash photolysis studies on phthalimides by Griesbeck *et al.* deduced that the electron transfer most likely takes place from the triplet state rather than the singlet state.<sup>81,288,297</sup> With regards to the possible routes for decarboxylation (route 1, 2 or 3) it is reasonable to assume the stability of intermediate **156** would play an important role in determining the preferred pathway. Work with phthalimides has shown similar carbon centred radicals are stable enough to undergo both intra- and intermolecular radical addition reactions, and in fact this is often the preferred fate.<sup>81,286,288,298</sup> However, the near quantitative yield of enecarbamate **134** and high yield of enamide **144** suggest that an intermediate such as **156** is short lived or that a concerted mechanism is more likely. That being said, work with phthalimides has shown elimination from similar carbon centred radicals can occur as a preferred route provided the leaving group is sufficient.<sup>287</sup> Perhaps the least likely route is route 3, which involves the formation of intermediate **157** and subsequent back electron

transfer from the maleimide to the carbon centred radical. Back electron transfers with phthalimides are seldom seen and only occur in the presence of strongly electron withdrawing groups adjacent to the radical.<sup>288</sup>

Based on current evidence and the work with phthalimides it seems most likely the reaction proceeds *via* electron transfer from the triplet state followed by a concerted radical decarboxylation-elimination. However, without further work the intricacies of this particular decarboxylation remain a mystery. The knowledge gained from the study of this reaction was employed towards the generation of more general photocleavable linkers which will be discussed in the next chapter.

### 2.3.6: Conclusions and future work

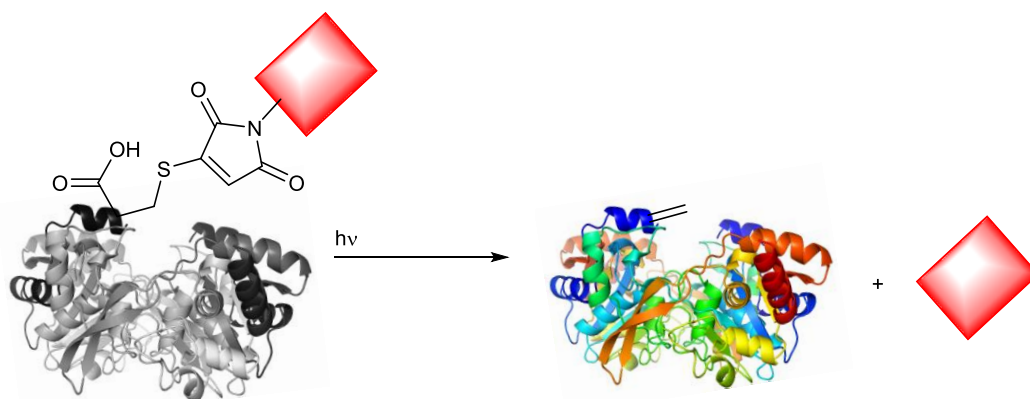
A novel thiomaleimide-mediated decarboxylation of C-terminal cysteine residues was discovered and studied using two small molecule cysteine models. The reaction proceeds rapidly to produce the corresponding enecarbamates and enamides in good yields (Scheme 77).



**Scheme 77**  
**The photochemical decarboxylation of C-terminal thiomaleimides to produce enecarbamates or enamides.**

These reactions provide the first example of a maleimide-mediated photochemical decarboxylation and expand the utility of maleimides into the realm of photocleavable linkers.

The utility of this approach is limited by the necessity of a C-terminal cysteine and an inability to isolate the released chemical payload, possibly due to extended polymerisation. This second problem precludes the use of this reaction for *in vivo* therapeutic applications due to toxicity concerns. However, the reaction could still find use in a research capacity for applications in which the identity of the released compound is unimportant e.g. photochemical protein uncaging (Scheme 78).

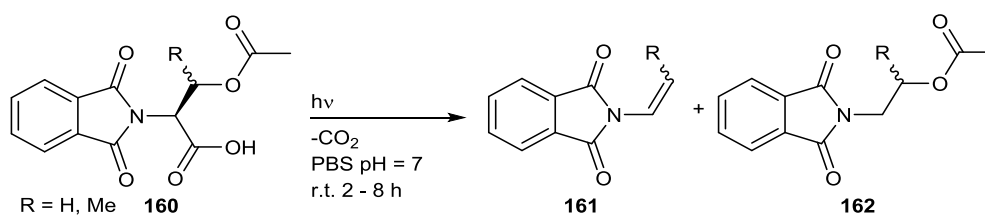


**Scheme 78**  
Utilising the maleimide-mediated C-terminal cysteine decarboxylation for protein uncaging.

## 2.4: Dithiomaleimide based photocleavable linkers

### 2.4.1: Aims and introduction

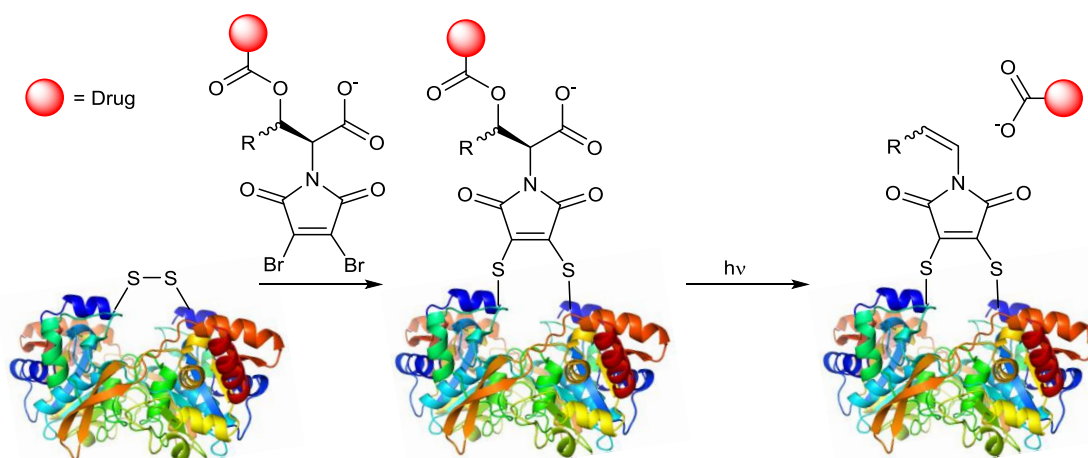
Given the significant drawbacks of the C-terminal-cysteine decarboxylation we decided to design a new set of photocleavable linkers based around the maleimide scaffold. The previous work demonstrated the ability of thiomaleimides to act as electron acceptors in photochemical electron transfer reactions and it was envisioned that this could be exploited in the design of improved maleimide based photocleavable linkers. Work by Griesbeck *et al.* showed *N*-phthaloyl-serine/threonine analogues can participate in photochemical elimination reactions *via* a decarboxylation.<sup>80,83,287</sup> A competition exists between elimination to form **161** and protonation to form **162**, with a better leaving group favouring elimination and *vice versa* (Scheme 79) (Section 1.1.3.1, page 23).



**Scheme 79**  
The photochemical decarboxylation-elimination reaction of acetylated *N*-phthaloyl-amino acid **160**.

Griesbeck *et al.* suggested this work could inform development of novel photocleavable linkers for protein uncaging. Though the reaction is high yielding, phthalimides are not ideal for biomodification as they have no built in point of attachment. A photocleavable linker based on a phthalimide structure would require an additional chemical moiety to react specifically with the protein. This complicates synthesis and decreases the appeal of this method. In addition to this the irradiation times are prohibitively long, requiring at least two hours of intense irradiation for efficient photocleavage.<sup>287</sup>

The work outlined in the previous chapter demonstrated the similarities between phthalimides and thiomaleimides in regards to decarboxylation reactions. It was hypothesised that if we could emulate the acetylated-*N*-phthaloyl-amino acid decarboxylation reaction with thiomaleimides we could develop a cysteine selective photocleavable linker (Scheme 80). This approach also holds several advantages over the previously described C-terminal-cysteine decarboxylation. The chemical payload is released as a more traditional leaving group rather than a thiomaleimide, potentially alleviating problems associated with polymerisation, and the reaction is no longer restricted to C-terminal cysteine residues. Removal of the latter restriction opens up the possibility of using dithiomaleimides, rather than monothiomaleimides, further expanding the utility of the reaction.



**Scheme 80**  
A conceptual scheme demonstrating thiomaleimide based photocleavable linkers.

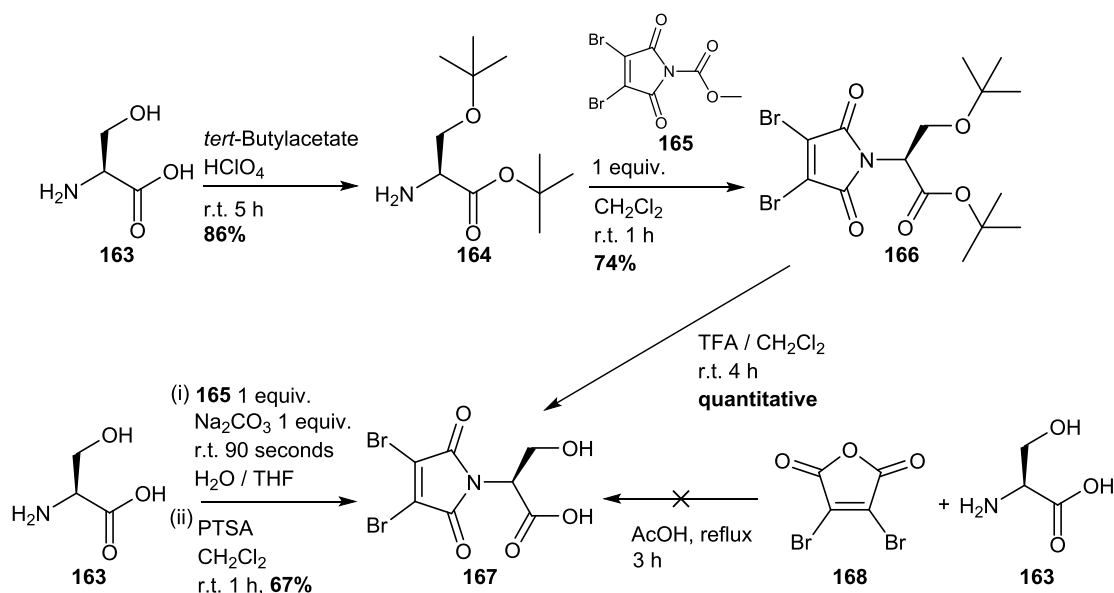
## 2.4.2: Synthesis of a simple cysteine-maleimide model

In order to test the proposed decarboxylation-elimination reaction a suitable model had to be synthesised. A dithiomaleimide-serine model was synthesised to closely mimic the previous work on phthalimides and allow for an effective comparison. Due to the novel nature of this work no previous synthetic routes to this compound exist and a considerable amount of strategy development was necessary. Several routes were explored to the desired compound which was eventually furnished in a good yield over three steps.

### 2.4.2.1: Synthesis of dibromomaleimide-*N*-L-serine

The first step in the process was the synthesis of dibromomaleimide-*N*-L-serine **167** which could serve as an intermediate in the synthesis of the final compound and also a useful synthetic building block for similar constructs. The first route to this compound was *via* dual *tert*-Butyl protected serine **164**. Protection of both the alcohol and carboxylic acid of the serine proceeded almost quantitatively in one step. Reaction of **164** with activated carbamate **165** and subsequent *tert*-Butyl deprotection yielded the desired

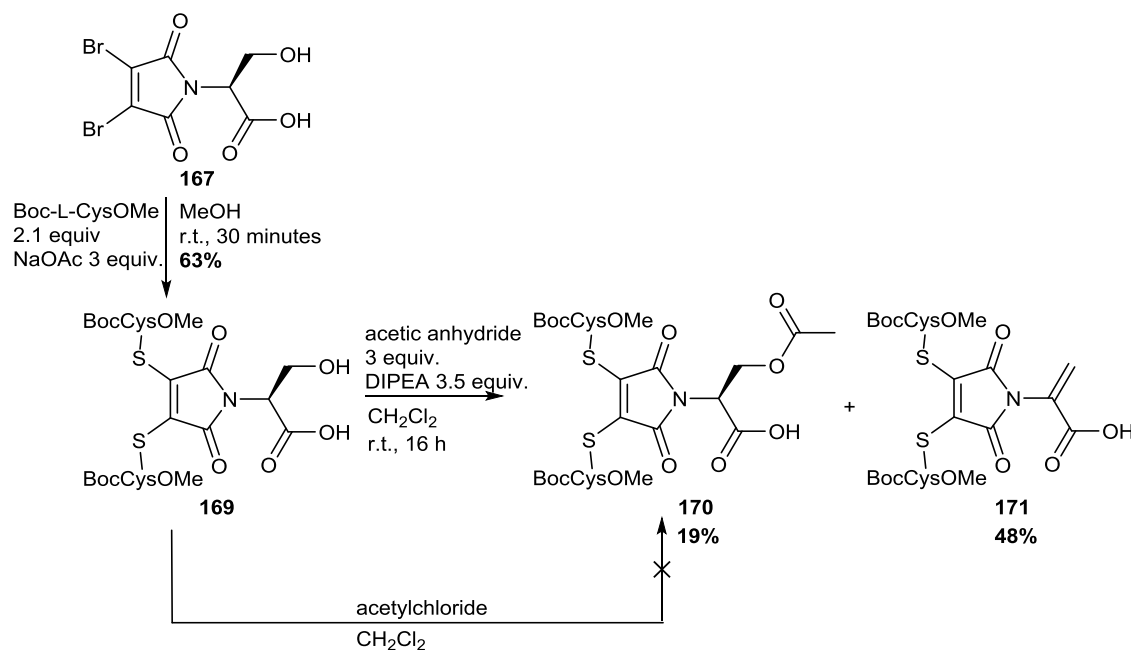
dibromomaleimide-N-L-serine **167** in an overall yield of 64%. Despite the success of this route we wished to eliminate the protection and deprotection steps and find a more direct path to dibromomaleimide-N-L-serine **167**. Difficulties were encountered due to the insolubility of L-serine **163** in the organic solvents typically employed in the reactions of amines with carbamate **165**. Equally problematic was the solubility and stability of carbamate **165** in aqueous solutions. Eventually a system was found which yielded the desired compound **167** in a 67% yield in a single step, improving on the overall yield of the three step route. This involved using a THF / H<sub>2</sub>O solvent mixture to solubilise both components and allow for attack of the amine on the carbamate. Immediate extraction with dichloromethane followed by treatment with *para*-toluenesulfonic acid promoted ring closing and formation of the product. Attempts to synthesise **165** *via* condensation of L-serine with dibromomaleic anhydride **168**, synthesised using a known protocol,<sup>156</sup> produced a complex mixture of products which could not be separated. These synthetic routes are summarised below (Scheme 81).



**Scheme 81**  
Synthetic routes to dibromomaleimide-N-L-serine **167**.

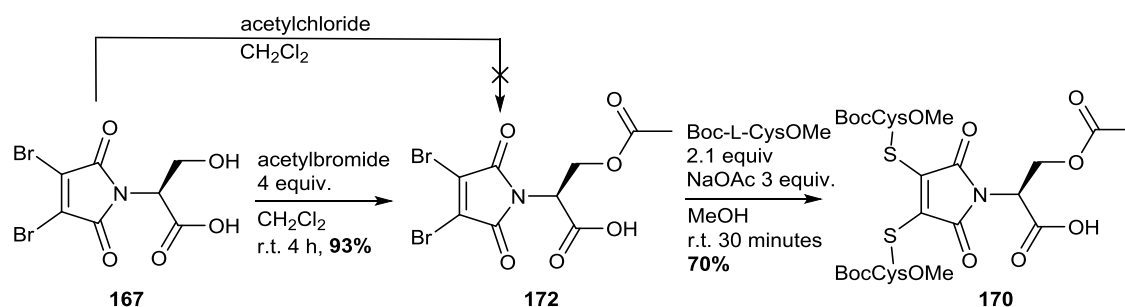
With a reliable route to dibromomaleimide-N-L-serine **167** several strategies for the synthesis of the final dithiomaleimide-serine model **170** were assessed. Displacement of the maleimide bromines for Boc-L-cys-OMe formed dithiomaleimide-serine **169**, though the isolated yield of this reaction was lower than expected due to purification difficulties. Unfortunately, acetylation of **169** proved difficult. Reaction with acetyl chloride gave a mixture of products, possibly due to Boc deprotection by the released hydrochloric acid. Attempts to react the serine alcohol with acetic anhydride produced dehydroalanine like product **171** as the major species. Despite this, desired acetylated dithiomaleimide-serine model **170** was isolated in a small yield. This indicates the desired product forms but subsequent deprotonation of the alpha proton results in elimination of the acetyl group and

formation of side product **171**. This unwanted reactivity could be minimised by decreasing reaction times, but a concurrent decrease in the consumption of starting material **169** limited the usefulness of this approach (Scheme 82).



**Scheme 82**  
Synthetic routes towards acetylated dithiomaleimide-serine model **170** via dithiomaleimide-serine **169**.

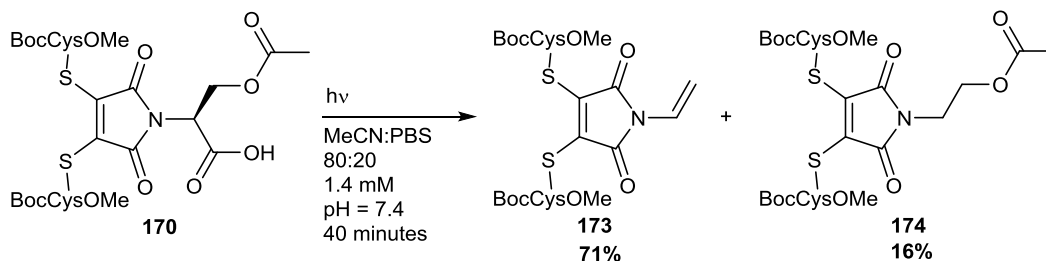
Greater success was found by first acetylating dibromomaleimide-N-L-serine **167** before introducing Boc-L-cys-OMe. Though acetylation using acetyl chloride was unsuccessful using the corresponding acyl bromide produced acetylated dibromomaleimide-serine **172** in an excellent yield under base free conditions. Substitution of the maleimide bromines for Boc-L-cys-OMe yielded the final product dithiomaleimide-serine model **170** in a good yield (Scheme 83).



**Scheme 83**  
Synthetic routes towards acetylated dithiomaleimide-serine model **170** via acetylated dibromomaleimide-serine **172**.

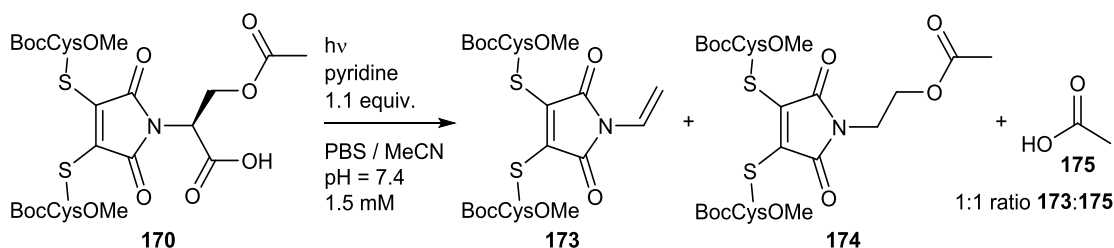
### 2.4.2.2: Irradiation of a simple cysteine model

Irradiation of acetylated dithiomaleimide-serine **170** in a buffer / acetonitrile solvent system resulted in the consumption of the starting material within 40 minutes. Purification of the resultant mixture yielded the suspected ene-maleimide **173** and also protonated side product **174** (Scheme 84).



**Scheme 84**  
The irradiation of acetylated dithiomaleimide-serine model **170**.

This result confirmed the hypothesis that thiomaleimides could undergo photochemical decarboxylation-elimination reactions, albeit in a lower yield than the corresponding phthalimides (95%<sup>287</sup>). Irradiation times were significantly reduced; 40 minutes with a 125 W lamp compared to two hours with an 800W lamp at millimolar concentrations. The two products formed were analogous to the product observed during the phthalimide work and provide another example of similarities between phthalimide and thiomaleimide photochemistry. To confirm the release of acetic acid the reaction was repeated in organic solvent with pyridine as a base in a sealed NMR tube (Scheme 85). Analysis after irradiation clearly showed the formation of acetic acid by both <sup>1</sup>H and <sup>13</sup>C NMR in a 1:1 ratio with compound **173**. Protonated side product **174** was also observed. The presence of acetic acid (**175**) released in equimolar quantities gives confidence that the released product is not undergoing further reactions.

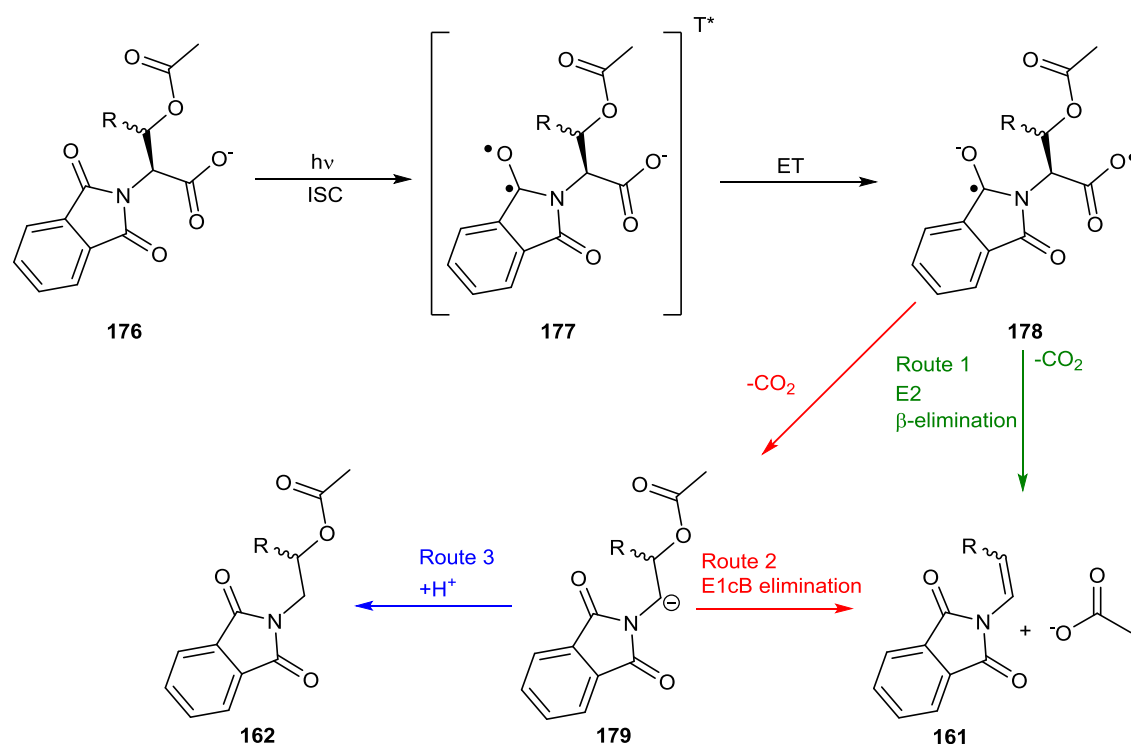


**Scheme 85**  
The irradiation of acetylated dithiomaleimide-serine model **170** in the presence of pyridine in DMSO-d<sub>6</sub>.

### 2.4.3: A postulated mechanism for thiomaleimide decarboxylation-elimination

As with the C-terminal decarboxylation discussed in the previous chapter a mechanism for this thiomaleimide decarboxylation can be inferred from the related decarboxylation

reactions of N-phthaloyl-amino acids.<sup>287</sup> Whilst no detailed study of this particular phthalimide photochemical decarboxylation-elimination has been performed the key photochemical steps are likely to be identical to the previously reported phthalimide decarboxylation reactions (Scheme 86). Photochemical excitation of the phthalimide (**176**) is followed by an intersystem crossing to the triplet state **177**. An electron is then transferred from the carboxylate to the triplet phthalimide to produce carboxylate radical **178**. Two pathways for the elimination of the acetate group were proposed; a direct E2  $\beta$ -elimination (route 1) or a two-step process involving an intermediate carbon anion (**179**) in an E1cB-like elimination (route 2). It is by this second route that protonated impurity **162** is formed. It was proposed that substitution at the beta position of the amino acid can influence the route for decarboxylation. The authors state that in both cases acetate is released, though do not specify how this occurs in the concerted mechanism. As the concerted elimination is radical in nature it stands to reason that the leaving group would be pushed out as a carboxy radical rather than the anionic acetate. It is possible that “back” electron transfer from the phthalimide to the carboxy radical occurs, regenerating the phthalimide and forming the acetate, though this is not explicitly addressed by the authors.

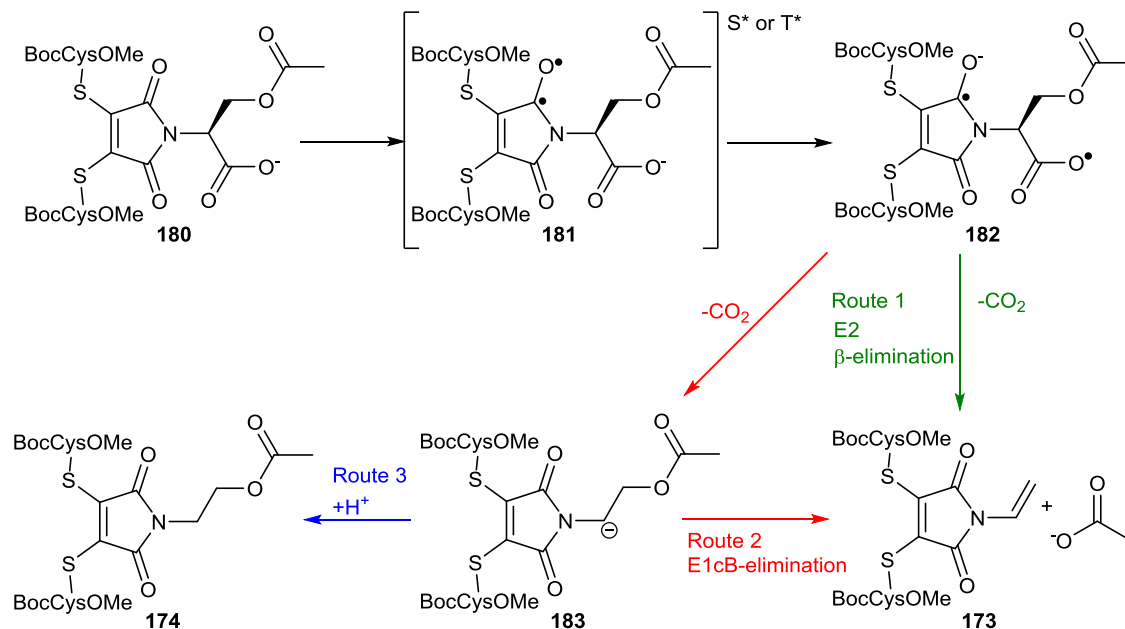


#### Scheme 86

The proposed mechanism for the formation of phthalimides **161** and **162** during the irradiation of acetylated N-phthaloyl-serine carboxylate **176**.

Based on this information a mechanism for the maleimide based decarboxylation can be proposed (Scheme 87). Photoexcitation of thiomaleimide-serine carboxylate **180** to the excited singlet/triplet state (**181**) is followed by electron transfer from the carboxylate to the

maleimide. Elimination can then occur *via* either a concerted E2  $\beta$ -elimination or a two step E1cB like mechanism. The increased presence of protonated product **174** suggests the two step route is more likely in the case of maleimides, as formation of such a product would be impossible through a concerted elimination. Of course it is entirely possible that a competition could be occurring between both routes.

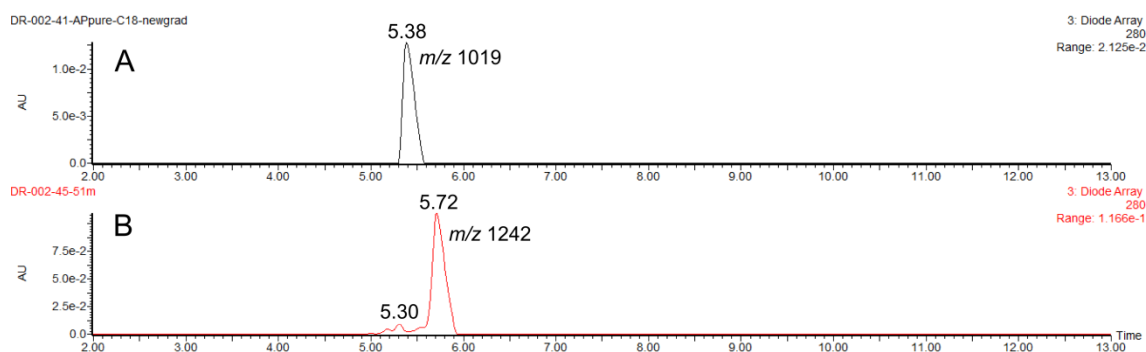
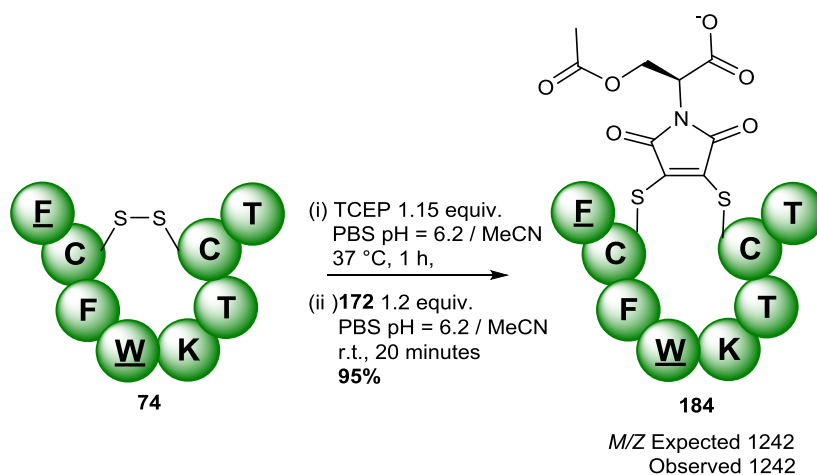


**Scheme 87**  
The proposed mechanism for the photochemical thiomaleimide decarboxylation-elimination reaction.

## 2.4.4: Photochemical cleavage from a peptide model

### 2.4.4.1: Preparing and irradiating a suitable Octreotide model

Given that the eventual aim of this work was to design photocleavable linkers that are compatible with proteins and peptides we decided to test the new photochemical decarboxylation on a peptide model. Octreotide **74** was employed for this purpose due to its simplicity and familiarity. A modified protocol for the modification of Octreotide **74** was devised and implemented. Reducing the disulfide with a slight excess of TCEP and subsequently reacting with acetylated dibromomaleimide-serine **172** yielded the desired Octreotide conjugate **184** (Scheme 88). The reaction was followed using LCMS and a clear change in retention time was observed (Scheme 88) (Figure 44). Analysis of this peak using both ES<sup>+</sup> and ES<sup>-</sup> ionisation modes showed the desired mass.



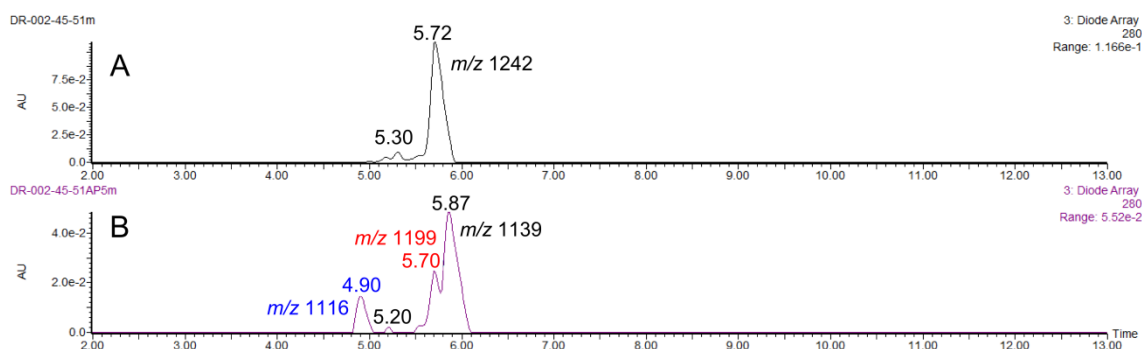
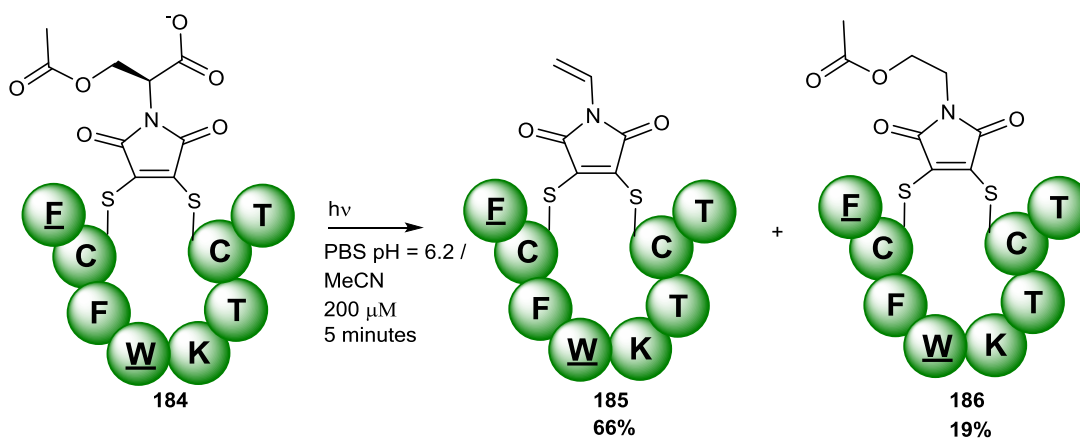
### Scheme 88

The modification of Octreotide **74** with acetylated dibromomaleimide-serine **172**.

### Figure 44

A UPLC trace showing the modification of Octreotide **74** with acetylated dibromomaleimide-serine **172**: (A) Octreotide **74**, (B) Octreotide conjugate **184**. See experimental section for ES spectra (Section 3.2.7.1, page 202, Figure 90).

Subsequent irradiation of Octreotide conjugate **184** resulted in complete consumption within five minutes and the formation of three new products (Scheme 89) (Figure 45). The peak at 5.87 minutes had an *m/z* value of 1140, which corresponds to the desired Octreotide ene-maleimide **185**. The secondary peak at 5.70 minutes had a *m/z* value of 1199, which corresponds to protonated Octreotide conjugate **186**. Based on the work done with small molecule model **170** this was entirely expected. Starting material **184** was not detected by the mass analyser in this peak, showing that despite the similar retention times between starting material **184** and side product **186** a full conversion had taken place. Though baseline separation of the two product peaks could not be achieved, splitting the peaks down the middle and integrating gives an approximated yield of 66% for the desired product **185** and 19% for the protonated species **186**. This is in agreement with the results obtained on the small molecule model. All integrations were performed on the UV-Vis trace scanning at 280 nm to prevent interference from the maleimide absorbance.



### Scheme 89

The irradiation of Octreotide conjugate 184. Irradiation was performed using a 5W 395 nm LED torch.

### Figure 45

A UPLC trace scanning at 280 nm of the crude mixture of products formed from the irradiation of Octreotide conjugate 184.  $m/z$  values are shown next to the corresponding peak and matched the expected values. See experimental section for ES spectra (Section 3.2.7.1, page 206, Figure 97 & Figure 98).

In addition to the two expected products an additional peptidic species was formed with a retention time of 4.90 minutes and an  $m/z$  value of 1116. This value matches exactly with Octreotide-succinimide **187**, a side product previously encountered during the *bis*-modification work discussed previously (Section 2.1.2, page 51) (Figure 46).

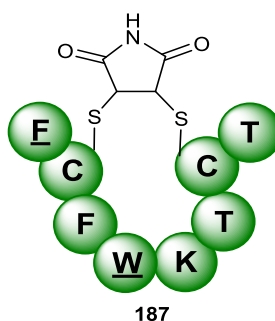
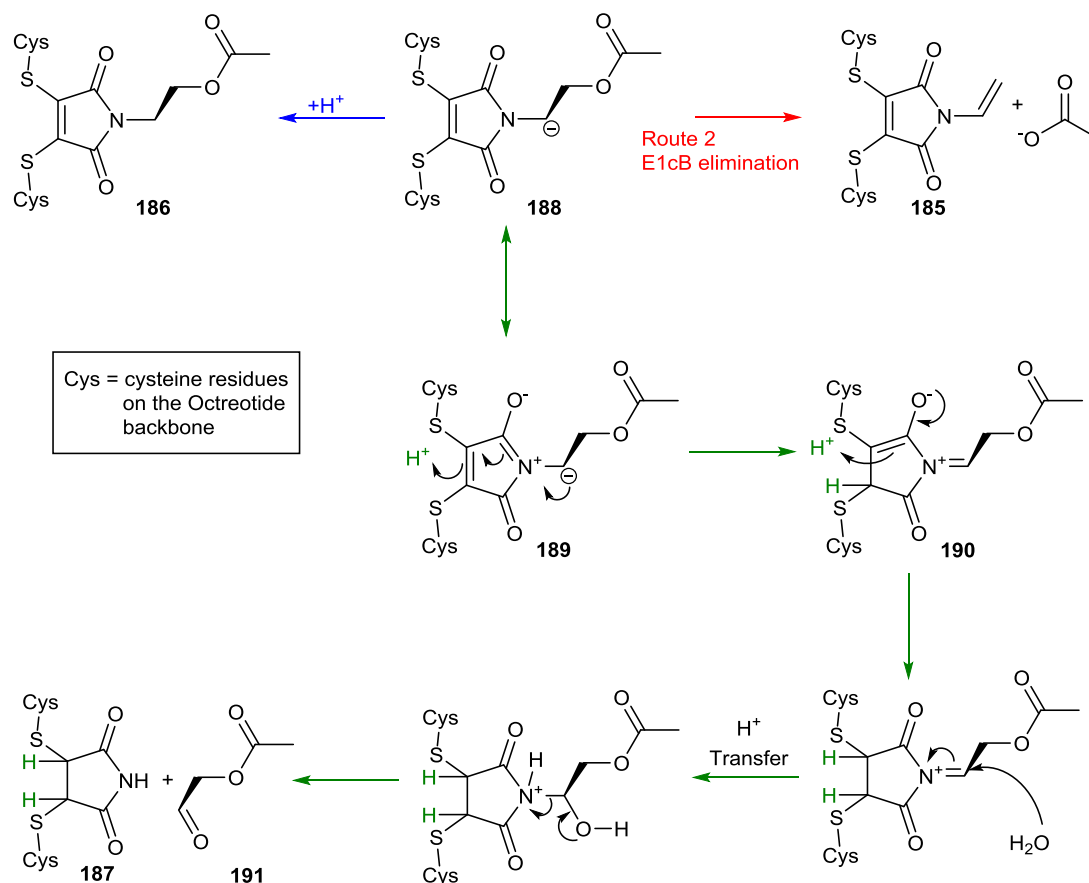


### Figure 46

Octreotide-succinimide **187** formed as a side product during the irradiation of Octreotide conjugate 184.

Injection of a pure sample of Octreotide-succinimide **187** showed the same retention time as the side-product observed during the irradiation of **184**, providing evidence for its formation. The unexpected formation of **187** poses the question as to how such a species could form under the reaction conditions. No obvious mechanism, given the knowledge gained from the small molecule work and the research on phthalimides, presents itself. One plausible route is *via* the protonation at the double bond of the maleimide after decarboxylative formation of anion **188**. This is best seen *via* alternate resonance form **189**. This could form an iminium ion (**190**) which is subsequently attacked by water, leading to cleavage of the N-C bond and formation of succinimide **187** (Scheme 90).



**Scheme 90**  
**A proposed mechanism for the photochemical formation of Octreotide-succinimide 187.**

Though protonation at the double bond seems unlikely when compared to elimination or direct protonation at the alpha position this mechanism does provide a route to the observed product. Attempts to observe aldehyde **191** by ESI mass spectrometry were unsuccessful, though given the reactive nature of aldehydes this was unsurprising.

## 2.4.5: Altering the scaffold of the thiomaleimide photocleavable linker

### 2.4.5.1: Synthesis of structurally varied dibromomaleimide linkers

Though the initial work on the simple model system was a success we felt that the reaction was not explored to a satisfactory level. A quick look at the basic scaffold of the photocleavable linker reveals several targets for modification, namely the alpha & beta positions and the leaving group (Figure 47). We were interested in how the photochemical decarboxylation-elimination would be affected by changes in these key positions and if possible improve the yield of the desired photochemical cleavage.

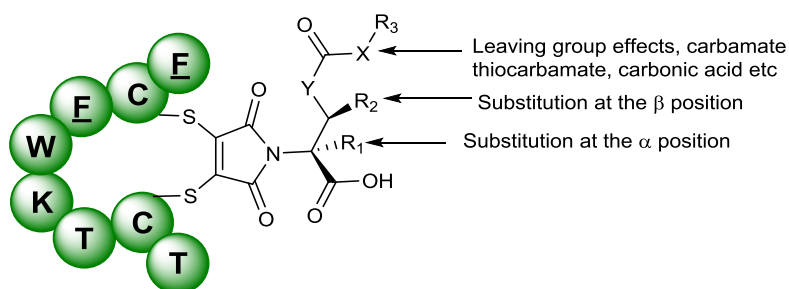
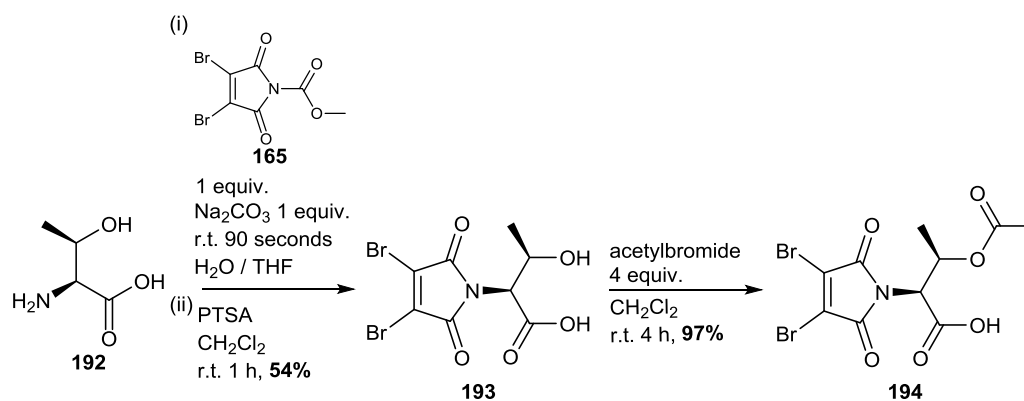


**Figure 47**  
A schematic showing the various points on the photocleavable scaffold which can be targeted for substitution.

These dibromomaleimides were subsequently inserted into the disulfide bond of Octreotide **74** and their photochemical reactivity studied using the UPLC-MS method previously developed. This provided a simple and reliable strategy to quickly compare the effects of these structural changes.

### Synthesis of acetylated dibromomaleimide-threonine

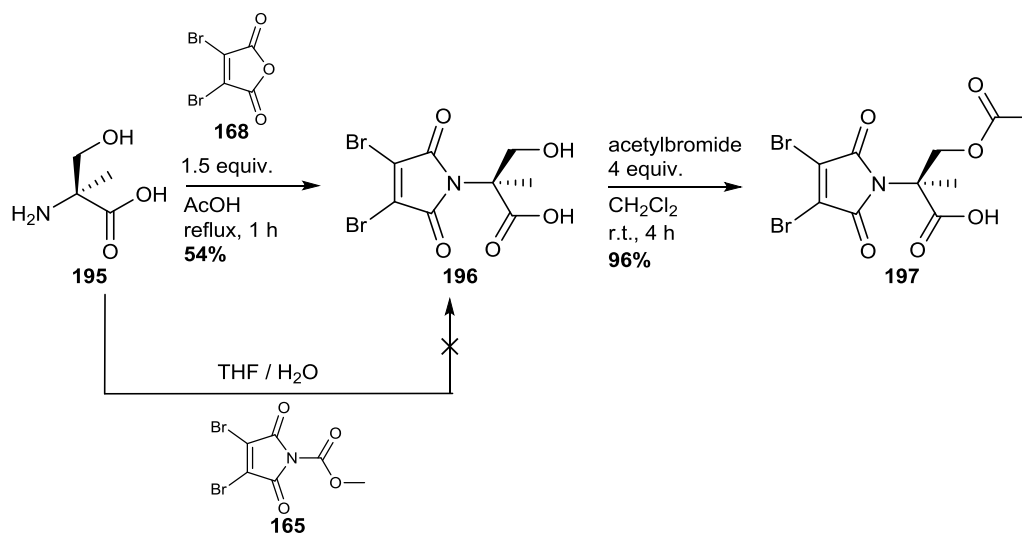
Work by Griesbeck *et al.* demonstrated N-phthaloyl-L-threonine is able to undergo efficient photochemical decarboxylation.<sup>287</sup> To test the effect of this alteration on the photochemical decarboxylation-elimination on thiomaleimides, acetylated dibromomaleimide-threonine **192** was synthesised. Reaction of L-threonine **192** with carbamate **165** gave dibromomaleimide-threonine **193** in a good yield. Subsequent acetylation furnished acetylated dibromomaleimide-threonine **194** in an overall yield of 52% (Scheme 91).



**Scheme 91**  
The synthesis of acetylated dibromomaleimide-threonine **194**.

### Synthesis of acetylated dibromomaleimide- $\alpha$ -Me-serine

The work with phthalimides was not extended to testing the ramifications of substitution at the alpha position of the amino acid, though given the influence of substitution at the beta position it is reasonable to assume some effect would be observed. In fact, any effect could be more pronounced as the alpha position is more directly involved in the two step E1cB mechanism of elimination. Acetylated dibromomaleimide- $\alpha$ -Me-serine **197** was synthesised in two steps using a modified version of the previously employed synthetic route. L- $\alpha$ -Me-serine **195** was reacted with dibromomaleic anhydride **168** to produce dibromomaleimide- $\alpha$ -Me-serine **196**. Attempts to produce **196** *via* reaction of L- $\alpha$ -Me-serine **195** with carbamate **163** were unsuccessful, with extended reaction times leading only to degradation of the carbamate starting material. TLC analysis of the reaction mixture indicated that the secondary amine was simply unable to react with the carbamate, the added steric bulk of the methyl group perhaps preventing nucleophilic attack.

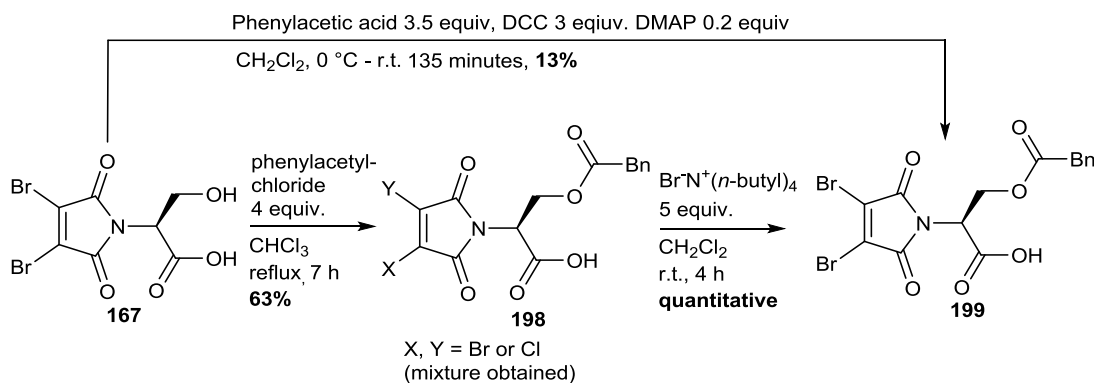


**Scheme 92**  
The synthesis of acetylated dibromomaleimide- $\alpha$ -Me-serine **197**.

Interestingly reaction of L- $\alpha$ -Me-serine **195** with dibromomaleic anhydride **168** proceeded well despite the same reaction producing a complex mixture when attempted with simple L-serine **163**. The addition of the methyl group appears to stabilise this serine analogue towards the reaction conditions. This suggests the side products seen in the reaction of L-serine **163** with dibromomaleic anhydride **168** (Scheme 81) are likely a result of enolisation.

### Synthesis of phenylacetyl-dibromomaleimide-serine

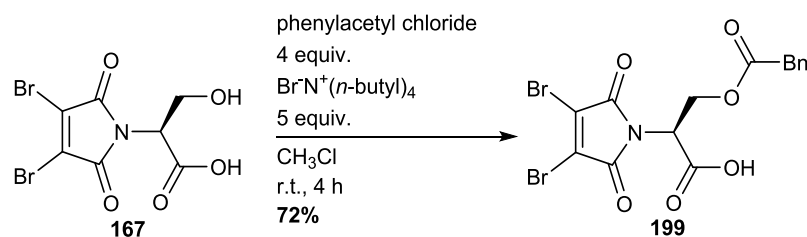
The effect of the leaving group on the efficiency of the decarboxylation-elimination was not thoroughly studied on phthalimides;<sup>287</sup> only two different groups were tested. We wanted to see what effect changing the leaving group from acetic acid to phenylacetic acid would have on the overall reactivity of these compounds. Several routes to target compound **199** were tested (Scheme 93). Attempts to form the ester *via* a HATU mediated coupling were unsuccessful, and a DCC coupling reaction furnished the product in a very poor yield. Cross reactivity of DMAP with dibromomaleimides has been previously noted in the lab so the low yield in this case was unsurprising. Reaction of dibromomaleimide-serine **167** with phenylacetyl chloride in refluxing chloroform furnished a mixture of three inseparable compounds of similar structure (**198**). Analysis of the mixture suggested a bromine-chlorine exchange had occurred as a result of the liberation of chlorine during the reaction. Fortunately, addition of excess tetra-*N*-butylammonium bromide to this mixture furnished the compound **199** in a good overall yield, presumably through a chlorine-bromine exchange.



#### Scheme 93

#### Routes towards the synthesis of phenylacetyl-dibromomaleimide-serine **199**.

Using this knowledge a one pot synthesis was devised in which the tetra-*N*-butylammonium bromide was added at the start of the reaction. This reaction proceeds at room temperature to furnish the desired compound in a single step and a good yield (Scheme 94).

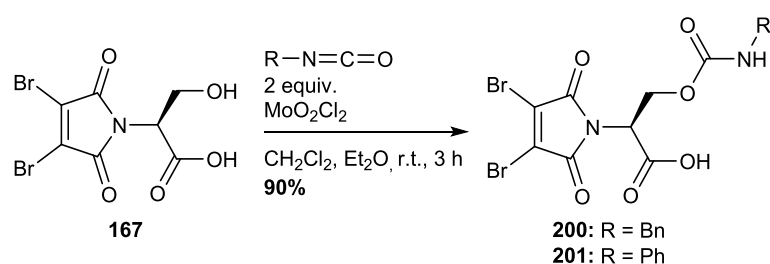


**Scheme 94**  
**Optimised synthesis of functionalised dibromomaleimide 199.**

The fact that the reaction between dibromomaleimide-serine **167** and phenylacetyl chloride in the presence of tetra-*N*-butylammonium bromide proceeds at room temperature suggests that phenylacetyl bromide acts as an intermediate. Previous attempts to react **167** with acyl chlorides at room temperature in the absence of base were ineffective, and conversion of acyl chlorides to acyl bromides by tetra-*N*-butylammonium bromide has been reported.<sup>306,307</sup>

### Synthesis of carbamate-dibromomaleimide-serine analogues

Many fluorophores and cytotoxic compounds contain amine functionality so developing a method to release amines would increase the utility of this reaction. Carbamic acids spontaneously decarboxylate in aqueous environments to release amines so are ideal leaving groups in this respect.<sup>308</sup> Carbamates are also far more hydrolytically stable than esters and are thus more desirable for *in vivo* applications.<sup>309,310</sup> carbamate-dibromomaleimides **200** and **201** were easily synthesised in base free conditions by the reaction of dibromomaleimide-serine **167** with the appropriate isocyanate in the presence of molybdenum(VI) dichloride dioxide (Scheme 95).<sup>311</sup>

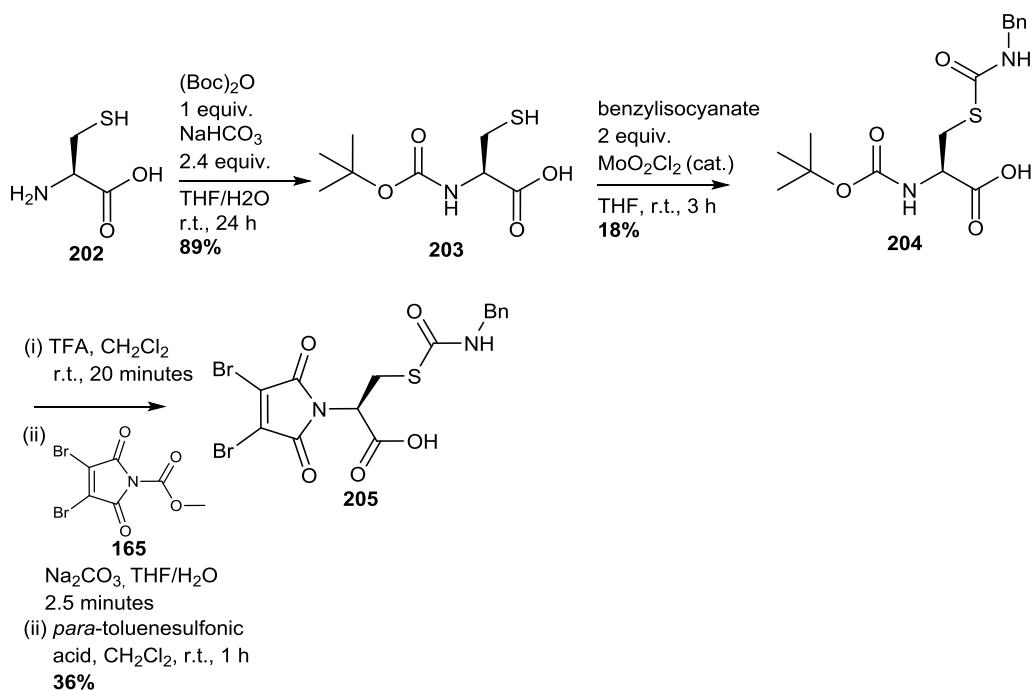


**Scheme 95**  
**The synthesis of carbamate-dibromomaleimide-serine analogues 200 and 201.**

### Synthesis of thiocarbamate-dibromomaleimide-serine

To see what effect exchanging oxygen for sulfur would have on the photochemical decarboxylation-elimination thiocarbamate-dibromomaleimide-serine **205** was synthesised. L-cysteine **202** was selectively N-Boc protected to produce Boc-cysteine **203**. Subsequent reaction with benzylisocyanate produced thiocarbamate **204**. This step was low yielding and highlights the limitations of this catalytic approach. One pot Boc deprotection and

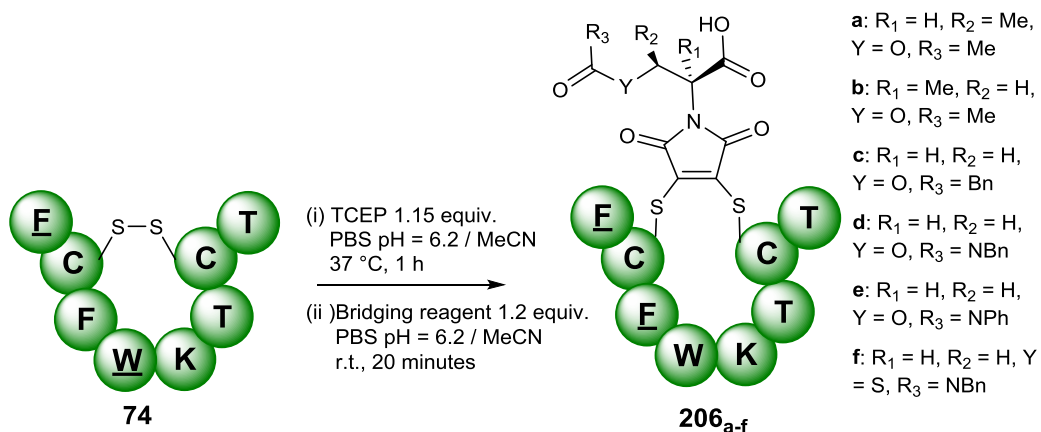
subsequent reaction with carbamate **165** produced thiocarbamate-dibromomaleimide-serine **205**.



**Scheme 96**  
The synthesis of thiocarbamate-dibromomaleimide-serine **205**.

#### 2.4.5.2: Comparing the effects of structural modifications

Octreotide **74** was reduced and modified with the newly synthesised library of dibromomaleimides according to the optimised protocol. Modification proceeded efficiently in each case with only trace amounts of native Octreotide **74** remaining in the cases of **206<sub>c</sub>** and **206<sub>d</sub>** (Scheme 97) (Figure 48).



**Scheme 97**  
The modification of Octreotide **74** with functionalised dibromomaleimide linkers.

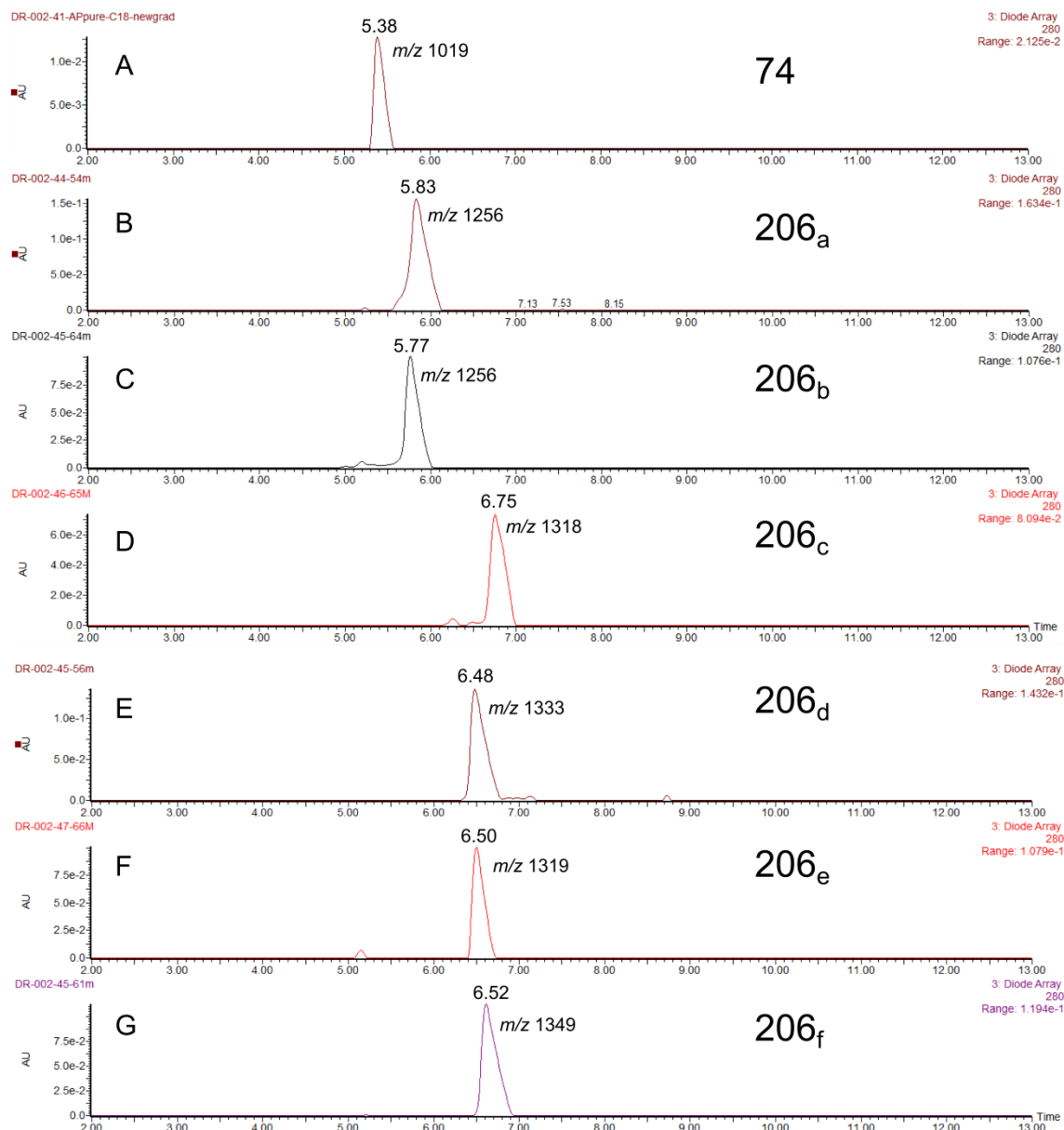
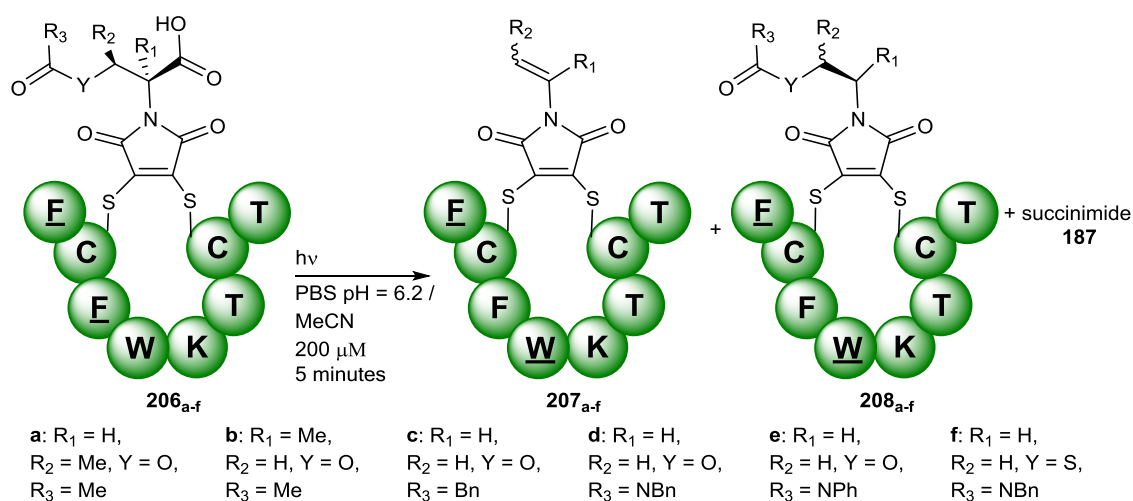


**Figure 48**  
**LCMS traces showing successful modification of Octreotide 74 with dibromomaleimides (B) 194, (C) 197, (D) 199, (E) 200, (F) 201, and (G) 205. All  $m/z$  values matched the expected. For full LCMS spectra see experimental section (section 3.2.7.1, page 202).**

Irradiation of Octreotide conjugates **206<sub>a-f</sub>** in buffer resulted in the complete consumption of starting material within five minutes (Scheme 98). In each case the desired ene-maleimide was observed, in addition to the protonated species and Octreotide succinimide **187**. No other products were observed (Figure 49), suggesting the reaction is not drastically affected by these modifications, though the ratios of the products were different in each case. The UPLC traces are shown below for each case and the results summarised in Table 2.



### Scheme 98

The irradiation of Octreotide conjugates **206<sub>a-f</sub>**. Irradiation was performed using a 5W 395 nm LED torch.

**Table 2**  
A summary of the products obtained from the irradiation of Octreotide conjugates **207<sub>a-f</sub>**.

	$R_1$	$R_2$	$R_3$	Y	ene- maleimide <b>185/207<sub>a-f</sub> / %</b>	protonated product <b>186/208<sub>a-f</sub> / %</b>	Succinimide <b>187 / %</b>
<b>184</b>	H	H	Me	O	66 <sup>(a)</sup>	19 <sup>(a)</sup>	15
<b>206<sub>a</sub></b>	H	Me	Me	O	50 <sup>(a)</sup>	26 <sup>(a)</sup>	24
<b>206<sub>b</sub></b>	Me	H	Me	O	80	0	20
<b>206<sub>c</sub></b>	H	H	Bn	O	83	17	0
<b>206<sub>d</sub></b>	H	H	NBn	O	52	29	19
<b>206<sub>e</sub></b>	H	H	NPh	O	65	25	10
<b>206<sub>f</sub></b>	H	H	NBn	S	31	40	29
<b>(a) Yield is approximated due to poor peak resolution.</b>							

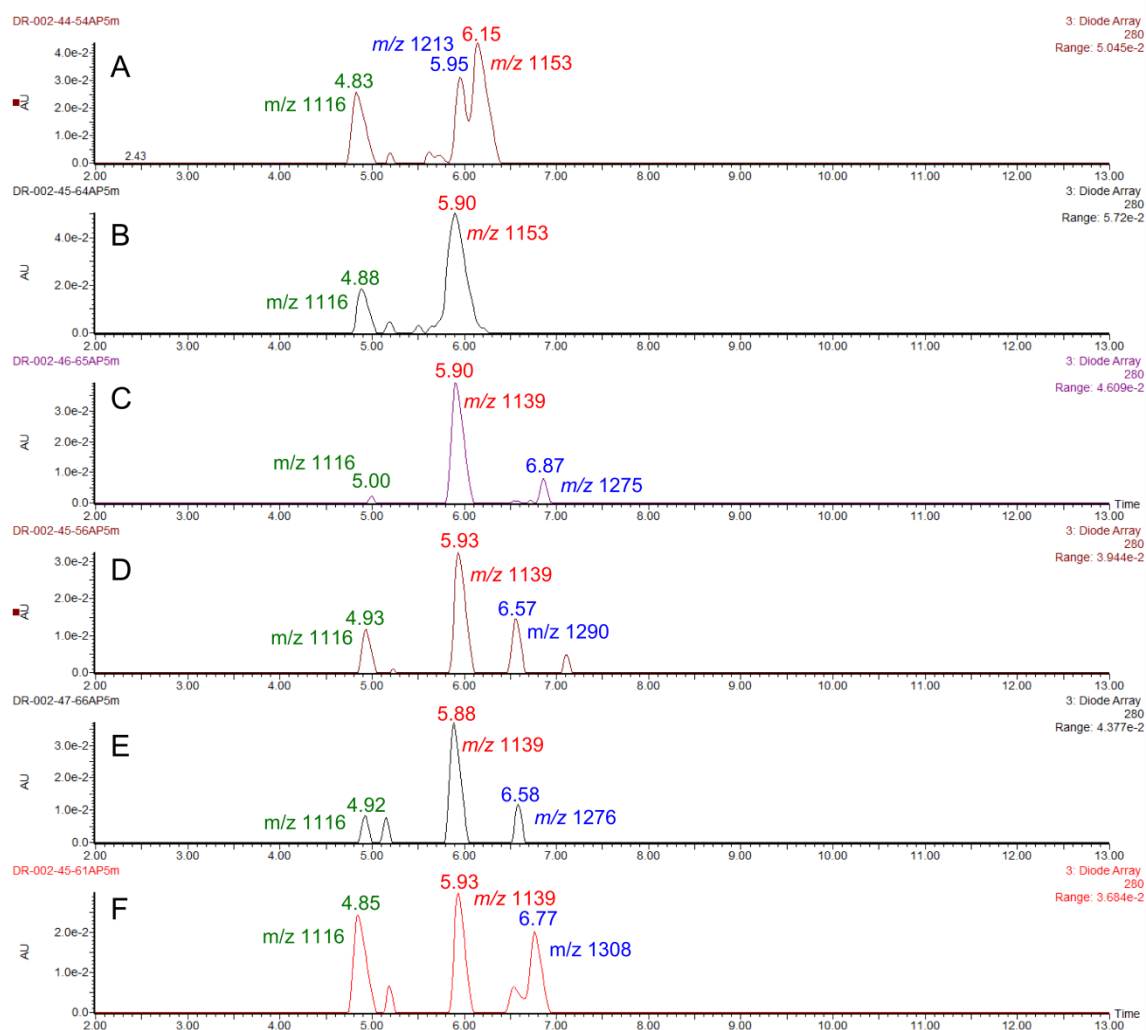


**Figure 49**  
**LCMS traces showing the irradiation of Octreotide conjugates 206<sub>a-f</sub>. (A) Irradiation of 206<sub>a</sub>, (B) Irradiation of 206<sub>b</sub>, (C) Irradiation of 206<sub>c</sub>, (D) Irradiation of 206<sub>d</sub>, (E) Irradiation of 206<sub>e</sub>, (F) Irradiation of 206<sub>f</sub>. ES+ *m/z* values are shown in the colour corresponding to the peak label and all matched the expected values. See experimental section for ES spectra (section 3.2.7.1).**

### The effect of methylation at the alpha and beta positions

Methylation at the beta position has a negative effect on the photocleavage, seeming to favour the formation of protonated product **208<sub>a</sub>** and succinimide **187**. Griesbeck *et al.* noticed a similar effect with N-phthaloyl-*allo*-threonine and argued that an unfavourable steric clash between the beta-methyl and the phthalimide discouraged concerted elimination by forcing the carboxylate and the leaving group away from the ideal antiperiplanar configuration (Figure 50). They argue that this forces the decarboxylation to proceed *via* the two step mechanism, consequently enabling protonation of the intermediate. It is important to note that the authors assign a higher priority to the clash between the carboxylate and the acetate than the clash between the acetate and the phthalimide.

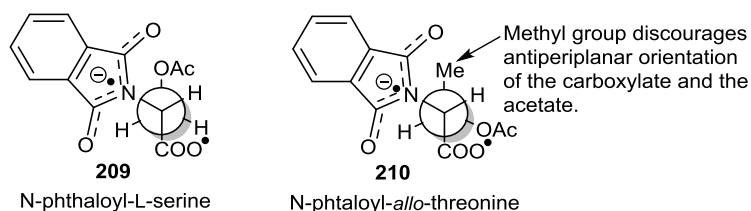


**Figure 50**  
Newman projections of the proposed transition states formed during the irradiation of N-phthaloyl-L-serine **209** and N-phthaloyl-*α*/o-threonine **210**.<sup>287</sup>

Though this same argument cannot be directly applied to the example of Octreotide conjugate **206<sub>a</sub>** it is possible the geometrical conformation forced by the beta-methyl is discouraging concerted elimination or encouraging a two step elimination.

In contrast methylating at the alpha position has a positive effect on the photocleavage efficiency. A 14% increase of the desired ene-maleimide is seen when compared to the unmethylated structure. Protonated species **208<sub>a</sub>** was not detected, either by LC or MS, though succinimide **187** was still observed. One potential reason behind this increase in yield takes into account the geometrical considerations. The addition of the methyl group on the alpha carbon could encourage an antiperiplanar orientation of the acetyl and carboxylate groups and promote concerted elimination, favouring formation of the ene-maleimide (Figure 51).

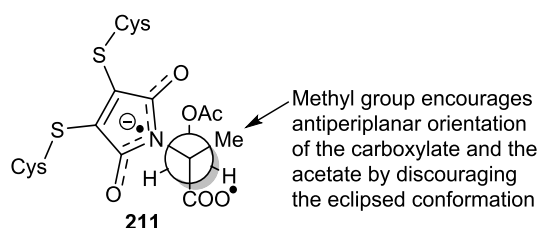
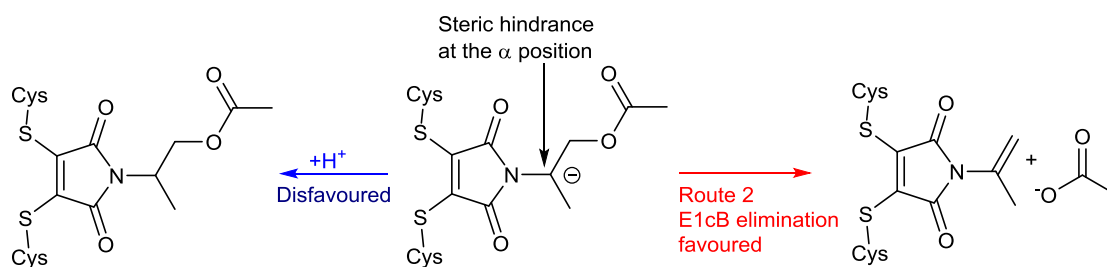


**Figure 51**  
A Newman projection of the hypothesised transition state of the irradiation of acetylated dithiomaleimide- $\alpha$ -Me-serine **211**.

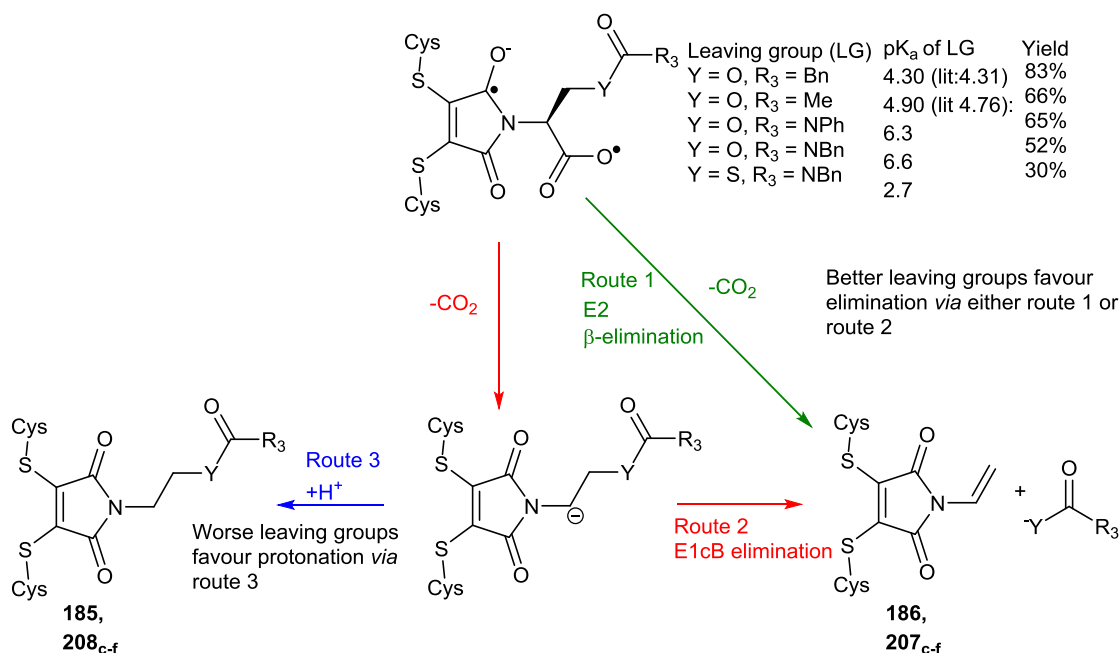
As with the phthalimide work this argument is conditional on the carboxylate being deemed more sterically repulsive than the maleimide. This gives priority to avoiding a clash between the carboxylate and the acetate, rather than between the acetate and the maleimide. Another explanation is that the additional bulk, however small, of the methyl group inhibits protonation for purely steric reasons. Thus even if the mechanism proceeds *via* the two step E1cB like mechanism protonation would be depressed and the elimination product favoured (Scheme 99). The presence of succinimide **187**, assuming the mechanism of protonation at the double bond proposed in Scheme 90 is correct, lends weight to this purely steric argument.



**Scheme 99**  
A possible explanation for the decrease in protonated product **208<sub>b</sub>** observed with Octreotide conjugate **206<sub>b</sub>**.

### The effect of changing the leaving group

This work also highlighted the importance of the leaving group on the efficiency of the reaction. Exchanging acetate for phenylacetate, benzyl carbamic acid, phenyl carbamic acid or benzylthiocarbamic acid as the leaving group (**206<sub>c-f</sub>**) produces significant changes in the yield of ene-maleimide **207<sub>c-f</sub>**. Since there are no significant geometrical differences between the standard scaffolds of Octreotide conjugates **184** and **206<sub>d-f</sub>** the differences in reactivity can be attributed mostly to the effect of the leaving group. The general trend is that the lower the  $pK_a$  of the leaving group the higher the decarboxylative yield. The exception to this rule is the benzylthiocarbamic acid **206<sub>i</sub>**, which has a very low calculated  $pK_a$  but also the lowest yield of decarboxylation. Chemical intuition suggests better leaving groups would favour elimination over protonation, so these results are unsurprising (Scheme 100). It is also in agreement with the work done with the phthalimides.<sup>287</sup>

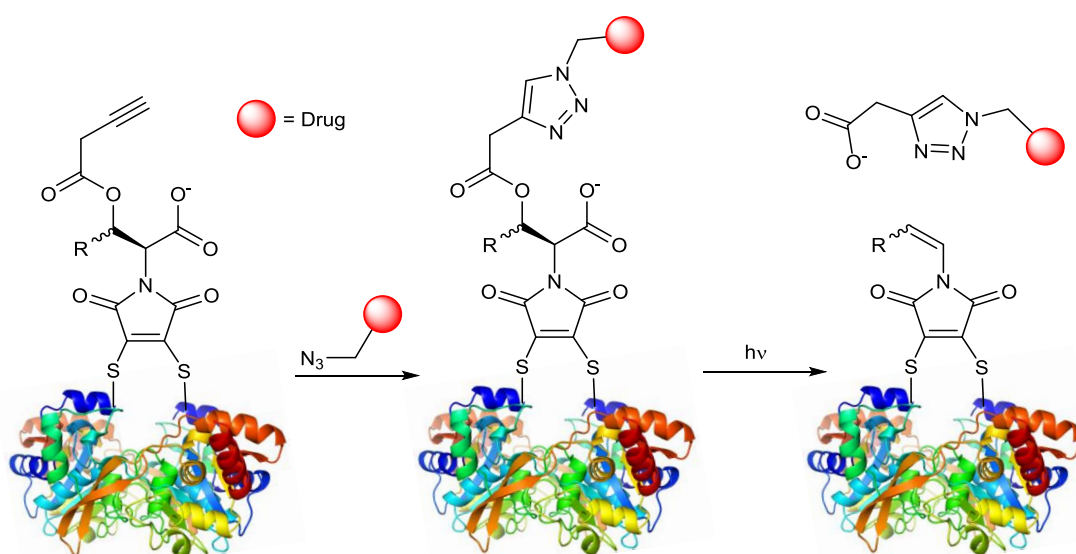


**Scheme 100**  
A proposed explanation for the effect of the leaving group on the thiomaleimide decarboxylation-elimination.  $pK_a$  values were calculated using the ACD i-Lab software. Literature values for phenylacetic acid<sup>312</sup> and acetic acid<sup>313</sup> were also obtained.

This work provided a more satisfactory insight into the photochemical thiomaleimide decarboxylation-elimination and informs the design of the next generation of maleimide based photocleavable linkers.

### 2.5.6: Developing a photocleavable antibody-drug-conjugate

The overall aim of this work was to develop a novel class of photocleavable linkers which could be used to create a photocleavable antibody drug conjugate. We envisioned creating a photocleavable alkyne “click” handle which upon functionalisation with a suitable cytotoxic payload could be utilised for this purpose (Scheme 101).



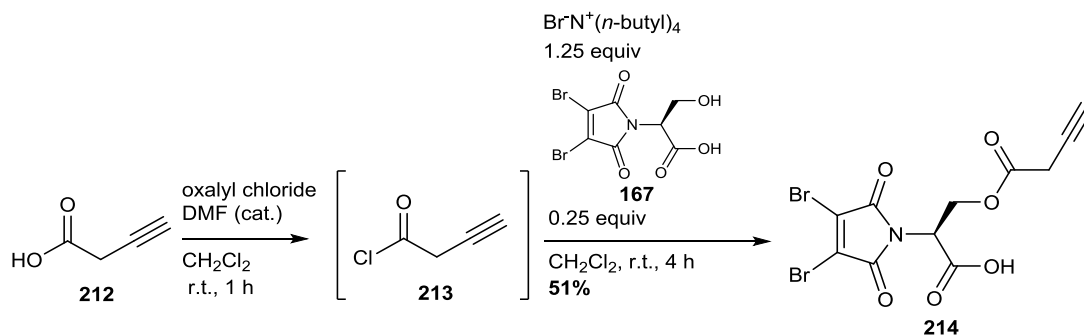
**Scheme 101**  
A hypothetical photocleavable protein-drug conjugate based on the thiomaleimide photocleavable linkers.

Proceeding *via* the alkyne handle expands the choice of chemical payloads to any azide functionalised moiety and increases the versatility of this approach when compared to direct attachment of the drug. This approach also simplifies synthesis by minimising the amount of time spent handling the toxic Doxorubicin on a synthetic scale.

#### 2.4.6.1: Synthesis of a photocleavable click handle

The first step towards the generation of the photocleavable ADC was deciding on the appropriate photocleavable linker. The previous work showed that the leaving group can have a profound effect on the yield of the photocleavage, with acetate leaving groups cleaving in higher yields than the corresponding carbamic acid leaving groups. For these reasons it was decided to synthesise alkyne-dibromomaleimide-serine **214** from 3-butynoic acid **212**. A one pot procedure was developed in which the acid chloride is generated *in situ* using oxalyl chloride. Subsequent addition of dibromomaleimide-serine **167** and tetra-*N*-butylammonium bromide furnishes the desired product in a good yield (Scheme 102).

Interestingly attempts to generate the acid bromide directly using oxalyl bromide were unsuccessful.

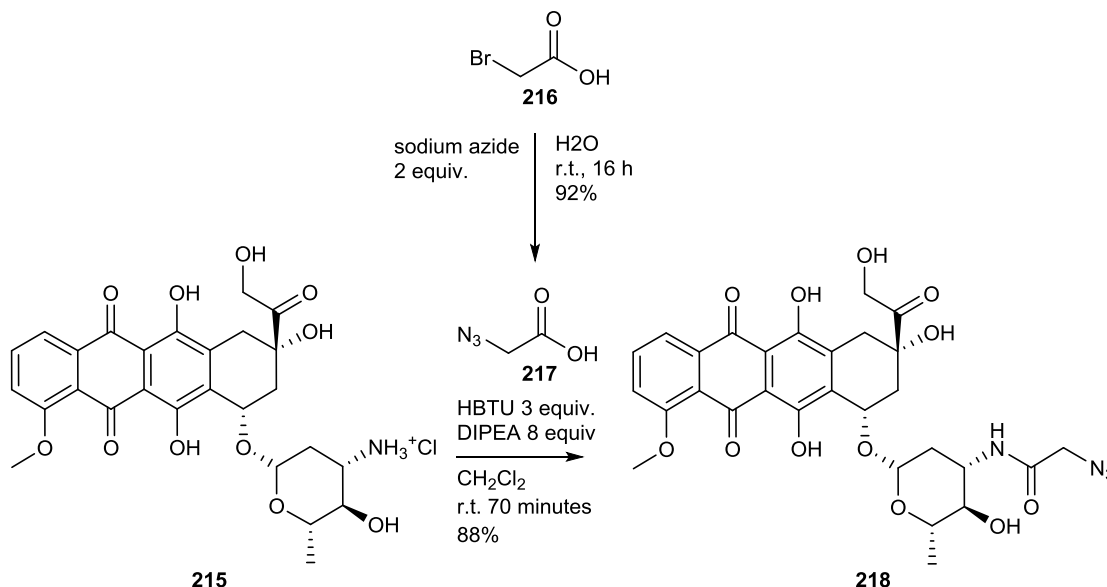


#### Scheme 102

The synthesis of photocleavable alkyne-dibromomaleimide-serine **214**.

#### 2.4.6.2: Synthesis of a doxorubicin-azide analogue

Doxorubicin, trade name Adriamycin, is a cytotoxic drug originally reported in 1969<sup>314</sup> and remains one of the most potent anti-tumour agents with FDA approval. Doxorubicin also displays reasonable absorbance and fluorescence which makes it easy to track by chromatographic methods. These characteristics, coupled with safety concerns over more toxic drugs, made Doxorubicin a logical choice for this work. 2-azidoacetic acid **217** was synthesised from bromoacetic acid **216** in a good yield and subsequently coupled to Doxorubicin.HCl **215** using HBTU and DIPEA (Scheme 103).



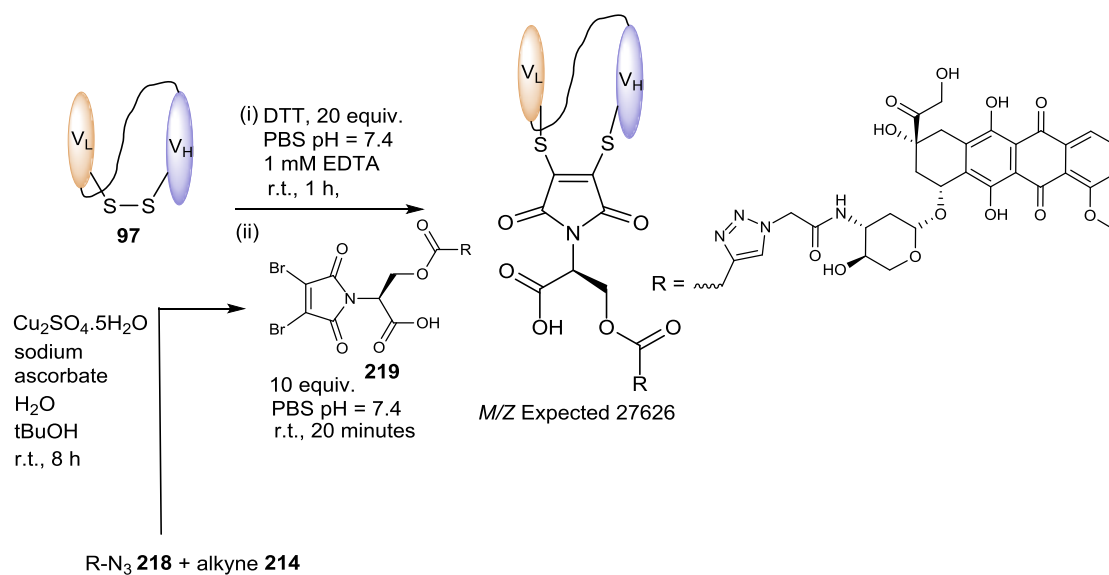
#### Scheme 103

The synthesis of Dox-azide **218**.

#### 2.4.6.3: Generation of a photocleavable scFv-Doxorubicin ADC

An Anti-CEA scFv (previously employed in section 2.2.2, page 68) was chosen as the antibody fragment of choice for the photocleavable ADC. The primary reason for this was

the fact that CEA does not internalise upon binding of the antibody, meaning the ADC remains attached to the cell membrane upon binding to the antigen. Any photochemically released drug will be released into the extra-cellular environment and subsequently internalise, either *via* a different receptor mediated process or by general endocytosis. A non-internalising antibody was chosen due to the high thiol content of the *intra*-cellular environment. As discussed previously thiomaleimides are cleaved from proteins in the presence of excess thiol. This would decrease the efficiency of the photochemical cleavage and lead to non-specific cleavage of the drug. Though non-internalising ADCs are less commonly employed there are several successful examples that demonstrate the validity of this approach.<sup>159,315,316</sup> The scFv, rather than the full antibody, was chosen primarily for its simplicity and availability. Anti-CEA scFv **97** was reduced and modified according to a previously optimised protocol. Dox-azide **218** and dibromomaleimide-alkyne **214** were “pre-clicked” before being added to a reduced sample of scFv **97** to produce Doxorubicin modified scFv **220**. The “pre-click” reaction was necessitated by the presence of a histidine tag on the scFv which binds copper and complicates Cu<sup>(ii)</sup> click reactions. LCMS confirmed successful modification. (Scheme 104) (Figure 52).



#### Scheme 104

The modification of scFv with “pre clicked” photocleavable Dox analogue **219**.

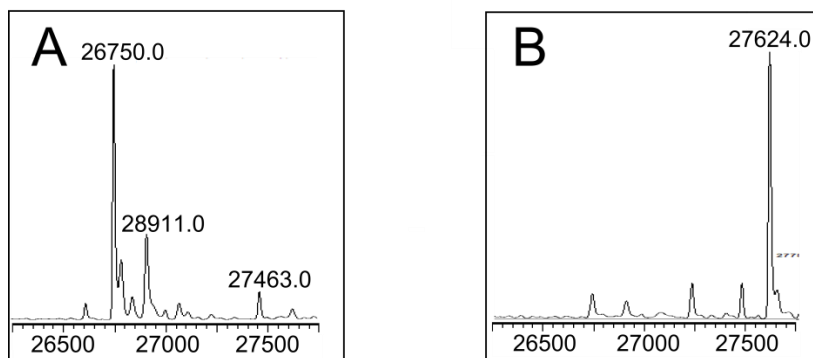
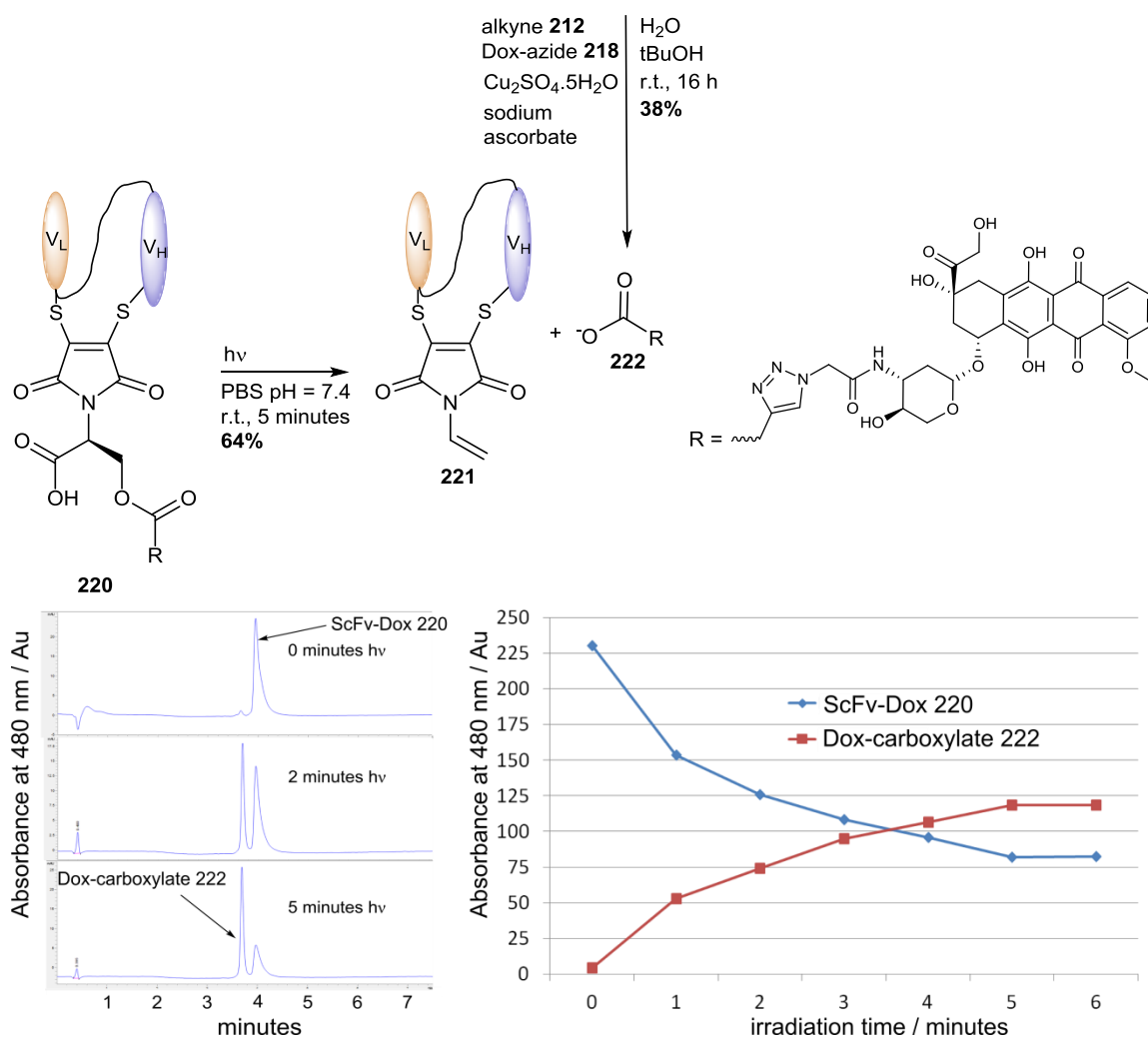


**Figure 52**  
**MS data (A) scFv 97 (B) Doxorubicin-ScFv analogue 220. See experimental section for full spectra (Section 3.2.7.2, page 211, Figure 106).**

Irradiation of modified scFv **220** resulted in cleavage of Doxorubicin analogue **222** in an overall yield of 64% within 5 minutes (Scheme 105). The release of Dox-carboxylate **222** and decrease of modified scFv **220** was monitored using HPLC scanning at 480 nm (Figure 53). A standard solution of Dox-carboxylic acid **222**, generated from a Cu<sup>(ii)</sup> click reaction of Dox-azide **218** and 3-butynoic acid **212**, was injected to confirm the identity of the released species. Extended irradiation times did not increase the concentration of Doxorubicin analogue **222**, suggesting the maximum achievable conversion in this system was reached within five minutes. No decrease in the absorbance at 280 nm was observed, showing the protein was stable to the irradiation and the decrease at 480 nm was due to release of Dox-carboxylic acid **222**.



### Scheme 105

The irradiation of scFv-Dox **220** and the synthesis of Dox-carboxylic acid **222**. Irradiation was performed using a 5W 395 nm LED torch.

### Figure 53

(A) A HPLC trace showing the release of Dox-carboxylate **222** and decrease in concentration of scFv-Dox **220**. (B) A graph showing the release of Dox-carboxylate **222** and decrease in concentration of scFv-Dox **220**. See experimental section for a HPLC trace of a standard solution of Dox-carboxylate **222** (section 3.1.2.4, page 171, Figure 61).

This reaction demonstrates a significant improvement in efficiency over the recently published photocleavable ADC based on a cyanine photocage, which reported a 62% yield after 33 minutes of irradiation with a much more powerful light source ( $25 \text{ mW} \cdot \text{cm}^{-1}$  compared to  $0.9 \text{ mW} \cdot \text{cm}^{-1}$ ). This suggests the above reaction is more efficient than the current state of the art. Though the yield was good it was lower than anticipated based on the work done with Octreotide **74**. It was hoped the adjacent triazole ring would inductively withdraw electrons from the ester and decrease the  $\text{pK}_a$  of the leaving group, leading to a high yield of released Doxorubicin-carboxylate **222**. Nevertheless, this work represents the first maleimide based photocleavable ADC and is a good example of the utility of maleimide photochemistry.

#### 2.4.6.4: Cell kill assay for the photocleaved Doxorubicin analogue

Before proceeding to test the cell killing efficacy of photocleavable scFv **220** we wished to get a measure of the cytotoxicity of the released compound. An accurate idea of the performance of the released drug would help to inform the experimental parameters for the work with the antibody fragment. Several dilutions of Doxorubicin-carboxylic acid **222** were prepared (10  $\mu\text{M}$  to 0.5  $\text{nm}$ ) and tested against three CEA expressing cell lines; HeLa, CaSki and Capan-1. As a control native Doxorubicin.HCl **215** was tested under the same conditions. Cell viability after three days was tested and expressed as a function of concentration of the Doxorubicin analogue (Figure 54). These experiments were performed by collaborators in the UCL Cancer Institute.

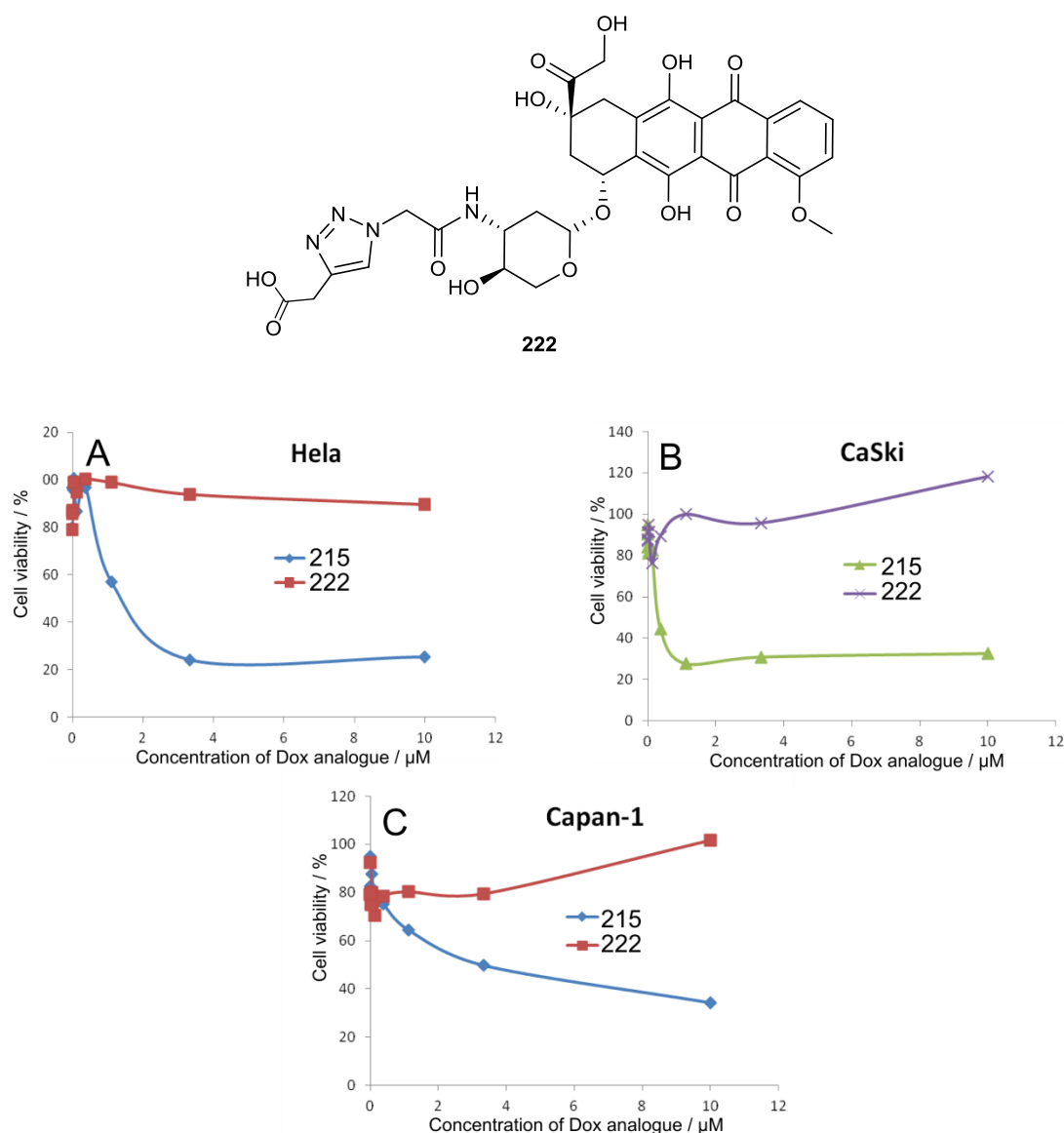
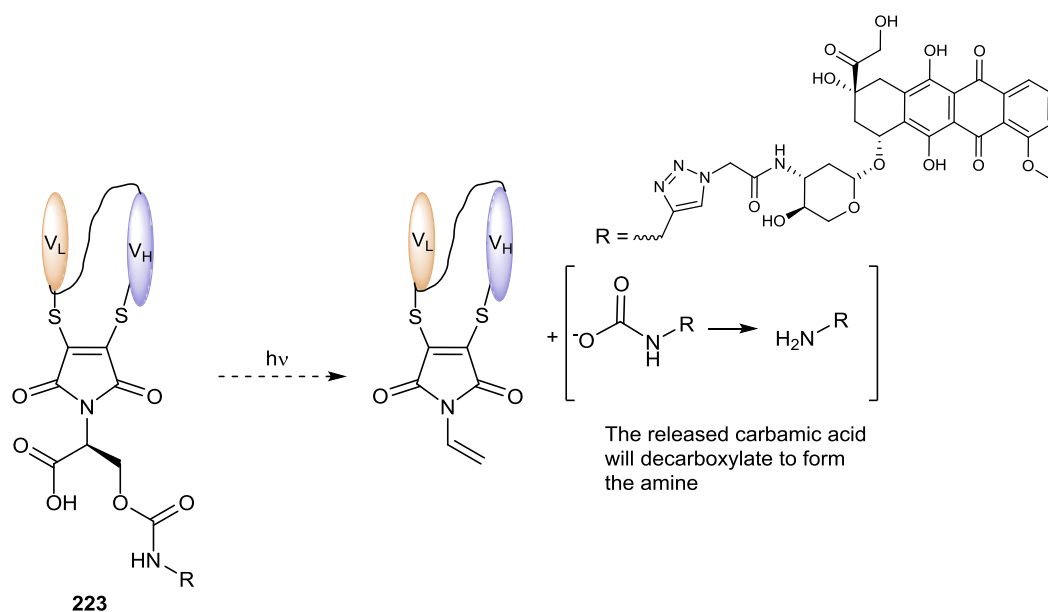


**Figure 54**  
Cell viability after three days as a function of concentration of Dox-carboxylic acid **222** and Doxorubicin **215** for three cell lines: (A) HeLa, (B) CaSki and (C) Capan-1. Data was analysed and compiled by Dr Enrique Rota of the UCL cancer institute.

Disappointingly no significant effect on the cell viability was seen in any of the cell lines treated with Dox-carboxylic acid **222**. Though a slight decrease in cell viability was seen with the Hela cell line, both CaSki and Capan-1 displayed an increase in the cell count after three days. Native Doxorubicin **215** behaved as expected in each case, demonstrating the validity of the cell lines. Though some decrease in activity was expected complete annulment of the cytotoxicity was not anticipated. These results demonstrate that the structural modification to Doxorubicin has a deleterious effect on the cytotoxicity of the drug. This observed effect could be caused by the inability of the drug to interact with the cellular target, or an inability to pass through the cell membrane. Though the mechanism of action of Doxorubicin is not fully understood it is generally accepted that the cytotoxic effects are caused by intercalation of the Doxorubicin pharmacophore with DNA in the nucleus of the cell. This intercalation inhibits the progression of topoisomerase II and prevents successful replication.<sup>317–320</sup> Though the sugar ring aids in the interaction with DNA, structure activity relationships of Doxorubicin analogues have shown that alterations to the ring, such as in Doxorubicin-carboxylic acid **222**, are typically well tolerated.<sup>321–324</sup> That being said it is entirely possible that the addition of the triazole ring and the carboxylic acid inhibit the desired interaction and annul the cytotoxicity of the drug. Carboxylic acid containing Doxorubicin analogues are not well reported, though an example was found in the literature in which cytotoxicity was retained with a Doxorubicin analogue containing a pendant carboxylic acid.<sup>322</sup> As mentioned previously it is entirely possible that Doxorubicin-carboxylic acid **222** is simply unable to pass through the cell membrane by passive transport. Native Doxorubicin **215** is known to cross the cell membrane *via* endocytosis, the relative hydrophobic aromatic ring system and positively charged amine aiding positive interactions with the lipid membrane. Doxorubicin-carboxylic acid **222** exists as a carboxylate within the extra-cellular environment thus may be less able to cross the lipid membrane than native Doxorubicin **215**. Regardless of the reasons it is clear that the addition of the pendant carboxylic acid tail has nullified the cytotoxicity of the drug and invalidates the use of doxorubicin-scFv **220** as a photocleavable ADC.

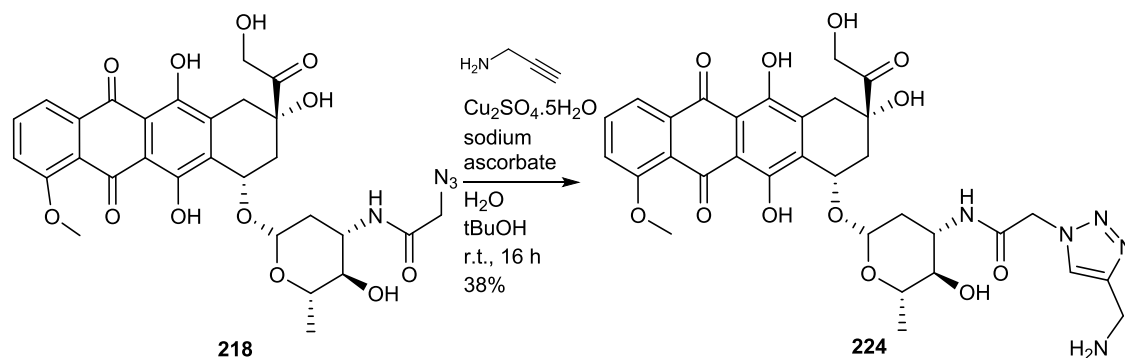
#### **2.4.6.5: Cell kill assay for Doxorubicin-amine**

As it was apparent releasing the Doxorubicin with a pendant carboxylic acid was not ideal a different approach was appraised. Though the photochemical thiomaleimide decarboxylation-elimination is less efficient with carbamic acid leaving groups the yields are still sufficiently high. Carbamic acids spontaneously decarboxylate to release amines, rather than carboxylates, which could be advantageous for the release of Doxorubicin analogues. By exchanging the ester for a carbamate in Doxorubicin-scFv **220** we hoped that the released drug would not suffer from the same potency issues as Dox-carboxylic acid **222** (Scheme 106).



**Scheme 106**  
**Proposed scFv-drug conjugate 223 utilising a carbamate link between the Doxorubicin analogue and the photocleavable scaffold.**

Because of time considerations Dox-amine **224** was synthesised and tested in a cell kill assay before time was spent developing a protocol to generate the proposed carbamate Doxorubicin-scFv **223**. Dox-amine **224** was synthesised in a single step *via* the Cu<sup>(ii)</sup> click reaction of Dox-azide **218** and propargyl amine (Scheme 107).



**Scheme 107**  
**The synthesis of Dox-amine 224.**

As with the previous cell kill assay several dilutions of Dox-amine **224** were prepared (10  $\mu\text{M}$  to 0.5 nM) and tested against three CEA expressing cell lines; Hela, CaSki and Capan-1. Cell viability after three days of incubation with Dox-amine **224** and Doxorubicin HCl **215** at 37  $^{\circ}\text{C}$  was tested and expressed as a function of the concentration of the Doxorubicin analogues (Figure 55). Once again this work was performed by collaborators at the UCL Cancer Institute.

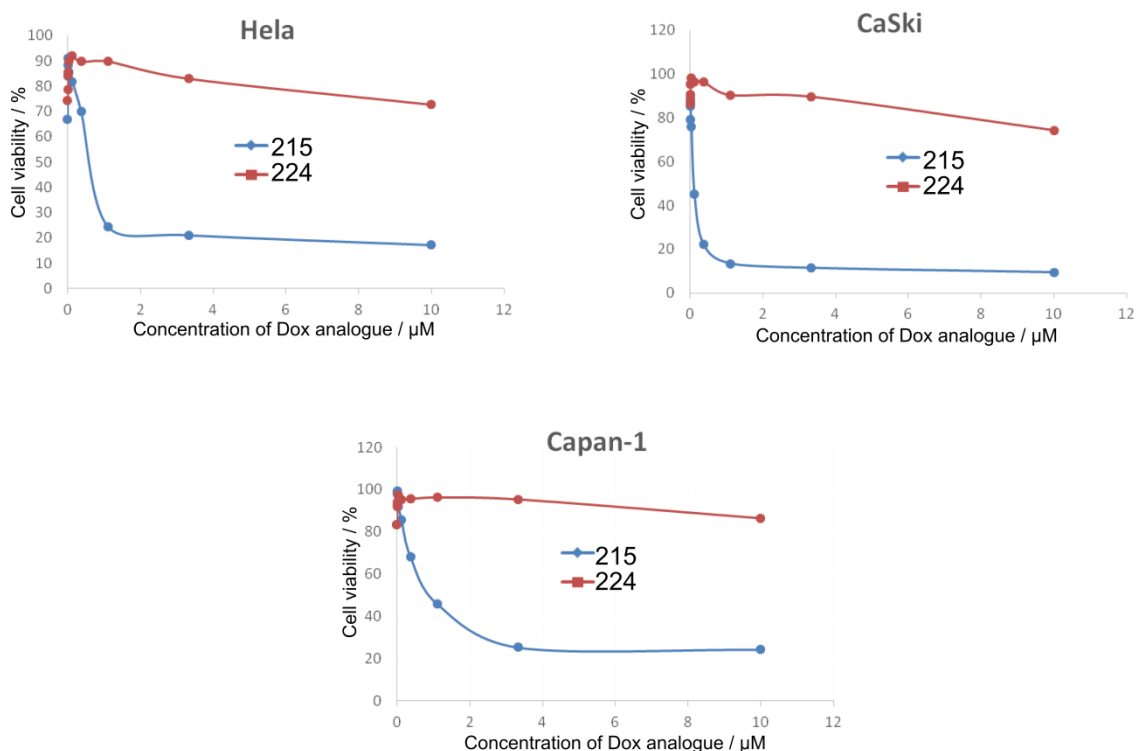
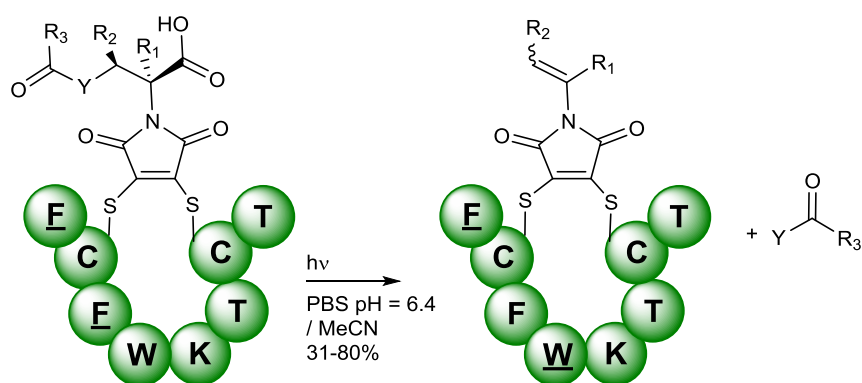


**Figure 55**  
**Cell viability after three days as a function of concentration of Dox-amine 224 and Doxorubicin 215 for three cell lines: (A) HeLa, (B) CaSki and (C) Capan-1.**

Disappointingly the results once again suggested the Dox-amine analogue **224** had only a minimal impact on the viability of the cells. The HeLa cell line represents the best case scenario with a 20% decrease in viability at a concentration of 10  $\mu\text{M}$ , though this is too high for any practical application. It is unlikely that Dox-amine **224** would have any trouble entering the cell, as in this case the structural modification should not drastically alter the interaction of the compound with the cell membrane. The ineffectiveness of this Doxorubicin analogue suggests that the triazole ring may be having a negative effect on the ability of the drug to interact with DNA.

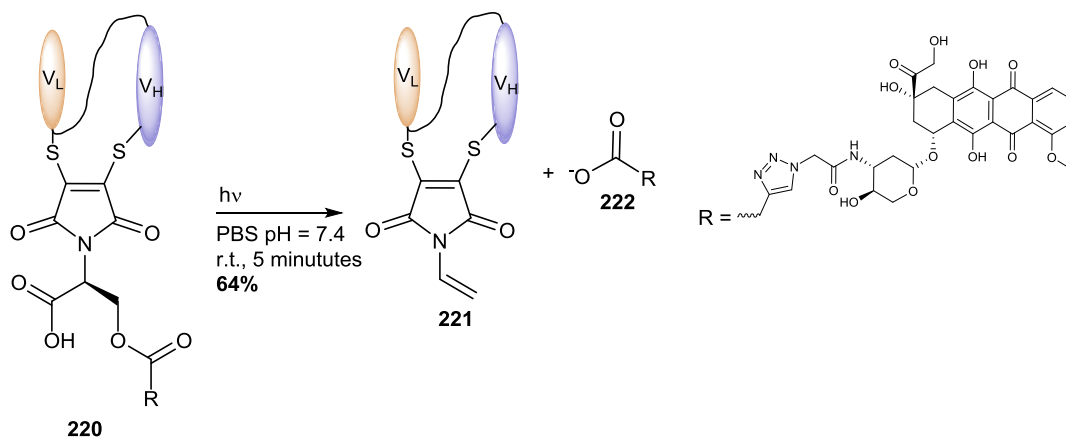
### 2.4.7: Conclusions

A novel photochemical decarboxylation-elimination reaction based on the thiomaleimide scaffold was explored (Scheme 108). The tolerance of the reaction towards a variety of structural modifications was tested and mechanistic insights drawn from the data obtained. This photochemical reaction represents an incredibly efficient photochemical decarboxylation, with irradiation times of less than five minutes compared to 6 - 24 hours for the comparable phthalimides.<sup>287</sup>



**Scheme 108**  
The novel thiomaleimide decarboxylation-elimination applied to several Octreotide conjugates.

The reaction was also employed to cleave a Doxorubicin analogue from an Anti-CEA scFv antibody fragment, demonstrating 64% cleavage within five minutes of irradiation (Scheme 109). The lower reaction times with a considerably less powerful photon source represent a significant advantage when compared to currently employed methods.<sup>245</sup>



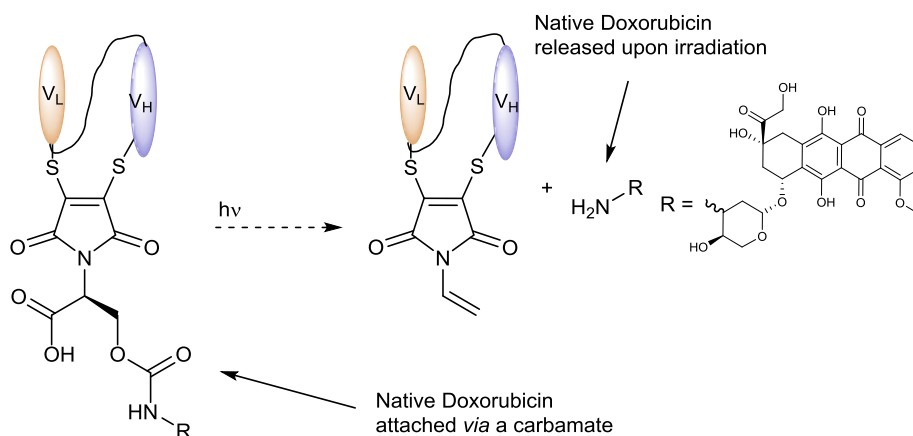
**Scheme 109**  
The photocleavable scFv-Dox conjugate based around novel thiomaleimide based photocleavable linkers.

The ease of synthesis, cysteine selectivity, low irradiation times, high cleavage yields and high wavelength of activation of these photocleavable linkers offer several significant benefits over the current state of the art and are certainly worthy of further investigation. Though work towards realising the final application is still underway current results suggest that these reagents could play an important role in the emerging field of photochemically activated antibody based therapeutics.

## 2.4.8: Future Work

### 2.4.8.1: Perfecting the photochemical-scFv-Doxorubicin conjugate

Though the “click” approach to generating a photocleavable ADC would be desirable it has become apparent that the changes to the Doxorubicin structure required to allow this approach have a considerable detrimental effect on the cytotoxicity of the drug. To remedy this situation a more direct approach will be taken by attaching the Doxorubicin directly to the photocleavable scaffold *via* a carbamate. Upon irradiation pure Doxorubicin **215** will be released, ensuring the desirable cytotoxic effect (Scheme 110).

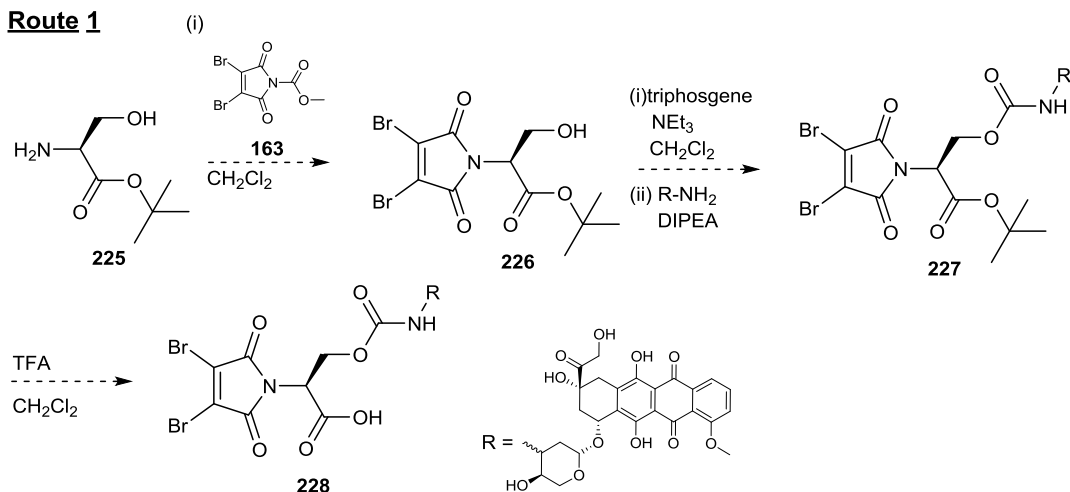


**Scheme 110**

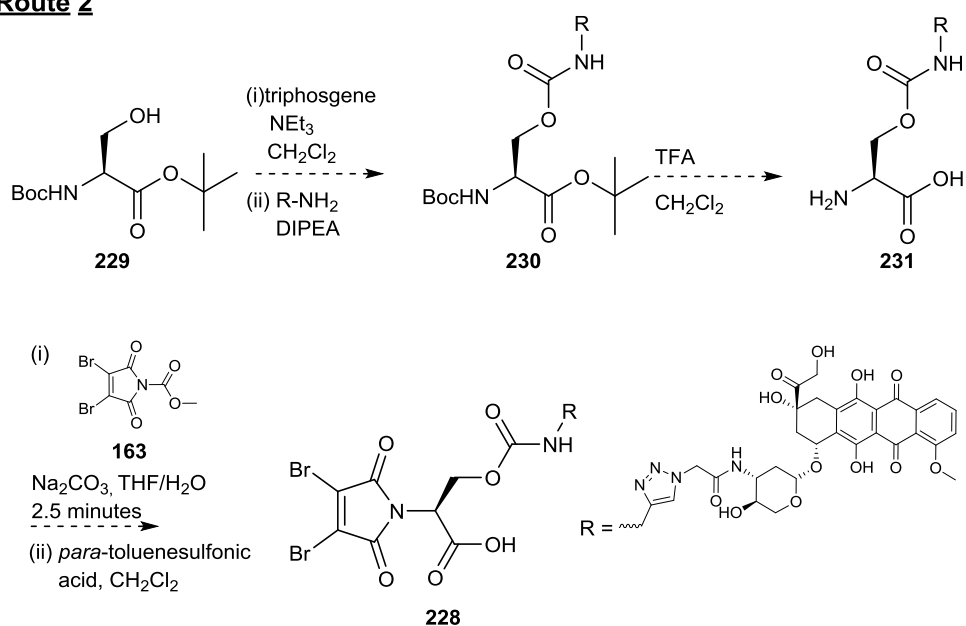
**A proposed method for utilising the thiomaleimide photocleavable linkers to release native Doxorubicin **215**.**

Two synthetic strategies towards the target dibromomaleimide have been designed (Scheme 111). The first route involves preparation of *tert*-Butyl protected dibromomaleimide-serine **225**, followed by conversion of the alcohol to a chloroformate and *in situ* reaction of the chloroformate with an amine to generate Doxorubicin functionalised dibromomaleimide carbamate **227**. Subsequent *tert*-Butyl deprotection would then reveal the necessary carboxylic acid to furnish target compound **228**. The second route starts from Boc-*tert*-Butyl protected serine **229**. Formation of the carbamate *via* the chloroformate is followed by deprotection of both the Boc and *tert*-Butyl groups in a single step to produce Dox-serine **231**. This species could then be reacted with activated dibromomaleimide **163** to produce the target compound **228**. In addition to proceeding *via* the chloroformate other coupling reagents such as carbonyldiimidazole and *para*-nitrophenolchloroformate could be explored for the formation of the carbamate.

### Route 1



### Route 2

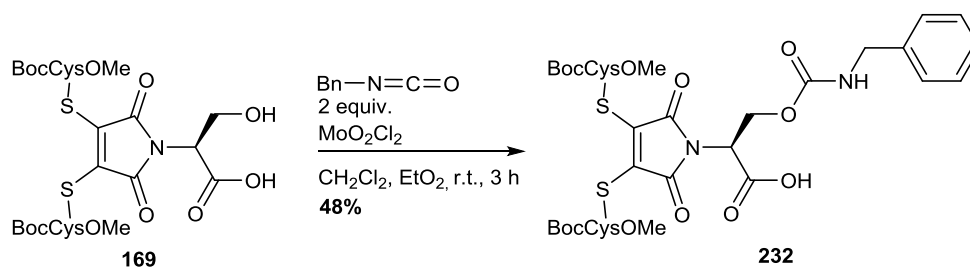


### Scheme 111

Proposed routes to the target doxorubicin releasing photocleavable linker **228**.

#### 2.4.8.2: Determining the quantum yield

Though the low reaction times of the photochemical thiomaleimide decarboxylation-elimination suggest a very efficient reaction it is necessary to obtain a quantum yield of photocleavage to get a true measure of the efficiency. Actinometry will be employed for this purpose and a direct comparison with a state of the art *O*-nitrobenzyl photocleavable linker will be made. Benzylcarbamate-dithiomaleimide-serine **232** has been synthesised for this purpose (Scheme 112).



**Scheme 112**  
The synthesis of benzylcarbamate-dithiomaleimide-serine **232**.

By monitoring the release of benzylamine as a function of absorbed photons a quantum yield of photocleavage will be obtained for these novel photocleavable linkers. A collaboration with Dr Michael Terzidis and Professor Richard Curry at the University of Surrey has already been established to complete this work.

### 2.4.8.3: Long term outlook

Given the advantages listed above the potential of this reaction is tremendous, though a significant body of work is still required to truly understand its intricacies and fully explore any possibilities. It would be interesting to alter the substitution on the maleimide alkene to test the affect that this would have on the efficiency of the reaction (Figure 56). It is known that the UV/Vis absorbance characteristics of maleimides are greatly affected by substitution at the alkene so it is reasonable to assume some effect on the efficiency of the reaction would be observed.

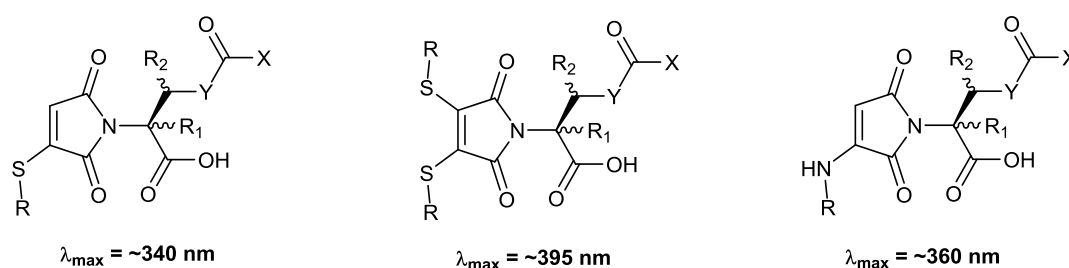
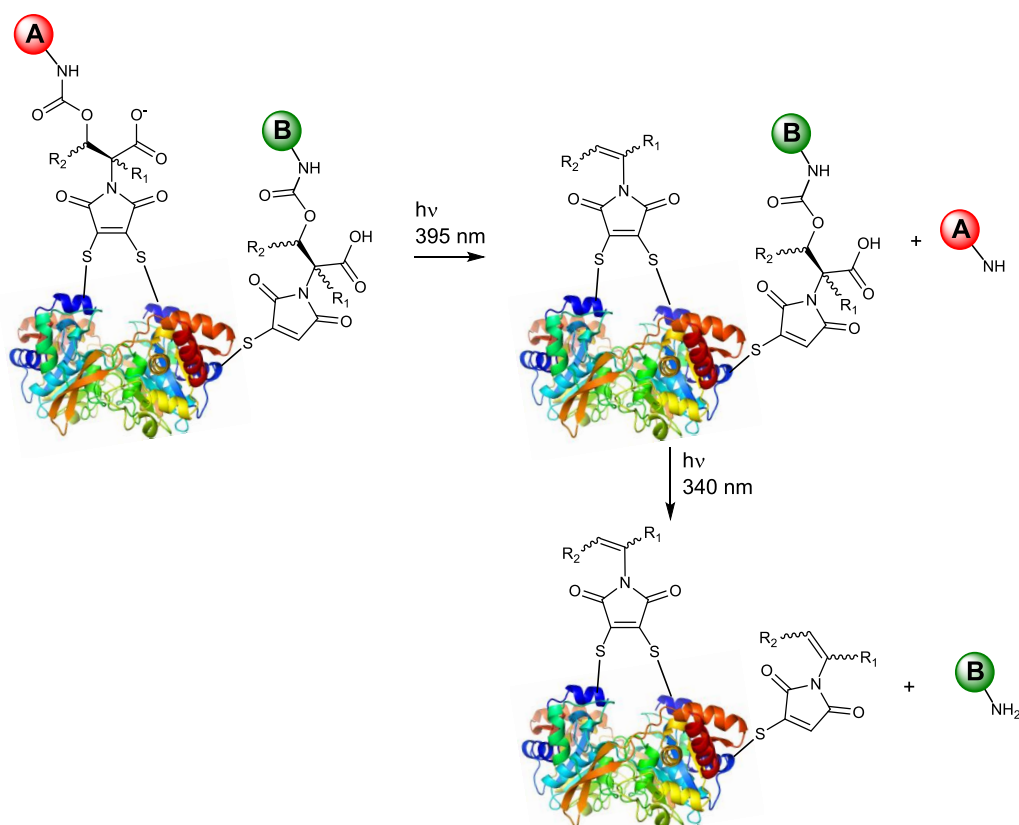


**Figure 56**  
Proposed modifications to the maleimide alkene of the photocleavable linkers.  $\lambda_{\max}$  values for thiomaleimides<sup>63</sup>, dithiomaleimides<sup>63</sup> and aminomaleimides<sup>325</sup> were obtained from the literature.

If substitution at the maleimide alkene was found to have no detrimental effect on the efficiency of the reaction a whole range of tuneable photocleavable linkers could be synthesised. This could lead to the development of an orthogonal system in which two different maleimide based photocleavable linkers are utilised to release two separate chemical payloads (Scheme 113).



**Scheme 113**  
**A conceptual application of orthogonal maleimide based photocleavable linkers.**

The two payloads could target separate therapeutic targets or even work synergistically to add a further layer of defence against off-target side effects i.e. payload A could be released in a pro-drug form and be subsequently converted to the active form by release of payload B. A “theranostics” approach could also be taken in which one payload is a therapeutic and the second is a diagnostic tool to monitor the effectiveness of the therapeutic.

Looking beyond the realm of photocleavable antibody drug conjugates this reaction could be employed for any application in which the incredibly efficient spatio-temporal release of a target compound is desired. Thus this reaction could be used in any application which currently employs photocleavable linkers i.e. protein purification,<sup>326</sup> solid phase synthesis,<sup>327</sup> photopolymerisation,<sup>21,92</sup> photorelease of fluorescent probes,<sup>328</sup> amongst many others.<sup>89</sup>

## 3: Experimental

### 3.1: Synthetic organic chemistry

#### 3.1.1: General experimental

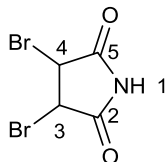
All reagents and starting materials were obtained from chemical suppliers, unless specifically stated otherwise, and were used as received. Reactions were monitored by thin layer chromatography using pre-coated SIL G/UV 254 plates purchased from VWR. Flash chromatography was carried out manually using Kiesegel 60 M 0.04/0.063 mm silica gel or automatically using a BioTage Isolera with KP-Snap or KP-Sil columns. Reverse phase chromatography was carried out using a BioTage Isolera 1 with 10g C-18 prepacked columns provided by BioTage. Petrol refers to petroleum ether (40 - 60 °C). NMR spectra were recorded using a Bruker AC300, AC500 or AC600 spectrometer (300 MHz, 500 MHz and 600 MHz respectively). Chemical shifts ( $\delta$ ) are given in ppm units relative to the solvent reference and coupling constants ( $J$ ) are measured in Hertz. Proton ( $^1\text{H}$ ) NMR multiplicities are shown as s (singlet), d (doublet), t (triplet), q (quartet), m (multiplet), dd (double doublet), dt (double triplet), etc. Protons adjacent to diastereomeric carbons are labeled ` and ``. HMBC, HSQC and DEPT were employed to aid with accurate assignments. Infrared spectra were recorded on a Perkin Elmer Spectrum 100 FTIR spectrometer (ATR mode). Melting points were determined using a Gallenkamp apparatus. High and low resolution mass spectrometry of organic molecules was performed using a VG70 SE (EI or CI) or an LCT Premier mass spectrometer (ES). Mass spectrometry data for compounds **141**, **217**, **218** and **224** were obtained from the EPSRC Mass Spectrometry facility at Swansea using an LTQ Orbitrap XL. UV/Vis spectra were obtained using a ThermoScientific NanoDrop 2000C running in cuvette mode, using a quartz cuvette with a path length of 1 cm<sup>3</sup>. Extinction coefficients for all compounds were calculated by taking measurements at 0.3, 0.2 and 0.1 mM and averaging the results. Optical rotation values were obtained using a Perkins Elmer model 343 polarimeter operating at 21 °C (Currently non-operational).

Irradiation at 365 nm was performed using a commercial 5W LED torch purchased from Advanced NDT Ltd with an irradiance measurement of approximately 20 mW·cm<sup>-3</sup> at 14 cm. For large scale reactions the UV torch was placed adjacent to the round bottomed flask inside a reflective chamber at a distance of 14 cm and the beam directed through the solution. For small scale HPLC reactions the UV torch was placed adjacent to a 7 ml sample vile inside a reflective chamber at a distance of 14 cm and the beam directed through the solution. When a mercury lamp is specified a 125 W lamp from Photochemical Reactors Ltd was used in combination with a water cooled Pyrex immersion well.

## 3.1.2: Synthesis

### 3.1.2.1: Synthesis of monobromomaleimide reagents

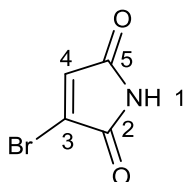
#### 2,3-dibromosuccinimide<sup>267</sup>



Maleimide (2.00 g, 20.0 mmol) was dissolved in CHCl<sub>3</sub> (15 ml), and bromine (1.16 ml, 20.0 mmol in 15 ml of CHCl<sub>3</sub>) was added dropwise over 10 minutes. The reaction mixture was refluxed for three hours, and then allowed to cool to room temperature. The yellow precipitate was filtered and washed with cold CHCl<sub>3</sub> (4 x 20 ml) to give the title compound as pale yellow crystals (4.20 g, 16.3 mmol) in an 81% yield.

m.p. 125.3 - 126.1 °C; <sup>1</sup>H NMR (500 MHz, CDCl<sub>3</sub>-d<sub>1</sub>) δ = 8.41 (1H, s, H-1), 4.73 (2H, s, H-3, 4); <sup>13</sup>C NMR (125 MHz, CDCl<sub>3</sub>-d<sub>1</sub>) δ = 169.8 (C-2,5), 42.8 (C-3,4); IR (solid, cm<sup>-1</sup>) 3284, 2988, 2947, 1790, 1730; MS (EI) m/z [M, relative intensity] 254.8 [<sup>79</sup>Br<sup>79</sup>BrM, 4.9], 256.8 [<sup>81</sup>Br<sup>79</sup>BrM, 10], 258.8 [<sup>81</sup>Br<sup>81</sup>BrM, 5]. Data matched the literature.<sup>267</sup>

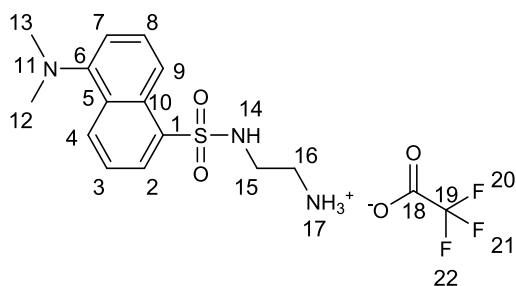
#### monobromomaleimide **93**<sup>267</sup>



2,3-dibromosuccinimide (1.00 g, 3.89 mmol) and sodium acetate trihydrate (1.59 g, 11.7 mmol) were dissolved in acetic acid (24 ml). The reaction mixture was refluxed for 90 minutes then cooled to room temperature. The solvent was evaporated, the crude solid dissolved in ethyl acetate (20 ml) and washed with sat. aqueous NaHCO<sub>3</sub> (3 x 20 ml). The organic phase was separated, dried over MgSO<sub>4</sub> and the solvent removed *in vacuo*. The impure solid was purified by flash chromatography (60% ethyl acetate in petrol) to afford the title compound **93** as a white powder (555 mg, 3.19 mmol) in an 82% yield.

m.p. 157.3 - 157.9 °C; <sup>1</sup>H NMR (500 MHz, CDCl<sub>3</sub>-d<sub>1</sub>) δ = 7.48 (1H, s, H-1), 6.89 (1H, s, H-4); <sup>13</sup>C (125 MHz, CDCl<sub>3</sub>-d<sub>1</sub>) δ = 168.0 (C-5), 164.9 (C-2), 132.9 (C-3), 132.3 (C-4); IR (solid, cm<sup>-1</sup>) 3231, 3104, 2681, 1780, 1763, 1708, 1578; MS (EI+) m/z [M, relative intensity] 174.9 [M<sup>79</sup>BrM+H, 100], 176.9 [M<sup>81</sup>BrM+H, 98]; Exact mass calcd for [C<sub>4</sub>H<sub>3</sub>NO<sub>2</sub><sup>79</sup>Br] 175.93417, found 175.93420. Data matched the literature.<sup>267</sup>

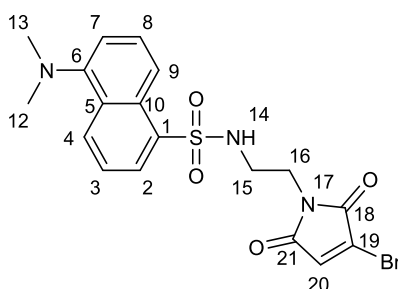
**2-((5-(dimethylamino)naphthalene)-1-sulfonamido)ethan-1-aminium 2,2,2-trifluoroacetate **108****<sup>151</sup>



*Tert*-Butyl (2-aminoethyl)carbamate (200 mg, 1.26 mmol) was dissolved in CH<sub>2</sub>Cl<sub>2</sub> (53 ml), and a solution of dansyl chloride (366 mg, 1.37 mmol) and triethylamine (455  $\mu$ l, 3.25 mmol) in CH<sub>2</sub>Cl<sub>2</sub> (53 ml) was added at room temperature. After stirring for four hours at room temperature the solvent was removed *in vacuo* and the residue was purified by flash chromatography (40% ethyl acetate in petrol) to afford a viscous oil. Trifluoroacetic acid (14 ml) was added and the cloudy grey solution was stirred for two hours at room temperature before all solvent was removed *in vacuo*. Dissolution in CH<sub>2</sub>Cl<sub>2</sub> and subsequent cooling to 0 °C resulted in precipitation of a solid which was collected and washed with Et<sub>2</sub>O (4 x 5 ml) to afford title compound **108** as a white solid (364 g, 0.895 mmol) in a 71% yield.

m.p. 159.4 – 161.4 °C (lit. m.p.160 - 162 °C<sup>151</sup>); <sup>1</sup>H NMR (600 MHz, MeCN-d<sub>3</sub>)  $\delta$  = 8.56 (1H, d, J = 8.7, H-4), 8.26 (1H, d, J = 8.7, H-2), 8.18 (1H, dd, J = 7.3, J = 1.1, H-9), 7.51 - 7.63 (2H, m, H-8, 3), 7.27 (1H, d, J = 7.3, H-7), 3.08 (2H, t, J = 6.0, H-15), 3.01 (2H, t, J = 6.0, H-16), 2.87 (6H, s, H-12, 13); <sup>13</sup>C NMR (150 MHz, MeCN-d<sub>3</sub>)  $\delta$  = 161.7 (q, J<sub>C-F</sub> = 27.3, C-18), 153.0 (C-6), 135.7 (C-1), 131.3 (C-4), 130.7 (C-10), 130.2 (C-5), 130.2 (C-9), 129.3 (C-8), 124.3 (C-3), 119.8 (C-2), 117.1 (C-19), 116.3 (C-7), 45.7 (C-12, 13), 41.0 (C-15), 41.0 (C-16); <sup>19</sup>F NMR (280 MHz, MeCN-d<sub>3</sub>)  $\delta$  = -70.5 (F-20 - 22); IR (solid, cm<sup>-1</sup>) 3090, 1659, 1624, 1530; MS (ES+) m/z [M, relative intensity] 362.2 [C<sub>14</sub>H<sub>15</sub>F<sub>3</sub>N<sub>2</sub>O<sub>4</sub>S, 100], 294.1 [M+H-TFA, 22]; Exact mass calcd for [C<sub>14</sub>H<sub>20</sub>N<sub>3</sub>O<sub>2</sub>S] 294.1276, found 294.1280. Data matched the literature<sup>151</sup>

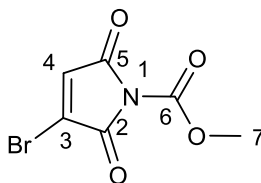
***N*-(2-(3-bromo-2,5-dioxo-2,5-dihydro-1*H*-pyrrol-1-yl)ethyl)-5-(dimethylamino)naphthalene-1-sulfonamide **110****<sup>151</sup>



Bromomaleic anhydride (21  $\mu$ l, 0.223 mmol) was added in a single portion to a solution of compound **108** (100 mg, 0.246 mmol) in AcOH (2.3 ml) and stirred at room temperature for 90 minutes before being raised to reflux for a further two hours. All solvent was removed *in vacuo* and the resulting crude material purified by flash chromatography (0 - 50% ethyl acetate in petrol) to afford a brown oil which was triturated with ethyl acetate to produce compound **110** as a brown solid (66 mg, 0.0146 mmol) in a 65% yield.

m.p. decomposition above 70 °C (lit. m.p. 70 - 71 °C<sup>151</sup>); <sup>1</sup>H NMR (600 MHz, MeCN-d<sub>3</sub>)  $\delta$  = 8.53 (1H, d, *J* = 8.7, H-4), 8.12 (2H, dd, *J* = 10.9, *J* = 8.3, H-2, 9), 7.39 - 7.73 (2H, m, H-3, 8), 7.26 (1H, d, *J* = 7.5, H-7), 6.67 (1H, s, H-20), 5.99 (1H, t, *J* = 6.2, H-14), 3.45 (1H, t, *J* = 6.2, H-16), 3.09 (2H, q, *J* = 6.2, H-15), 2.88 (6H, s, H-12, 13); <sup>13</sup>C NMR (150 MHz, MeCN-d<sub>3</sub>)  $\delta$  = 169.3 (C-21), 166.3 (C-18), 152.9 (C-6), 135.9 (C-1), 132.9 (C-20), 131.3 (C-4), 131.1 (C-10), 130.6 (C-5), 130.3 (C-19), 130.1 (C-9), 129.3 (C-8), 124.4 (C-3), 119.9 (C-2), 116.4 (C-7), 45.7 (C-12, 13), 41.4 (C-15), 39.2 (C-16); IR (solid, cm<sup>-1</sup>) 3326, 3093, 2950, 2838, 1717, 1585; MS (EI) *m/z* [*M*, relative intensity] 450.9 [<sup>79</sup>BrM, 97], 452.9 [<sup>81</sup>BrM, 100]; Exact mass calcd for [C<sub>18</sub>H<sub>18</sub><sup>79</sup>BrN<sub>3</sub>O<sub>4</sub>S] 451.02014, found 451.02069. Data matched the literature.<sup>151</sup>

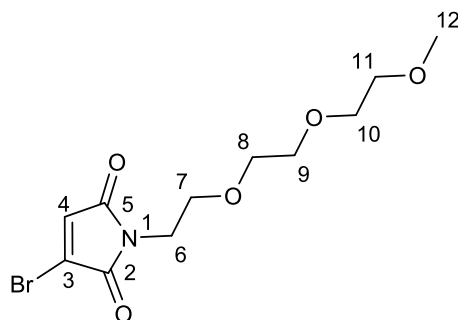
**methyl 3-bromo-2,5-dioxo-2,5-dihydro-1*H*-pyrrole-1-carboxylate **112****<sup>145</sup>



Monobromomaleimide **93** (100 mg, 0.572 mmol) and *N*-methylmorpholine (62.5  $\mu$ l, 0.572 mmol) were dissolved in tetrahydrofuran (5 ml). Methyl chloroformate (44  $\mu$ L, 0.527 mmol) was added dropwise and the reaction stirred at room temperature for 30 minutes. CH<sub>2</sub>Cl<sub>2</sub> (10 ml) was added and the organic phase washed with saturated aqueous Na<sub>2</sub>CO<sub>3</sub> (3 x 3 ml). The organic layer was dried over MgSO<sub>4</sub> and all solvent was removed *in vacuo* to yield title compound **112** as a pale pink solid (130 mg, 0.555 mmol) in a 97% yield.

m.p. 121.3 - 122.7 °C (lit. m.p 120 - 122 °C<sup>145</sup>); <sup>1</sup>H NMR (600 MHz, CDCl<sub>3</sub>-d<sub>1</sub>) δ = 7.02 (1H, s, H-4) 4.02 (3H, s, H-7); <sup>13</sup>C (125 MHz, CDCl<sub>3</sub>-d<sub>1</sub>) δ = 163.32 (C-5), 160.90 (C-2), 147.57 (C-6), 133.32 (C-4), 133.14 (C-3), 54.74 (C-7); IR (solid, cm<sup>-1</sup>) 2966, 1814, 1769, 1729; 1606; MS (CI<sup>+</sup>) m/z [M, relative intensity] 234.0 [<sup>79</sup>BrM+H, 8], 236.0 [<sup>89</sup>BrM+H, 9]; Exact mass calcd for [C<sub>6</sub>H<sub>5</sub>NO<sub>4</sub><sup>79</sup>Br] 233.93965, found 233.93922. Data matched the literature.<sup>145</sup>

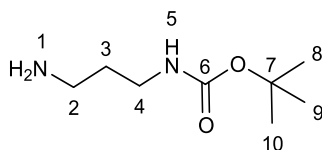
### 3-bromo-1-(2-(2-(2-methoxyethoxy)ethoxy)ethyl)-1H-pyrrole-2,5-dione **114**



Compound **112** (120 mg, 0.513 mmol) was dissolved in CH<sub>2</sub>Cl<sub>2</sub> (20 ml), 2-(2-(2-methoxyethoxy)ethoxy)ethanamine (84.0 mg, 0.513 mmol) was added and the reaction stirred at room temperature for two hours. The solvent was removed *in vacuo* and the crude product was purified by flash chromatography (2 - 10% MeOH in CH<sub>2</sub>Cl<sub>2</sub>) to produce title compound **114** as a yellow oil (130 mg, 0.404 mmol) in a 79% yield.

<sup>1</sup>H NMR (600 MHz, CDCl<sub>3</sub>-d<sub>1</sub>) δ = 6.70 (1H, s, H-4), 3.77 (2H, t, J = 6.0, H-6), 3.65 (2H, t, J = 6.0, H-7) 3.58 - 3.63 (6H, m, H-8, 9, 10), 3.53 (2H, t, J = 4.8, H-11), 3.37 (3H, s, H-12); <sup>13</sup>C (150 MHz, CDCl<sub>3</sub>-d<sub>1</sub>) δ = 168.56 (C-5), 165.37 (C-2), 132.01 (C-3), 131.48 (C-4), 72.0, 70.7 (x 2), 70.2 (C-8, 9, 10, 11), 67.78 (C-7), 59.20 (C-12), 38.31 (C-6); IR (film, cm<sup>-1</sup>) 2970, 2875, 1720, 1588; MS (EI) m/z [M, relative intensity] 201.9 [M<sup>79</sup>Br-C<sub>5</sub>H<sub>11</sub>O<sub>3</sub>, 80], 203.9 [M<sup>81</sup>Br-C<sub>5</sub>H<sub>11</sub>O<sub>3</sub>, 82]; Exact mass calcd for [C<sub>11</sub>H<sub>16</sub>BrNO<sub>5</sub>] 321.02119, found 321.02157. Data matched the literature.<sup>267</sup>

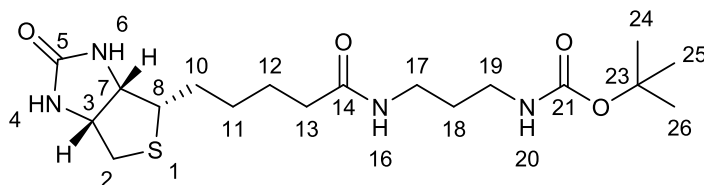
### *tert*-Butyl (3-aminopropyl)carbamate **115**<sup>329</sup>



Di-*tert*-Butyl dicarbonate (200 mg, 0.917 mmol) was dissolved in CHCl<sub>3</sub> (16 ml) and added dropwise over three hours to a solution of 1,3-diaminopropane (765 μL, 9.17 mmol) in CHCl<sub>3</sub> (50 ml) at 0 °C. After this time the solution was returned to room temperature and allowed to stir for 15 hours. The solution was then diluted with CHCl<sub>3</sub> (100 ml) and washed with K<sub>2</sub>CO<sub>3</sub> (2 x 50 ml) followed by H<sub>2</sub>O (2 x 50 ml). The organic layer was separated, dried over MgSO<sub>4</sub>, and then concentrated *in vacuo* to produce **115** as an orange oil (155 mg, 0.890) in a 97% yield. Product was taken on without further purification: <sup>1</sup>H NMR (600 MHz, CDCl<sub>3</sub>-d<sub>1</sub>) δ = 5.10 (1H, br. s., H-5), 3.10 (2H, q, J = 6.6, H-4), 2.68 (2H, t, J = 6.6, H-2),

1.54 (2H, q, J = 6.6, H-3), 1.45 (2H, br. s., H-1), 1.36 (9H, s, H-8, 9, 10);  $^{13}\text{C}$  (125 MHz,  $\text{CDCl}_3\text{-d}_1$ )  $\delta$  = 156.3 (C-6), 79.5 (C-7), 39.7 (C-2) 38.4 (C-4), 33.4 (C-3) 28.5 (C-8, 9, 10); IR (solid,  $\text{cm}^{-1}$ ) 3356, 2971, 2940, 2871, 1737, 1680, 1583; MS (EI)  $m/z$  [M, relative intensity] 175.2 [M+H, 100]. Spectra matched the literature.<sup>329</sup>

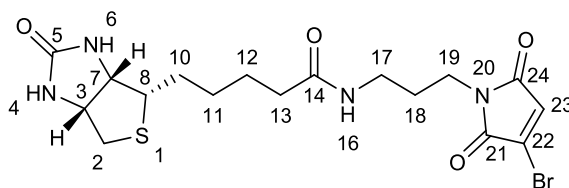
***tert*-Butyl (3-(5-((4S)-2-oxohexahydro-1H-thieno[3,4-d]imidazol-4-yl)pentanamido)propyl)carbamate 116**



D-Biotin (295 mg, 1.21 mmol), HBTU (398 mg, 1.05 mmol) and DIPEA (221  $\mu\text{L}$ , 1.27 mmol) were dissolved in DMF (5 ml) and stirred for 20 minutes at room temperature. This mixture was then added dropwise over 20 minutes to a solution of *tert*-Butyl (3-aminopropyl)carbamate **115** (140 mg, 0.804 mmol) in DMF (3 ml) and stirred for two hours at room temperature. After this time toluene (70 ml) was added and all solvent was removed *in vacuo*. The crude residue was purified by column chromatography (2% - 10% MeOH/ $\text{CH}_2\text{Cl}_2$  followed by subsequent purification in 70% ethyl acetate in petrol) to yield title compound **116** as a yellow oil (225 mg, 0.512 mmol) in a 70% yield.

$^1\text{H}$  NMR (600 MHz,  $\text{CDCl}_3\text{-d}_1$ )  $\delta$  = 6.91 (1H, s, H-16), 6.73 (1H, s, H-20), 5.80 (1H, s, H-4), 5.14 (1H, s, H-6) 4.40 - 4.55 (1H, m, H-3) 4.25 - 4.32 (1H, m, H-7), 3.10-3.15 (3H, m, H-8 + H-19), 2.89 (1H, dd, J = 12.6, J = 8.5, H-2'), 2.72 (1H, dd, J = 12.6, J = 8.5, H-2''), 2.32 (2H, t, J = 7.5, H-17), 2.19 (2H, t, J = 7.8, H-13), 1.74 - 1.59 (6H, m, H-10, 12, 18),  $\delta$ 1.37-1.47 (11H, m, H-11, H-24-26);  $^{13}\text{C}$  (125 MHz,  $\text{CDCl}_3\text{-d}_1$ )  $\delta$  = 173.92 (C-14) 164.31(C-5), 156.72 (C-21), 79.36 (C-23) 62.01 (C-3), 60.32 (C-7), 55.88 (C-8), 40.68 (C-2), 37.35 (C 19) 36.64 (C-17), 36.06 (C-13) 30.04, 29.80, 25.94, 24.89 (C-10, 11, 12, 18), 28.54 (C 24-26); IR (solid,  $\text{cm}^{-1}$ ) 3450, 2960, 1744, 1608, 1550; MS (CI)  $m/z$  [M, relative intensity] 401.2 [M+H, 6] 301.2 [ $\text{C}_{13}\text{H}_{25}\text{N}_4\text{O}_2\text{S}$ , 100]; Exact mass calcd for [ $\text{C}_{18}\text{H}_{33}\text{N}_4\text{O}_4\text{S}$ ] 401.22170, found 401.22256.

**N-(3-(3-bromo-2,5-dioxo-2,5-dihydro-1H-pyrrol-1-yl)propyl)-5-((4S)-2-oxohexahydro-1H-thieno[3,4-d]imidazol-4-yl)pentanamide 117**



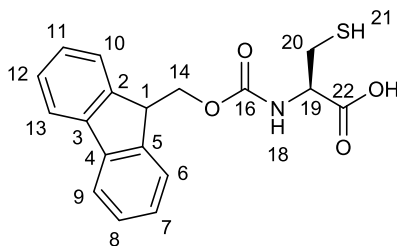
Compound **116** (100 mg, 0.250 mmol) was dissolved in trifluoroacetic acid (5 ml) and stirred for 15 hours. After this time toluene (50 ml) was added and the solvent removed *in vacuo*. The crude material was dissolved in acetic acid (10 ml) and bromomaleic anhydride

(45.0 mg, 0.250 mmol) was added. The reaction was heated under reflux for three hours, then allowed to return to room temperature. All solvents were removed *in vacuo* and the crude residue purified by flash chromatography (2% to 10% MeOH in CH<sub>2</sub>Cl<sub>2</sub>) to afford title compound **117** as a white powder (75.0 mg, 0.164 mmol) in a 66% yield.

<sup>1</sup>H NMR (400 MHz, MeOD-d<sub>4</sub>) δ = 7.96 (1H, br. s., H-16), 7.13 (1H, s, H-23), 4.48 - 4.53 (1H, m, H-3), 4.34 (1H, dd, J = 7.5, J = 4.4, H-7), 3.59 (2H, t, J = 7.2, H-19), 3.23 - 3.27 (1H, m, H-8), 3.20 (2H, q, J = 9.2, H-17), 2.95 (1H, dd, J = 12.8, J = 5.0, H-2'), 2.72 (1H, d, J = 12.8, H-2''), 2.22 (2H, t, J = 11.6, H-13), 1.57 - 1.85 (6H, m, H-10, 12, 18), 1.44 - 1.52 (2H, m, H-11); <sup>13</sup>C NMR (150 MHz, DMSO-d<sub>6</sub>) δ = 172.0 (C-14), 169.0 (C-21), 165.6 (C-24), 162.7 (C-5), 132.6 (C-23), 130.4 (C-22), 61.0 (C-3), 59.2 (C-7), 55.4 (C-8), 41.4 (C-2), 36.3 (C-19), 36.1 (C-17), 35.2 (C-13), 28.2, 28.1, 28.1 (C-10, C-12, C-18), 25.3 (C-11); IR (solid, cm<sup>-1</sup>) 3287, 2932, 2861, 1779, 1700, 1645, 1590, 1548; MS (ES+) m/z [M, relative intensity] 481.1 [M<sup>79</sup>BrM+Na, 98], 483.1 [M<sup>81</sup>BrM+Na, 100]; Exact mass calcd for [C<sub>17</sub>H<sub>23</sub><sup>79</sup>BrN<sub>4</sub>O<sub>4</sub>SNa] 481.0521, found 481.0533.

### 3.1.2.2: Synthesis of C-terminal cysteine models

#### (((9H-fluoren-9-yl)methoxy)carbonyl)-L-cysteine **132**

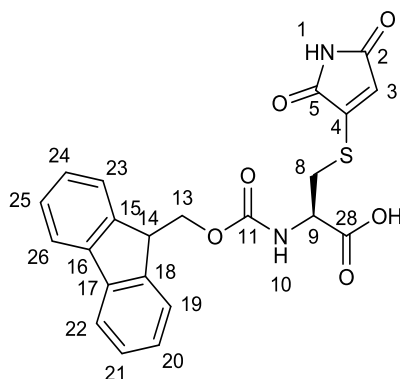


Fmoc-Cys-(Trt)-OH (1.00 g, 1.71 mmol) was suspended in CH<sub>2</sub>Cl<sub>2</sub> (68 ml) and stirred under argon at room temperature. To this suspension triisopropylsilane (2 ml, 9.76 mmol) was added, followed by trifluoroacetic acid (8 ml, 104 mmol). The solution was stirred for 10 minutes at room temperature, before all solvent was removed *in vacuo*. Excess trifluoroacetic acid was azeotropically removed by co-evaporation with CH<sub>2</sub>Cl<sub>2</sub>. The resulting white solid was placed onto filter paper and washed with hexane (8 x 30 ml), before being dried under vacuum to produce title compound **132** as a white solid (563 mg, 1.64 mmol) in a 96% yield.

m.p. 115.5 - 117.0 °C; <sup>1</sup>H NMR (600 MHz, DMSO-d<sub>6</sub>) δ = 7.90 (2H, d, J = 7.4, H-13, 9), 7.74 (2H, d, J = 7.4, H-10, 6), 7.70 (1H, d, J = 8.0, H-18), 7.42 (2H, t, J = 7.4, H-12, 8), 7.33 (2H, t, J = 7.4, H-7, 11), 4.31 (2H, d, J = 6.5, H-14), 4.24 (1H, t, J = 6.5, H-1), 4.12 (1H, dt, J = 8.0, J = 4.3, H-19), 2.85 - 2.93 (1H, m, H-20'), 2.70 - 2.77 (1H, m, H-20''), 1.23 (1H, broad s, H-21); <sup>13</sup>C NMR (150 MHz, DMSO-d<sub>6</sub>) δ = 171.9 (C-22), 156.1 (C-16), 143.8 (C-2, 5), 140.8 (C-3, 4), 127.7 (C-7, 11), 127.1 (C-8, 12), 125.3 (C-6, 10), 120.2 (C-9, 13), 65.7 (C-14), 56.6 (C-19), 46.6 (C-1), 25.5 (C-20); IR (solid, cm<sup>-1</sup>) 3312, 1696, 1531, 1447, 1426;

MS (ES+) m/z [M, relative intensity] 366.1 [M+Na] 100], 179.1 [C<sub>14</sub>H<sub>11</sub>, 7]; Exact mass calcd for [C<sub>18</sub>H<sub>17</sub>NO<sub>4</sub>SNa] 366.0776, found 366.0748.

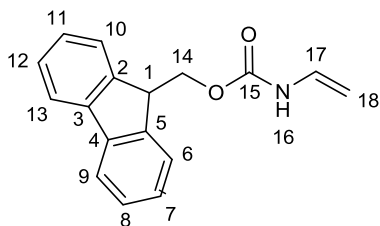
**N-(((9H-fluoren-9-yl)methoxy)carbonyl)-S-(2,5-dioxo-2,5-dihydro-1H-pyrrol-3-yl)-L-cysteine **133****



Fmoc-cysteine **132** (177 mg, 0.515 mmol) and sodium acetate (93.0 mg, 1.133 mmol) were dissolved in MeOH (10 ml) and stirred for five minutes under argon. Monobromomaleimide **93** (100 mg, 0.567 mmol) was subsequently added and the solution stirred for 20 minutes at room temperature. All solvent was removed *in vacuo*, the crude material suspended in ethyl acetate (25 ml) and washed with 10% aqueous citric acid (12 ml). The organic layer was collected, dried over MgSO<sub>4</sub> and all solvent removed *in vacuo*. Purification by flash chromatography (2% - 8% MeOH in CH<sub>2</sub>Cl<sub>2</sub> with 1% AcOH) afforded title compound **133** as a light orange powder (200 mg, 0.457 mmol) in a 90% yield.

m.p. decomposition above 120 °C; <sup>1</sup>H NMR (600 MHz, DMSO-d<sub>6</sub>) δ = 11.03 (1H, s, H-29), 7.91(1H, br. s, H-10), 7.89 (2H, d, J = 7.5, H-22, 26), 7.70 (2H, dd, J = 7.5, J = 3.1, H-19, 23), 7.42 (2H, t, J = 7.5, H-21, 25), 7.32 (2H, t, J = 7.5, H-20, 24), 6.49 (1H, s, H-3), 4.25 - 4.35 (3H, m, H-13, 9), 4.23 (1H, t, J = 7.2, H-14), 3.43 (1H, dd, J = 13.5, J = 4.3, H-8'), 3.25 (1H, dd, J = 13.5, J = 9.3, H-8''); <sup>13</sup>C NMR (150 MHz, DMSO-d<sub>6</sub>) δ = 171.4 (C-28), 170.9 (C-2), 169.3 (C-5), 156.0 (C-11), 150.0 (C-4), 143.8 (C-15, 18), 140.7 (C-17, 16), 127.7 (C-20, 24), 127.1 (C-21, 25), 125.2 (C-19, 23), 120.2 (C-22, 26), 119.5 (C-3), 65.9 (C-13), 52.5 (C-9), 46.6 (C-14), 32.7 (C-8); IR (solid, cm<sup>-1</sup>) 3316, 1735, 1705, 1685, 1529, 1448; MS (ES+) m/z [M, relative intensity] 461.1 [M+Na, 100], 366.1 [M-C<sub>4</sub>H<sub>2</sub>O<sub>2</sub>N+Na, 5], 179.1[C<sub>14</sub>H<sub>11</sub>,1]; Exact mass calcd for [C<sub>22</sub>H<sub>18</sub>N<sub>2</sub>O<sub>6</sub>SNa] 461.0783, found 461.0760; ε<sub>344</sub> (MeOH) = 3523 M<sup>-1</sup>·cm<sup>-1</sup>.

### (9H-fluoren-9-yl)methyl vinylcarbamate **134**

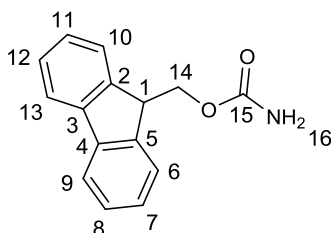


#### Method 1

Compound **133** (40.0 mg, 0.0912 mmol) and sodium acetate (8.22 mg, 0.100 mmol) were dissolved in MeOH (240 ml) and the entire solution degassed with argon for 30 minutes. The solution was irradiated using a medium pressure mercury lamp for one hour. All solvent was removed *in vacuo* at room temperature and the resulting crude material was washed with Et<sub>2</sub>O (3 x 20 ml). The organic washings were collected and the organic solvent evaporated *in vacuo* to yield enamide **134** as a white solid (22 mg, 0.0867 mmol) in a 95% yield. 5 mg (0.0188 mmol) of the product was dissolved in MeOD-d<sub>4</sub> containing sodium acetate (5 mg, 0.0610 mmol) for stabilisation.\*Under non-basic conditions degradation to amide **136** was observed\*

m.p. decomposes above 130 °C; <sup>1</sup>H NMR (600 MHz, MeOD-d<sub>4</sub>) δ = 7.80 (2H, d, J = 7.5, H-9, 13), 7.66 (2H, d, J = 7.5, H-9, 6, 10), 7.39 (2H, t, J = 7.5, H-8, 12), 7.32 (2H, t, J = 7.5, H-7, 11), 6.63 (1H, dd, J = 15.8, J = 9.0, H-17), 4.55 (1H, d, J = 15.8, H-18a), 4.41 (2H, d, J = 6.8, H-14), 4.23 (2H, m, H-18b + H-1); <sup>13</sup>C NMR (150 MHz, MeOD-d<sub>4</sub>) δ = 156.2 (C-15), 145.1 (2, 5), 142.6 (3, 4), 131.4 (C-17), 128.8 (C-7,11), 128.2 (C-8, 12), 126.1 (C-6, 10), 121.0 (C-9, 13) 93.8 (C-18) 68.0 (C-14), 48.3 (C-1); IR (solid, cm<sup>-1</sup>) 3313, 2922, 2852, 1699, 1649; MS (EI) m/z [M, relative intensity] 265.1 [M+H, 3], 178.1 [Fmoc-CH<sub>3</sub>,100]; Exact mass calcd for [C<sub>17</sub>H<sub>15</sub>NO<sub>2</sub>Na] 288.1000, found 288.0989.

### (9H-fluoren-9-yl)methyl carbamate **136**

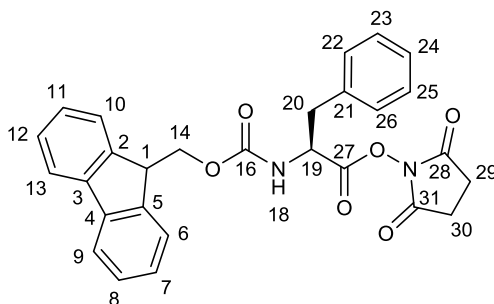


Enecarbamate **134** (20.0 mg, 0.0750 mmol) was dissolved in CH<sub>3</sub>Cl (1 ml) and 0.5 ml of dilute HCl (0.1 M) was added. The solution was stirred vigorously at room temperature for 30 minutes before all solvent was removed *in vacuo* to yield title compound **136** as a white solid (18.0 mg, 0.0750 mmol) in a quantitative yield.

m.p. 198.5 - 201.5 °C; (lit. m.p. 192 - 195 °C<sup>330</sup>); <sup>1</sup>H NMR (600 MHz, CDCl<sub>3</sub>-d<sub>1</sub>) δ = 7.78 (2H, d, J = 7.5, H-9, 13), 7.61 (2H, d, J = 7.5, H-6, 10), 7.42 (2H, t, J = 7.5, H-8, 12), 7.33

(2H, t, J = 7.5, H-11, 7), 4.60 (2H, broad s, H-16), 4.42 (2H, d, J = 7.0, H-14), 4.25 (1H, t, J = 7.0, H-1); <sup>13</sup>C NMR (150 MHz, CDCl<sub>3</sub>-d<sub>1</sub>) δ = 156.7 (C-15), 143.9 (C-2, 5), 141.4 (C-3, 4), 127.9 (C-7, 11), 127.2 (C-8, 12), 125.1 (C-6, 10), 120.1 (C-9, 13), 67.0 (C-14), 47.2 (C-1); IR (solid, cm<sup>-1</sup>); MS (ES+) m/z [M, relative intensity] 262.1 [M+Na, 70], 179.1 [C<sub>14</sub>H<sub>11</sub>, 5]; Exact mass calcd for [C<sub>15</sub>H<sub>13</sub>NO<sub>2</sub>Na] 262.0844, found 262.0824.

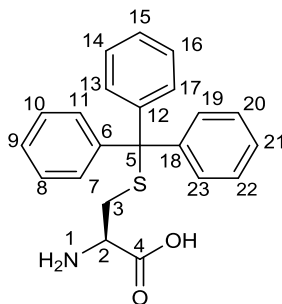
**2,5-dioxopyrrolidin-1-yl (((9H-fluoren-9-yl)methoxy)carbonyl)-L-phenylalaninate**  
**138**



Fmoc-L-Phe (3.00 g, 7.74 mmol) and N-Hydroxysuccinimide (897 mg, 7.74 mmol) were suspended in CH<sub>2</sub>Cl<sub>2</sub> (90 ml) and stirred under argon at room temperature. 1-Ethyl-3-(3-dimethylaminopropyl)carbodiimide was added and the resulting solution stirred for four hours. All solvent was removed *in vacuo* and the resulting white solid dissolved in CH<sub>2</sub>Cl<sub>2</sub> (50.0 ml). The organic layer was washed with 10% aqueous citric acid (10 ml), followed by saturated Na<sub>2</sub>CO<sub>3</sub> (30 ml) and finally brine (2 x 30 ml). The organic layer was dried over MgSO<sub>4</sub> and all solvent removed *in vacuo* to produce title compound **138** as a white powder (3.50 g, 7.22 mmol) in a 97% yield.

m.p. 68 - 71 °C; <sup>1</sup>H NMR (600 MHz, CDCl<sub>3</sub>-d<sub>1</sub>) δ = 7.77 (2H, d, J = 7.5, H-9, 13), 7.54 (2H, dd, J = 7.5, J = 3.4, H-6, 10), 7.41 (2H, t, J = 7.5, H-8, 12), 7.26 - 7.34 (7H, m, H-7, 11, 22 - 26), 5.27 (1H, d, J = 8.6, H-18), 5.06 (1H, dt, J = 8.6, J = 6.0, H-19), 4.45 (1H, dd, J = 10.6, J = 7.2, H-14'), 4.35 (1H, dd, J = 10.6, J = 7.2, H-14''), 4.19 (1H, t, J = 7.2, H-1), 3.33 (1H, dd, J = 14.2, J = 6.0, H-20'), 3.23 (1H, dd, J = 14.2, J = 6.0, H-20''), 2.82 (4H, s H-29 + 30); <sup>13</sup>C NMR (150 MHz, CDCl<sub>3</sub>-d<sub>1</sub>) δ = 168.8 (C-28, 31), 167.6 (C-27), 155.4 (C-16), 143.9 (C-2, 5), 141.4 (C-3, 4), 134.5 (C-21), 129.8 (C-26, 22), 128.9 (C-25, 23), 127.9 (C-7, 11), 127.7 (C-24), 127.2 (C-8, 12), 125.3 (C-6, 10), 120.1 (C-9, 13), 67.3 (C-14), 53.1 (C-19), 47.2 (C-1), 38.1 (C-20), 25.7 (C-29 + 30); IR (solid, cm<sup>-1</sup>) 3329, 1737, 1702; MS (EI) m/z [M, relative intensity] 484.1 [M+H, 1], 178.1 [C<sub>14</sub>H<sub>11</sub>, 100], 165.1 [C<sub>13</sub>H<sub>9</sub>, 17]; Exact mass calcd for [C<sub>28</sub>H<sub>24</sub>N<sub>2</sub>O<sub>6</sub>] 484.16344, found 484.163121.

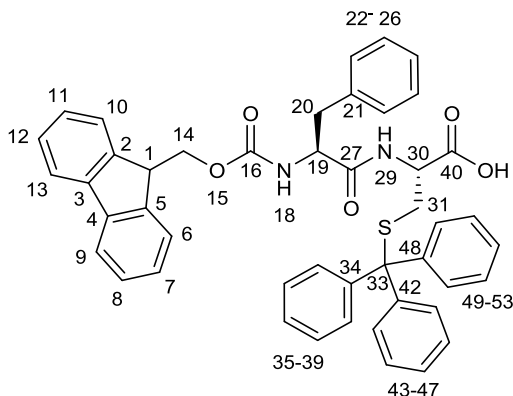
## S-Trityl-L-cysteine **140**



Fmoc-Cys-Trt-OH (600 mg, 1.02 mmol) was dissolved in piperidine (10.0 ml, 30% in DMF) and stirred at room temperature for one hour. All solvent and excess piperidine was removed by co-evaporation with toluene to leave a crude white solid. This solid was transferred to filter paper and washed with hexane (12 x 10 ml) to produce title compound **140** as a white powder (366 mg, 1.01 mmol) in a quantitative yield.

m.p. decomposition above 190 °C; <sup>1</sup>H NMR (600 MHz, DMSO-d<sub>6</sub>) δ = 7.30 - 7.28 (15H, m, Phe), 2.91 (1H, dd, J = 9.2, J = 4.3 Hz, H-2), 2.57 (1H, dd, J = 12.6, J = 4.3, H-3'), 2.40 (1H, dd, J = 12.6, J = 9.2, H-3''); <sup>13</sup>C NMR (150 MHz, DMSO-d<sub>6</sub>) δ = 167.9 (C-4), 144.3 (C-6, 12, 18), 129.2 (C-7, 11, 13, 17, 19, 23), 128.1 (C-8, 10, 14, 16, 20, 22), 126.8 (C-9, 15, 21), 66.0 (C-5), 53.4 (C-2), 33.5 (C-3); IR (solid, cm<sup>-1</sup>) 3051, 1650; MS (ES+) m/z [M, relative intensity] 243.1 [C(C<sub>6</sub>H<sub>5</sub>)<sub>3</sub>, 100]; Exact mass calcd for [C<sub>22</sub>H<sub>21</sub>NO<sub>2</sub>SNa] 386.1191, found 386.1198.

## N-(((9H-fluoren-9-yl)methoxy)carbonyl)-L-phenylalanyl)-S-trityl-L-cysteine **141**

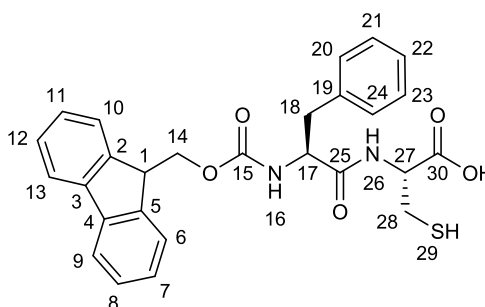


N,N-Diisopropylethylamine (0.570 ml, 3.3 mmol) was added to a suspension of compounds **138** (800 mg, 1.65 mmol) and **140** (602 mg, 1.65 mmol) in DMF (35 ml) and stirred at room temperature for one hour. Toluene (100 ml) was added and all solvent removed *in vacuo* to produce a crude gum. Purification by flash chromatography (1 - 6% MeOH in CH<sub>2</sub>Cl<sub>2</sub> with 1% AcOH) produced dipeptide **141** as a white powder (640 mg, 0.87 mmol) in a 53% yield.

m.p. 109.5 - 111.0 °C; <sup>1</sup>H NMR (600 MHz, DMSO-d<sub>6</sub>) δ = 8.44 (1H, d, J = 7.3, H-18), 7.88 (2H, d, J = 7.6, H-9, 13), 7.65 (1H, d, J = 8.7, H-29), 7.62 (2H, d, J = 7.6, H-6, 10), 7.40 (2H, t, J = 7.6, H-8, 12), 7.12 - 7.35 (22H, m, H-7, 11, 22-26, 35-39, 43-47, 49-53), 4.31

(1H, td, J = 8.7, J = 3.4, H-30), 4.18 (1H, td, J = 7.3, J = 5.2, H-19), 4.03 - 4.14 (3H, m, H-1, 14', 14''), 3.00 (1H, dd, J = 13.7, J = 3.4, H-31'), 2.75 (1H, dd, J = 13.7, J = 3.4, H-31''), 2.52 (1H, dd, J = 12.1, J = 5.2, H-20'), 2.42 (1H, dd, J = 12.1, J = 5.2, H-20''); <sup>13</sup>C NMR (150 MHz, DMSO-d<sub>6</sub>) δ = 171.7 (C-40), 171.6 (C-27), 155.8 (C-16), 144.2 (C-48, 42, 34), 143.8 (C-2,5), 140.7 (C-4, 3), 138.1 (C-21), 125.3-129.3 (C-7,11, C-6,10, C-8,12, C-22-26, 35-39, 43-47, 49-53) 120.1 (C-9, 13), 66.2 (C-33), 65.7 (C-14), 56.0 (C-30), 55.0 (C-19), 46.5 (C-1), 40.0 (C-31), 37.4 (C-20); IR (solid, cm<sup>-1</sup>) 3287, 3089, 1712, 1623 1592; MS (ES+) m/z [M, relative intensity] 731.3 [M+H, 100]; Exact mass calcd for [C<sub>46</sub>H<sub>40</sub>N<sub>2</sub>O<sub>5</sub>S] 731.2585, found 731.2578.

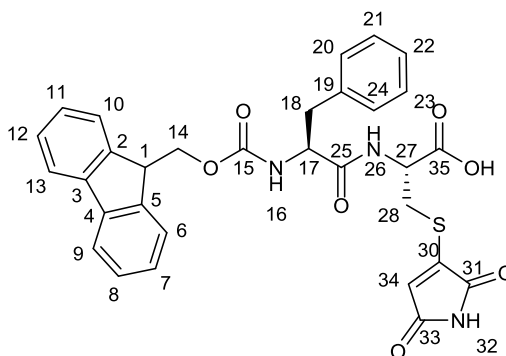
**(((9H-fluoren-9-yl)methoxy)carbonyl)-L-phenylalanyl-L-cysteine **142****



Triisopropylsilane (480 μl, 2.33 mmol) and trifluoroacetic acid (2.4 ml) were added to a solution of **141** (300 mg, 0.408 mmol) in CH<sub>2</sub>Cl<sub>2</sub> (20 ml) and stirred at room temperature for 15 minutes. All solvent was removed *in vacuo*, and excess trifluoroacetic acid was co-evaporated with Et<sub>2</sub>O (4 x 20 ml). The resulting white solid was transferred to filter paper and washed with hexane (5 x 30 ml) to give title compound **142** (190 mg, 0.387 mmol) as a white solid in a 95% yield.

m.p. decomposition above 130 °C; <sup>1</sup>H NMR (600 MHz, DMSO-d<sub>6</sub>) δ = 8.36 (1H, d, J = 7.7, H-16), 7.88 (2H, d, J = 7.5, H-9, 13), 7.68 (1H, d, J = 8.9, H-26), 7.63 (2H, t, J = 7.5, H-6, 10), 7.41 (2H, dt, J = 7.5, J = 5.1, H-8, 12), 7.32 (2H, t, J = 7.5, H-11, 7), 7.23 - 7.31 (4H, m, H-20, 21, 23, 24), 7.18 (1H, t, J = 7.5, H-22), 4.45 (1H, td, J = 7.7, J = 4.7, H-17), 4.34 (1H, td, J = 8.9, J = 3.7, H-27), 4.11 - 4.21 (3H, m, H-1, 14), 3.03 (1H, dd, J = 13.6, J = 3.7, H-28'), 2.90 (1H, ddd, J = 13.5, J = 8.5, J = 4.6, H-28''), 2.75 - 2.84 (2H, m, H-18), 2.43 (1H, t, J = 8.5, H-29); <sup>13</sup>C NMR (150 MHz, DMSO-d<sub>6</sub>) δ = 171.8 (C-30), 171.5 (C-25), 155.8 (C-15), 143.8 (C-2,5), 140.7 (C-3,4), 138.1 (C-19), 129.3 (C-20, 24), 128.1 (C-21, 23), 127.7 (C-7, 11), 127.1 (C-8, 12), 126.3 (C-22), 125.4 (C-6, 10), 120.1 (C-9, 13), 65.7 (C-14), 56.0 (C-17), 54.4 (C-27), 46.6 (C-1), 37.4 (C-18), 25.6 (C-28); IR (solid, cm<sup>-1</sup>) 3302, 3062, 2901, 1700, 1688, 1656; MS (ES+) m/z [M, relative intensity] 513.1 [M+Na], 75], 206.1 [C<sub>11</sub>H<sub>13</sub>NOS<sub>2</sub>]; Exact mass calcd for [C<sub>27</sub>H<sub>26</sub>N<sub>2</sub>O<sub>5</sub>S]+Na 513.1460, found 513.1456.

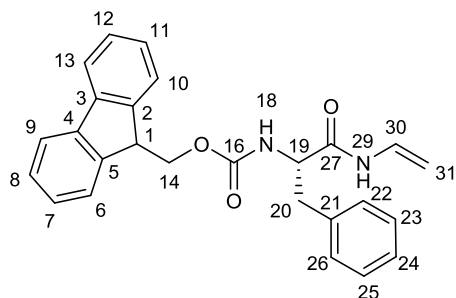
**N-(((9H-fluoren-9-yl)methoxy)carbonyl)-L-phenylalanyl)-S-(2,5-dioxo-2,5-dihydro-1H-pyrrol-3-yl)-L-cysteine **143****



Compound **142** (50 mg, 0.102 mmol) and sodium acetate (18.4 mg, 0.224 mmol) were dissolved in MeOH (2 ml) and stirred for five minutes under argon. Monobromomaleimide **93** (20 mg, 0.112 mmol) was subsequently added and the solution stirred for 30 minutes at room temperature. All solvent was removed *in vacuo*, the crude material suspended in ethyl acetate (5 ml) and washed with 10% aqueous citric acid (2 ml). The organic layer was collected, dried over MgSO<sub>4</sub> and all solvent removed *in vacuo*. Purification by flash chromatography (2% - 8% MeOH in CH<sub>2</sub>Cl<sub>2</sub> with 1% AcOH) afforded cysteine-maleimide **143** as an off white wax (47 mg, 0.080 mmol) in a 79% yield.

<sup>1</sup>H NMR (600 MHz, DMSO-d<sub>6</sub>) δ = 7.87 (2H, d, J = 7.5, H-9, 13), 7.73 (2H, d, J = 7.9, H-16), 7.62 (2H, t, J = 6.6, H-6, 10), 7.40 (2H, td, J = 7.5, J = 4.5, H-8, 12), 7.22 - 7.34 (7H, m, H-7, 11, 20, 21, 23, 24, 26), 7.17 (1H, t, J = 7.1, H-22), 6.49 (1H, s, H-34), 4.41 - 4.55 (1H, m, H-17), 4.27 (1H, t, J = 7.4, H-27), 4.08 - 4.15 (3H, m, H-1, 14), 3.44 (2H, dd, J = 13.4, J = 5.1, H-28`), 3.30 (3H, dd, J = 13.4, J = 7.4, H-28`), 3.03 (1H, dd, J = 13.7, J = 3.2, H-18`), 2.76 (1H, dd, J = 13.7, J = 11.3, H-18`); <sup>13</sup>C NMR (150 MHz, DMSO-d<sub>6</sub>) δ = 171.7 (C-35), 171.4 (C-25), 169.3 (C-33), 167.6 (C-31), 155.5 (C-15), 151.1 (C-30), 143.8 (C-2,5), 140.6 (C-3,4), 138.0 (C-19), 129.3 (C-20, 24), 128.2 (C-21, 23), 127.7 (C-7, 11), 127.1 (C-8, 12), 126.2 (C-22), 125.1 (C-6, 10), 119.8 (C-9, 13), 119.2 (C-34), 65.6 (C-14), 56.3 (C-17), 55.1 (C-27), 46.5 (C-1), 37.3 (C-18), 33.1 (C-28); IR (solid, cm<sup>-1</sup>) 3300, 3123, 2932, 1710, 1651, 1535; MS (ES+) m/z [M, relative intensity] 608.2 [M+Na, 50], 586.2 [M+H, 35], 179.1[C<sub>14</sub>H<sub>11</sub>,1]; Exact mass calcd for [C<sub>31</sub>H<sub>27</sub>N<sub>3</sub>O<sub>7</sub>S] 586.1648, found 586.1668; ε<sub>344</sub> (MeOH) = 3321 M<sup>-1</sup>·cm<sup>-1</sup>.

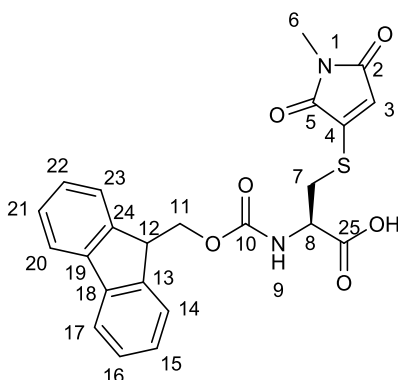
**(9H-fluoren-9-yl)methyl (S)-(1-oxo-3-phenyl-1-(vinylamino)propan-2-yl)carbamate**  
**144**



Dipeptide **143** (30.0 mg, 0.0512 mmol) and sodium acetate (4.62 mg, 0.0563 mmol) were dissolved in MeOH (135 ml) and the entire solution degassed with argon for 30 minutes. The solution was irradiated using the UVG-2 torch for 60 minutes. All solvent was removed *in vacuo* at room temperature and the resulting crude material washed with Et<sub>2</sub>O (3 x 15 ml). Collection of the organic washings and subsequent evaporation gave enamide **144** as a white solid (17 mg, 0.0414 mmol) in an 81% yield.

m.p. 152.0 - 152.8 °C; <sup>1</sup>H NMR (600 MHz, CDCl<sub>3</sub>-d<sub>1</sub>) δ = 7.77 (2H, d, J = 7.5, H-13, 9), 7.53 (2H, t, J = 7.5, H-6, 10), 7.41 (2H, t, J = 7.5, H-8, 12), 7.15 - 7.34 (7H, m, H-24, 25, 23, 26, 22, 11, 7), 6.87 (1H, dt, J = 15.4, J = 9.8, H-30), 4.50 (1H, d, J = 15.8, H-31a), 4.47 (1H, dd, J = 8.5, 5.5, H-19), 4.43 (1H, d, J = 8.7, H-31b), 4.39 (2H, overlapping multiplet, H-14), 4.19 (1H, t, J = 6.8, H-1), 3.16 (1H, dd, J = 13.0, 8.5, H-20'), 3.06 (1H, dd, J = 13.0, 5.5, H-20''); <sup>13</sup>C NMR (150 MHz, CDCl<sub>3</sub>-d<sub>1</sub>) δ = 168.3 (C-27), 154.4 (C-16), 143.7 (C-2, 5), 141.4 (C-3, 4), 129.4 (C-30), 129.0 (C-7,11), 127.9 -120.2 (C-6, 8, 9, 10, 12, 13, 21-26), 97.1 (C-31), 67.3 (C-14), 56.4 (C-19), 47.2 (C-1), 38.3 (C-20); IR (solid, cm<sup>-1</sup>) 3289, 2953, 1685, 1665, 1643; MS (ES+) m/z [M, relative intensity] 435.2 [M+Na, 100], 175.1 [C<sub>11</sub>H<sub>13</sub>NO, 15]; Exact mass calcd for [C<sub>26</sub>H<sub>24</sub>N<sub>2</sub>O<sub>3</sub>Na] 435.1685, found 435.1673.

**N-(((9H-fluoren-9-yl)methoxy)carbonyl)-S-(1-methyl-2,5-dioxo-2,5-dihydro-1H-pyrrol-3-yl)-L-cysteine 146**

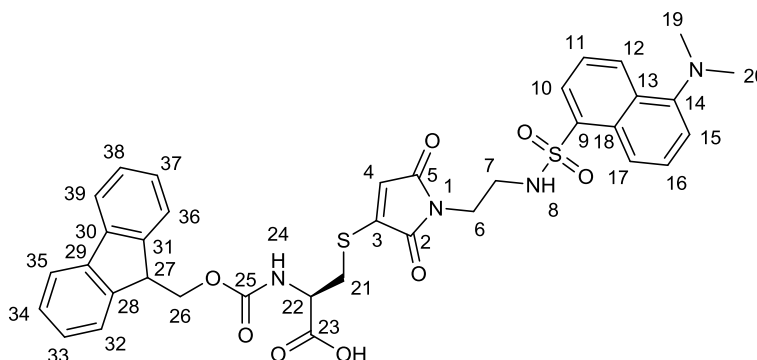


Fmoc-cysteine **132** (200 mg, 0.582 mmol) and sodium acetate (105 mg, 1.28 mmol) were dissolved in MeOH (11.3 ml) and stirred for five minutes under argon. N-Methylmonobromomaleimide (121 mg, 0.640 mmol) was subsequently added and the solution stirred for 20 minutes at room temperature. All solvent was removed *in vacuo*, the

crude material suspended in ethyl acetate (35 ml) and washed with 10% aqueous citric acid (15 ml). The organic layer was collected, dried over MgSO<sub>4</sub> and all solvent removed *in vacuo*. Purification by flash chromatography (2% - 6% MeOH in CH<sub>2</sub>Cl<sub>2</sub> with 1% AcOH) afforded title compound **146** as a light orange powder (242 mg, 0.535 mmol) in a 92% yield.

m.p. 105 - 107 °C; <sup>1</sup>H NMR (600 MHz, DMSO-d<sub>6</sub>) δ = 7.98 (1H, d, J = 8.3, H-9), 7.89 (2H, d, J = 7.5, H-17, 20), 7.70 (2H, d, J = 7.5, H-14, 23), 7.42 (2H, t, J = 7.5, H-16, 21), 7.32 (2H, t, J = 7.5, H-15, 22), 6.59 (1H, s, H-3), 4.26 - 4.35 (3H, m, H-11, 8), 4.17 - 4.26 (1H, m, H-12), 3.46 (1H, dd, J = 13.7, J = 4.7, H-7'), 3.27 (1H, dd, J = 13.7, J = 9.4, H-7''), 2.85 (3H, s, H-6); <sup>13</sup>C NMR (150 MHz, DMSO-d<sub>6</sub>) δ = 171.3 (C-25), 169.5 (C-2), 167.9 (C-5), 156.0 (C-10), 149.5 (C-4), 143.8 (C-13, 24), 140.8 (C-18, 19), 127.7 (C-15, 22), 127.1 (C-16, 21), 125.2 (C-14, 23), 120.2 (C-17, 20), 118.7 (C-3), 65.9 (C-11), 52.4 (C-8), 46.6 (C-12), 32.4 (C-7); IR (solid, cm<sup>-1</sup>) 3311, 1702, 1675, 1535; MS (ES+) m/z [M, relative intensity] 475.1 [M+Na, 100]; Exact mass calcd for [C<sub>23</sub>H<sub>20</sub>N<sub>2</sub>O<sub>6</sub>SNa] 475.0940, found 475.0952; ε<sub>354</sub> (MeOH) = 3813 M<sup>-1</sup>·cm<sup>-1</sup>.

**N-(((9H-fluoren-9-yl)methoxy)carbonyl)-S-(1-(2-((5-(dimethylamino)naphthalene)-1-sulfonamido)ethyl)-2,5-dioxo-2,5-dihydro-1H-pyrrol-3-yl)-L-cysteine **148****



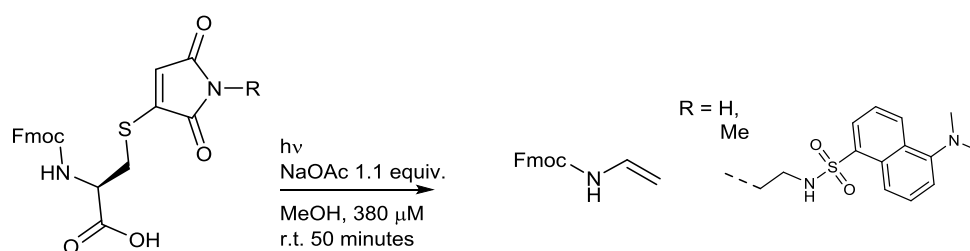
Fmoc-L-Cysteine **132** (16.0 mg, 0.0465 mmol) and sodium acetate (8.4 mg, 0.102 mmol) were dissolved in MeOH (1.5 ml) and stirred under argon for five minutes. Compound **110** (21.0 mg, 0.0465 mmol) was added resulting in a cloudy suspension. MeOH was added dropwise until complete dissolution (20 ml) and the mixture stirred at room temperature for one hour. All solvent was removed *in vacuo*, the crude material suspended in CH<sub>2</sub>Cl<sub>2</sub> (15 ml) and washed with 10% aqueous citric acid. The organic layer was collected, dried over MgSO<sub>4</sub> and all solvent removed *in vacuo*. The crude material was purified by flash chromatography (2 - 5% MeOH in CH<sub>2</sub>Cl<sub>2</sub> with 1% AcOH) to produce compound **148** as an orange solid (11.0 mg, 0.0154 mmol) in a 33% yield.

<sup>1</sup>H NMR (600 MHz, MeOD-d<sub>4</sub>) δ = 8.48 (2H, d, J = 8.3, H-12), 8.19 (1H, d, J = 8.7, H-17), 8.10 (2H, d, J = 7.1, H-10), 7.77 (2H, d, J = 7.7, H-35, 39), 7.65 (2H, t, J = 7.7, H-32, 36), 7.43 - 7.55 (2H, H-11, 16), 7.36 (2H, td, J = 7.7, J = 3.0, H-34, 38), 7.29 (2H, q, J = 7.7, H-33, 37), 7.22 (2H, d, J = 7.5, H-15), 5.92 (1H, s, H-4), 4.40 (2H, m, H-22, 26'), 4.34 (1H,

dd,  $J = 10.5$ ,  $J = 7.0$ , H-26''), 4.21 (1H, t,  $J = 7.0$ , H-27), 3.41 (3H, m, H-21', 6), 3.16 - 3.25 (1H, m, H-21''), 3.10 (2H, t,  $J = 5.8$ , H-7), 2.84 (6H, s, H-19, 20);  $^{13}\text{C}$  NMR (150 MHz, MeOD- $d_4$ )  $\delta = 170.5$  (C-23), 170.5 (C-5), 169.0 (C-2), 153.0 (C-25), 151.1 (C-14), 145.2 (C-28, 31), 145.2 (C-3), 142.6 (C-29, 30), 136.6 (C-9), 131.4 (C-12), 131.0 (C-18), 130.7 (C-13), 130.4 (C-17), 129.3 (C-16), 128.8 (C-33, 37), 128.2 (C-34, 38), 126.2 (C-32, 36), 124.3 (C-11), 120.9 (C-10), 120.6 (C-35, 39), 119.0 (C-4), 116.2 (C-15), 68.1 (C-26), 47.9 (C-27), 45.8 (C-19, 20), 41.5 (C-7), 38.7 (C-6), 34.6 (C-21); MS (ES+)  $m/z$  [M, relative intensity] 715.2 [M+H, 20]; Exact mass calcd for  $[\text{C}_{36}\text{H}_{35}\text{N}_4\text{O}_8\text{S}_2]$  715.1896, found 715.1918;  $\epsilon_{336}$  (MeOH) =  $4672 \text{ M}^{-1}\cdot\text{cm}^{-1}$ .

### 3.1.2.3: HPLC analysis of the Irradiation of C-terminal cysteine models

#### General method for the irradiation of C-terminal cysteine models



Sodium acetate (1.1 equiv.) was added to a solution of C-terminal cysteine model (**133**, **146** or **148**) in MeOH (0.1 ml, 380  $\mu\text{M}$  solution). The mixture was irradiated using the 365 nm UVG-2 torch for 50 minutes, with samples taken every 10 minutes for analysis by LCMS. LCMS was performed on a Waters Acquity uPLC connected to Waters Acquity Single Quad Detector and a photodiode array. Flow rate was set at 0.600 ml/min. A Hypersil Gold (100 x 2.1 mm) column at 50  $^{\circ}\text{C}$  was employed. Solvent A is  $\text{H}_2\text{O}$  (0.1% formic acid), solvent B is MeCN (0.1% formic acid) Mobile phase: 95:5 A:B; gradient over 15 min to 5:95 A:B. MS mode ES+ ; scan range:  $m/z$   $\frac{1}{4}$  100–1000; scan time: 0.25 s. A capillary voltage of 3.5 kV and a cone voltage of 50 V was employed.

#### UV/Vis traces for injected standards.

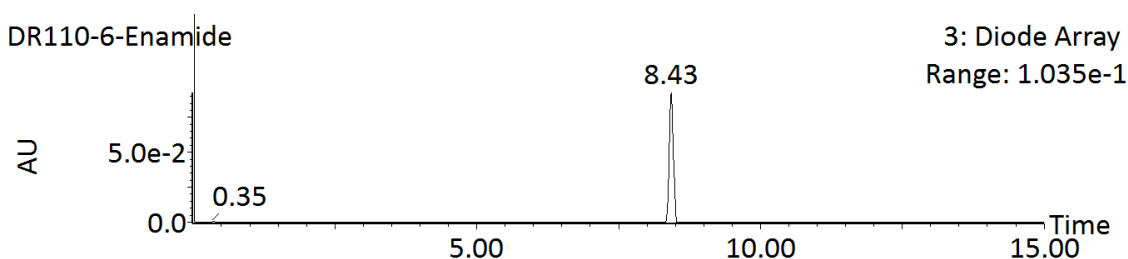


**Figure 57**  
UV/Vis trace for enecarbamate **134**.

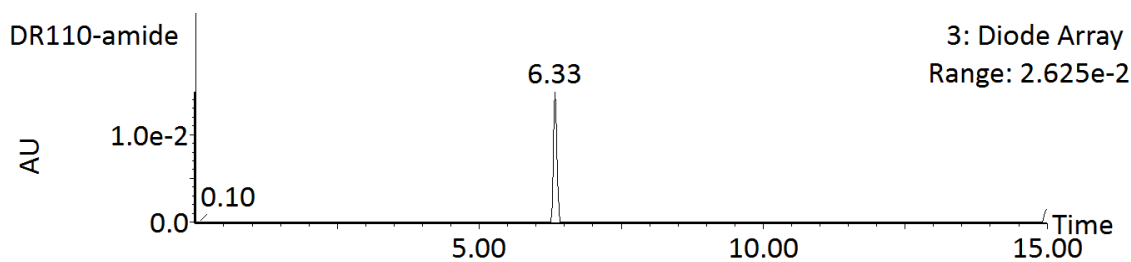


**Figure 58**  
UV/Vis trace for carbamate 136.

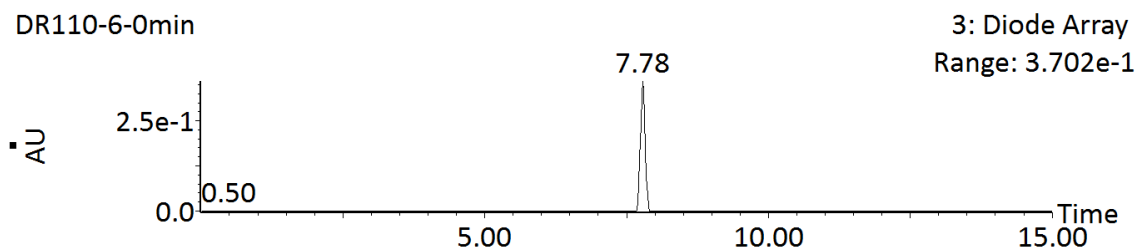


**Figure 59**  
UV/Vis trace for Fmoc-L-cys-N-methylmaleimide 146.

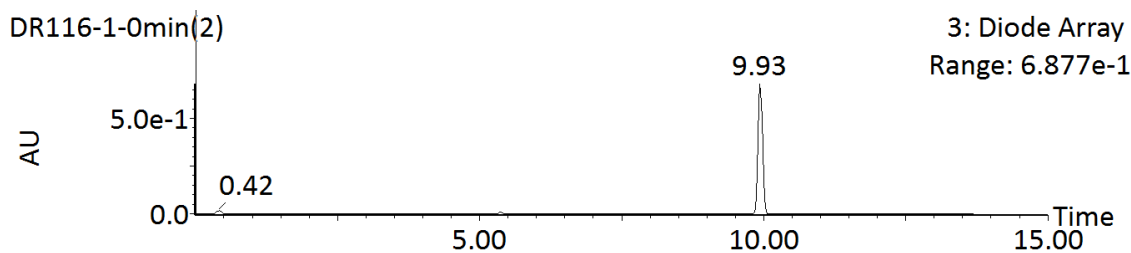
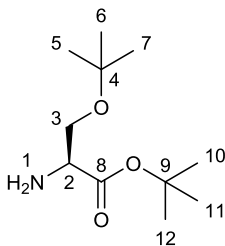


**Figure 60**  
UV/Vis trace for Fmoc-L-cys-N-dansylmaleimide 148

### 3.1.2.4: Synthesis of photocleavable linkers

#### *Tert*-Butyl O-(*tert*-butyl)-L-serinate 164

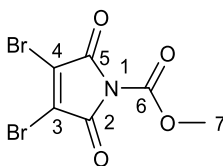


L-Serine (1.00 g, 9.43 mmol) was suspended in *tert*-Butylacetate (30 ml) and stirred under argon. Perchloric acid (0.900 ml, 70% in water, 10.4 mmol) was added and the mixture stirred for five hours. After this time saturated NaHCO<sub>3</sub> (100 ml) was added and the solution stirred for 30 minutes. The mixture was extracted with CH<sub>2</sub>Cl<sub>2</sub> (2 x 150 ml), the organic layers combined and washed with brine (100 ml), and then dried over MgSO<sub>4</sub>. All

solvent was removed *in vacuo* to afford title compound **164** as a clear oil (1.76 g, 8.11 mmol) in an 86% yield.

$^1\text{H}$  NMR (600 MHz,  $\text{CDCl}_3\text{-d}_1$ )  $\delta$  = 3.61 (1H, dd,  $J$  = 8.5, 4.6, H-3'), 3.55 (1H, dd,  $J$  = 8.5, , H-3''), 3.48 (1H, t,  $J$  = 4.2, H-2), 2.15 (2H, s, H-1), 1.47 (9H, s, H-10, 11, 12), 1.17 (9H, s, H-5, 6, 7);  $^{13}\text{C}$  NMR (150 MHz,  $\text{CDCl}_3\text{-d}_1$ )  $\delta$  = 173.2 (C-8), 81.3 (C-9), 73.0 (C-4), 63.8 (C-3), 55.6 (C-2), 28.2 (C-10, 11, 12), 27.5 (C-5, 6, 7); IR (solid,  $\text{cm}^{-1}$ ) 3379.04 (br), 2974.21 (m), 2850.51 (m), 1731.98 (s); MS (ES+)  $m/z$  [M, relative intensity] 218.2 ([M+H], 100); Exact mass calcd for  $[\text{C}_{11}\text{H}_{24}\text{NO}_3]$  218.1756, found 218.1750.

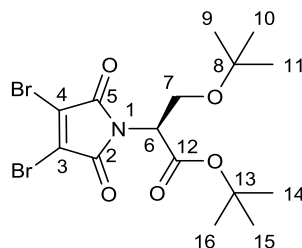
#### methyl 3,4-dibromo-2,5-dioxo-2,5-dihydro-1H-pyrrole-1-carboxylate **165**



N-Methylmorpholine (18.8 mmol, 2.10 ml) and methyl chloroformate (18.8 mmol, 1.45 ml) were added sequentially to a solution of 2,3-dibromomaleimide (18.8 mmol, 4.80 g) in tetrahydrofuran (80 ml). The solution was stirred at room temperature for 30 minutes, before all solvent was removed *in vacuo*. The crude material was dissolved in  $\text{CH}_2\text{Cl}_2$  (300 ml) and washed with brine (100 ml). The organic layer was dried over  $\text{MgSO}_4$  and all solvent removed to produce title compound **165** as a pale purple powder (5.70 g, 18.2 mmol) in a 97% yield.

m.p. 115 - 117  $^\circ\text{C}$  (lit. m.p. 115 - 118  $^\circ\text{C}$ <sup>145</sup>);  $^1\text{H}$  NMR (500 MHz,  $\text{CDCl}_3\text{-d}_1$ )  $\delta$  = 4.00 (3H, s, H-7);  $^{13}\text{C}$  NMR (125 MHz,  $\text{CDCl}_3\text{-d}_1$ )  $\delta$  = 159.3 (C-6), 147.0 (C-2, 5), 131.5 (C-3, 4), 54.9 (C-7); IR (solid,  $\text{cm}^{-1}$ ) 2961, 1808, 1765, 1724, 1600; MS (ES+)  $m/z$  [M, relative intensity] 310.7 [ $^{79}\text{Br}^{79}\text{Br}+\text{H}$ , 49], 312.7 [ $^{81}\text{Br}^{79}\text{Br}+\text{H}$ , 100], 314.7 [ $^{81}\text{Br}^{81}\text{Br}+\text{H}$ , 51]; Exact mass calcd for  $[\text{C}_6\text{H}_4^{79}\text{Br}_2\text{NO}_4]$  310.8423, found 310.8421. Data matched the literature.<sup>145</sup>

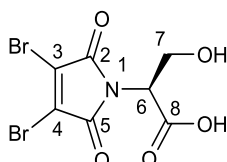
**tert-Butyl (S)-3-(tert-butoxy)-2-(3,4-dibromo-2,5-dioxo-2,5-dihydro-1H-pyrrol-1-yl)propanoate 166**



Compound **164** (0.902 g, 4.15 mmol in 5 ml CH<sub>2</sub>Cl<sub>2</sub>) was added to a stirring solution of carbamate **165** (1.3 g, 4.15 mmol) in CH<sub>2</sub>Cl<sub>2</sub> (60 ml). The solution was left to stir at room temperature for 60 minutes. After this time all solvent was removed *in vacuo* and the crude material purified by flash chromatography (10 - 20% ethyl acetate in petrol) to yield **166** as a dark yellow oil (1.40 g, 3.08 mmol) in a 74% yield.

<sup>1</sup>H NMR (600 MHz, MeOD-d<sub>4</sub>) δ = 4.83 (1H, dd, J = 9.6, 6.2, H-6), 3.89 - 3.91 (2H, m, H-7', 7''), 1.45 (9H, s, H14, 15, 16), 1.12 (9H, s, H-9, 10, 11); <sup>13</sup>C NMR (150 MHz, MeOD-d<sub>4</sub>) δ = 167.5 (C-12), 164.8 (C-2, 5), 130.6 (C-3, 4), 84.5 (C-13), 75.0 (C-8), 59.6 (C-6), 56.2 (C-7), 28.1 (C-14, 15, 16), 27.7 (C-9, 10, 11); IR (solid, cm<sup>-1</sup>) 3052, 2964, 1742, 1602; MS (ES+) m/z [M, relative intensity] 452.0 [<sup>79</sup>Br<sup>79</sup>BrM+H, 49], 454.0 [<sup>81</sup>Br<sup>79</sup>BrM+H, 100], 456.0 [<sup>81</sup>Br<sup>81</sup>BrM+H, 51]; Exact mass calcd for [C<sub>15</sub>H<sub>2</sub><sup>79</sup>Br<sub>2</sub>NO<sub>5</sub>] 451.9786, found 451.9708.

**(S)-2-(3,4-dibromo-2,5-dioxo-2,5-dihydro-1H-pyrrol-1-yl)-3-hydroxypropanoic acid 167**



**Method 1**

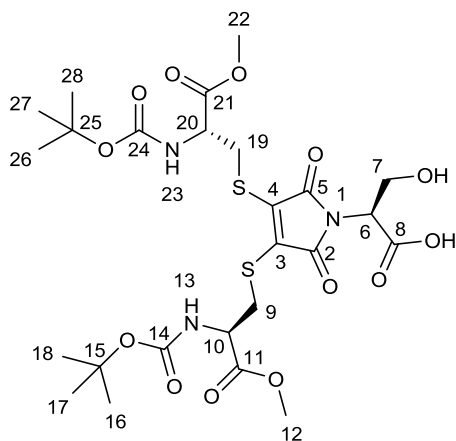
L-Serine (0.554 g, 5.27 mmol) and sodium carbonate (0.558 g, 5.27 mmol) were dissolved in a tetrahydrofuran:water mixture (50:50, 56 ml) and stirred under argon at room temperature for five minutes. Carbamate **165** (1.65 g, 5.27 mmol) was added in a single portion and the resulting solution stirred for 90 seconds before being acidified to pH = 2-3 through addition of solid citric acid. The solution was extracted with CH<sub>2</sub>Cl<sub>2</sub> (4 x 112 ml) and dried over a generous amount of MgSO<sub>4</sub>. All solvent was removed *in vacuo* and the crude material dissolved in CH<sub>2</sub>Cl<sub>2</sub> (56 ml). A spatula tip of para-toluenesulfonic acid (~100 mg) was added and the solution stirred at room temperature for one hour. All solvent was removed *in vacuo* and the crude material purified by flash chromatography (0 - 4% MeOH in CH<sub>2</sub>Cl<sub>2</sub> with 1% AcOH) to produce title compound **167** as white crystals (1.20 g, 3.52 mmol) in a 67% yield. Standing at room temperature resulted in transformation of the solid to a clear gum.

## Method 2

Trifluoroacetic acid (20 ml) was added slowly to a solution of compound **166** (0.5 g, 1.1 mmol) in CH<sub>2</sub>Cl<sub>2</sub> (40 ml) at 0 °C. The solution was returned to room temperature and allowed to stir for four hours. All solvent was removed *in vacuo* to produce title compound **167** as a white solid (346 mg, 1.01 mmol) in a quantitative yield. Standing at room temperature resulted in transformation of the solid to a clear gum.

<sup>1</sup>H NMR (600 MHz, MeOD-d<sub>4</sub>) δ = 4.89 (1H, dd, J = 8.7, J = 6.4, H-6), 4.10 - 4.13 (2H, m, H-7, 7''); <sup>13</sup>C NMR (150 MHz, MeOD-d<sub>4</sub>) δ = 170.0 (C-8), 165.0 (C-2, 5), 130.6 (C-3, 4), 59.7 (C-7), 57.1 (C-6); IR (solid, cm<sup>-1</sup>) 3489, 2970, 2901, 1719, 1593; MS (ES+) m/z [M, relative intensity] 363.9 [<sup>79</sup>Br<sup>79</sup>BrM+Na, 49], 365.9 [<sup>81</sup>Br<sup>79</sup>BrM+Na, 100], 367.9 [<sup>81</sup>Br<sup>81</sup>BrM+Na, 51]; Exact mass calcd for [C<sub>7</sub>H<sub>5</sub><sup>79</sup>Br<sub>2</sub>NO<sub>5</sub>Na] [M+Na] 363.8432, found 363.8637.

### (S)-2-(3,4-bis(((R)-2-((tert-butoxycarbonyl)amino)-3-methoxy-3-oxopropyl)thio)-2,5-dioxo-2,5-dihydro-1H-pyrrol-1-yl)-3-hydroxypropanoic acid **169**

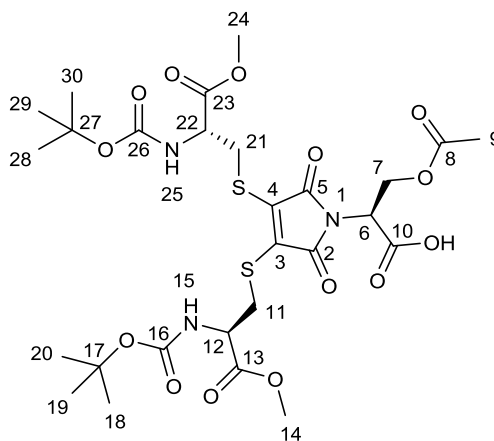


Compound **167** (350 mg, 1.02 mmol) and sodium acetate (258 mg, 3.15 mmol) were dissolved in MeOH (23 ml). Boc-L-Cys-OMe (504 mg, 2.14 mmol) was added and the reaction stirred under argon at room temperature for 40 minutes. All solvent was removed *in vacuo*, the crude material dissolved in ethyl acetate (30 ml) and washed with 10% aqueous citric acid (10 ml). The organic layer was collected, dried over MgSO<sub>4</sub> and all solvent removed *in vacuo*. The crude material was purified by flash chromatography (ethyl acetate with 0.5% AcOH) to produce title compound **169** (614 mg, 0.942 mmol) in a 92% yield. Further purification was performed (0 - 4% MeOH in CH<sub>2</sub>Cl<sub>2</sub> with 1% AcOH) to produce a pure sample (420 mg, 0.644) in a 63% yield.

m.p. 115.0 - 117.0 °C; <sup>1</sup>H NMR (600 MHz, DMSO-d<sub>6</sub>) δ = 7.47 (2H, d, J = 8.3, H-23, 13), 4.65 (1H, t, J = 7.5, H-6), 4.26 (2H, ddd, J = 10.0, J = 8.3, J = 4.3, H-10, 20), 3.89 (2H, d, J = 7.5, H-7), 3.77 (2H, dd, J = 13.4, J = 4.3, H-9, 19), 3.64 (3H, s, H-12, 22), 3.40 (2H, dd, J = 13.4, J = 10.0, H-9, 19), 1.38 (18H, s, H-16, 17, 18, 26, 27, 28); <sup>13</sup>C NMR (150 MHz, DMSO-d<sub>6</sub>) δ = 170.8 (C-11, 21), 168.7 (C-8), 165.4 (C-2, 5), 155.3 (C-14, 24), 134.9 (C-3,

4), 78.7 (C-15, 25), 57.9 (C-7), 54.9 (C-6), 53.8 (C-10, 20), 52.3 (C-12, 22), 32.2 (C-9,19), 28.1 (C-16, 17, 18, 26, 27, 28); IR (solid,  $\text{cm}^{-1}$ ) 3370, 2978, 1705, 1512; MS (ES+)  $m/z$  [M, relative intensity] 674.2 [M+Na, 95], 652.2 [M+H, 40]; Exact mass calcd for [C<sub>25</sub>H<sub>37</sub>N<sub>3</sub>O<sub>13</sub>S<sub>2</sub>Na] 652.1846, found 652.1849.

**(S)-3-acetoxy-2-(3,4-bis(((R)-2-((tert-butoxycarbonyl)amino)-3-methoxy-3-oxopropyl)thio)-2,5-dioxo-2,5-dihydro-1H-pyrrol-1-yl)propanoic acid **170****



**Method 1**

Compound **172** (320 mg, 0.491 mmol) and N,N-Diisopropylethylamine (214  $\mu\text{l}$ , 1.73 mmol) were dissolved in  $\text{CH}_2\text{Cl}_2$  (7 ml). Acetic anhydride (139  $\mu\text{l}$ , 1.47 mmol) was added and the reaction stirred under argon at room temperature for 16 hours. All organic solvent was removed *in vacuo*, the crude material dissolved in ethyl acetate (20 ml) and washed with 10% aqueous citric acid (7 ml). The organic layer was collected, all solvent removed *in vacuo* and dried over  $\text{MgSO}_4$ . Purification by flash chromatography (40% ethyl acetate in  $\text{CH}_2\text{Cl}_2$  with 1% AcOH) yielded **170** (65 mg, 0.094 mmol) in a 19% yield. Compound **171** (150 mg, 0.237 mmol) was also obtained in a yield of 48%.

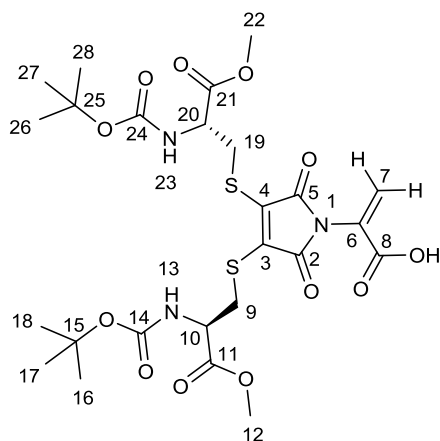
**Method 2**

Compound **172** (683 mg, 1.77 mmol) and sodium acetate (450 mg, 5.49 mmol) were dissolved in MeOH (39 ml). Boc-L-Cys-OMe (875 mg, 3.72 mmol) was added and the solution stirred under argon at room temperature for 30 minutes, resulting in a bright yellow solution. All solvent was removed *in vacuo*, the crude material dissolved in ethyl acetate (60 ml) and washed with 10% aqueous citric acid (20 ml). The organic layer was collected, dried over  $\text{MgSO}_4$  and all solvent removed *in vacuo*. The crude material was purified by flash chromatography (0 - 5% MeOH in  $\text{CH}_2\text{Cl}_2$  in 1% AcOH) to yield title compound **170** as a yellow powder (856 mg, 1.23 mmol) in a 70% yield.

m.p. 78.6 - 79.9  $^{\circ}\text{C}$ ;  $^1\text{H}$  NMR (600 MHz,  $\text{MeOD-d}_4$ )  $\delta$  = 4.96 (1H, dd,  $J$  = 9.8,  $J$  = 3.9, H-6), 4.73 (1H, dd,  $J$  = 11.5,  $J$  = 3.9, H-7'), 4.50 (1H, dd,  $J$  = 11.5,  $J$  = 9.8, H-7''), 4.41 (2H, dd,  $J$  = 8.3,  $J$  = 4.5, H-12, 22), 3.86 (2H, dd,  $J$  = 13.7,  $J$  = 4.5, H-11', 21'), 3.73 (6H, s, H-14, 24), 3.50 (2H, dd,  $J$  = 13.7,  $J$  = 8.3, H-11'', 21''), 2.01 (3H, s, H-9), 1.44 (18H, s, H-18, 19, 20,

28, 29, 30);  $^{13}\text{C}$  NMR (150 MHz, MeOD- $d_4$ )  $\delta$  = 172.4 (C-8), 172.4 (C-13, 23), 169.7 (C-10), 166.8 (C-2, 5), 157.7 (C-16, 26), 137.3 (C-3, 4), 80.9 (C-17, 27), 62.3 (C-7), 55.3 (C-6), 53.1 (C-14, 24), 52.8 (C-12, 22), 34.0 (C-11, 21), 28.7 (C-18, 19, 20, 28, 29, 30), 20.7 (C-9); IR (solid,  $\text{cm}^{-1}$ ) 3370, 2977, 1743, 1708, 1508; MS (ES+)  $m/z$  [M, relative intensity] 711.2 [M+H<sub>2</sub>O, 100], 716.2 [M+Na, 75], 694.2 [M+H, 45]; Exact mass calcd for [C<sub>27</sub>H<sub>40</sub>N<sub>3</sub>O<sub>14</sub>S<sub>2</sub>] 694.1952, found 694.1918.

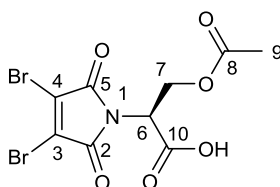
**2-(3,4-bis(((R)-2-((tert-butoxycarbonyl)amino)-3-methoxy-3-oxopropyl)thio)-2,5-dioxo-2,5-dihydro-1H-pyrrol-1-yl)acrylic acid 171**



See experimental procedure for compound **170**.

m.p. 74.6 - 76.9 °C;  $^1\text{H}$  NMR (600 MHz, MeOD- $d_4$ )  $\delta$  = 6.58 (3H, s, H-7a), 5.96 (1H, s, H-7b), 4.46 (2H, dd,  $J$  = 8.4,  $J$  = 4.4, H-10, 20), 3.87 (2H, dd,  $J$  = 13.9,  $J$  = 4.4, H-9', 19''), 3.74 (6H, s, H-12, 22), 3.52 (2H, dd,  $J$  = 13.9,  $J$  = 8.4, H-9'', 19'), 1.43 (18H, s, H-16, 17, 18, 26, 27, 28);  $^{13}\text{C}$  NMR (150 MHz, MeOD- $d_4$ )  $\delta$  = 172.3 (C-11, 21), 165.8 (C-2, 5), 165.2 (C-8), 157.7 (C-14, 24), 137.7 (C-3, 4), 131.2 (C-6), 128.7 (C-7), 81.0 (C-15, 25), 55.3 (C-10, 20), 52.9 (C-12, 22), 33.3 (C-9, 19), 28.6 (C-16, 17, 18, 26, 27, 28); IR (solid,  $\text{cm}^{-1}$ ) 3367, 2977, 1712, 1640, 1510; MS (ES+)  $m/z$  [M, relative intensity] 656.2 [M+Na, 100], 634.2 [M+H, 30]; Exact mass calcd for [C<sub>25</sub>H<sub>36</sub>N<sub>3</sub>O<sub>12</sub>S<sub>2</sub>Na] 656.1740, found 656.1750.

**(S)-3-acetoxy-2-(3,4-dibromo-2,5-dioxo-2,5-dihydro-1H-pyrrol-1-yl)propanoic acid 172**

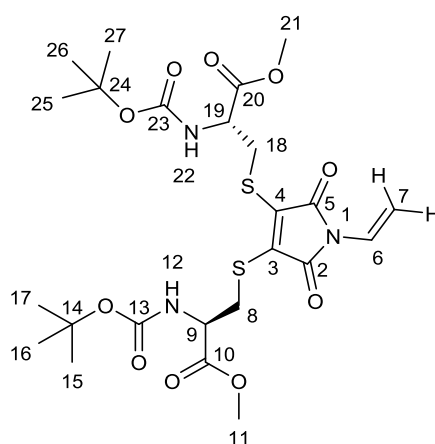


Acetyl bromide (0.432 ml, 5.84 mmol) in CH<sub>2</sub>Cl<sub>2</sub> (7.5 ml) was added dropwise to a solution of compound **167** (500 mg, 1.46 mmol) in CH<sub>2</sub>Cl<sub>2</sub> (7.5 ml). The solution was stirred under argon at room temperature for four hours. After this time a 10% aqueous citric acid solution (5 ml) was slowly added and the solution stirred for five minutes. The organic layer was separated, dried over MgSO<sub>4</sub> and all solvent removed *in vacuo*. The crude material was

purified by flash chromatography (0 - 5% MeOH in CH<sub>2</sub>Cl<sub>2</sub> with 1% AcOH) to yield title compound **172** as a white solid (520 mg, 1.35 mmol) in a 93% yield.

m.p. 63.2 - 65.2 °C; <sup>1</sup>H NMR (600 MHz, MeOD-d<sub>4</sub>) δ = 5.09 (1H, dd, J = 9.9, J = 4.3, H-6), 4.72 (1H, dd, J = 11.7, J = 4.3, H-7'), 4.53 (1H, dd, J = 11.7, J = 9.9, H-7''), 1.97 - 2.05 (3H, m, H-9); <sup>13</sup>C NMR (150 MHz, MeOD-d<sub>4</sub>) δ = 177.8 (C-8), 170.6 (C-10), 164.5 (C-2, 5), 130.2 (C-3, 4), 66.6 (C-6), 60.2 (C-7), 20.1 (C-9); IR (solid, cm<sup>-1</sup>) 3452, 3124, 2945, 1717, 1594; MS (ES+) m/z [M, relative intensity] 380.9 [<sup>79</sup>Br<sup>79</sup>BrM+H, 49], 382.9 [<sup>79</sup>Br<sup>81</sup>BrM+H, 100], 384.9 [<sup>81</sup>Br<sup>81</sup>BrM+H, 49]; Exact mass calcd for [C<sub>9</sub>H<sub>8</sub><sup>79</sup>Br<sub>2</sub>NO<sub>6</sub>] 380.8484, found 380.8486.

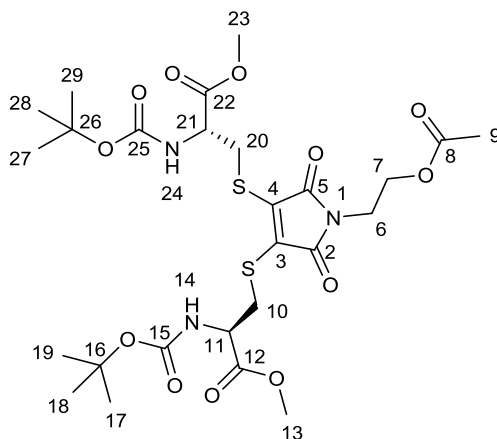
**dimethyl 3,3'-((2,5-dioxo-1-vinyl-2,5-dihydro-1H-pyrrole-3,4-diyl)bis(sulfanediyl))(2R,2'R)-bis(2-((tert-butoxycarbonyl)amino)propanoate) **173****



Compound **170** (100 mg, 0.144 mmol) was dissolved in MeCN:phosphate buffer pH = 7.4 (80:20, 96 ml), degassed with argon for 30 minutes and irradiated at room temperature with a medium pressure mercury lamp for 40 minutes. The solution was subsequently acidified to pH = 2-3 through addition of solid citric acid and extracted with CH<sub>2</sub>Cl<sub>2</sub> (2 x 125 ml). The organic layers were combined, dried over MgSO<sub>4</sub> and all solvent removed *in vacuo*. The crude mixture was purified by flash chromatography (0 - 20% ethyl acetate in petrol) to produce compound **173** as an orange solid (60 mg, 0.102 mmol) in a 71% yield and compound **174** as a yellow solid (15 mg, 0.0230 mmol) in a 16% yield.

m.p. 78.0 – 80.6 °C; <sup>1</sup>H NMR (400 MHz, MeOD-d<sub>4</sub>) δ = 6.68 (1H, dd, J = 16.3, J = 9.9, H-6), 5.82 (1H, d, J = 16.3, 7a), 4.92 (1H, d, J = 9.9, 7b), 4.50 (2H, dd, J = 8.0, J = 4.3, H-9, 19), 3.92 (2H, dd, J = 13.8, J = 4.3, H-8', 18'), 3.77 (6H, s, H-11, 21), 3.53 (2H, dd, J = 13.8, J = 8.0, H-8'', 18''), 1.45 (18H, s, H-15, 16, 17, 25, 26, 27); <sup>13</sup>C NMR (150 MHz, DMSO-d<sub>6</sub>) δ = 170.8 (C-10, 20), 164.2 (C-2, 5), 155.3 (C-13, 23), 136.5 (C-3, 4), 123.7 (C-6), 102.5 (C-7), 78.7 (C-14, 24), 53.9 (C-9, 19), 52.3 (C-11, 21), 32.2 (C-8, 18), 28.1 (C-15, 16, 17, 25, 26, 27); IR (solid, cm<sup>-1</sup>) 2978, 2496, 1751, 1703, 1675, 1637, 1517; MS (ES+) m/z [M, relative intensity] 590.2 [M+H, 100]; Exact mass calcd for [C<sub>24</sub>H<sub>36</sub>N<sub>3</sub>O<sub>10</sub>S<sub>2</sub>] 590.1842, found 590.1865.

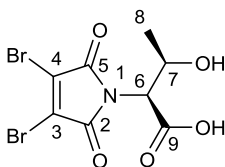
**dimethyl 3,3'-((1-(2-acetoxyethyl)-2,5-dioxo-2,5-dihydro-1H-pyrrole-3,4-diyl)bis(sulfanediyl)(2R,2`R)-bis(2-((tert-butoxycarbonyl)amino)propanoate) 174**



See experimental procedure for compound **173**.

$^1\text{H}$  NMR (600 MHz, MeOD- $d_4$ )  $\delta$  = 4.44 (3H, dd,  $J$  = 8.5,  $J$  = 4.7, H-11, 21), 4.21 (2H, t,  $J$  = 5.8, H-7), 3.87 (2H, dd,  $J$  = 13.9,  $J$  = 4.7, H-10', 20'), 3.77 (2H, t,  $J$  = 5.8, H-6), 3.73 (6H, s, H-13, 23), 3.46 (2H, dd,  $J$  = 13.9,  $J$  = 8.5, H-10'', 20''), 2.00 (3H, s, H-9), 1.44 (18H, s, H-17, 18, 19, 27, 28, 29);  $^{13}\text{C}$  NMR (150 MHz, MeOD- $d_4$ )  $\delta$  = 172.7 (C-8), 172.4 (C-12, 22), 167.5 (C-2, 5), 157.6 (C-15, 25), 137.3 (C-3, 4), 81.0 (C-16, 26), 62.7 (C-7), 55.5 (C-11, 21), 53.1 (C-13, 23), 38.7 (C-6), 34.0 (C-10, 20), 28.7 (C-17, 18, 19, 27, 28, 29), 20.8 (C-9); IR (solid,  $\text{cm}^{-1}$ ) 2977, 2928, 1741, 1702, 1505; MS (ES+)  $m/z$  [ $M$ , relative intensity] 672.2 [ $M+\text{Na}$ , 100] 650.2 [ $M+\text{H}$ , 20]; Exact mass calcd for [ $\text{C}_{26}\text{H}_{40}\text{N}_3\text{O}_{12}\text{S}_2$ ] 650.2053, found 650.2056.

**(2S,3R)-2-(3,4-dibromo-2,5-dioxo-2,5-dihydro-1H-pyrrol-1-yl)-3-hydroxybutanoic acid 193**

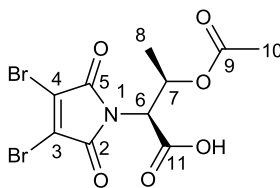


L-Threonine (0.762 g, 6.39 mmol) and sodium carbonate (0.677 g, 6.39 mmol) were dissolved in a tetrahydrofuran:water mixture (50:50, 68 ml) and stirred under argon at room temperature for five minutes. Carbamate **165** (2 g, 6.39 mmol) was added in a single portion and the resulting solution stirred for 90 seconds before being acidified to pH = 2 - 3 through addition of solid citric acid. The solution was extracted with  $\text{CH}_2\text{Cl}_2$  (4 x 112 ml) and dried over a generous amount of  $\text{MgSO}_4$ . All solvent was removed *in vacuo* and the crude material dissolved in  $\text{CH}_2\text{Cl}_2$  (56 ml). A spatula tip of para-toluenesulfonic acid (~100 mg) was added and the solution stirred at room temperature for one hour. All solvent was removed *in vacuo* and the crude material purified by flash chromatography (0 - 4% MeOH in  $\text{CH}_2\text{Cl}_2$  with 1% AcOH) to produce title compound **193** as a grey solid (1.24 g, 3.47

mmol) in a 54% yield. Standing at room temperature resulted in transformation of the solid to a cloudy gum.

$^1\text{H}$  NMR (600 MHz,  $\text{CDCl}_3\text{-d}_1$ )  $\delta$  = 4.86 (1H, d,  $J$  = 4.3, H-6), 4.66 (1H, dq,  $J$  = 6.4,  $J$  = 4.3, H-7), 1.25 (3H, d,  $J$  = 6.4, H-8);  $^{13}\text{C}$  NMR (150 MHz,  $\text{CDCl}_3\text{-d}_1$ )  $\delta$  = 170.6 (C-9), 164.5 (C-2, 5), 130.2 (C-3, 4), 66.6 (C-7), 60.2 (C-6), 20.1 (C-8); IR (solid,  $\text{cm}^{-1}$ ) 3429, 2980, 2924, 1788, 1716, 1594; MS (ES+)  $m/z$  [M, relative intensity] 355.9 [ $^{79}\text{Br}^{79}\text{Br}+\text{H}$ , 49], 357.9 [ $^{79}\text{Br}^{81}\text{Br}+\text{H}$ , 100], 359.9 [ $^{81}\text{Br}^{81}\text{Br}$ , 51]; Exact mass calcd for  $[\text{C}_8\text{H}_8^{79}\text{Br}_2\text{NO}_5]$  355.8769, found 355.8770.

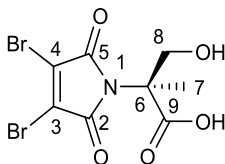
**(2S,3R)-3-acetoxy-2-(3,4-dibromo-2,5-dioxo-2,5-dihydro-1H-pyrrol-1-yl)butanoic acid 194**



Acetyl bromide (0.200 ml, 2.75 mmol) in  $\text{CH}_2\text{Cl}_2$  (3.5 ml) was added dropwise to a solution of compound **193** (245 mg, 0.686 mmol) in  $\text{CH}_2\text{Cl}_2$  (3.5 ml). The solution was stirred under argon at room temperature for four hours. After this time a 10% aqueous citric acid solution (3 ml) was slowly added and the solution stirred for five minutes. The organic layer was separated, dried over  $\text{MgSO}_4$  and all solvent removed *in vacuo*. The crude material was purified by flash chromatography (0 - 5% MeOH in  $\text{CH}_2\text{Cl}_2$  with 1% AcOH) to yield title compound **194** as a white solid (265 mg, 0.666 mmol) in a 97% yield.

$^1\text{H}$  NMR (500 MHz,  $\text{CDCl}_3\text{-d}_1$ )  $\delta$  = 5.64 (1H, dq,  $J$  = 6.5,  $J$  = 5.4, H-7), 4.84 (1H, d,  $J$  = 5.4, H-6), 2.01 (3H, s, H-10), 1.35 (3H, d,  $J$  = 6.5, H-8);  $^{13}\text{C}$  NMR (125, MHz,  $\text{CDCl}_3\text{-d}_1$ )  $\delta$  = 170.2 (C-9), 170.0 (C-11), 162.9 (C-2, 5), 129.8 (C-3, 4), 67.5 (C-7), 56.6 (C-6), 21.0 (C-10), 18.2 (C-8); IR (solid,  $\text{cm}^{-1}$ ) 3452, 3065, 2924, 1724, 1594; MS (ES+)  $m/z$  [M, relative intensity] 397.9 [ $^{79}\text{Br}^{79}\text{BrM}+\text{H}$ , 49], 399.9 [ $^{79}\text{Br}^{81}\text{BrM}+\text{H}$ , 100], 401.9 [ $^{81}\text{Br}^{81}\text{BrM}+\text{H}$ , 51]; Exact mass calcd for  $[\text{C}_{10}\text{H}_{10}^{79}\text{Br}_2\text{NO}_6]$  397.8879, found 397.8882.

**(S)-2-(3,4-dibromo-2,5-dioxo-2,5-dihydro-1H-pyrrol-1-yl)-3-hydroxy-2-methylpropanoic acid 196**

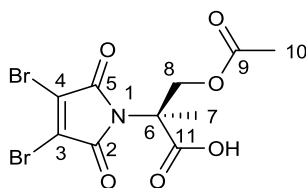


Dibromomaleic anhydride (75 mg, 0.293 mmol) and  $\alpha$ -methyl-L-serine (23.3 mg, 0.195 mmol) were dissolved in AcOH (1.3 ml) and raised to reflux over 20 minutes. The solution was stirred at reflux for 40 minutes before being returned to room temperature. A solution of 10% aqueous citric acid (10 ml) was subsequently added and the aqueous layer

extracted with CH<sub>2</sub>Cl<sub>2</sub> (3 x 20 ml). The organic layers were combined, dried over MgSO<sub>4</sub> and all solvent was removed *in vacuo*. The crude material was purified by flash chromatography (1 - 3% MeOH in CH<sub>2</sub>Cl<sub>2</sub> with 1% AcOH) to yield title compound **196** as an off-white wax (37 mg, 0.104 mmol) in a 54% yield.

<sup>1</sup>H NMR (600 MHz, MeOD-d<sub>4</sub>) δ = 4.15 (1H, d, J = 11.7, H-8'), 3.83 (1H, d, J = 11.7, H-8''), 1.81 (3H, s, H-7); <sup>13</sup>C NMR (150 MHz, MeOD-d<sub>4</sub>) δ = 174.1 (C-9), 165.6 (C-2, 5), 130.4 (C-3, 4), 67.2 (C-6), 65.0 (C-8), 20.4 (C-7); IR (solid, cm<sup>-1</sup>) 3483, 3093, 2994, 1724; MS (ES-) m/z [M, relative intensity] 352.9 [<sup>79</sup>Br<sup>79</sup>BrM-H, 49], 354.9 [<sup>81</sup>Br<sup>79</sup>BrM-H, 100], 356.9 [<sup>81</sup>Br<sup>81</sup>BrM-H, 51]; Exact mass calcd for [C<sub>8</sub>H<sub>6</sub>NO<sub>5</sub><sup>79</sup>Br<sub>2</sub>] 352.8535, found 352.8525.

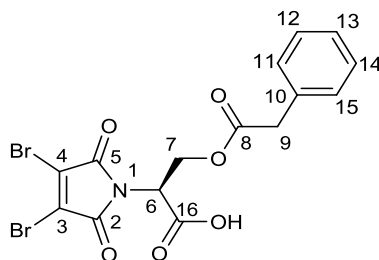
**(S)-3-acetoxy-2-(3,4-dibromo-2,5-dioxo-2,5-dihydro-1H-pyrrol-1-yl)-2-methylpropanoic acid 197**



Acetyl bromide (20.9 μl, 0.282 mmol) in CH<sub>2</sub>Cl<sub>2</sub> (0.4 ml) was added dropwise to a solution of compound **196** (25 mg, 0.0704 mmol) in CH<sub>2</sub>Cl<sub>2</sub> (0.4 ml). The solution was stirred under argon at room temperature for four hours. After this time a 10% citric acid solution (1 ml) was slowly added and the solution stirred for five minutes. CH<sub>2</sub>Cl<sub>2</sub> (2 ml) was added before the organic layer was separated, dried over MgSO<sub>4</sub> and all solvent removed *in vacuo*. The crude material was purified by flash chromatography (0 - 5% MeOH in CH<sub>2</sub>Cl<sub>2</sub> with 1% AcOH) to yield title compound **197** as a clear glass (25 mg, 0.0627 mmol) in an 89% yield.

<sup>1</sup>H NMR (600 MHz, CDCl<sub>3</sub>-d<sub>1</sub>) δ = 4.71 (1H, d, J = 11.7, H-8'), 4.52 (1H, d, J = 11.7, H-8''), 2.06 (3H, s, H-10), 1.92 (3H, s, H-7); <sup>13</sup>C NMR (150 MHz, CDCl<sub>3</sub>-d<sub>1</sub>) δ = 174.5 (C-11), 170.8 (C-9), 163.7 (C-2, 5), 129.7 (C-3, 4), 64.9 (C-8), 63.4 (C-6), 20.8 (C-10), 20.2 (C-7); IR (film, cm<sup>-1</sup>) 3501, 2976, 1722, 1604; MS (ES-) m/z [M, relative intensity] 394.9 [<sup>79</sup>Br<sup>79</sup>BrM-H, 49], 396.9 [<sup>81</sup>Br<sup>79</sup>BrM-H, 49], 398.9 [<sup>81</sup>Br<sup>81</sup>BrM-H, 49]; Exact mass calcd for [C<sub>10</sub>H<sub>10</sub><sup>79</sup>Br<sub>2</sub>NO<sub>6</sub>] 397.8875, found 397.8858.

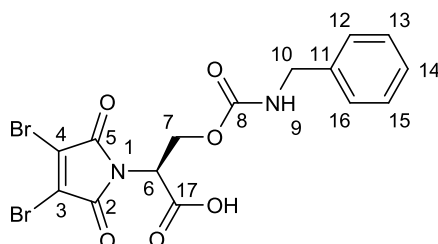
**2-(3,4-dibromo-2,5-dioxo-2,5-dihydro-1H-pyrrol-1-yl)-3-(2-phenylacetoxy)propanoic acid **199****



Compound **167** (30.0 mg, 0.0879 mmol) and tetra-*n*-butylammonium bromide (142 mg, 0.440 mmol) were dissolved in CH<sub>3</sub>Cl (1 ml) and stirred under argon in a dried round bottomed flask. Phenylacetyl chloride (46.5  $\mu$ l, 0.352 mmol) was added in a single portion and the reaction stirred at room temperature for four hours. After this time MeOH (0.5 ml) was added and all solvent removed *in vacuo*. The crude material was dissolved in ethyl acetate (5 ml) and washed with 10% aqueous citric acid (2 x 2 ml). The organic layer was collected, dried over MgSO<sub>4</sub> and all solvent removed *in vacuo*. The resulting crude material was purified by flash chromatography (0 - 25% acetone in CH<sub>2</sub>Cl<sub>2</sub> with 1% AcOH) to yield title compound **199** as a clear gum (29 mg, 0.063 mmol) in a 72% yield.

<sup>1</sup>H NMR (600 MHz, CDCl<sub>3</sub>-d<sub>1</sub>)  $\delta$  = 7.12 - 7.32 (5H, m, H-11-15), 5.09 (1H, dd, J = 10.3, J = 4.7, H-6), 4.78 (1H, dd, J = 11.8, J = 4.7, H-7'), 4.59 (1H, dd, J = 11.8, J = 10.4, H-7''), 3.58 (2H, d, J = 2.8, H-9); <sup>13</sup>C NMR (150 MHz, CDCl<sub>3</sub>-d<sub>1</sub>)  $\delta$  = 171.1 (C-8), 170.3 (C-16), 162.8 (C-2, 5), 133.3 (C-10), 129.7 (C-3, 4), 129.3 (C-11, 15), 128.8 (C-12, 14), 127.5 (C-13), 60.4 (C-6), 51.8 (C-7), 41.2 (C-9); IR (solid, cm<sup>-1</sup>); MS (ES+) m/z [M, relative intensity] 459.9 [<sup>79</sup>Br<sup>79</sup>BrM+H, 39], 461.9 [<sup>81</sup>Br<sup>79</sup>BrM+H, 84], 463.9 [<sup>81</sup>Br<sup>81</sup>BrM+H, 40]; Exact mass calcd for [C<sub>15</sub>H<sub>11</sub>Br<sub>2</sub>NO<sub>6</sub>] 459.9026, found 459.9025.

**(S)-3-((benzylcarbamoyl)oxy)-2-(3,4-dibromo-2,5-dioxo-2,5-dihydro-1H-pyrrol-1-yl)propanoic acid **200****

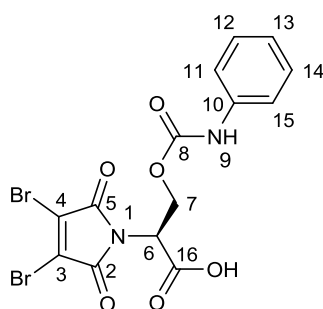


Compound **167** (200 mg, 0.587 mmol) was dissolved in CH<sub>2</sub>Cl<sub>2</sub> (5.6 ml, 10% diethylether) and stirred under argon. Benzyl isocyanate (145  $\mu$ l, 1.174 mmol) was added followed by a catalytic amount of powdered MoO<sub>2</sub>Cl<sub>2</sub> (5 mg), and the solution stirred at room temperature for four hours. The solution was subsequently washed with 10% aqueous citric acid (2 ml) and the aqueous layer extracted with CH<sub>2</sub>Cl<sub>2</sub> (2 x 5 ml). The organic layers were collected, dried over MgSO<sub>4</sub> and all solvent removed *in vacuo*. The crude material was

purified by flash chromatography (0 - 3% MeOH in CH<sub>2</sub>Cl<sub>2</sub> with 1% AcOH) to yield title compound **200** as a yellow gum (184 mg, 0.387 mmol) in a 66% yield.

m.p. 63.2 - 65.2 °C; <sup>1</sup>H NMR (600 MHz, MeOD-d<sub>4</sub>) δ = 7.18 - 7.33 (6H, m, H-9, 12-16), 5.11 (1H, dd, J = 10.2, J = 4.5, H-6), 4.70 (1H, dd, J = 11.7, J = 4.5, H-7), 4.59 (1H, dd, J = 11.7, J = 10.2, H-7), 4.22 (2H, s, H-10); <sup>13</sup>C NMR (150 MHz, MeOD-d<sub>4</sub>) δ = 169.2 (C-17), 164.6 (C-2, 5), 158.2 (C-8), 140.3 (C-11), 130.7 (C-3, 4), 129.5 (C-12, 16), 128.2 (C-13, 15), 128.1 (C-14), 62.0 (C-6), 54.0 (C-7), 45.4 (C-10); IR (solid, cm<sup>-1</sup>) 3443, 2912, 1743, 1601, 1513; MS (ES+) m/z [M, relative intensity] 475.0 [<sup>79</sup>Br<sup>79</sup>BrM+H, 49], 477.0 [<sup>79</sup>Br<sup>81</sup>BrM+H, 100], 479.0 [<sup>81</sup>Br<sup>81</sup>BrM+H, 51]; Exact mass calcd for [C<sub>15</sub>H<sub>13</sub>Br<sub>2</sub>N<sub>2</sub>O<sub>6</sub>] 474.9140, found 474.9133.

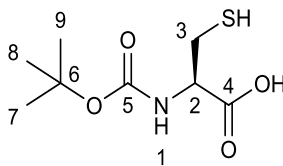
**(S)-2-(3,4-dibromo-2,5-dioxo-2,5-dihydro-1H-pyrrol-1-yl)-3-(phenylcarbamoyloxy) propanoic acid 201**



Compound **167** (68 mg, 0.200 mmol) was dissolved in Et<sub>2</sub>O (2 ml) and stirred under argon at room temperature. Phenyl isocyanate (43.5 μl, 0.400 mmol) was added, followed by a catalytic amount of powdered MoO<sub>2</sub>Cl<sub>2</sub> (5 mg), and the solution stirred at room temperature for three hours. All solvent was removed *in vacuo* and the product purified by flash chromatography (0 - 3% MeOH in CH<sub>2</sub>Cl<sub>2</sub> with 1% AcOH) to yield title compound **201** as a yellow solid (83 mg, 0.180 mmol) in a 90% yield.

m.p. 67.2 - 69.5 °C; <sup>1</sup>H NMR (600 MHz, CDCl<sub>3</sub>-d<sub>1</sub>) δ = 7.24 - 7.42 (5H, m, H-11-15), 7.09 (1H, t, J = 6.5, H-9), 5.19 (1H, dd, J = 9.5, J = 4.2, H-6), 4.85 (1H, dd, J = 11.9, J = 4.2, H-7), 4.68 (1H, dd, J = 11.9, J = 9.5, H-7); <sup>13</sup>C NMR (150 MHz, CDCl<sub>3</sub>-d<sub>1</sub>) δ = 169.5 (C-16), 165.9 (C-2, 5), 152.7 (C-8), 129.9 (C-3, 4), 137.2 (C-10) 119.0-130 (C-11-15), 61.5 (C-7), 52.6 (C-6); IR (solid, cm<sup>-1</sup>) 3293, 2971, 1722, 1595, 1530; MS (EI) m/z [M, relative intensity] 459.9 [<sup>79</sup>Br<sup>79</sup>BrM, 49], 461.9 [<sup>81</sup>Br<sup>79</sup>BrM, 100], 463.9 [<sup>81</sup>Br<sup>81</sup>BrM, 51]; Exact mass calcd for [C<sub>14</sub>H<sub>10</sub><sup>79</sup>Br<sub>2</sub>N<sub>2</sub>O<sub>6</sub>] 459.8900, found 459.8901.

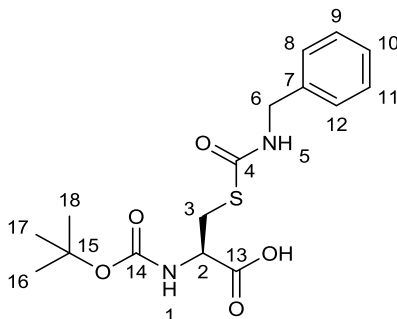
**(*tert*-Butoxycarbonyl)-L-cysteine 203<sup>331</sup>**



L-Cysteine (2.00 g, 16.5 mmol) and NaHCO<sub>3</sub> (3.40 g, 40 mmol) were dissolved in water:tetrahydrofuran (1:2.5, 50 ml). Di-*tert*-Butyl dicarbonate (3.60 g, 16.5 mmol) was added in a single portion and the reaction stirred at room temperature for 24 hours. After this time the reaction was cooled to 0 °C, ethyl acetate (50 ml) was added and the pH adjusted to pH = 2-3 *via* addition of 2M HCl. The organic layer was separated, and the aqueous layer washed with ethyl acetate (2 x 50 ml). The organic layers were combined, dried over MgSO<sub>4</sub> and all solvent was removed *in vacuo* to yield title compound **203** as a clear viscous oil (3.25 g, 14.7 mmol) in an 89% yield.

<sup>1</sup>H NMR (600 MHz, DMSO-d<sub>6</sub>) δ = 7.06 (1H, d, J = 8.3, H-1), 4.05 (1H, m, H-2), 2.83 (1H, m, H-3'), 2.69 (1H, m, H-3''), 1.37 (9H, s, H-7, 8, 9); <sup>13</sup>C NMR (150 MHz, DMSO-d<sub>6</sub>) δ = 172.1 (C-4), 155.4 (C-5), 78.3 (C-6), 56.2 (C-2), 48.6 (C-3), 28.2 (C-7, 8, 9); IR (film, cm<sup>-1</sup>) 3392, 2978, 1696, 1505; MS (ES+) m/z [M, relative intensity] 239.1 [M+NH<sub>4</sub>, 52]. Data matched the literature.<sup>331</sup>

**S-(benzylcarbamoyl)-N-(*tert*-Butoxycarbonyl)-L-cysteine 204**

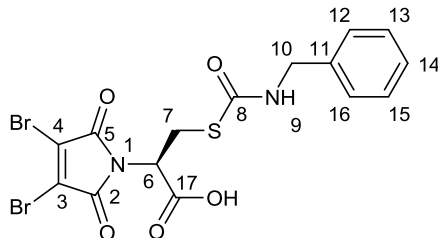


(*tert*-Butoxycarbonyl)-L-cysteine **203** (550 mg, 2.49 mmol) and benzyl isocyanate (0.614 ml, 4.98 mmol) were dissolved in THF (24 ml) and stirred under argon. A spatula tip of MoO<sub>2</sub>Cl<sub>2</sub> was added and the solution stirred at room temperature for three hours. After three hours all solvent was removed *in vacuo* and the crude material purified by flash chromatography (0 - 3% MeOH in CH<sub>2</sub>Cl<sub>2</sub> with 1% AcOH) to produce title compound **204** as a yellow gum (160 mg, 0.451 mmol) in a 18% yield.

<sup>1</sup>H NMR (600 MHz, DMSO-d<sub>6</sub>) δ = 8.74 (2H, t, J = 5.7, H-5), 7.21 - 7.35 (5H, m, H-8-12), 7.10 (1H, d, J = 9.2, H-1), 4.31 (2H, dd, J = 5.7, J = 3.4, H-6), 3.99 (1H, td, J = 9.2, J = 4.5, H-2), 3.33 (1H, dd, J = 13.6, J = 4.5, H-3'), 2.93 (1H, dd, J = 13.6, J = 9.2, H-3''), 1.38 (9H, s, H-16, 17, 18); <sup>13</sup>C NMR (150 MHz, DMSO-d<sub>6</sub>) δ = 172.4 (C-13), 165.6 (C-4), 155.3 (C-14), 139.0 (C-7), 128.4 (C-8, 12), 127.2 (C-9, 11), 127.0 (C-10), 78.2 (C-15), 54.1 (C-2),

44.0 (C-6), 30.5 (C-3), 28.2 (C-16, 17, 18); IR (solid,  $\text{cm}^{-1}$ ) 3311, 2987, 1728, 1665, 1508; MS (ES+)  $m/z$  [M, relative intensity] 355.1 [M+H, 100], 255.1 [ $\text{C}_{11}\text{H}_{15}\text{N}_2\text{O}_3\text{S}$ , 40]; Exact mass calcd for [ $\text{C}_{16}\text{H}_{23}\text{N}_2\text{O}_5\text{S}$ ] 355.328, found 355.1330.

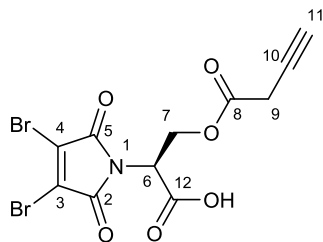
**(R)-3-((benzylcarbamoyl)thio)-2-(3,4-dibromo-2,5-dioxo-2,5-dihydro-1H-pyrrol-1-yl)propanoic acid 205**



Compound **204** (60.0 mg, 0.169 mmol) was dissolved in  $\text{CH}_2\text{Cl}_2$  (1 ml) before trifluoroacetic acid (1 ml) was added and the solution stirred at room temperature for 20 minutes. All solvent was removed *in vacuo* and the crude material dissolved in a THF: $\text{H}_2\text{O}$  mixture (50:50, 1.8 ml). The solution was added in a single portion to a round bottomed flask containing carbamate **165** (53.0 mg, 0.169 mmol) and sodium carbonate (72 mg, 0.676 mmol) and the resulting mixture was stirred at room temperature for three minutes. The solution was subsequently acidified through addition of solid citric acid to  $\text{pH} = 2-3$ , the aqueous layer extracted with  $\text{CH}_2\text{Cl}_2$  (4 x 4 ml) and then the organic layer dried over  $\text{MgSO}_4$ . All solvent was removed *in vacuo*, the crude material dissolved in  $\text{CH}_2\text{Cl}_2$  (1.8 ml) and a spatula tip (~10 mg) of para-toluenesulfonic acid was added. After stirring at room temperature for one hour all solvent was removed *in vacuo* and the crude material was purified by flash chromatography (0 - 7% MeOH in  $\text{CH}_2\text{Cl}_2$  with 1% AcOH) to yield title compound **205** as a yellow gum (30 mg, 0.0613 mmol) in a 36% yield.

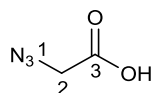
$^1\text{H}$  NMR (600 MHz,  $\text{MeOD-d}_4$ )  $\delta = 7.06 - 7.40$  (5H, m, H-12-16), 4.98 (1H, dd,  $J = 10.9$ ,  $J = 4.1$ , H-6), 4.34 (2H, s, H-10), 3.69 (1H, dd,  $J = 14.7$ ,  $J = 4.1$ , H-7'), 3.47 (1H, dd,  $J = 14.7$ ,  $J = 10.9$ , H-7'');  $^{13}\text{C}$  NMR (150 MHz,  $\text{MeOD-d}_4$ )  $\delta = 170.3$  (C-17), 167.8 (C-8), 164.7 (C-2, 5), 139.7 (C-11), 130.6 (C-3, 4), 129.6 (C-12, 16), 128.4 (C-13, 15), 128.2 (C-14), 55.2 (C-6), 45.7 (C-10), 29.7 (C-7); IR (solid,  $\text{cm}^{-1}$ ) 3423, 2912, 1728, 1672; MS (EI)  $m/z$  [M, relative intensity] 490.0 [ $^{79}\text{Br}^{79}\text{BrM}$ , 49], 492.0 [ $^{81}\text{Br}^{79}\text{BrM}$ , 100], 494.0 [ $^{81}\text{Br}^{81}\text{BrM}$ , 51]; Exact mass calcd for [ $\text{C}_{15}\text{H}_{12}\text{Br}_2\text{N}_2\text{O}_5\text{S}$ ] 489.8828, found 489.8805.

**(S)-3-(but-3-ynoyloxy)-2-(3,4-dibromo-2,5-dioxo-2,5-dihydro-1H-pyrrol-1-yl)propanoic acid 214**



3-Butynoic acid (39 mg, 0.468 mmol) was dissolved in  $\text{CH}_2\text{Cl}_2$  (1 ml). DMF (catalytic, 4  $\mu\text{l}$ ) and oxalyl chloride (42.3  $\mu\text{l}$ , 0.491 mmol) were added and the reaction stirred at room temperature for one hour. Tetra-*n*-butylammonium bromide (188 mg, 0.585 mmol) was added, followed by compound **167** (40.0 mg, 0.117 mmol), and the reaction stirred at room temperature for four hours. After this time MeOH (0.5 ml) was added and all solvent removed *in vacuo*. The resulting crude material was purified by flash chromatography (0 - 30% acetone in  $\text{CH}_2\text{Cl}_2$  with 1% AcOH) to yield title compound **214** as a white wax (29 mg, 0.063 mmol) in a 51% yield.

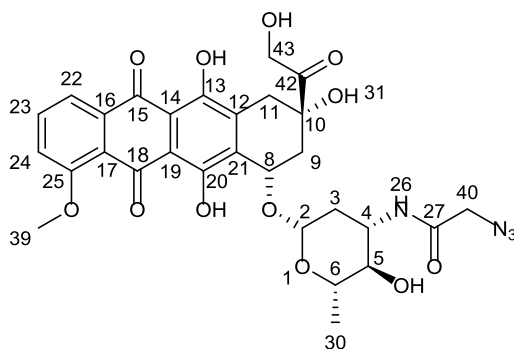
**2-azidoacetic acid 217**<sup>332</sup>



Bromoacetic acid (2.00 g, 14.4 mmol) was added over five minutes to a stirring solution of sodium azide (1.87 g, 28.8 mmol) in  $\text{H}_2\text{O}$  (8.4 ml). The solution was subsequently stirred at room temperature for 16 hours before conc. HCl (7 ml) was added dropwise to quench the reaction. The aqueous mixture was extracted with  $\text{Et}_2\text{O}$  (4 x 10 ml) and all solvent was removed *in vacuo* to produce title compound **217** as a clear liquid (1.33 g, 13.2 mmol) in a 92% yield.

$^1\text{H}$  NMR (600 MHz,  $\text{CDCl}_3\text{-d}_1$ )  $\delta$  = 3.99 (2H, s, H-2);  $^{13}\text{C}$  NMR (150 MHz,  $\text{CDCl}_3\text{-d}_1$ )  $\delta$  = 174.5 (C-3), 50.1 (C-2); IR (solid,  $\text{cm}^{-1}$ ) 3243, 2920, 2104, 1716; MS (CI)  $m/z$  [M, relative intensity] 102.1 [M+H, 46]; Exact mass calcd for  $[\text{C}_2\text{H}_4\text{N}_3\text{O}_2]$  102.0298, found 102.0299. Data matched the literature.<sup>332</sup>

**Doxorubicin-azide 218**

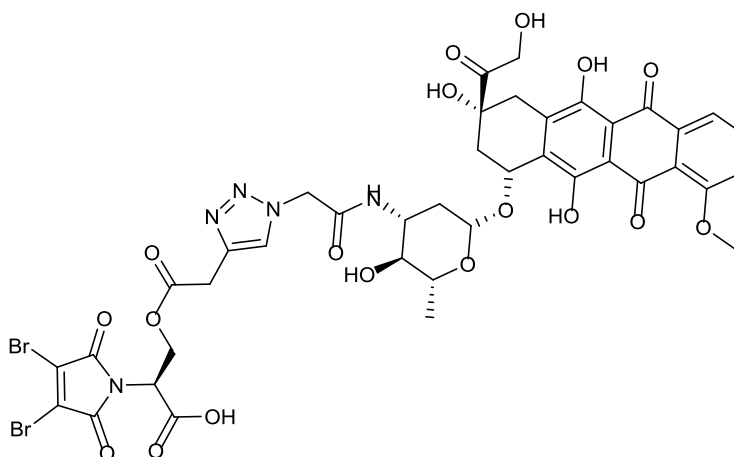


Doxorubicin hydrochloride (20.0 mg, 0.0345 mmol) was suspended in CH<sub>2</sub>Cl<sub>2</sub> (3.8 ml) and stirred at room temperature. A solution of compound **217** (3.5 mg, 0.0345 mmol) and HBTU (39.4 mg, 0.104 mmol) dissolved in CH<sub>2</sub>Cl<sub>2</sub> (7.4 ml) was added dropwise over three minutes and the entire solution was stirred at room temperature for 70 minutes. The reaction mixture was washed with sat. aqueous NaHCO<sub>3</sub> (5 ml), followed by brine (5 ml), and dried over MgSO<sub>4</sub>. All organic solvent was removed *in vacuo* and the crude material purified by column chromatography (0 - 10% MeOH in ethyl acetate) to produce title compound **218** as a red solid (20.0 mg, 0.0320 mmol) in a 93% yield.

<sup>1</sup>H NMR (600 MHz, MeOD-d<sub>4</sub>) δ = 7.64 - 7.72 (2H, m, H-23, 24), 7.41 (1H, d, J = 8.2, H-22), 5.37 (1H, d, J = 3.8, H-2), 4.99 (1H, br. s, H-8), 4.74 (2H, d, J = 5.3, H-43), 4.27 (1H, q, J = 6.5, H-6), 4.12 - 4.19 (1H, m, H-4), 3.94 (3H, s, H-39), 3.85 (2H, s, H-40), 3.62 (1H, br. s, H-5), 2.97 (1H, d, J = 18.0, H-11'), 2.78 (1H, d, J = 18.0, H-11''), 2.33 (1H, d, J = 14.4, H-9'), 2.10 (1H, dd, J = 14.4, J = 4.7, H-9''), 1.98 (1H, td, J = 13.2, J = 3.8, H-3'), 1.76 (1H, dd, J = 13.2, J = 4.7, H-3''), 1.27 (3H, d, J = 6.6, H-30); <sup>13</sup>C NMR (150 MHz, MeOD-d<sub>4</sub>) δ = 214.7 (C-42), 187.7 (C-15), 187.4 (C-18), 169.5 (C-27), 162.2 (C-25), 157.2 (C-13), 156.0 (C-20), 137.1 (C-16), 136.1 (C-23), 135.6 (C-12), 135.0 (C-21), 121.2 (C-17), 120.4 (C-22), 120.1 (C-24), 112.2 (C-14), 112.0 (C-19), 102.1 (C-2), 77.3 (C-10), 71.2 (C-8), 69.7 (C-5), 68.4 (C-6), 65.7 (C-43), 57.0 (C-39), 52.8 (C-40), 47.3 (C-4), 37.2 (C-9), 33.9 (C-11), 30.4 (C-3), 17.3 (C-30); IR (solid, cm<sup>-1</sup>) 3387, 2932, 2225, 1719, 1672, 1636, 1573; MS (ES-) m/z [M, relative intensity] 625.2 [M-H, 100], 647.2 [M+Na, 22]; Exact mass calcd for [C<sub>29</sub>H<sub>30</sub>N<sub>4</sub>O<sub>12</sub>] 652.1787, found 625.1780;

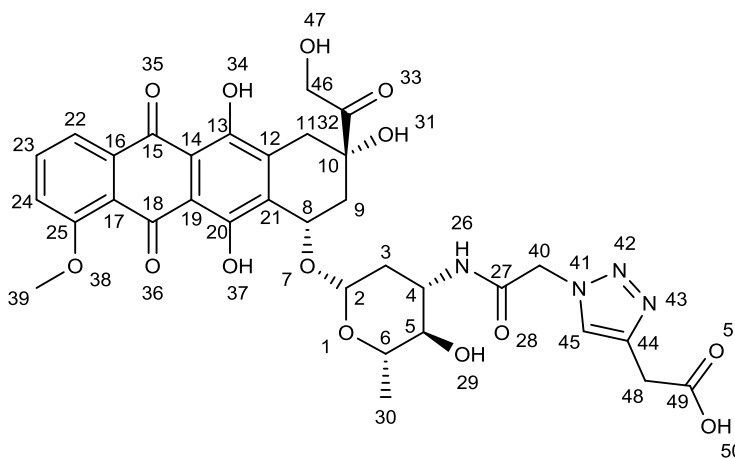
<sup>1</sup>H NMR (600 MHz, CDCl<sub>3</sub>-d<sub>1</sub>) δ = 5.14 (1H, dd, J = 9.9, J = 4.5, H-6), 4.86 (1H, dd, J = 11.9, J = 4.5, H-7'), 4.61 (1H, dd, J = 11.9, J = 9.9, H-7''), 3.27 (2H, d, J = 2.8, H-9), 2.17 (1H, t, J = 2.8, H-11); <sup>13</sup>C NMR (150 MHz, CDCl<sub>3</sub>-d<sub>1</sub>) δ = 170.4 (C-12), 167.5 (C-8), 163.0 (C-2, 5), 129.9 (C-3, 4), 74.9 (C-10), 72.4 (C-11), 61.4 (C-6), 51.8 (C-7), 25.7 (C-9); IR (solid, cm<sup>-1</sup>) 3290 (s), 2900, 2832, 1742, 1707, 1587; MS (ES+) m/z [M, relative intensity] 407.9 [<sup>79</sup>Br<sup>79</sup>BrM+H, 49], 409.9 [<sup>79</sup>Br<sup>81</sup>BrM+H, 100], 411.9 [<sup>81</sup>Br<sup>81</sup>BrM+H, 49]; Exact mass calcd for [C<sub>11</sub>H<sub>9</sub><sup>79</sup>Br<sub>2</sub>NO<sub>6</sub>] 407.8713, found 407.8719.

## Dox-dibromomaleimide **219**



Sodium ascorbate and  $\text{Cu}_2\text{SO}_4 \cdot \text{H}_2\text{O}$  (20  $\mu\text{l}$ , 47.8 mM suspension of each in degassed 50:50  $\text{H}_2\text{O}$  and *t*-BuOH) were added to a stirring solution of alkyne **214** (47.8 mM) and Dox-azide **218** (239 mM) in a degassed mixture of water and *t*-BuOH (50:50, 100  $\mu\text{l}$ ). The resulting solution was stirred in the dark at room temperature for 4 hours. After this time LCMS showed no trace of starting material **214** and confirmed successful click reaction to Dox-dibromomaleimide **219**. MS (ES+)  $m/z$  [M, relative intensity] 1036.0 [M+H, 100].

## Dox-Carboxylic acid **222**



Sodium ascorbate and  $\text{Cu}_2\text{SO}_4 \cdot \text{H}_2\text{O}$  (100  $\mu\text{l}$ , 47.8 mM suspension of each in degassed 50:50  $\text{H}_2\text{O}$  and *t*-BuOH) were added to a stirring solution of 3-butynoic acid (4.00 mg, 0.0478 mmol) and Dox-azide **218** (15.0 mg, 0.0239 mmol) in a mixture of degassed  $\text{H}_2\text{O}$  and *t*-BuOH (50:50, 0.5 ml). The resulting solution was stirred in the dark at room temperature for 16 hours. Acetic acid (50  $\mu\text{l}$ ) was added, all solvent removed *in vacuo* and the crude product dry loaded onto C18 silica. Purification by reverse phase chromatography (0-95% MeCN in  $\text{H}_2\text{O}$ ) gave a crude red material which was subsequently washed with  $\text{CH}_2\text{Cl}_2$  (5 x 1 ml) to yield title compound **222** as a red solid (7.0 mg, 0.00986 mmol) in a 41% yield.

$^1\text{H}$  NMR (600 MHz, DMSO- $d_6$ )  $\delta$  = 14.05 (2H, s, H-34), 13.28 (2H, s., H-37), 8.20 (1H, d,  $J$  = 8.2, H-26), 7.91 (2H, br. s., H-23, 24), 7.84 (1H, s, H-45), 7.65 (1H, s, H-22), 5.46 (1H, br. s., H-31), 5.15 - 5.33 (1H, m, H-2), 5.03 (3H, m, H-8, 40), 4.95 (2H, br. s., H-29), 4.86 (1H, br. s., H-47), 4.56 (2H, br. s., H-46), 4.17 (1H, q,  $J$  = 6.6, H-6), 3.99 (4H, br. s., H-4, 39), 3.60 (2H, s, H-48), 3.42 (1H, br. s., H-5), 2.96 (2H, dd,  $J$  = 18.2,  $J$  = 5.6, H-11), 2.19 (1H, d,  $J$  = 13.6, H-9`), 2.12 (1H, dd,  $J$  = 13.2,  $J$  = 5.6, H-9``), 1.88 (1H, td,  $J$  = 12.7,  $J$  = 3.6, H-3`), 1.49 (1H, dd,  $J$  = 12.7,  $J$  = 3.6, H-3``), 1.13 (3H, d,  $J$  = 6.6, H-30);  $^{13}\text{C}$  NMR (150 MHz, DMSO- $d_6$ )  $\delta$  = 213.9 (C-32), 186.7 (C-15), 186.6 (C-18), 171.6 (C-49), 164.7 (C-27), 160.8 (C-25), 156.1 (C-13), 154.5 (C-20), 140.2 (C-44), 136.3 (C-16), 135.6 (C-23), 134.8 (C-12), 134.1 (C-21), 124.8 (C-45), 120.1 (C-17), 119.8 (C-22), 119.0 (C-24), 110.9 (C-14), 110.7 (C-19), 100.2 (C-2), 75.0 (C-10), 70.1 (C-8), 67.8 (C-5), 66.6 (C-6), 63.7 (C-46), 56.6 (C-39), 51.5 (C-40), 45.5 (C-4), 36.8 (C-9), 32.1 (C-11), 31.5 (C-48), 29.7 (C-3), 17.0 (C-30); IR (solid,  $\text{cm}^{-1}$ ) 3403, 3312, 2893, 1787, 1717, 1611, 1543; MS (ES-)  $m/z$  [ $M$ , relative intensity] 709.2 [ $M$ -H, 100], 731.2 [ $M$ +Na, 60]; Exact mass calcd for  $[\text{C}_{33}\text{H}_{33}\text{N}_4\text{O}_{14}]$  709.1999, found 709.1994;

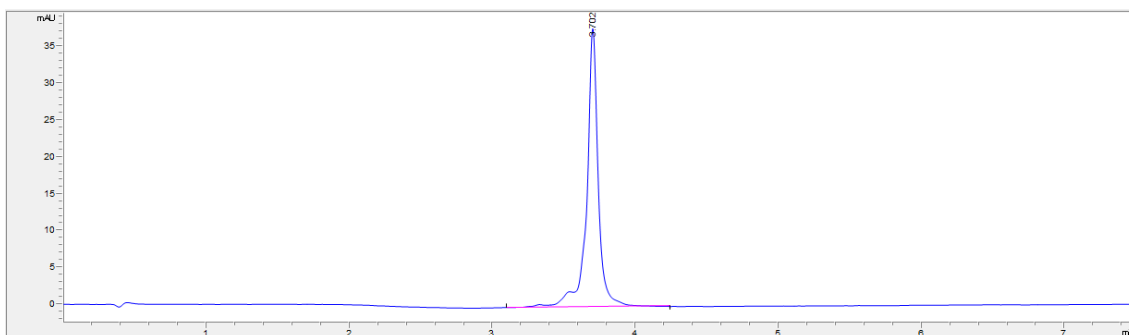
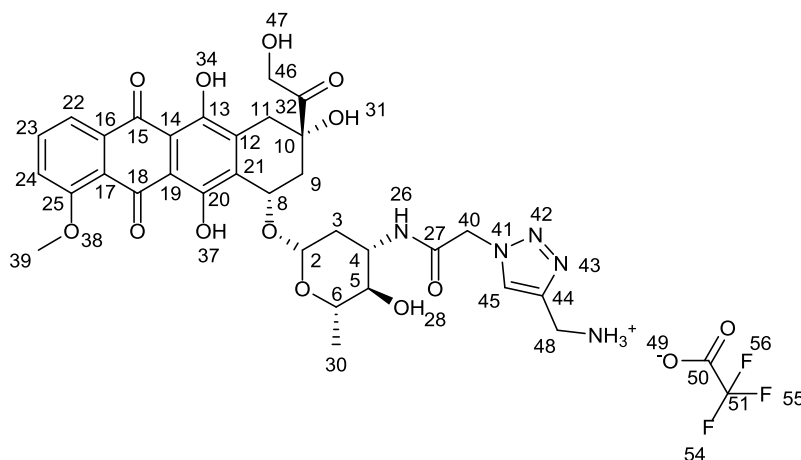


**Figure 61**  
A HPLC chromatogram of Dox-carboxylic acid 222

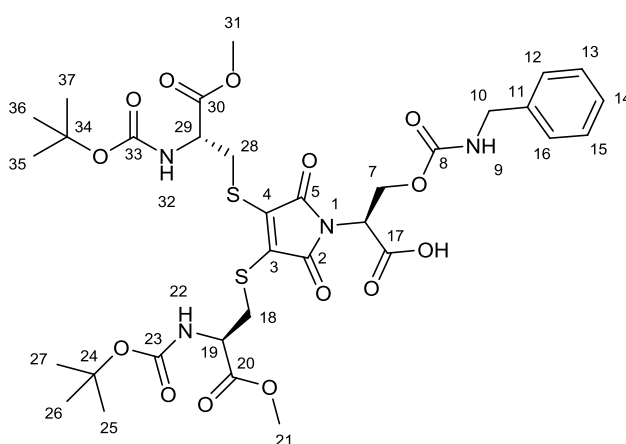
### Dox-amine 224



Sodium ascorbate and  $\text{Cu}_2\text{SO}_4 \cdot \text{H}_2\text{O}$  (100  $\mu\text{l}$ , 51.0 mM suspension of each in degassed 50:50  $\text{H}_2\text{O}$  and  $t\text{-BuOH}$ ) were added to a stirring solution of propargylamine (2.81 mg,

0.0510 mmol) and Dox-azide **218** (16 mg, 0.0255 mmol) in a 50:50 mixture of degassed H<sub>2</sub>O and *t*-BuOH (0.5 ml). The resulting solution was stirred in the dark at room temperature for two hours. All solvent was removed *in vacuo* and the crude product dissolved in H<sub>2</sub>O (5 ml, 0.1% trifluoroacetic acid). The aqueous layer was washed with CH<sub>2</sub>Cl<sub>2</sub>, the organic layer discarded, and the water removed *in vacuo* to produce a crude red solid which was purified by reverse phase C-18 silica (0-95% MeCN in H<sub>2</sub>O with 0.1% trifluoroacetic acid) to yield title compound **224** as a red wax (9.0 mg, 0.011 mmol) in a 43% yield. <sup>1</sup>H NMR (600 MHz, DMSO-*d*<sub>6</sub>) δ = 14.02 (1H, s, H-37), 13.29 (1H, s, H-34), 8.27 (1H, d, J = 8.2, H-26), 8.20 (2H, br. s., H-49), 8.03 (1H, s, H-45), 7.89 - 7.93 (2H, m, H-23, 24), 7.67 (1H, dd, J = 6.5, J = 3.3, H-22), 5.25 (1H, d, J = 2.9, H-2), 5.13 (2H, d, J = 3.3, H-40), 4.95 (1H, dd, J = 5.7, J = 3.1, H-8), 4.55 (2H, s, H-46), 4.16 (1H, q, J = 6.7, H-6), 4.06 - 4.13 (2H, m, H-48), 3.94 - 4.03 (4H, m, H-4, 39), 3.41 (1H, br. s., H-5), 2.96 (2H, d, J = 4.7, H-11), 2.18 (1H, dd, J = 14.0, J = 3.1, H-9'), 2.14 (1H, dd, J = 14.0, J = 5.7, H-9''), 1.89 (1H, td, J = 12.6, J = 3.9, H-3'), 1.50 (1H, dd, J = 12.6, J = 4.7, H-3''), 1.14 (3H, d, J = 6.7, H-30); <sup>13</sup>C NMR (150 MHz, DMSO-*d*<sub>6</sub>) δ = 213.8 (C-32), 186.6 (C-15), 186.6 (C-18), 164.5 (C-27), 160.8 (C-25), 158.0 (q, J<sub>C-F</sub> = 25.5, C-50), 156.1 (C-13), 154.5 (C-20), 139.8 (C-44), 136.3 (C-16), 135.6 (C-23), 134.8 (C-12), 134.2 (C-21), 125.6 (C-45), 120.0 (C-17), 119.8 (C-22), 119.1 (C-24), 110.8 (C-14), 110.7 (C-19), 100.3 (C-2), 74.9 (C-10), 70.2 (C-8), 67.9 (C-5), 66.6 (C-6), 63.6 (C-46), 56.6 (C-39), 51.7 (C-40), 45.5 (C-4), 36.7 (C-9), 33.9 (C-48), 32.1 (C-11), 29.7 (C-3), 17.0 (C-30); <sup>19</sup>F NMR (282MHz, DMSO-*d*<sub>6</sub>) δ = -73.9 (F-54 - 56); IR (solid, cm<sup>-1</sup>) 3395, 2956, 2893, 1754, 1694, 1643, 1585; (ES+) *m/z* [M, relative intensity] 682.2 [M-TFA, 100], 268.1 [C<sub>11</sub>H<sub>18</sub>N<sub>5</sub>O<sub>3</sub>, 30]; Exact mass calcd for [C<sub>32</sub>H<sub>36</sub>N<sub>5</sub>O<sub>12</sub>] 682.2350, found 682.2352.

**(S)-3-((benzylcarbamoyleoxy)-2-(3,4-bis(((R)-2-((tert-butoxycarbonyl)amino)-3-methoxy-3-oxopropyl)thio)-2,5-dioxo-2,5-dihydro-1H-pyrrol-1-yl)propanoic acid **232****



Compound **169** (19.2 mg, 0.0295 mmol) was dissolved in CH<sub>2</sub>Cl<sub>2</sub>/EtO<sub>2</sub> (1.0 ml, 50/50) and stirred under argon. Benzyl isocyanate (7.3 μl, 0.0589 mmol) was added, followed by a spatula tip of powdered MoO<sub>2</sub>Cl<sub>2</sub>, and the solution stirred at room temperature for three

hours. All solvent was removed *in vacuo*. The crude material was purified by flash chromatography (0 - 10% MeOH in CH<sub>2</sub>Cl<sub>2</sub> with 1% AcOH, multiple columns required) to yield title compound **232** as a yellow glass (11 mg, 0.0140 mmol) in a 48% yield.

<sup>1</sup>H NMR (600 MHz, MeOD-d<sub>4</sub>) δ = 7.17 - 7.33 (5H, m, 12, 13, 14, 15, 16), 5.00 (1H, dd, J = 10.2, J = 4.3, H-6), 4.75 (1H, dd, J = 11.1, J = 4.3, H-7'), 4.49 (1H, td, J = 11.1, J = 10.2, H-7''), 4.41 (2H, dd, J = 8.7, J = 4.8, H-19, 29), 4.25 (2H, d, J = 2.3, H-10), 3.85 (2H, dd, J = 13.8, J = 4.8, H-18', 28'), 3.71 (6H, br. s., H-21, 31), 3.49 (2H, dd, J = 13.8, J = 8.7, H-18'', 28''), 1.39 - 1.46 (18H, m, H-25, 26, 27, 35, 36, 37); <sup>13</sup>C NMR (150 MHz, MeOD-d<sub>4</sub>) δ = 172.4 (C-17), 166.8 (C-2, 5), 158. (C-23, 33), 140.3 (C-11), 137.1 (C-3, 4), 129.5 (C-12, 16), 128.2 (C-15, 13), 128.1 (C-14), 81.0 (C-24, 34), 62.2 (C-7), 56.0 (C-19, 29), 53.1 (C-21, 31, 6), 45.4 (C-10), 34.0 (C-18, 28), 30.8, 29.5, 28.7 (C-25, 26, 27, 35, 36, 37); IR (solid, cm<sup>-1</sup>) 3370, 2977, 2929, 1709 (broad, sharp); MS (ES+) m/z [M, relative intensity] 807.2 [M+Na, 40] 865.2 [M-C<sub>5</sub>H<sub>9</sub>O<sub>2</sub>, 100]; Exact mass calcd for [C<sub>33</sub>H<sub>44</sub>O<sub>14</sub>N<sub>4</sub>S<sub>2</sub>Na] 807.2188, found 807.2184; ε<sub>480</sub> = 3705 M<sup>-1</sup>·cm<sup>-1</sup>.

## 3.2: Chemical Biology Experimental

### 3.2.1: General experimental

All buffers were passed through a microfilter before use to remove particulates and the pH adjusted using 1 M HCl or 1 M NaOH. pH was measured using a Hanna Instruments pH 210 electronic pH meter. When spin filtration devices are mentioned VivaSpin (GE Healthcare) 3000, 5000 or 10000 molecular weight cut off devices were employed. Where appropriate PD-10 desalting columns from GE Healthcare were used for protein purification. Protein concentrations were determined photometrically using either a Jenway 2705 spectrophotometer or a ThermoScientific Nanodrop 2000C. For small scale centrifugation Eppendorf 5415 R and VWR Galaxy 14D microcentrifuges were employed. For large scale Fab fragment preparation an Eppendorf 5810 R centrifuge was used. An Eppendorf thermomixer comfort heating block was used for temperature and agitation controlled experiments.

Octreotide was purchased from LKT laboratories. Rituxan **100** and Herceptin **125** were purchased from the UCLH pharmacy, Anti-CEA scFv **97** was expressed according to literature procedure by Dr Berend Tolner and Dr Maria Livanos of the UCL Cancer Institute. Digests of Rituxan and Herceptin were prepared using Pierce Fab fabrication kits according to modified versions of the manufacturers protocol.

#### Photochemistry on protein and peptide samples

Irradiation of Octreotide, Rituxan Fab and Herceptin Fab was performed using a commercial 5W LED torch purchased from Advanced NDT Ltd with an irradiance measurement of approximately  $20 \text{ mWcm}^{-3}$  at 14 cm. Protein and peptide samples were placed in a plastic cuvette with the LED positioned 14 cm above, and the whole apparatus was encased in reflective foil. When a single LED system is specified a custom built 5W LED was provided by collaborators at the University of York. Samples were placed into a plastic cuvette with the LED position 1 cm above, and the whole apparatus was encased in reflective foil. Irradiation of scFv conjugate **220** was performed using a Tank007 UV torch with an irradiance measurement of  $6 \text{ mW}\cdot\text{cm}^{-3}$  at a distance of 1 cm.

#### Buffers

All buffers were adjusted to the desired pH using 1M HCl or 1M NaOH. When varying amounts of EDTA are specified the exact amount is outlined in the protocol.

Phosphate buffer pH = 6.2: 50:50 MeCN:phosphate buffer (pH = 6.2, 50 mM  $\text{NaH}_2\text{PO}_4$ ).

Acetate buffer pH = 3.1: 20 mM sodium acetate

Digest buffer pH = 6.8: 50 mM  $\text{NaH}_2\text{PO}_4$ , 150 mM NaCl, 1 mM EDTA,

PBS pH = 7.4: 2.7 mM KCl, 137 mM NaCl, 10 mM  $\text{Na}_2\text{HPO}_4$ , 1.8 mM  $\text{KH}_2\text{PO}_4$ , (varying amounts of EDTA)

PBS pH = 6: 24.6 mM Na<sub>2</sub>HPO<sub>4</sub>, 154.4 mM KH<sub>2</sub>PO<sub>4</sub>.

PBS pH = 8: 189.3 mM Na<sub>2</sub>HPO<sub>4</sub>, 0.9 mM KH<sub>2</sub>PO<sub>4</sub>.

BBS pH = 8: 5 mM sodium borate, 25 mM NaCl, (varying amounts of EDTA).

### **SDS-PAGE methods**

Non-reducing 12% acrylamide gels were made using standard procedures. A 4% stacking gel was utilised. Samples (22 µM) were mixed 1:1 with a 1X SDS-loading buffer (1 g SDS, 3 ml glycerol, 6 ml 0.5 M Tris buffer PH 6.8, 2 mg R-250 dye was diluted 1 in 6 with dd H<sub>2</sub>O), heated for two minutes at 75 °C and loaded onto the gel with a total volume of 4 µL. Samples were run at constant current (30 mA) for 40 minutes in 1 x SDS running buffer and stained with Coomassie. Gel-Pro analyser version 3.1.00.00 from Media Cybernetics was used for densitometry analysis.

#### **3.2.1.1: HPLC methods**

##### **Octreotide**

A Kinetex 5u XN-C18 100A (260 x 4.60 mm) column at 40 °C using a Shimadzu LC-10AD liquid chromatography apparatus equipped with a Shimadzu DGU-14A diode array. Flow rate was set at 1.00 ml/min. Solvent A is H<sub>2</sub>O (0.1% formic acid), solvent B is MeCN (0.1% formic acid). Mobile phase: 75:25 A:B; gradient to 35:65 A:B over 24.5 minutes: gradient to 5:95 A:B up to 26 minutes, followed by 75:25 A:B to completion of 30 minutes. For analytical work an injection volume of 20 µl at 10 µM was used. For semi-preparative purification of **90** an injection volume of 100 µl at 100 µM was employed.

##### **Anti-CEA scFv**

A Hypersil Gold C4 (50 x 2.1 mm) column at 50 °C was employed on a Agilent Technologies 1260 Infinity LC equipped with a Agilent Technologies 1260 Infinity photodiode array. Flow rate was set at 0.600 ml/min. Solvent A is H<sub>2</sub>O (0.1% formic acid), solvent B is MeCN (0.1% formic acid). Mobile phase: 95:5 A:B; gradient over 6 minutes to 5:95 A:B. An Injection volume of 10 µl at 20 µM was used.

#### **3.2.1.2: MALDI-TOF methods**

MALDI-TOF was performed on a Shimadzu Biotech Axima CFR in reflectron mode, with laser power set at 75.

#### **3.2.1.3: Tandem-MS methods**

Tandem MS was performed on a ThermoScientific Finnigan LTQ fitted with a Hypersil Gold C18 column (100 mm x 2.1 mm). Flow rate was set at Solvent A is H<sub>2</sub>O (0.1% formic acid), solvent B is MeOH (0.1% formic acid). Mobile phase: 95:5 A:B; gradient over 10 minutes to 5:95 A:B. Ionisation was performed in ES+ mode with a collision energy of 35% for the MS<sup>2</sup> spectra. An injection volume of 25 µl was employed. Spray voltage was 4.5 kV, capillary

temperature 280 °C. MS scans consisted of three averaged “microscans”, each with a maximum injection time of 200 ms.

#### **3.2.1.4: LCMS methods**

LCMS for Octreotide, anti-CEA scFv and Herceptin was performed on a Waters Acquity uPLC connected to Waters Acquity Single Quad Detector and a photodiode array. Flow rate was set at 0.600 ml/min. LCMS for Rituxan Fab was performed on a ThermoScientific MSQ Plus connected to an Accela 1250 pump and Accela UV-Vis detector. Flow rate was set at 0.600 ml/min. All deconvoluted mass spectra were produced using the software provided by the manufacturer.

##### **Octreotide [2+2] work**

An Acquity UPLC BEH C18 (50 x 2.1 mm) column at 50 °C was employed; Solvent A is H<sub>2</sub>O (0.1% formic acid), solvent B is MeCN (0.1% formic acid). Mobile phase: 95:5 A:B; gradient over 4 minutes to 5:95 A:B. MS mode ES<sup>+</sup> ; scan range: m/z ¼ 250–2,000; scan time: 0.25 s. A capillary voltage of 3.5 kV and a cone voltage of 50 V was employed. Injection volumes of 10 µl at 200 µM were used. Injection volumes of 10 µl at 300 µM were used.

##### **Octreotide decarboxylation work**

An Agilent SB-C18 (20 x 2.1 mm) column at 50 °C was employed. Solvent A is H<sub>2</sub>O (0.1% formic acid), solvent B is MeCN (0.1% formic acid). Mobile phase: 95:5 A:B up to 2 minutes: gradient to 30:70 A:B up to 12.5 minutes: gradient to 5:95 A:B up to 15 minutes A:B. MS mode ES<sup>+</sup>/ES<sup>-</sup> ; scan range: m/z ¼ 250–2,000; scan time: 0.25 s. A capillary voltage of 3.5 kV and a cone voltage of 50 V was employed. Injection volumes of 10 µl at 200 µM were used.

##### **Rituxan Fab**

A Hypersil Gold C4 (50 x 2.1 mm) column at 50 °C was used for separation. Solvent A is H<sub>2</sub>O (0.1% formic acid), solvent B is MeCN (0.1% formic acid). Mobile phase: 95:5 A:B; gradient over 4 min to 5:95 A:B. MS mode ES<sup>+</sup> ; scan range: m/z ¼ 250–2,000; scan time: 0.25 s. A capillary voltage of 3.5 kV and a cone voltage of 50 V was employed. Injection volumes of 7 µl at 10 µM were used.

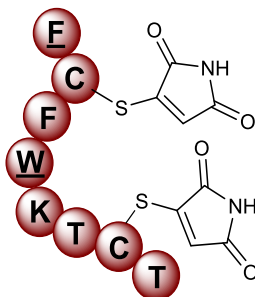
##### **Herceptin Fab**

A Hypersil Gold C4 (50 x 2.1 mm) column at 50 °C was used for separation. Solvent A is H<sub>2</sub>O (0.1% formic acid), solvent B is MeCN (0.1% formic acid). Mobile phase: 95:5 A:B; gradient over 4 min to 5:95 A:B. MS mode ES<sup>+</sup> ; scan range: m/z ¼ 250–2,000; scan time: 0.25 s. A capillary voltage of 3.5 kV and a cone voltage of 50 V was employed. Injection volumes of 10 µl at 10 µM were used. Deconvolution was performed using the MaxEnt 1 algorithm pre-installed on MassLynx software.

## 3.2.2: Octreotide photoactivation

### 3.2.2.1: Modification of Octreotide

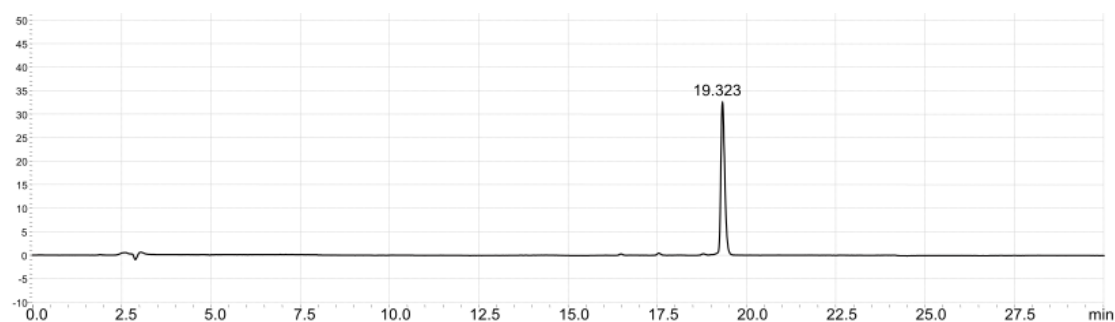
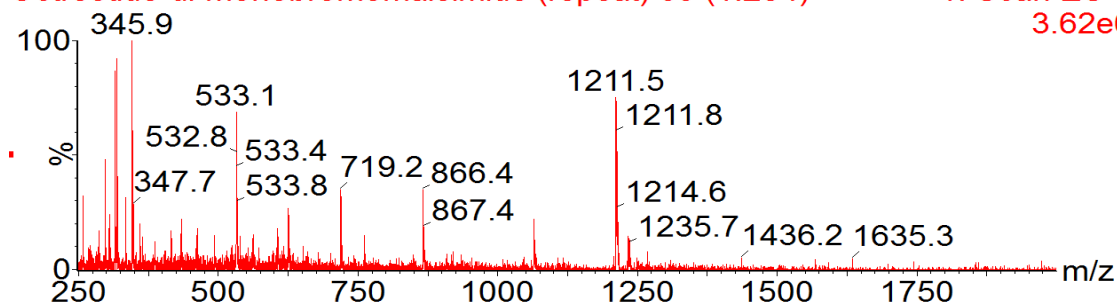
#### Preparation of *bis*-modified Octreotide **90**



A solution of reduced Octreotide **92** (300 mM in 50:50 PBS pH = 6.2:MeCN, 1.00 ml) was added dropwise to a solution of bromomaleimide **93** (300 mM in 50:50 PBS pH = 6.2:MeCN, 100 equiv., 100  $\mu$ l) over five minutes. After 30 minutes at room temperature the solution was placed into dialysis cups (2 KDa MWCO) and dialysed with deionised water overnight. All solvent was subsequently removed by lyophilisation, the peptide dissolved in deionised water and purified by HPLC. HPLC yield of 70%. Analysis by MALDI-TOF confirmed successful conjugation to produce conjugate **90**. Expected mass 1211, observed mass 1211 (relative to pure Octreotide 1018).

Octreotide-di-monobromomaleimide (repeat) **69** (1.284)

1: Scan ES+  
3.62e6



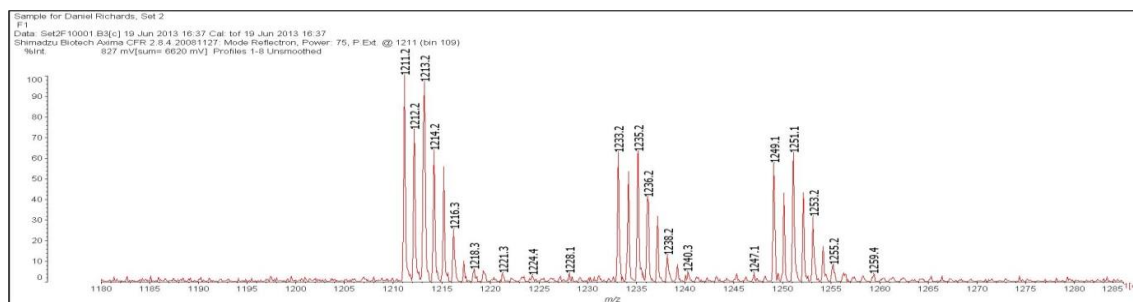
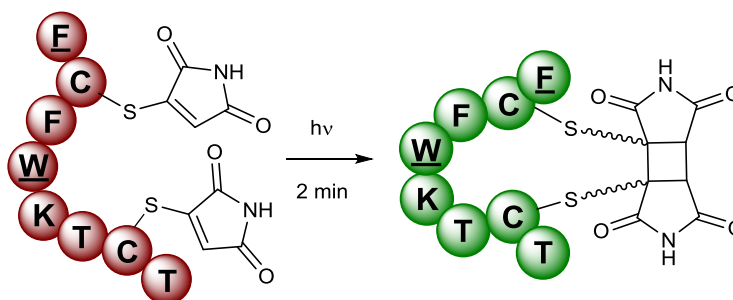


**Figure 62**  
**LCMS spectra of crude *bis*-modified Octreotide 90. HPLC trace and MALDI spectra for purified Octreotide conjugate 90.**

### Preparation of bridged Octreotide 91



Purified conjugate **90** (300  $\mu$ M in 50:50 PBS pH = 6.2:MeCN, 60  $\mu$ l) was placed in a 1 cm<sup>3</sup> cuvette and irradiated for two minutes using the 365 nm UVG-2 torch. The subsequent solution was analysed by HPLC. Extended irradiation times effected no change in the HPLC trace, indicating the reaction had gone to completion: Peaks labelled A (16.14 minutes), B (16.49 minutes), C (17.26 minutes) and D (17.64 minutes) were analysed by MALDI-TOF (expected mass 1211, observed mass 1211). Additionally, the eluent was collected between 15.0 and 20.0 minutes and analysed by MALDI-TOF (Expected mass 1211, observed mass 1211).

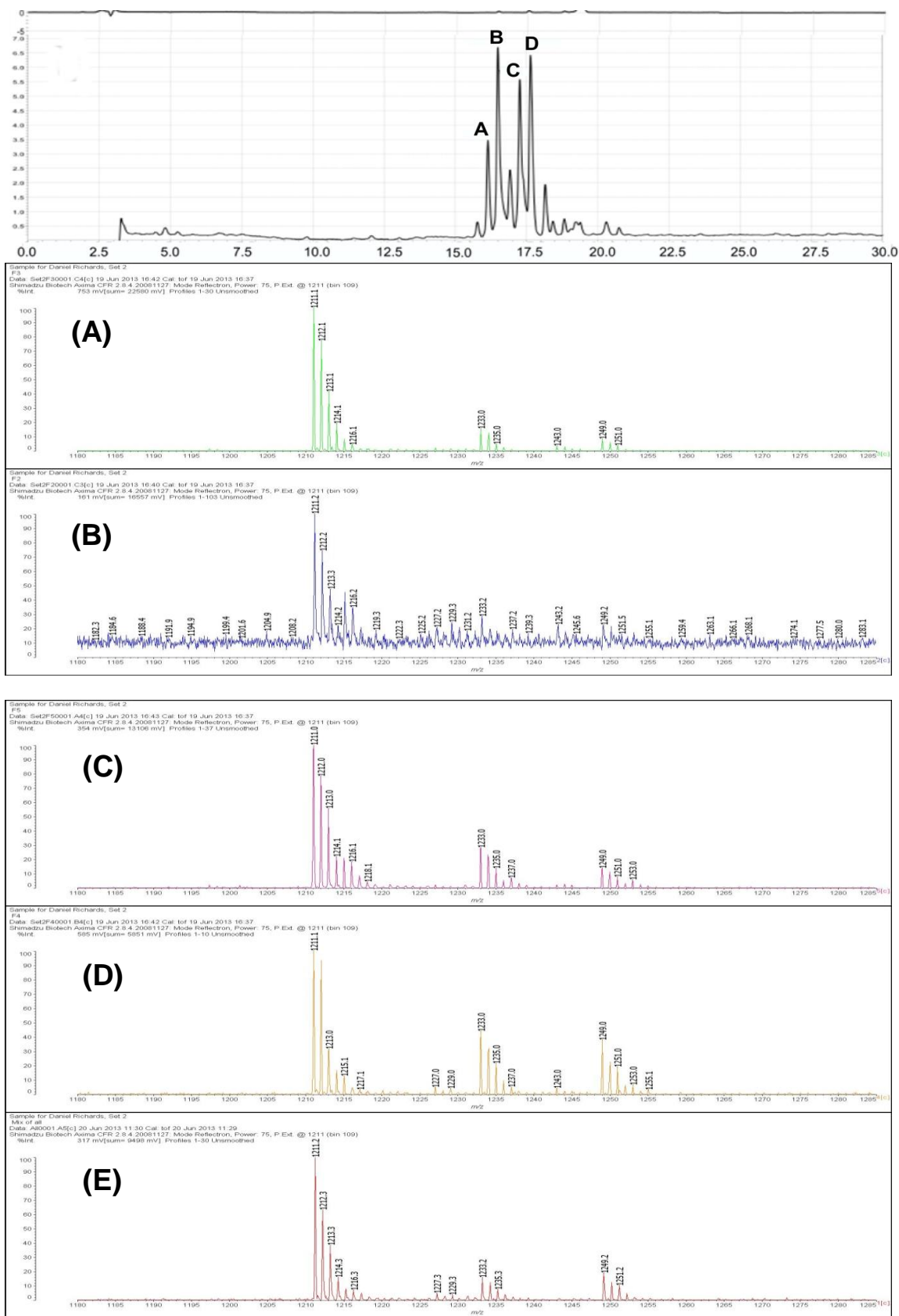
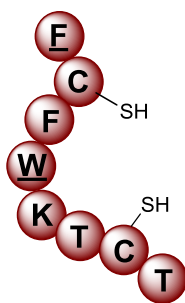


**Figure 63**  
**HPLC trace for the irradiation of Octreotide conjugate 90. MALDI-TOF spectrum for (A) peak A, (B) peak B, (C) peak C, (D) peak D, and (E) the combined eluent from 15.0 to 20.0 minutes.**

## Preparation of reduced Octreotide 92



*Tris*(2-carboxyethyl)phosphine (TCEP) (30 mM in 50:50 PBS pH = 6.2:MeCN, 1.5 equiv., 15  $\mu$ l) was added to a solution of Octreotide **74** (300  $\mu$ M in 50:50 PBS pH = 6.2:MeCN, 1 ml) and left to react at 37  $^{\circ}$ C for one hour. LCMS analysis of the solution revealed successful reduction to reduced Octreotide **92**. Expected mass 1021, observed mass 1021.

octreotide reduced peptide (repeat) 72 (1.339)

1: Scan ES+  
4.15e7

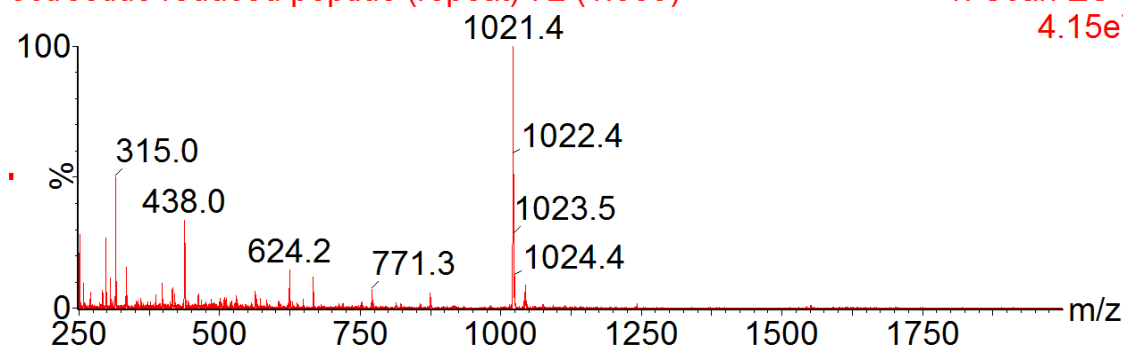
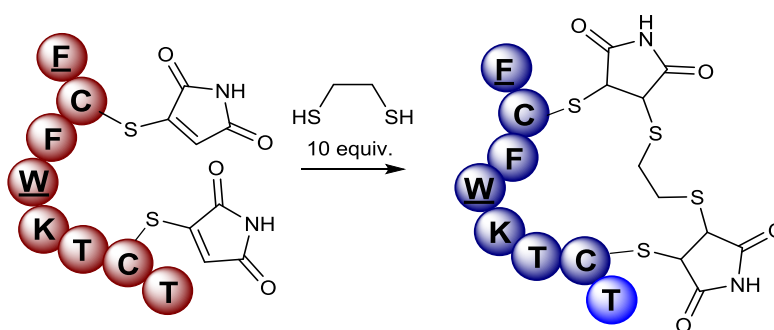


Figure 64  
LCMS spectrum for reduced Octreotide 92.

## 3.2.2.2: Thiol reactivity of Octreotide conjugates

### Preparation of EDT bridged Octreotide 95



Ethanedithiol (100 mM in 50:50 PBS pH = 6.2:MeCN, 10 equiv., 0.3  $\mu$ l) was added to a solution of conjugate **90** (100  $\mu$ M in 50:50 PBS pH = 6.2:MeCN, 30  $\mu$ l). After 30 minutes LCMS confirmed successful reaction: Expected mass 1306, observed mass 1306.

Octreotide-di-monobromo-bridge(repeat) 70 (1.302)

1: Scan ES+  
1.15e6

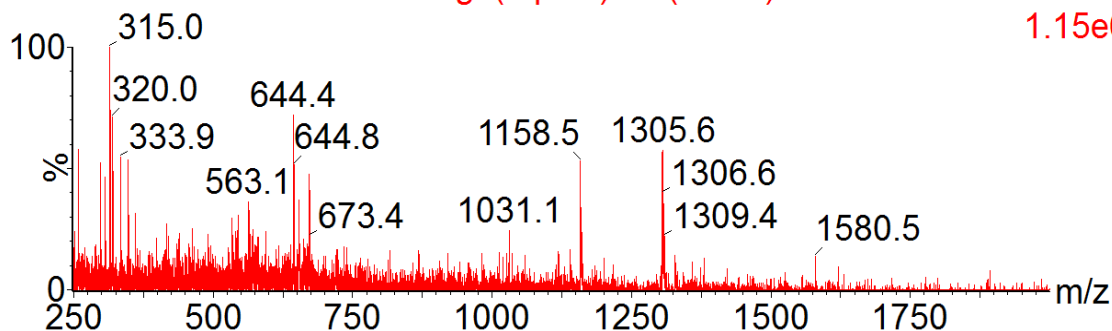
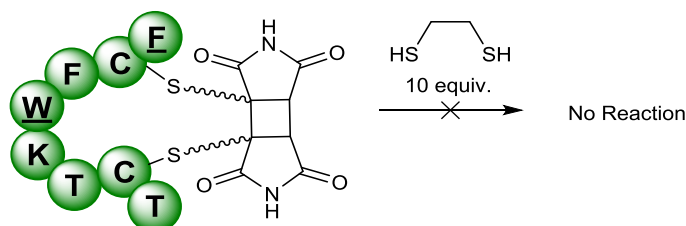


Figure 65  
LCMS of Octreotide conjugate 90 + ethanedithiol to generate conjugate 95.

Treatment of bridged conjugate 91 with ethanedithiol



Ethanedithiol (100 mM in 50:50 PBS pH = 6.2:MeCN, 10 equiv., 0.3  $\mu$ l) was added to a solution of bridged Octreotide **91** (100  $\mu$ M in 50:50 PBS pH = 6.2:MeCN, 30  $\mu$ l). After 30 minutes LCMS showed no change, indicating no reaction had taken place.

octreotide di-monobromomaleimide after 15m mercury with edt (002-5) 60 (1.1

4.74e6

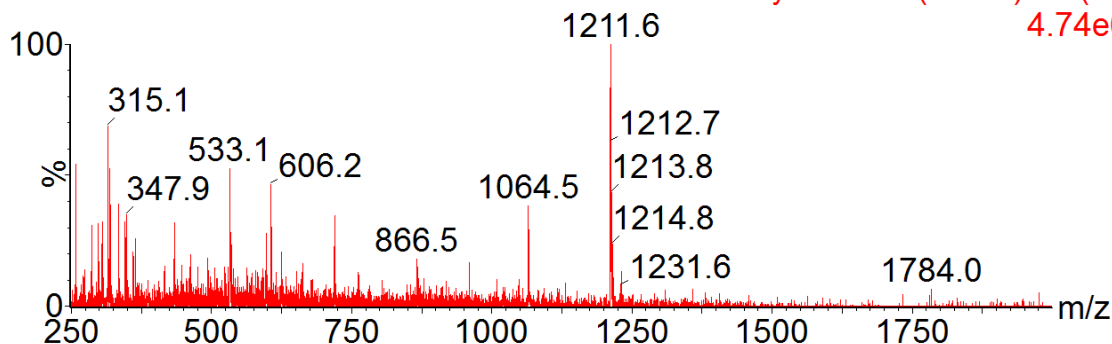


Figure 66  
LCMS of conjugate 91 + ethanedithiol.

### 3.2.2.4: Electrophysiology data

Worked was performed by Dr Muriel Nobles

#### Cell culture

Cell culture methods and the generation of stable cell lines were carried out as previously described.<sup>333</sup> HEK293 cells (human embryonic kidney cell line) stably expressing Kir3.1 and Kir3.2A channels were maintained in minimum essential medium supplemented with 10% foetal calf serum and 727  $\mu$ g of G418 (Invitrogen), at 37  $^{\circ}$ C in humidified atmosphere (95% O<sub>2</sub>, 5% CO<sub>2</sub>). Cells were transiently transfected with SSTR2 DNA (Missouri S&T

cDNA Resource Center) along with pEGFP-N1 (Clontech) for visualization of transfected cells using epifluorescence. Transfections were performed with 5  $\mu$ l of Fugene HD (Roche) and 800 ng SSTR2 DNA and 40 ng EGFP DNA.

### Electrophysiology

Whole cell patch-clamp current recordings were performed with an Axopatch 200B amplifier (Axon Instruments) using fire polished pipettes with a resistance of 4-5 M $\Omega$  pulled from filamented borosilicated glass capillaries (Harvard Apparatus, 1.5 mm OD x 1.17 mm ID). Data was acquired and analysed via a Digidata 1322A interface (Axon Instruments) and pCLAMP software (version 10.2, Axon Instruments). Cells were clamped at -50 mV. The extracellular solution was: NaCl (135 mM), KCl (5.4 mM), CaCl<sub>2</sub> (2 mM), MgCl<sub>2</sub> (1 mM), NaH<sub>2</sub>PO<sub>4</sub> (0.33 mM), H-HEPES (5 mM), Glucose (10 mM), buffered to pH 7.4 with NaOH. The intracellular solution was: potassium D-gluconate (110 mM), KCl (20 mM), NaCl (10 mM), MgCl<sub>2</sub> (1 mM), MgATP (2 mM), EGTA (2 mM), Na<sub>2</sub>GTP (0.3 mM), buffered to pH 7.2 with KOH. Octreotide **74** and conjugates **90** and **91** were administered by a gravity driven system, at a concentration of 0.01, 0.1 or 1  $\mu$ M until the current reaches a maximum value. All experiments were done at room temperature. All peptides for testing were kept at -80 °C avoiding repetitive thawing/freezing. Currents were elicited by holding cells at -50 mV and stepping to potentials between -120 and +60 mV in 10 mV increments for 360 ms. Current densities were measured at -120 mV and all data are presented as means  $\pm$  S.E.M. Data were analysed for statistical significance using one way ANOVA with a post-hoc test.

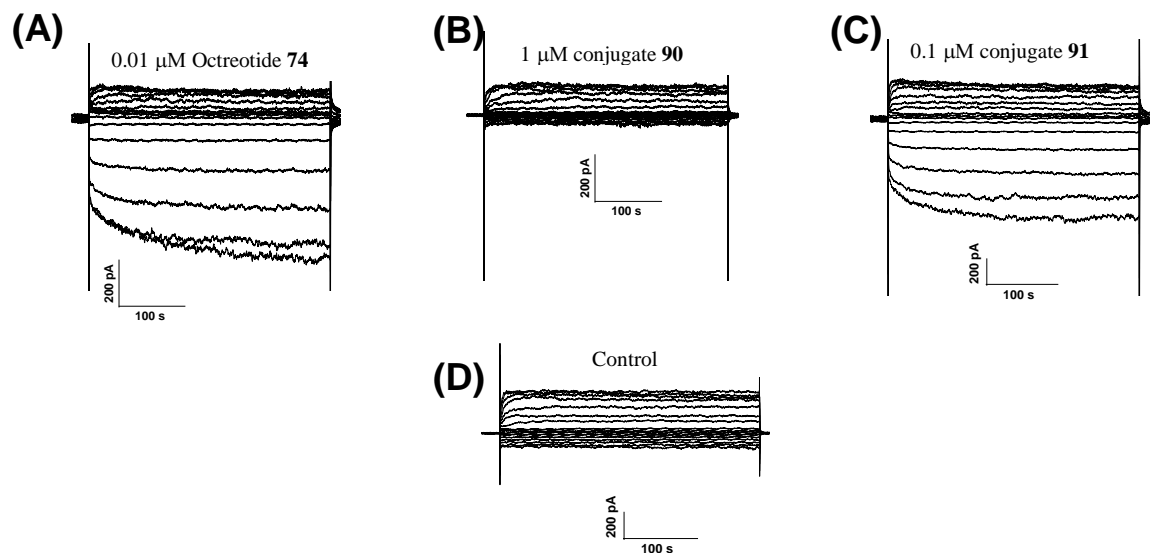


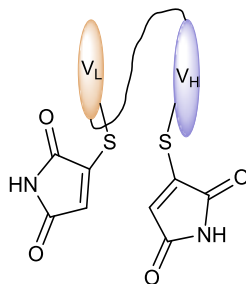
**Figure 67**

(A) Current activation from native Octreotide 74 (0.01  $\mu$ M). (B) Current activation from *bis*-modified Octreotide 90 (1  $\mu$ M) (C) Current activation from bridged Octreotide 91 (0.1  $\mu$ M). (D) Current without agonist. The maximum current values obtained were as follows: native Octreotide 74 (10 nM,  $-73.7 \pm 5.9$  pA/pF, n=10), conjugate 90 (1  $\mu$ M,  $-2.1 \pm 0.9$  pA/pF, n=9,  $p < 0.0001$  compared to Octreotide 74) and conjugate 91 (100 nM,  $-16.1 \pm 4.7$  pA/pF, n=10,  $p < 0.0001$  compared to Octreotide 74).

### 3.2.3: Anti-CEA scFv fragment

#### 3.2.3.1: Anti-scFv fragment modification

##### Preparation of *bis*-modified anti-CEA scFv **98**



A solution of dithiothreitol (DTT) (70 mM in PBS + 10% MeCN, 20 equiv., 2.4  $\mu$ l) was added to a solution of scFv **97** (70  $\mu$ M in PBS pH = 7.4 + 10% MeCN, 120  $\mu$ L) and left to react for one hour at room temperature. After this time the solution was purified by spin filtration (5 kDa MWCO) into PBS pH = 7.4 + 1mM EDTA. After purification the solution of reduced scFv was readjusted to 70  $\mu$ L and added dropwise to a solution of monobromomaleimide **93** (70 mM in MeCN, 100 equiv., 7.0  $\mu$ l) and left to react for 15 minutes. The solution was once again purified by spin filtration (5 KDa MWCO) into PBS pH = 7.4. Analysis by LCMS and SDS-PAGE confirmed conjugate **98**. Expected mass 26944, observed mass 26935. See main text for SDS-PAGE (section 2.2.2, page 70, Figure 27).

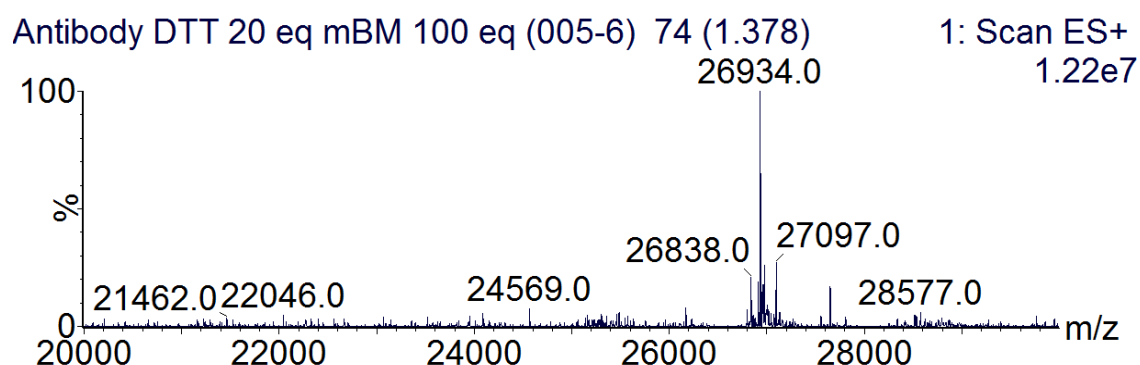
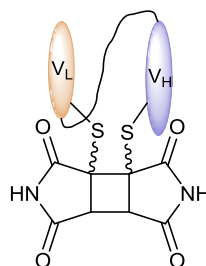


**Figure 68**  
Deconvoluted mass spectrum for scFv conjugate **98**.

##### Generation of bridged scFv **99**



Anti-CEA scFv conjugate **98** (70  $\mu$ M in PBS pH = 7.4, 100  $\mu$ l) was added to a cuvette and irradiated using the 365 nm single LED at a distance of 1 cm for 60 minutes. Analysis by

SDS-PAGE and LCMS confirmed successful photocycloaddition to produce anti-CEA scFv conjugate **99**. Expected mass 26935, observed mass 26935. See main text for SDS-PAGE (section 2.2.2, page 70, Figure 27). Densitometry gave a bridging yield of 71%.

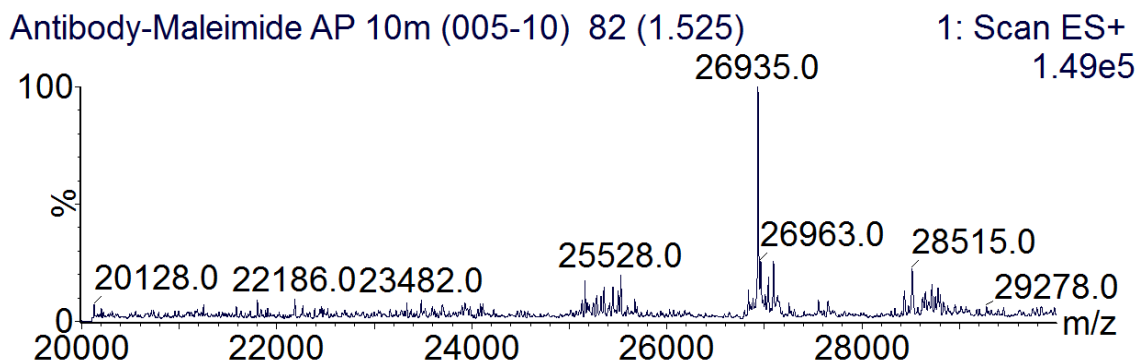
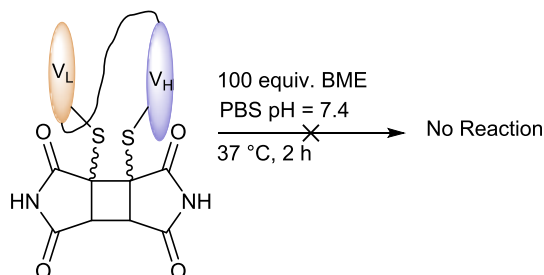


**Figure 69**  
Deconvoluted mass spectrum for scFv conjugate **99**.

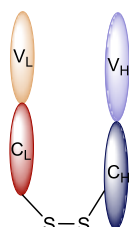
### 3.2.3.2: Thiol stability of a bridged anti-CEA scFv conjugate



A solution of  $\beta$ -mercaptoethanol (70 mM in PBS pH = 7.4, 100 equiv., 10  $\mu$ l) was added to bridged scFv conjugate **99** (70  $\mu$ M in PBS pH = 7.4 + 10% MeCN, 100  $\mu$ l) and left to react for 2 hours at 37 °C. SDS-PAGE and LCMS data matched the data for bridged scFv conjugate **99** indicating no reaction had taken place. Pure scFv conjugate **97** was subjected to the same conditions and complete reduction was seen by SDS-PAGE. See main text for SDS-PAGE (section 2.2.2, page 71, Figure 28).

## 3.2.4: Rituxan

### 3.2.4.1: Preparation of Rituxan Fab



DTT (10 mM in PBS, 0.5 ml) was added to a solution of papain (0.6 ml) in a Pierce fabrication filter and spun in a centrifuge at 5000 g for one minute. A further 0.5 ml DTT (10 mM in PBS) was added and the centrifugation repeated. The filter was once again filled with DTT (0 mM in PBS, 0.5 ml) and left to shake in the dark at 25 °C for one hour. The

resin was then washed with digest buffer (4 x 0.4 ml) and a solution of Rituxan **100** (7.00 mg·ml<sup>-1</sup>, 0.6 ml in PBS) added. The suspension was agitated at 1100 rpm in the dark at 37 °C for 20 hours. The resin was separated from the digest by centrifugation at room temperature, washed with PBS (3 x 0.5 ml) and both the digest and washes combined. The combined fractions were then buffer exchanged into PBS pH = 7.4 + 10mM EDTA and the total volume was adjusted to 2 ml. The sample was then applied to a NAb protein A column and incubated at room temperature under constant agitation for one hour. The Fab fraction was eluted according to manufacturer's protocol by washing the column with PBS (3 x 1 ml). Analysis of the solution by SDS-PAGE and LCMS confirmed successful production of Rituxan Fab **101**. Observed mass 47169.

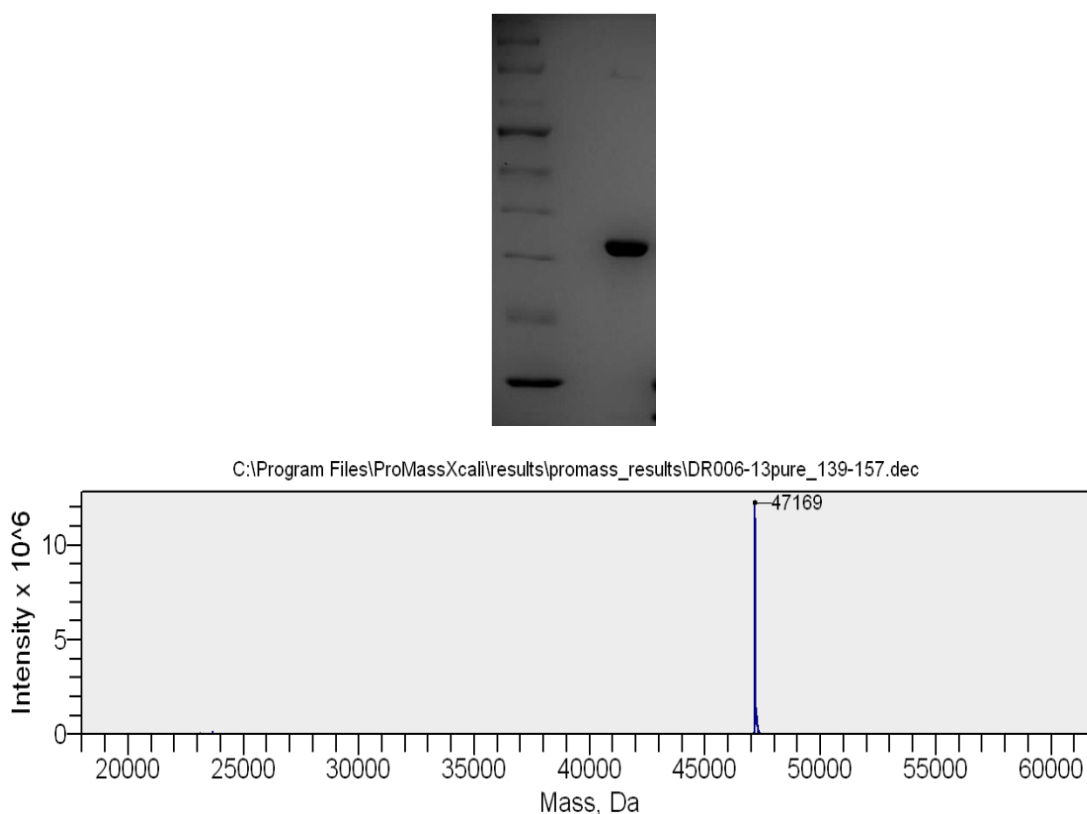


**Figure 70**  
**SDS-PAGE and deconvoluted mass spectrum for Rituxan Fab 101.**

### 3.2.4.2: Modification of Rituxan Fab

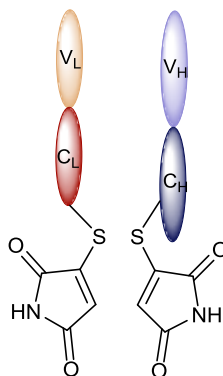
#### Preparation of *bis*-modified Rituxan Fab fragments

A general method for the modification of Rituxan Fab fragment **101** is shown below.

Rituxan Fab **101** (20 µM in PBS pH 7.4 + 10 mM EDTA, 200 µl) was reduced with TCEP (20 mM in PBS pH = 7.4, 10 equiv., 2 µl) at 37 °C for 90 minutes. The appropriate bromomaleimide (20 mM in MeCN, 100 equiv., 19 µl), was added and the reaction was left at room temperature for 30 minutes. The solution was purified by spin filtration (5 kDa MWCO) into PBS pH = 7.4 and the concentration adjusted to 20 µM ( $\epsilon_{280} = 68590$

$M^{-1}\cdot\text{cm}^{-1}$ ). Analysis by SDS-PAGE and LCMS confirmed Rituxan-Fab conjugate **102** or **119**<sub>a-d</sub>.

### Rituxan Fab conjugate **102**



Expected mass of light chain 23126, observed mass 23125. Expected mass of heavy chain 24237, observed mass 24236. See main text for SDS-PAGE (section 2.2.3.2, page 73, Figure 30)

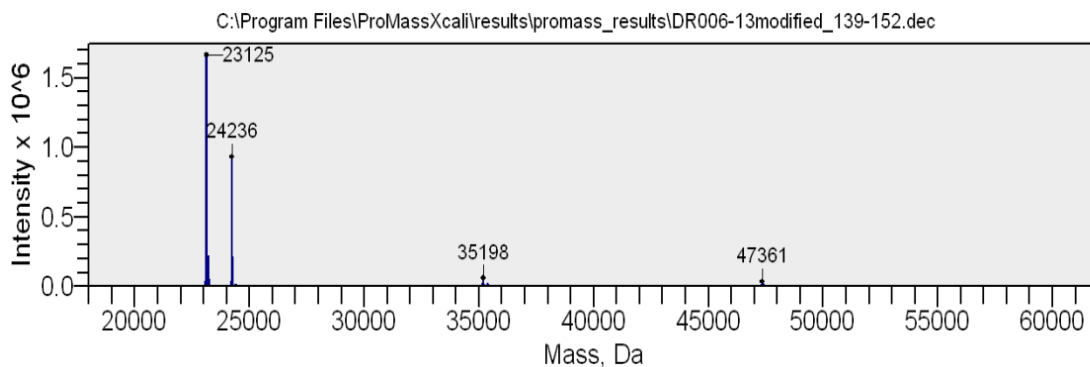
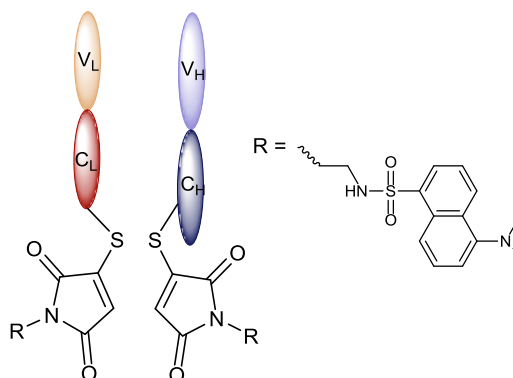


**Figure 71**  
Deconvoluted mass spectrum for Rituxan Fab conjugate **102**.

### Rituxan Fab conjugate **118**<sub>a</sub>



Expected mass of light chain 23402, observed mass 23401. Expected mass of heavy chain 24513, observed mass 24511. See main text for SDS-PAGE (section 2.2.3.5, page 78, Figure 32).

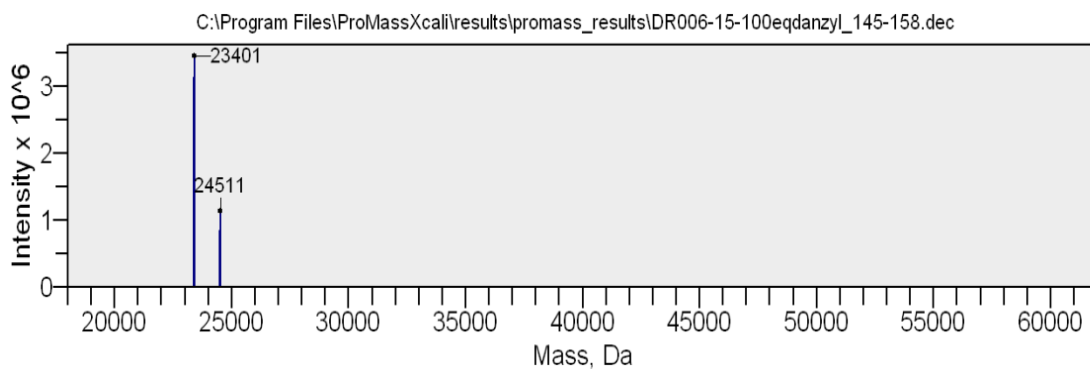
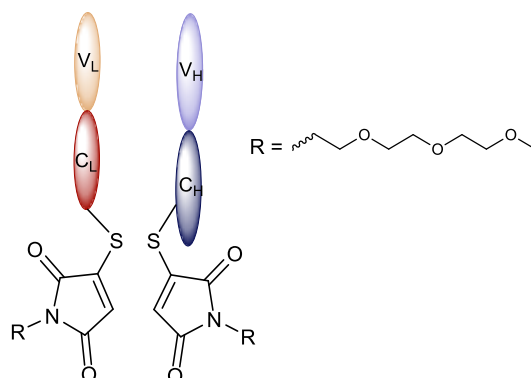


**Figure 72**  
Deconvoluted mass spectrum for Rituxan Fab Conjugate 118<sub>a</sub>.

**Rituxan Fab conjugate 118<sub>b</sub>**



Expected mass of light chain 23273, observed mass 23270. Expected mass of heavy chain 24384, observed mass 24380. See main text for SDS-PAGE (section 2.2.3.5, page 78, Figure 32).

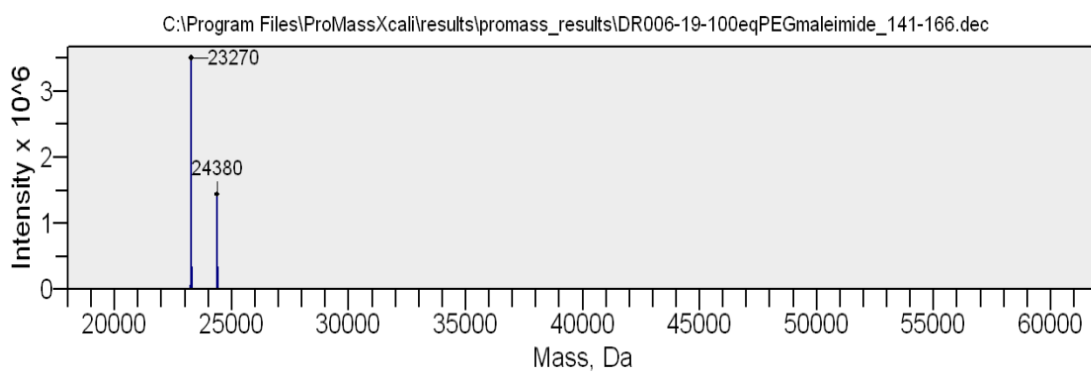
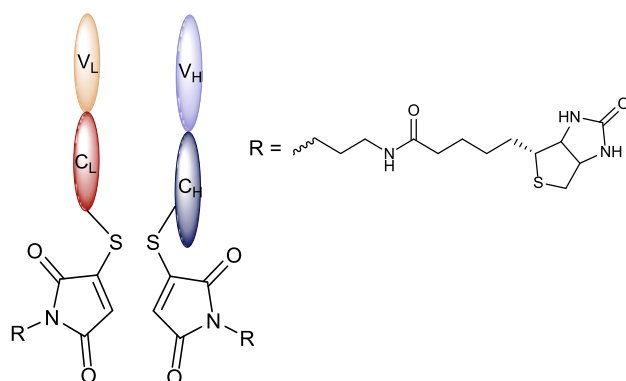


**Figure 73**  
Deconvoluted mass spectrum for Rituxan Fab Conjugate 118<sub>b</sub>.

### Rituxan Fab conjugate 118<sub>c</sub>



Expected mass of light chain 23410, observed mass 23408. Expected mass of heavy chain 24520, observed mass 24519. See main text for SDS-PAGE (section 2.2.3.5, page 78, Figure 32).

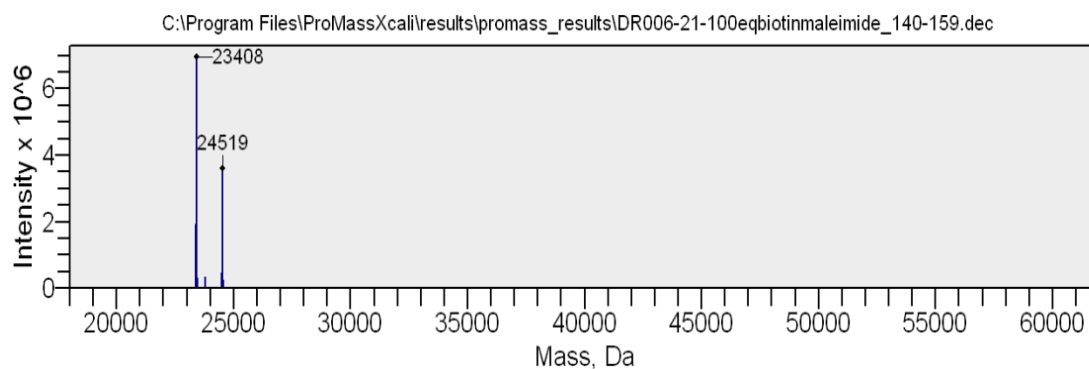
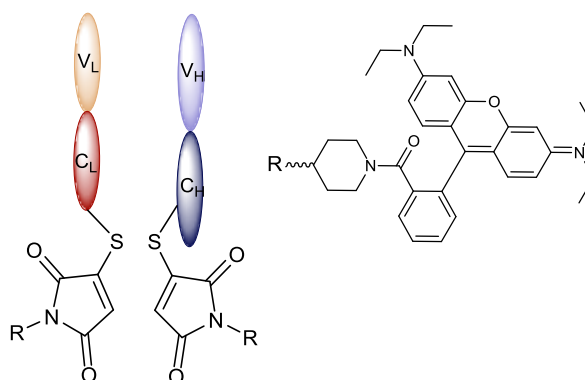


**Figure 74**  
Deconvoluted mass spectrum for Rituxan Fab Conjugate 118<sub>c</sub>.

### Rituxan Fab conjugate 118<sub>d</sub>



Expected mass of light chain 23635, observed mass 23635. Expected mass of heavy chain 24746, observed mass 24745. See main text for SDS-PAGE (section 2.2.3.5, page 78, Figure 32).

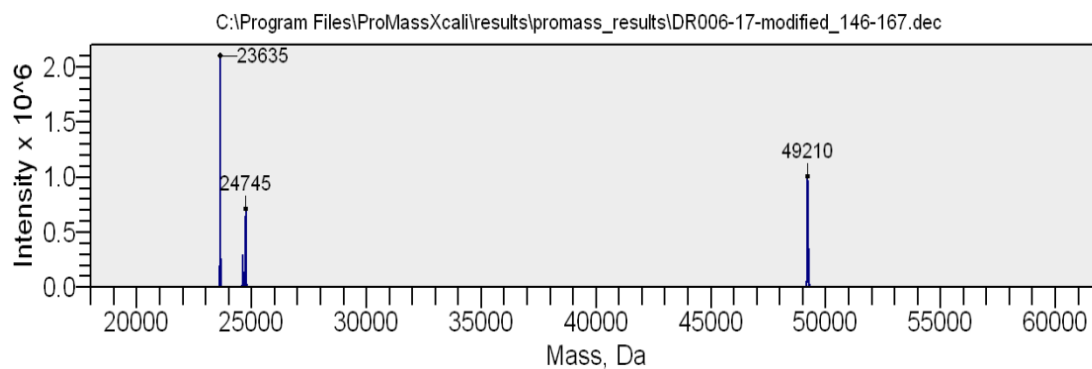


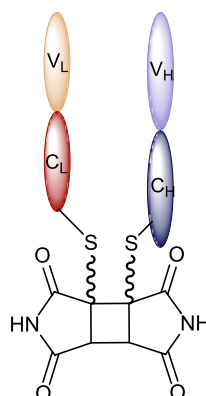
**Figure 75**  
Deconvoluted mass spectrum for Rituxan Fab Conjugate **118<sub>d</sub>**.

### Irradiation of Rituxan Fab conjugates

A general method for the generation of bridged Rituxan Fab Fragments **103** and **119<sub>b,c</sub>** is shown below.

*Bis*-modified Rituxan Fab conjugate **102** or **118<sub>b,c</sub>** (20  $\mu$ M in PBS pH = 7.4, 50  $\mu$ l) was added to a cuvette and irradiated using the 365 nm single LED at a distance of 1 cm for 30 minutes. For *bis*-modified Rituxan Fab conjugates **102**, **118<sub>b</sub>** and **118<sub>c</sub>** analysis by SDS-PAGE and LCMS confirmed successful photocycloaddition to produce bridged Rituxan Fab conjugates **103** or **119<sub>b,c</sub>**. Decarboxylated Rituxan Fab was also observed (expected mass 22953). For *bis*-modified Rituxan Fab conjugate **118<sub>a</sub>** only the decarboxylative side product was observed. For *bis*-modified Rituxan Fab conjugate **118<sub>d</sub>** no reaction was observed by LCMS.

### Bridged Rituxan Fab conjugate **103**



Expected mass 47363, observed mass 47362. See main text for SDS-PAGE (section 2.2.3.5, page 78, Figure 32). Densitometry gives a bridging yield of 85%.

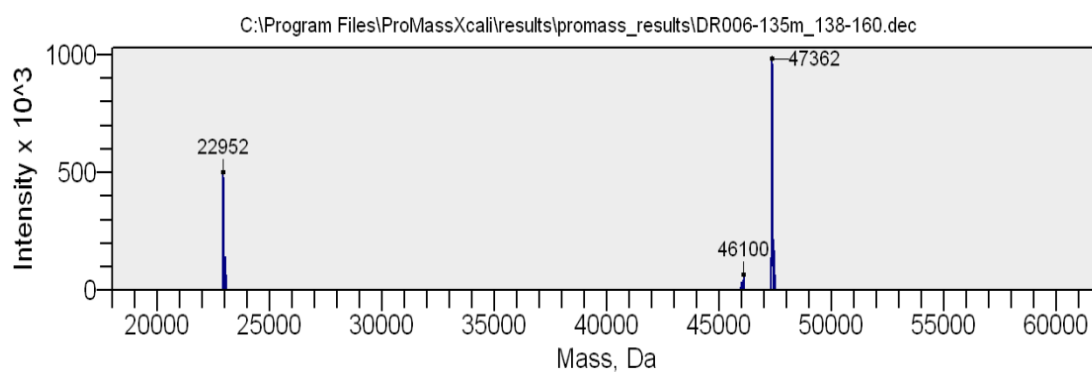
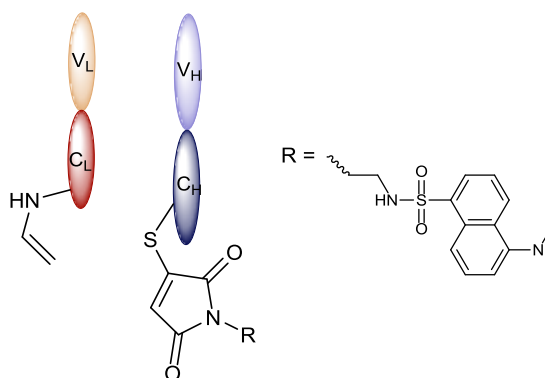


**Figure 76**  
Deconvoluted mass spectrum for Rituxan Fab Conjugate 103.

**Irradiation of Rituxan Fab conjugate 118<sub>a</sub>.**



Expected mass of light chain 22953, observed mass 22954. Expected mass of heavy chain 24513, observed mass 24513. The peak at 23400 indicates unreacted starting *bis*-modified Rituxan Fab conjugate **118<sub>a</sub>** (starting material). See main text for SDS-PAGE (section 2.2.3.5, page 78, Figure 32).

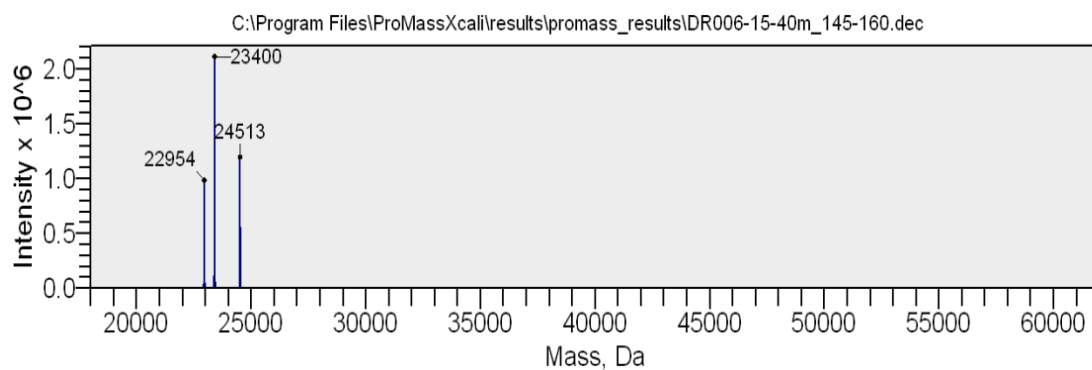
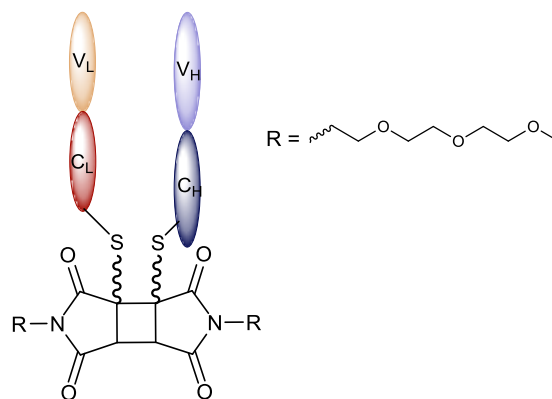


**Figure 77**  
Deconvoluted mass spectrum after the irradiation of Rituxan Fab 118<sub>a</sub>.

### Bridged Rituxan Fab conjugate 119<sub>b</sub>



Expected mass 47657, observed mass 47648. See main text for SDS-PAGE (section 2.2.3.5, page 78, Figure 32). Densitometry gives a bridging yield of 80%.

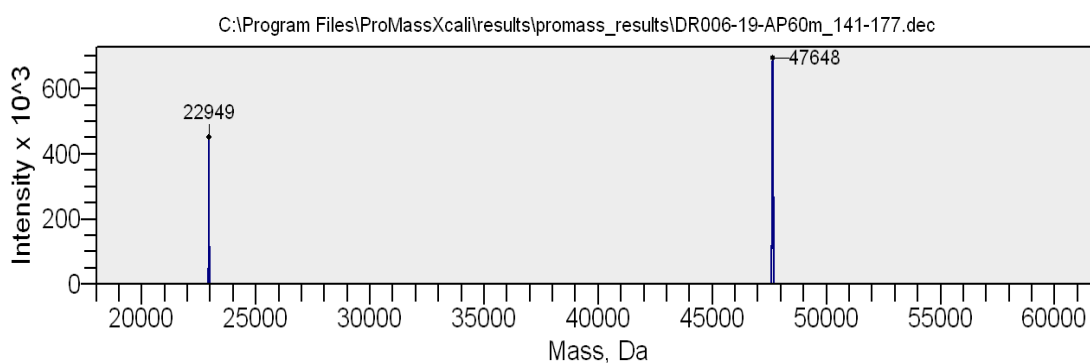
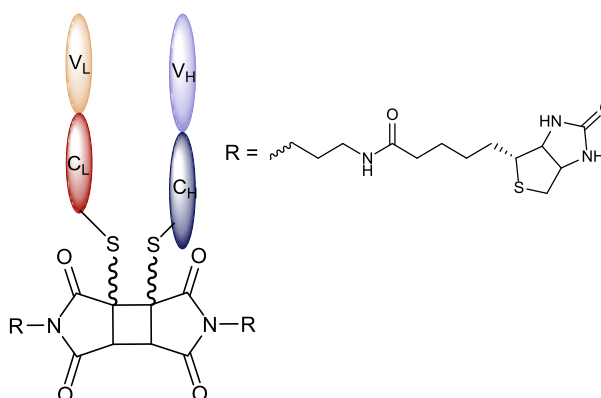


**Figure 78**  
Deconvoluted mass spectrum for Rituxan Fab Conjugate 119<sub>b</sub>.

### Bridged Rituxan Fab conjugate 119<sub>c</sub>



Expected mass 47930, observed mass 47931. See main text for SDS-PAGE (section 2.2.3.5, page 78, Figure 32). Densitometry gives a bridging yield of 80%.

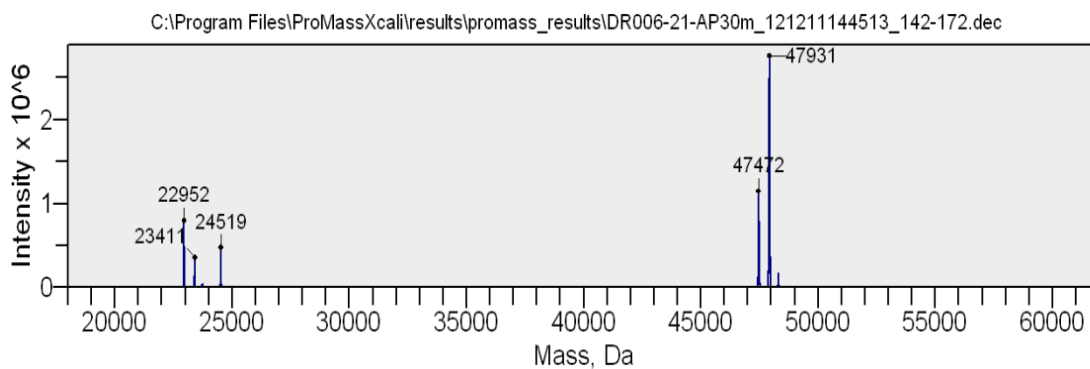
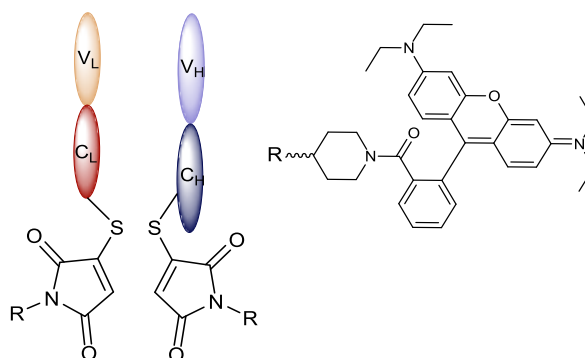


**Figure 79**  
Deconvoluted mass spectrum for Rituxan Fab Conjugate 119c.

**Irradiation of Rituxan Fab conjugate 118<sub>d</sub>.**



Expected mass of light chain 22953, observed mass 22954. Expected mass of heavy chain 24513, observed mass 24513. The peak at 23400 indicates unreacted starting *bis*-modified Rituxan Fab conjugate 118<sub>d</sub>. No reaction was observed by LCMS. See main text for SDS-PAGE (section 2.2.3.5, page 78, Figure 32).

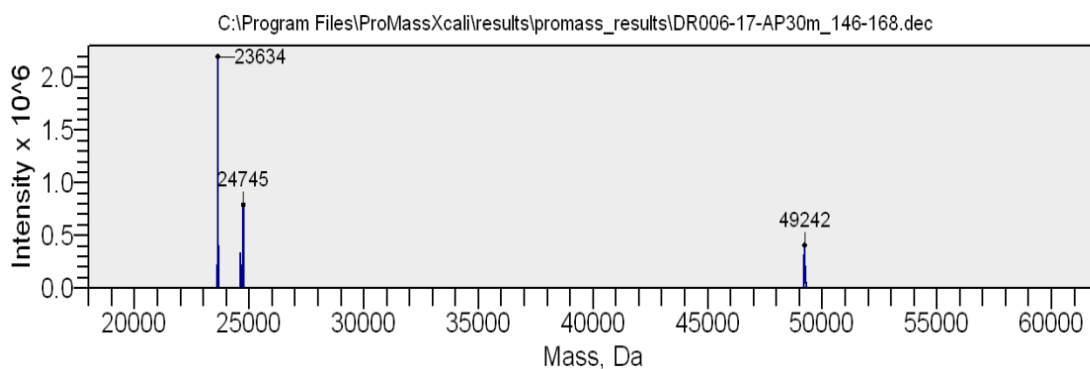
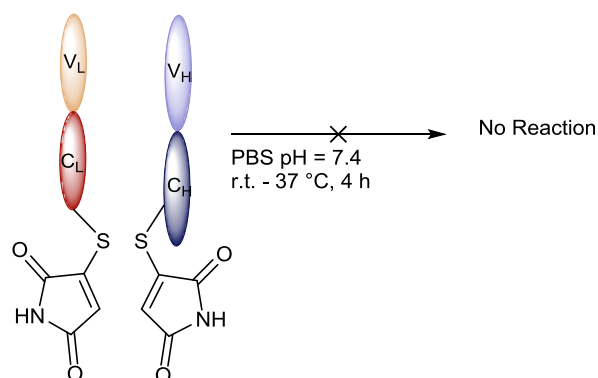


**Figure 80**  
Deconvoluted mass spectrum for after the irradiation of Rituxan Fab 118<sub>d</sub>.

## Non-irradiated control reaction with Rituxan Fab conjugate **102**



*Bis*-modified Rituxan Fab conjugate **102** (20  $\mu$ M, 50  $\mu$ l in PBS pH = 7.4) was added to a cuvette and left for one hour at 37 °C. Analysis by SDS-PAGE (Figure 81) showed no change and LCMS data matched that of the starting material **102**.

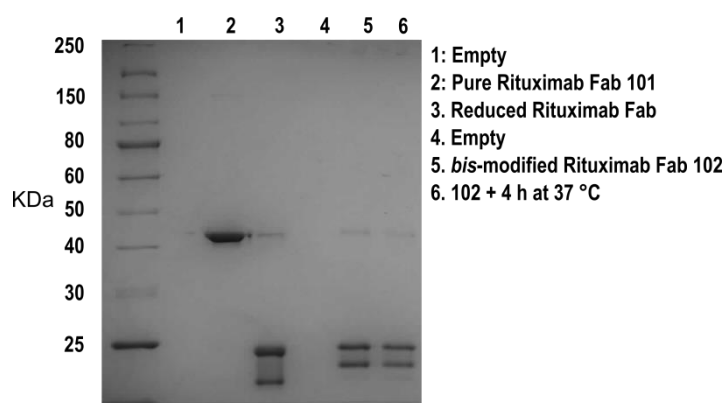
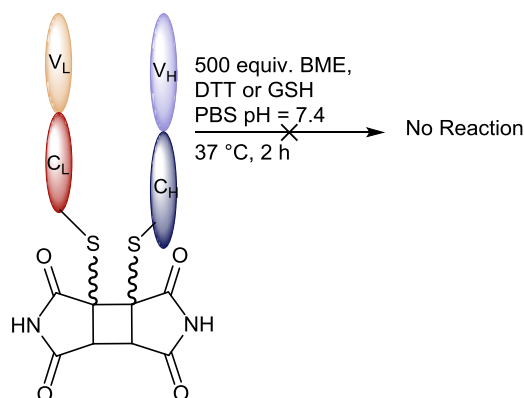


**Figure 81**  
SDS-PAGE showing no reaction of Rituxan Fab conjugate **102** upon incubation at 37 °C. Identical results were obtained at room temperature.

### 3.2.4.3: Thiol stability of bridged Rituxan Fab conjugates

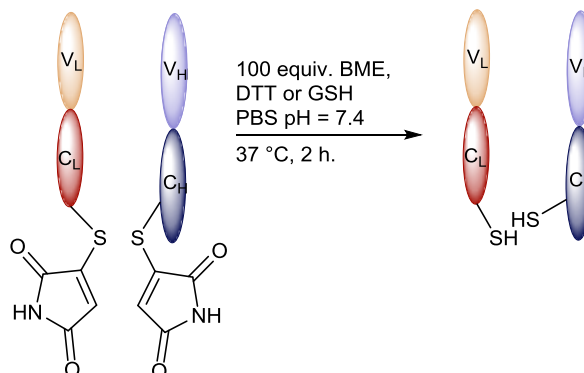
#### Thiol stability of bridged Rituxan Fab **103**



Rituxan Fab conjugate **103** was separated into 3 x 30  $\mu$ l aliquots (22  $\mu$ M in PBS pH = 7.4) and each aliquot reacted with a specific thiol (dithiothreitol, glutathione,  $\beta$ -mercaptoethanol 220 mM in PBS pH = 7.4, 500 equiv., total thiol concentration 11 mM, 1.5  $\mu$ l). The solutions

were incubated at 37 °C for four hours. Analysis by SDS-PAGE demonstrated the stability of the bridge. See main text for SDS-PAGE. LCMS also showed no change.

### Thiol stability of *bis*-modified Rituxan Fab **102**



Rituxan Fab conjugate **102** was separated into 3 x 30  $\mu$ l aliquots (22  $\mu$ M, PBS pH = 7.4) and each aliquot reacted with a specific thiol (dithiothreitol, glutathione,  $\beta$ -mercaptoethanol 22 mM in PBS pH = 7.4, 100 equiv., 3  $\mu$ l). The solutions were incubated at 37 °C for 2 hours. Analysis by LCMS revealed complete cleavage of the maleimides from the antibody fragment to yield reduced Rituxan Fab **105**. Expected mass of light chain 23029, observed mass 23029. Expected mass of heavy chain 24139, observed mass 24140.

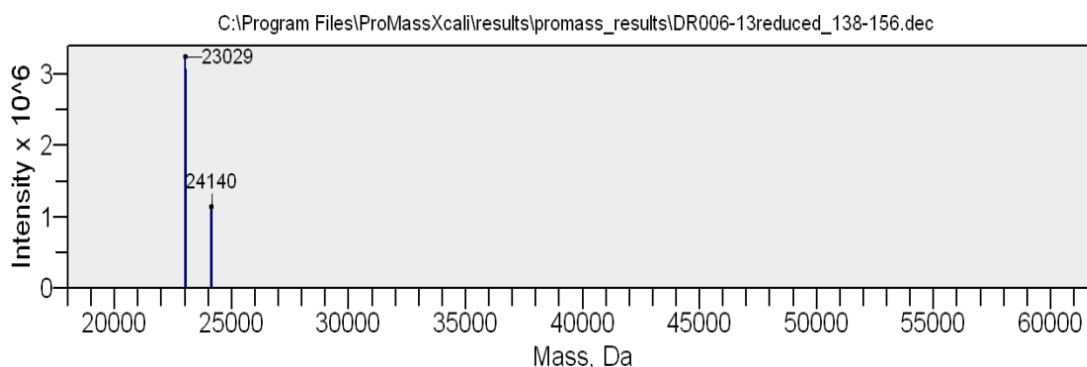
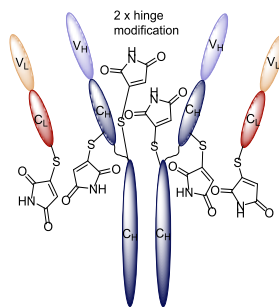


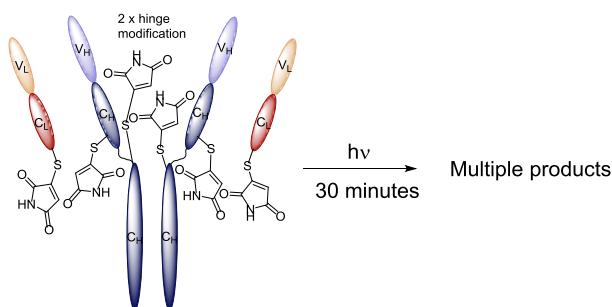
**Figure 82**  
Deconvoluted mass spectrum for reduced Rituxan Fab **105**.

### 3.2.4.4: Modification of Rituxan



Rituxan (20  $\mu$ M in BBS pH = 8 + 10mM EDTA, 60  $\mu$ l) was reduced with TCEP (20 mM in BBS pH = 8, 10 equiv., 0.6  $\mu$ l) for 2 hours at 37  $^{\circ}$ C. After this time monobromomaleimide **93** (80 mM in MeCN, 800 equiv., 12  $\mu$ l) was added and left to react at room temperature for 30 minutes. Purification was performed by buffer swapping into PBS pH = 7.4 using 10 KDa MWCO filters. Analysis by SDS-PAGE provided evidence for the formation of Rituxan conjugate **120**. See main text for SDS-PAGE (section 2.2.4, page 80, Figure 34).

### Irradiation of modified Rituxan



Rituxan conjugate **120** (60  $\mu$ M in PBS pH = 7.4, 40  $\mu$ l) was added to a cuvette and irradiated using a single 365 nm 5W LED at a distance of 1 cm at room temperature for 30 minutes. SDS-PAGE analysis revealed a complex mixture (section 2.2.4, page 80, Figure 34).

## 3.2.5: Herceptin

### 3.2.5.1: Preparation of Herceptin Fab

Immobilized pepsin (0.15 ml) was washed with acetate buffer (4 x 0.3 ml, 20 mM sodium acetate trihydrate, pH 3.1). Herceptin **125** (6.55 mg·ml<sup>-1</sup> in digest buffer, 0.5 ml) was added and the mixture incubated for five hours under constant agitation (1100 rpm) at 37  $^{\circ}$ C. The digest solution was separated from the resin beads, which were washed with digest buffer (3 x 0.4 ml). The washes were combined with the digest solution and the volume adjusted to 0.5 ml using spin filtration. Immobilised papain (0.5 ml, 0.25 mg·ml<sup>-1</sup>) was incubated in buffer (10 mM DTT in digest buffer) at 37  $^{\circ}$ C with constant agitation (1100 rpm) for one hour. The papain resin was subsequently filtered and washed with digest buffer (4 x 0.4 ml) and the pepsin digest solution prepared earlier was added. The mixture was incubated at 37  $^{\circ}$ C with constant agitation (1100 rpm) for 16 hours. The resin was separated from the

digest *via* spin filtration and washed with BBS (3 x 0.4 ml, 25 mM sodium borate, 25 mM NaCl, 0.5 mM EDTA). The digest and the washes were combined and buffer swapped for BBS using spin filtration columns (10000 MWCO), and the volume was adjusted to 0.5 ml. Yield of Her-Fab **8** was determined by UV/Vis spectroscopy ( $\epsilon_{280} = 68590 \text{ M}^{-1}\cdot\text{cm}^{-1}$ ,  $2.55 \text{ mg}\cdot\text{ml}^{-1}$ , 61%). Her-Fab **127** was confirmed using SDS-PAGE and LCMS. Observed mass 47645.

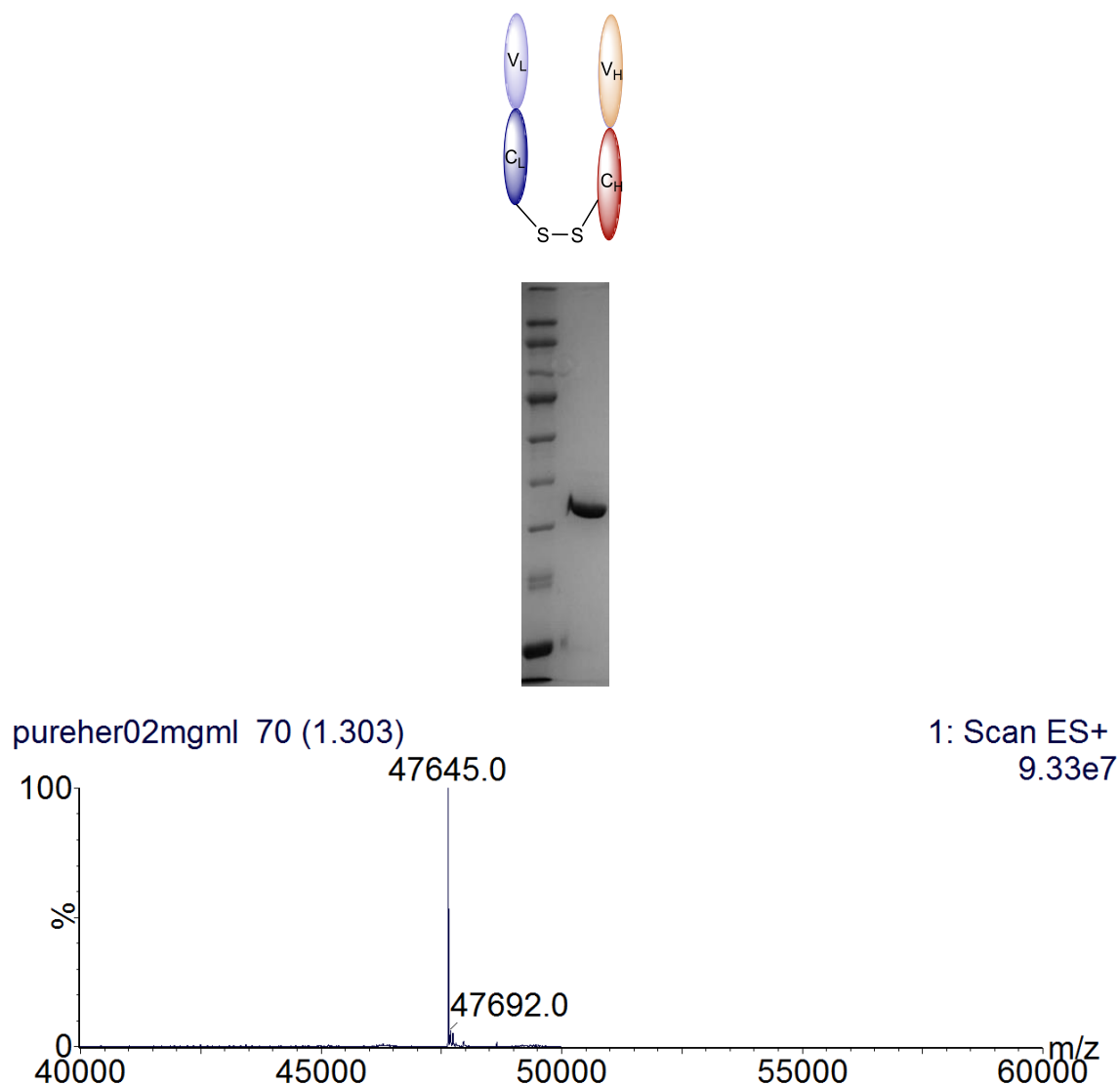


**Figure 83**  
SDS-PAGE and deconvoluted mass spectrum for Herceptin Fab **127**.

### 3.2.5.2: Modification of Herceptin Fab

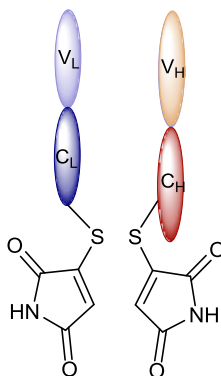
#### **Bis-modification of Herceptin Fab 125**

A general method for the modification of Herceptin Fab fragment **125** is shown below.

Herceptin Fab **125** ( $22 \mu\text{M}$  in BBS,  $200 \mu\text{l}$ ) was reduced with TCEP ( $22 \text{ mM}$  in BBS, 5 equiv.,  $1 \mu\text{l}$ ) at  $37 \text{ }^\circ\text{C}$  for 90 minutes. The appropriate bromomaleimide (**93**, **114**, **117**) ( $22 \text{ mM}$  in DMF, 100 equiv.,  $19 \mu\text{l}$ ) was added and the reaction was left at room temperature for

30 minutes. The solution was subsequently purified by desalting column (G-25, GE Healthcare) and buffer swapped into PBS pH = 6 using spin filtration (5 KDa MWCO).

#### Herceptin Fab conjugate 128<sub>a</sub>



Expected mass of light chain 23545, observed mass 23544. Expected mass of heavy chain 24307, observed mass 24305. For SDS-PAGE see main text (section 2.2.5.2, page 83, Figure 36).

DR014-41-maleimide 82 (1.530)

1: Scan ES+  
9.60e6

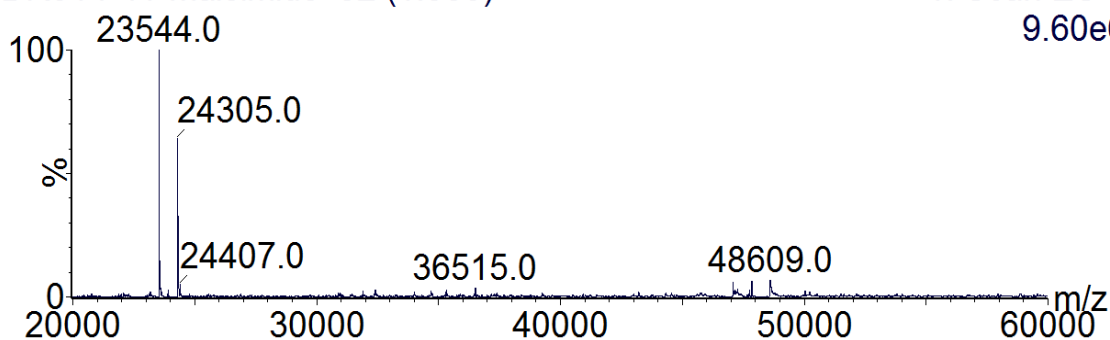
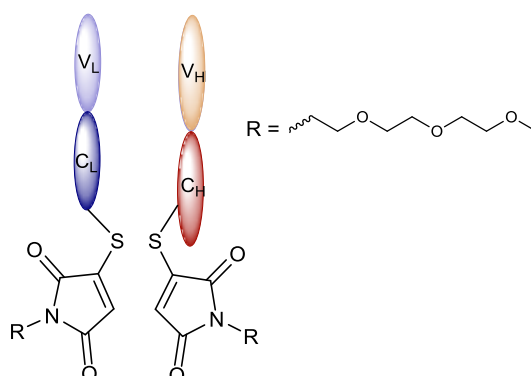


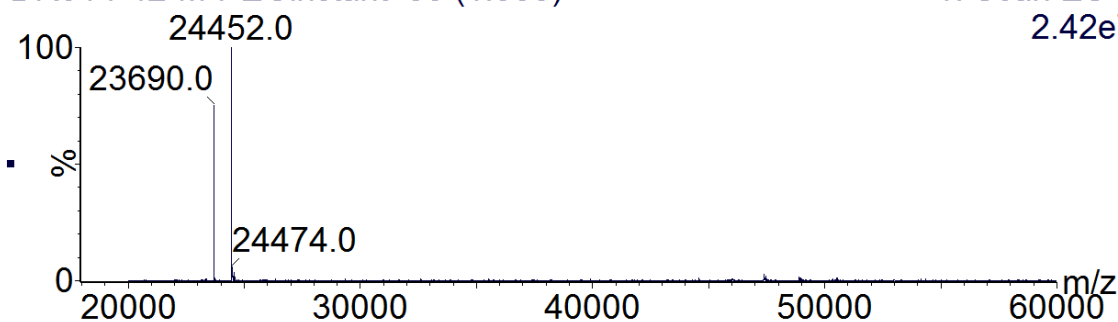
**Figure 84**  
Deconvoluted mass spectrum for Herceptin Fab Conjugate 128<sub>a</sub>.

#### Herceptin Fab conjugate 128<sub>b</sub>



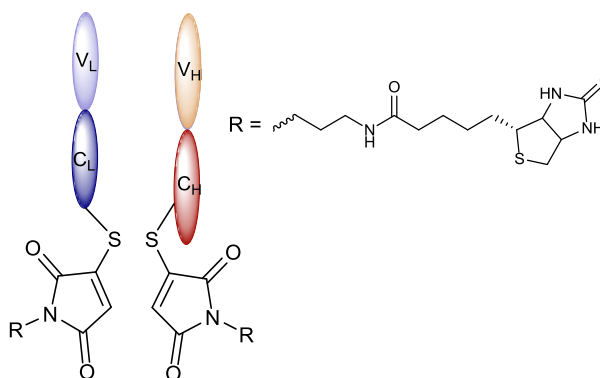
Expected mass of light chain 23692, observed mass 23690. Expected mass of heavy chain 24454, observed mass 24452. For SDS-PAGE see main text (section 2.2.5.2, page 83, Figure 36).

DR014-42-M-PEGinstant 85 (1.585)

1: Scan ES+  
2.42e7

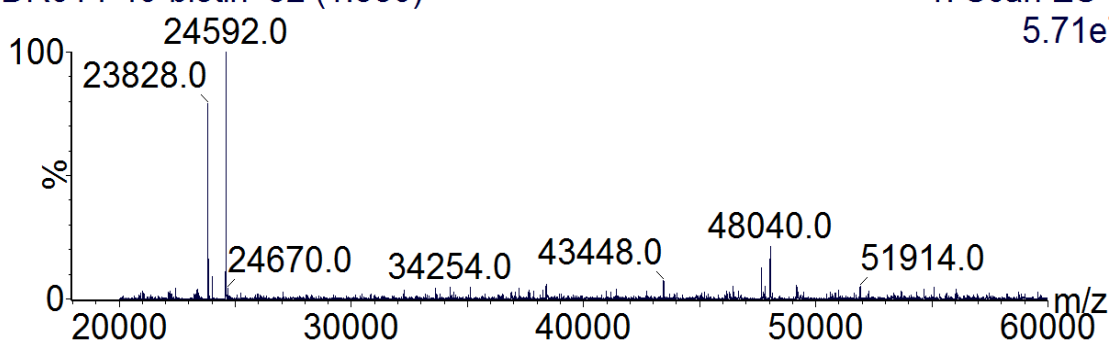
**Figure 85**  
Deconvoluted mass spectrum for Herceptin Fab Conjugate 128<sub>b</sub>.

### Herceptin Fab conjugate 128<sub>c</sub>



Expected mass of light chain 23829, observed mass 23828. Expected mass of heavy chain 24591, observed mass 24592. For SDS-PAGE see main text (section 2.2.5.2, page 83, Figure 36).

DR014-40-biotin 82 (1.530)

1: Scan ES+  
5.71e7

**Figure 86**  
Deconvoluted mass spectrum for Herceptin Fab Conjugate 128<sub>c</sub>.

### Irradiation of Herceptin Fab conjugates

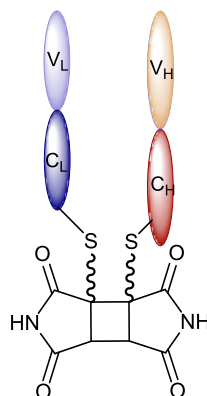
A general method for the generation of bridged Herceptin Fab Fragments **129<sub>a-c</sub>** is shown below.

*Bis*-modified Herceptin Fab conjugate **128<sub>a-c</sub>** (22  $\mu$ M in PBS pH = 6, 120  $\mu$ l) was added to a cuvette and irradiated using the UVG-2 365 nm torch for two minutes. Analysis by SDS-

PAGE and LCMS confirmed successful photocycloaddition to produce bridged Herceptin conjugates **129<sub>a-c</sub>**. In each case decarboxylative side product Herceptin Fab conjugate **130** was also observed (expected mass 23372).

For Herceptin Fab conjugate **128<sub>a</sub>** the same procedure was performed at pH = 8. See main text for details.

#### Bridged Herceptin Fab conjugate **129<sub>a</sub>**



Expected mass 47851, observed mass 47852. For SDS-PAGE see main text (section 2.2.5.2, page 83, Figure 36). Densitometry gave a bridging yield of 85%.

DR014-41-maleimideAP 79 (1.472)

1: Scan ES+  
1.25e7

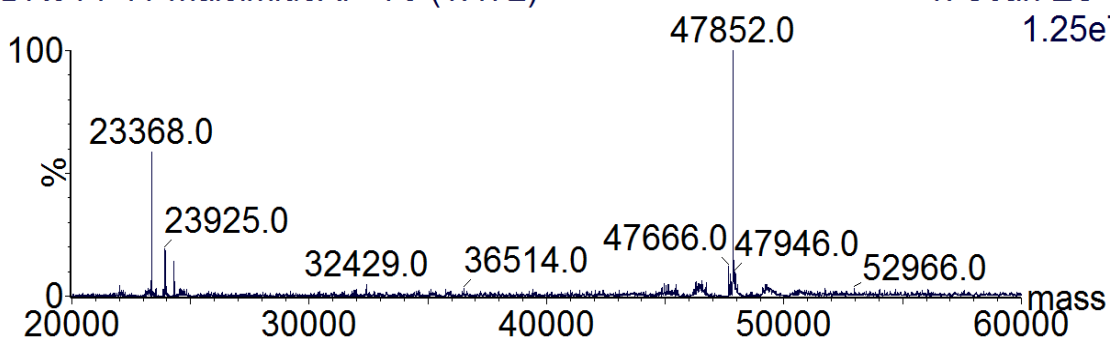
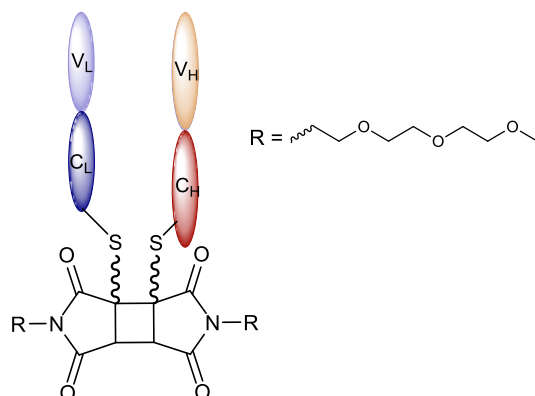


**Figure 87**  
Deconvoluted mass spectrum for Herceptin Fab Conjugate **129<sub>a</sub>**.

### Bridged Herceptin Fab conjugate 129<sub>b</sub>



Expected mass 48146, observed mass 48155. For SDS-PAGE see main text (section 2.2.5.2, page 83, Figure 36). Densitometry gave a bridging yield of 80%.

### DR014-41-pegAP 79 (1.470)

1: Scan ES+  
1.40e7

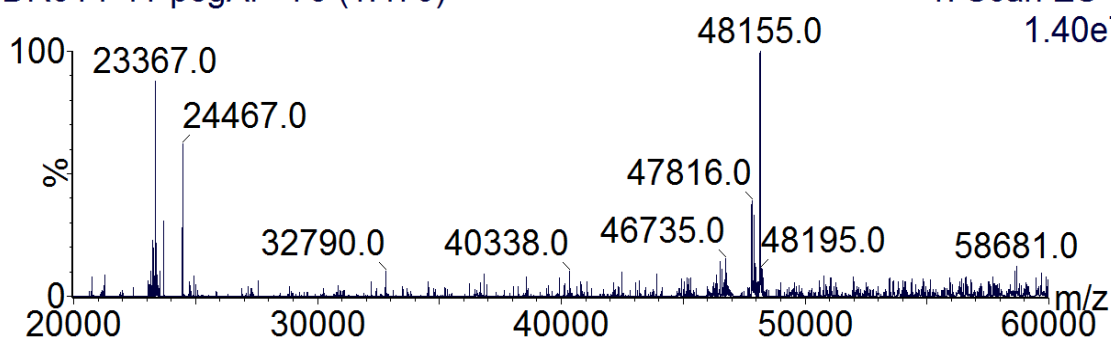
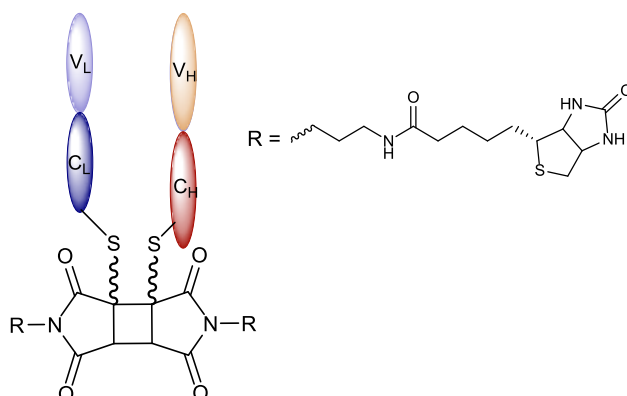


**Figure 88**  
Deconvoluted mass spectrum for Herceptin Fab Conjugate 129<sub>b</sub>.

### Bridged Herceptin Fab conjugate 129<sub>c</sub>



Expected mass 48428, observed mass 48441. For SDS-PAGE see main text (section 2.2.5.2, page 83, Figure 36). Densitometry gave a bridging yield of 80%.

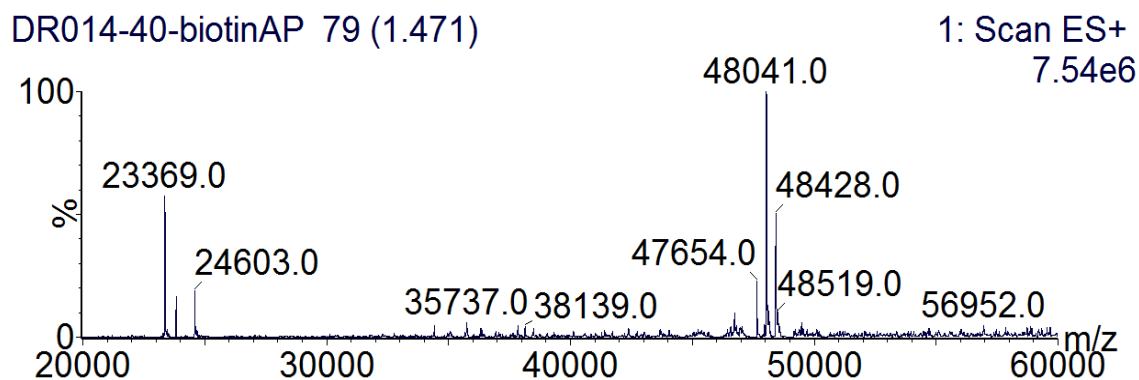


**Figure 89**  
Deconvoluted mass spectrum for Herceptin Fab Conjugate 129c.

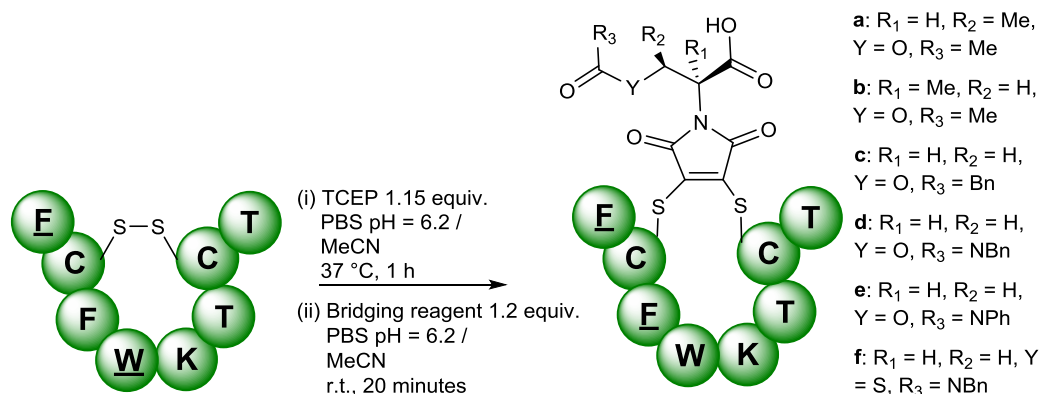
### 3.2.5.3: ELISA data for Herceptin conjugates

A 96-well plate was coated overnight at 4 °C with HER2 (0.25 µg·ml<sup>-1</sup> in PBS, 100 µl). As a negative control one row was coated with only PBS. The solutions were removed and each well washed (2 x PBS). The wells were subsequently coated with a 1% BSA solution in PBS for 1 hour at room temperature. After this the wells were emptied and washed (3 x PBS). Solutions of Herceptin Fab **125**, Herceptin Fab conjugate **129<sub>a</sub>** and Herceptin Fab conjugate **129<sub>a</sub>** in PBS pH = 7.4 were prepared in the following dilutions: 22 nM, 7.33 nM, 2.44 nM, 0.814 nM, 0.272 nM and 0.0905 nM. The dilutions were placed into the wells, each dilution repeated 3 times, and incubated for two hours at room temperature. As negative controls PBS only and Herceptin Fab **125** at 22 nM in the absence of HER2 were also subjected to the same protocol. The solutions were removed and the wells washed (2 x 0.1% Tween 20 in PBS, 3 x PBS). Detection antibody (100 µl of anti-human IgG, Fab-specific-HRP solution, 4 µl of a 1:5000 solution diluted further in 20 ml of PBS) was added and left for 1 hour at room temperature. The solutions were removed and the wells washed (2 x 0.1% Tween 20 in PBS, 3 x PBS). Finally, an OPD solution (0.5 mg·ml<sup>-1</sup> OPD in phosphate-citrate buffer with sodium perborate, 100 µl) was added to each well. After 2 minutes the reaction was stopped through addition of 4 M HCl (50 µl). Absorbance was measured at 490 nm and corrected by subtracting the average of negative controls. See main text for data. Protocol was taken from a literature procedure.<sup>144</sup> Data was analysed using GraphPad PRISM software. Absorbance values were normalised to the highest value, and lines were fit using non-linear regression (log[inhibitor] vs. response - variable slope, four parameters). IC<sub>50</sub> values were reported as obtained.

### 3.2.7: Dithiomaleimide photocleavable linkers

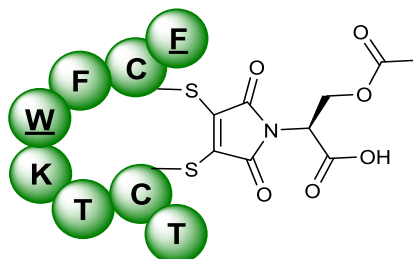
#### 3.2.7.1: Modification of Octreotide

A general experimental for the modification of Octreotide **74**.



*Tris*(2-carboxyethyl)phosphine (TCEP) (30 mM in 50:50 PBS pH = 6.2:MeCN, 1.15 equiv., 1.15  $\mu$ l) was added to a solution of Octreotide **74** (300  $\mu$ M in 50:50 PBS pH = 6.2:MeCN, 100  $\mu$ l) and left to react at 37 °C for 90 minutes. The appropriate bridging reagent (**172**, **194**, **197**, **199**, **200**, **201**, **205**) (30 mM, 1.2 equiv., 1.2  $\mu$ l in MeCN) was added and the mixture left at room temperature for 20 minutes. Analysis by LCMS showed complete bridging to Octreotide conjugates **184**, **206**<sub>a-f</sub>. See main text for LC traces (section 2.4.4.1 & 2.4.5.2).

#### Octreotide Conjugate **184**



Expected mass 1243, observed mass 1243 (ES<sup>-</sup> mode).

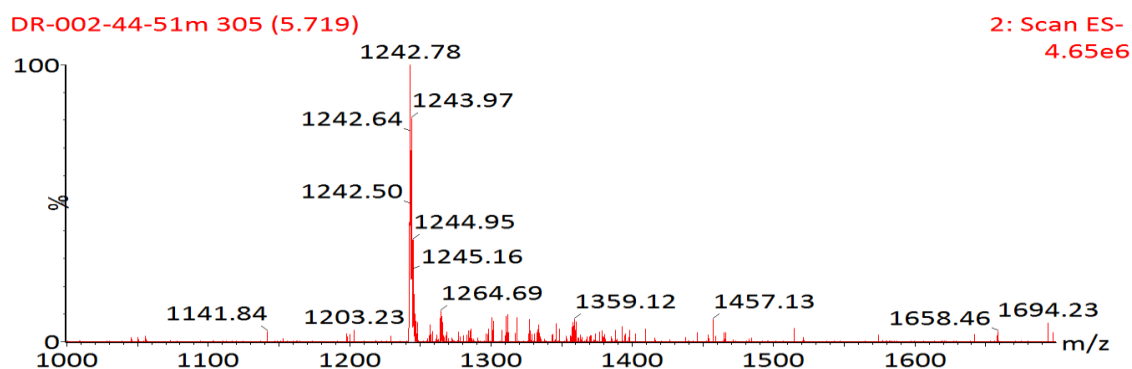
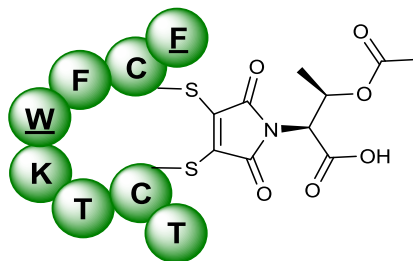
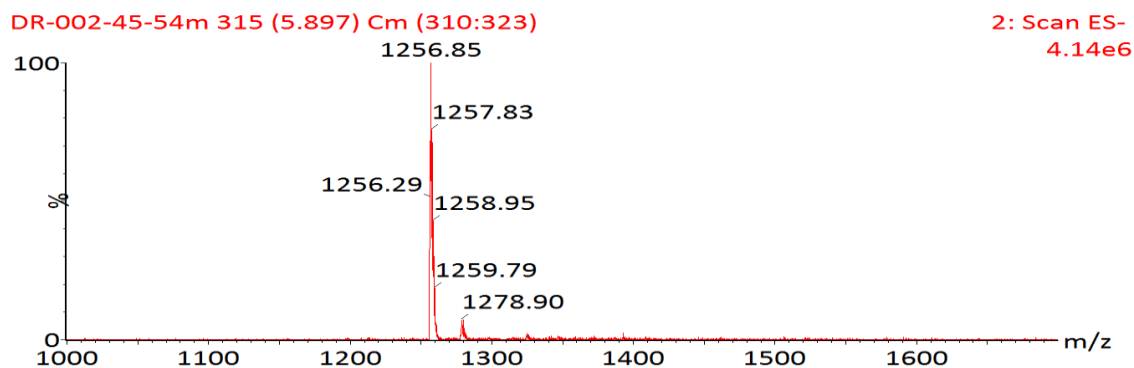


Figure 90  
ES negative mode spectrum of Octreotide conjugate **184**.

### Octreotide Conjugate 206<sub>a</sub>

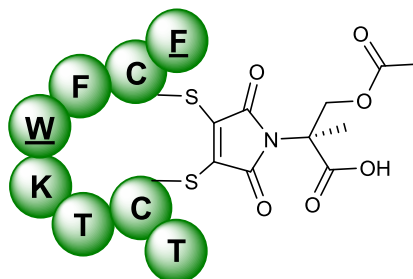


Expected mass 1257, observed mass 1257 (ES<sup>-</sup> mode).



**Figure 91**  
ES negative mode spectrum of Octreotide conjugate 206<sub>a</sub>.

### Octreotide Conjugate 206<sub>b</sub>



Expected mass 1257, observed mass 1257 (ES<sup>-</sup> mode).

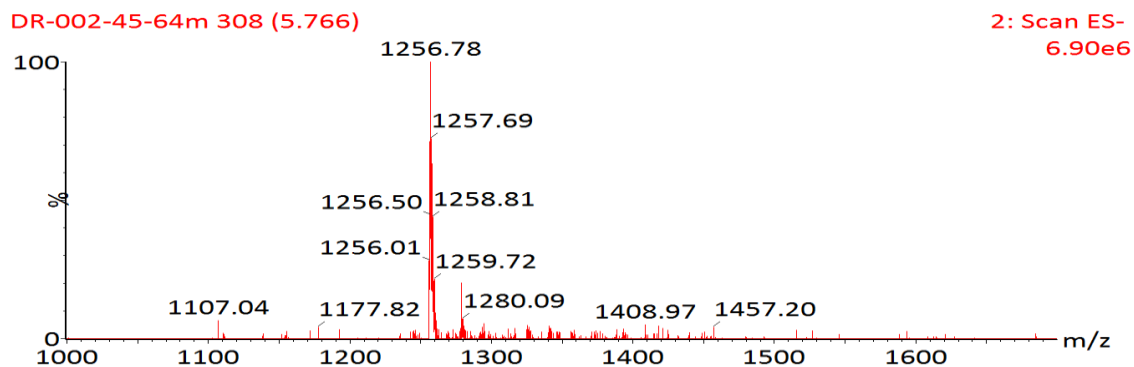
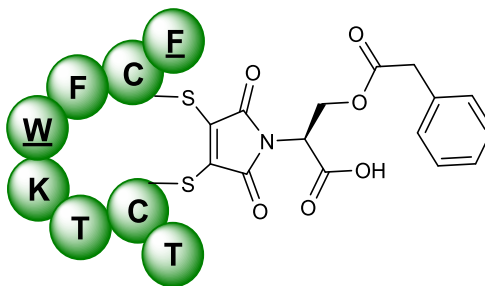


**Figure 92**  
ES negative mode spectrum of Octreotide conjugate 206<sub>b</sub>.

### Octreotide Conjugate 206<sub>c</sub>



Expected mass 1319, observed mass 1319 (ES<sup>-</sup> mode).

DR-002-46-65M 366 (6.859) Cm (358:366)

2: Scan ES-  
2.58e6

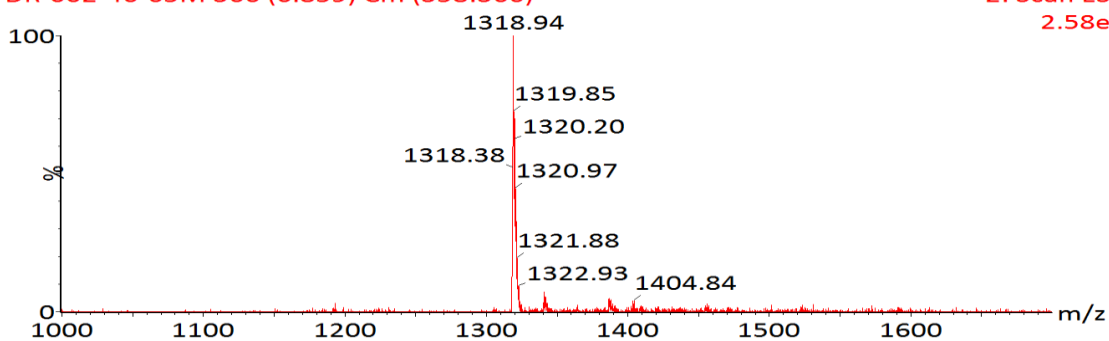
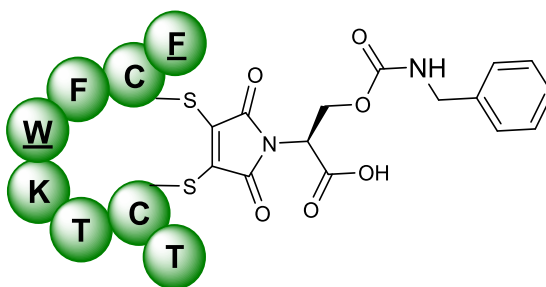


**Figure 93**  
ES negative mode spectrum of Octreotide conjugate 206<sub>c</sub>.

### Octreotide Conjugate 206<sub>d</sub>



Expected mass 1334, observed mass 1334 (ES<sup>-</sup> mode).

DR-002-45-56m 346 (6.484) Cm (344:352)

2: Scan ES-  
4.81e6

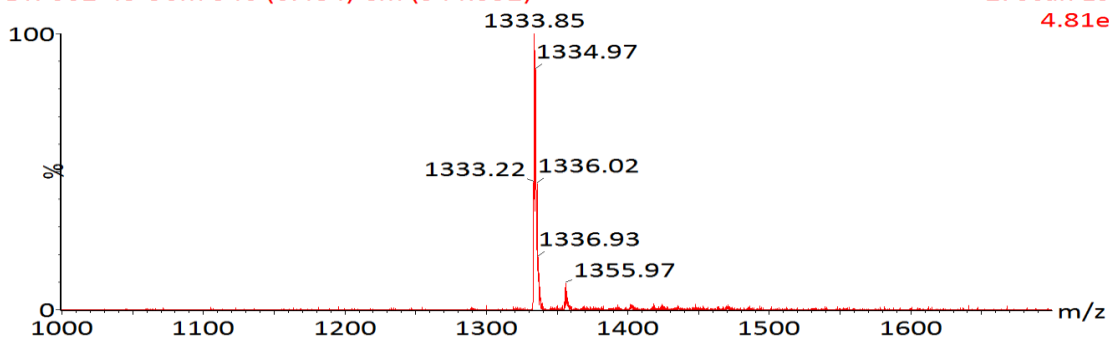
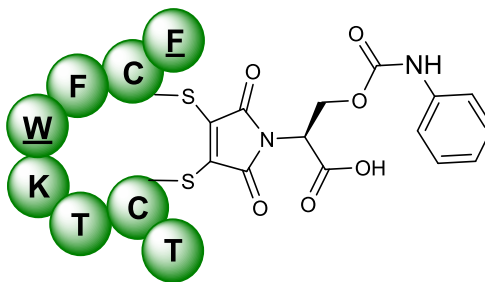


**Figure 94**  
ES negative mode spectrum of Octreotide conjugate 206<sub>d</sub>.

### Octreotide Conjugate 206<sub>e</sub>



Expected mass 1320, observed mass 1320 (ES<sup>-</sup> mode).

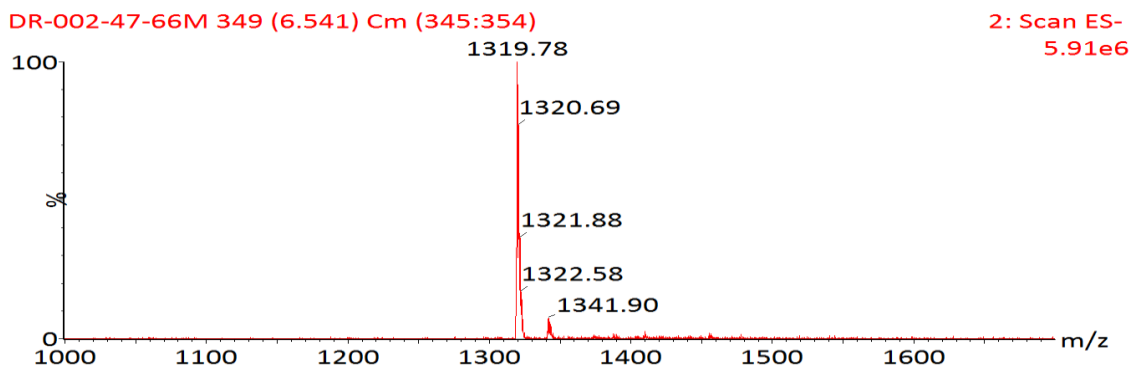
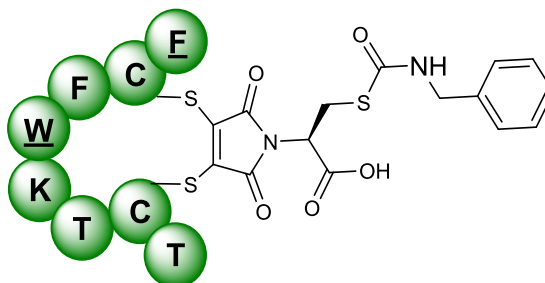


**Figure 95**  
ES negative mode spectrum of Octreotide conjugate 206<sub>e</sub>.

### Octreotide Conjugate 206<sub>f</sub>



Expected mass 1350, observed mass 1350 (ES<sup>-</sup> mode).

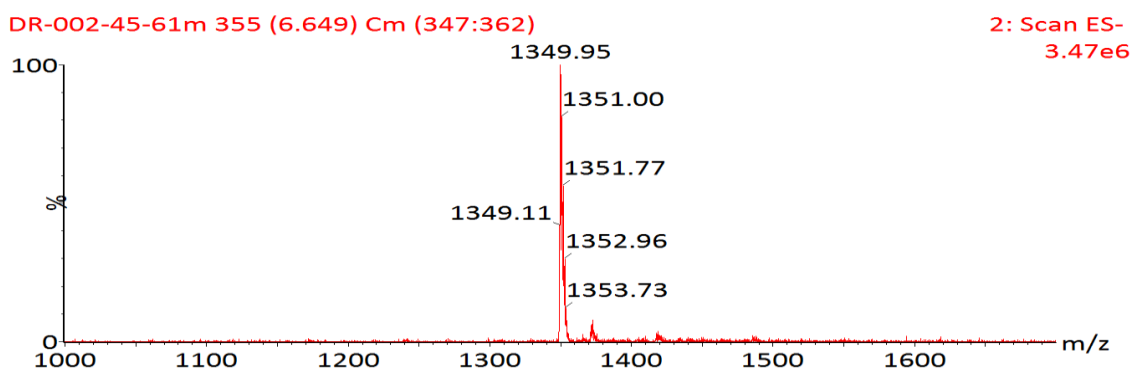
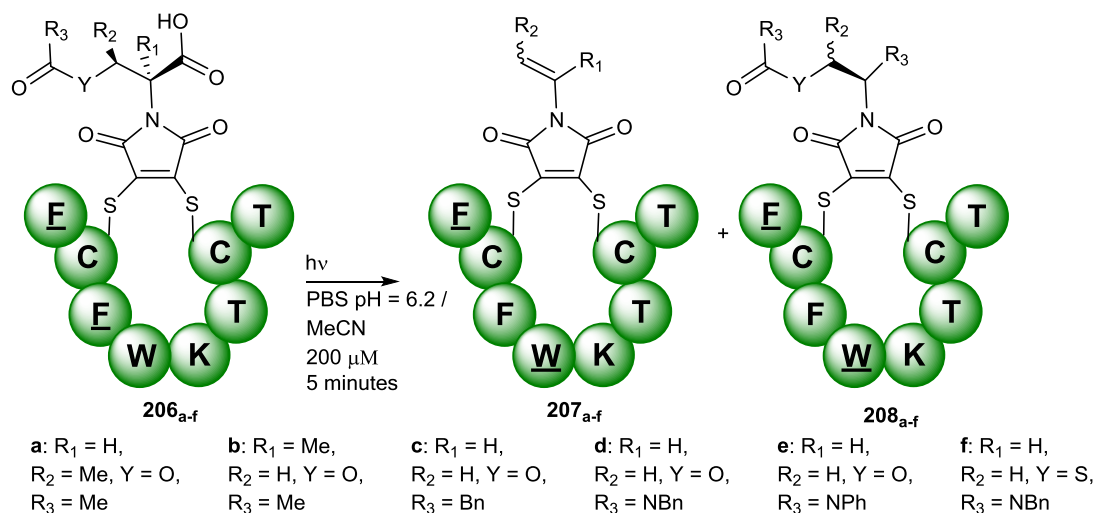


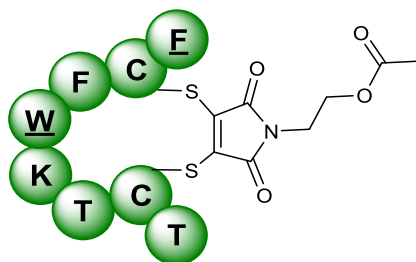
**Figure 96**  
ES negative mode spectrum of Octreotide conjugate 206<sub>f</sub>.

## A general experimental for the Irradiation of Octreotide conjugates



Octreotide conjugate **184** or **206<sub>a-f</sub>** (200 μM in 50:50 PBS pH = 6.2:MeCN, 40 μl) was added to a 1.5 ml Eppendorf tube and irradiated using a 395 nm LED held at a distance of 4 cm for five minutes. After this time the sample was analysed by LCMS which revealed a mixture of the products. See main text for LC details and yields.

### Octreotide Conjugate 186



Expected mass 1199, observed mass 1199 (ES<sup>-</sup> mode).

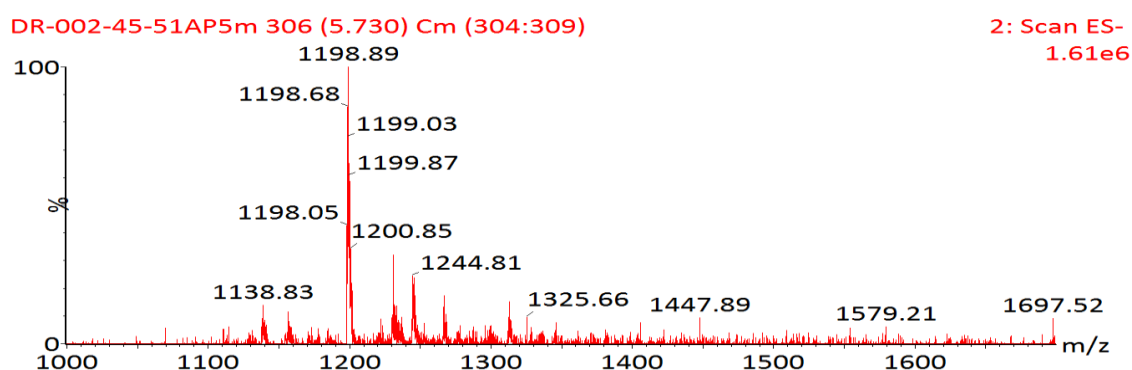
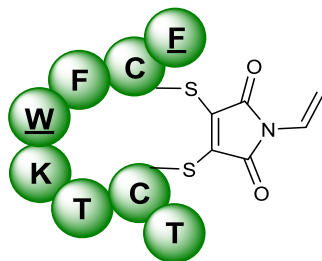


**Figure 97**  
ES negative mode spectrum of Octreotide conjugate 186.

### Octreotide Conjugate 207<sub>c</sub>



Expected mass 1339, observed mass 1339 (ES<sup>-</sup> mode).

DR-002-46-65AP5m 317 (5.939) Cm (315:323)

2: Scan ES-  
1.76e6

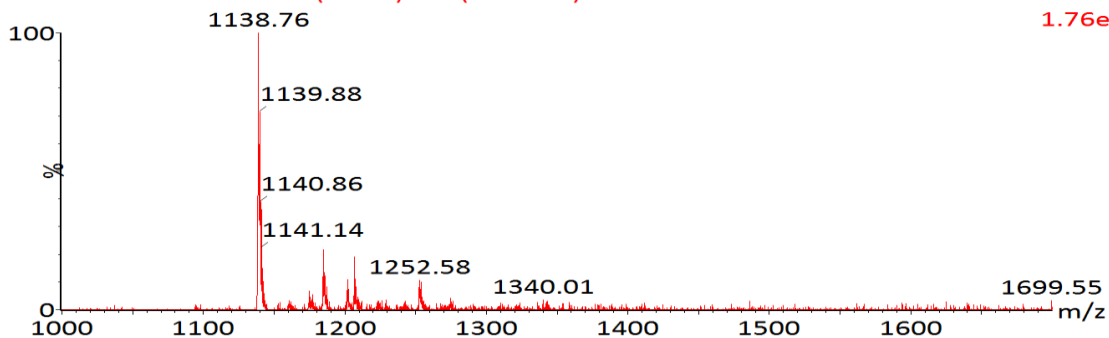
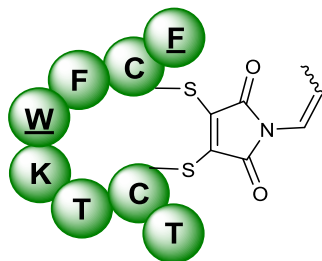


**Figure 98**  
ES negative mode spectrum of Octreotide conjugate 207<sub>c</sub>.

### Octreotide Conjugate 207<sub>a</sub>



Expected mass 1153, observed mass 1153 (ES<sup>-</sup> mode).

DR-002-44-54AP5m 330 (6.182) Cm (326:335)

2: Scan ES-  
3.12e6

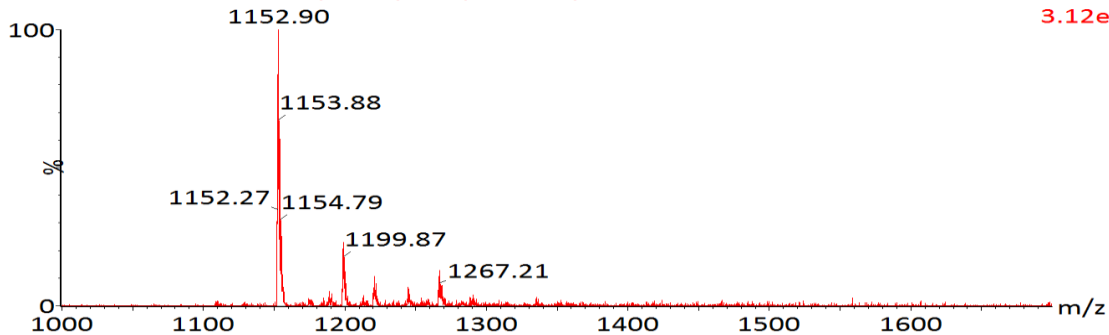
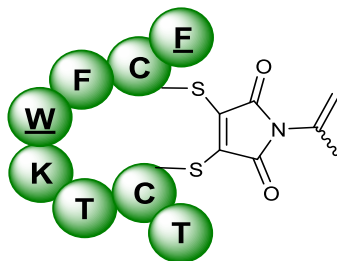


**Figure 99**  
ES negative mode spectrum of Octreotide conjugate 207<sub>a</sub>.

### Octreotide Conjugate 207<sub>b</sub>



Expected mass 1153, observed mass 1153 (ES<sup>-</sup> mode).

DR-002-45-64AP5m 318 (5.956) Cm (317:325)

2: Scan ES-  
2.40e6

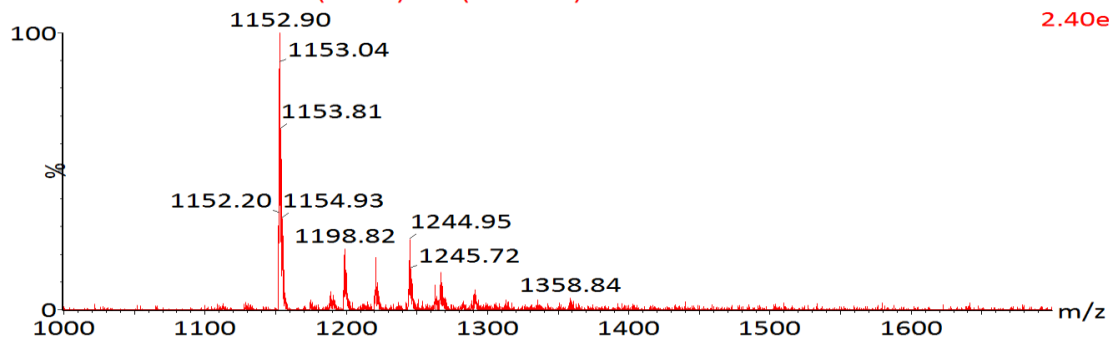
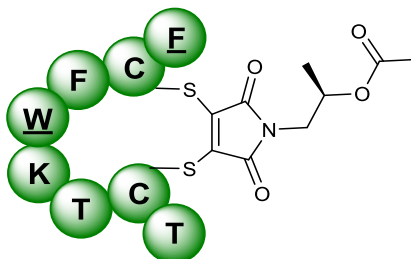


**Figure 100**  
ES negative mode spectrum of Octreotide conjugate 207<sub>b</sub>.

### Octreotide Conjugate 208<sub>a</sub>



Expected mass 1213, observed mass 1213 (ES<sup>-</sup> mode).

DR-002-45-54AP5m 323 (6.047) Cm (316:327)

2: Scan ES-  
9.32e5

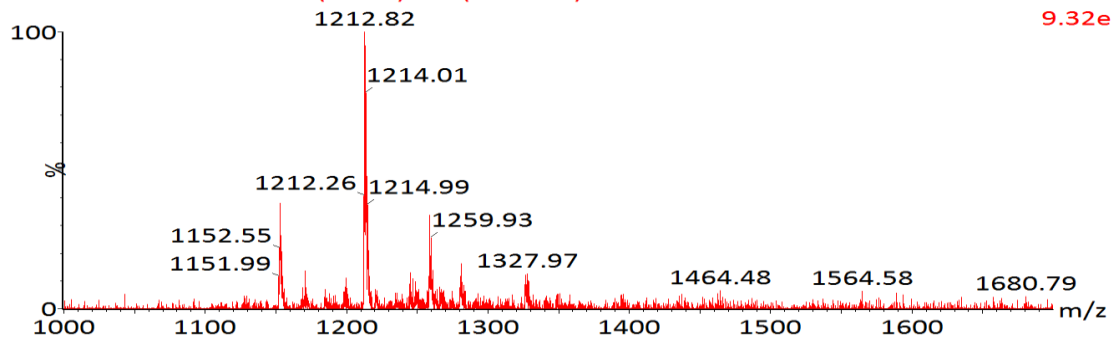
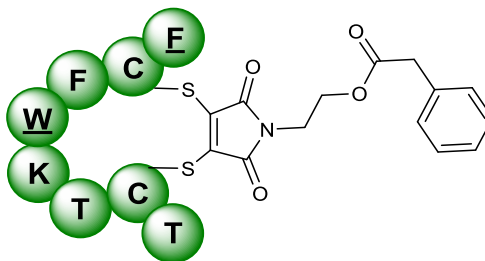


**Figure 101**  
ES negative mode spectrum of Octreotide conjugate 208<sub>a</sub>.

### Octreotide Conjugate 208<sub>c</sub>



Expected mass 1275, observed mass 1275 (ES<sup>-</sup> mode).

DR-002-46-65AP5m 366 (6.858) Cm (365:371)

2: Scan ES-  
4.88e5

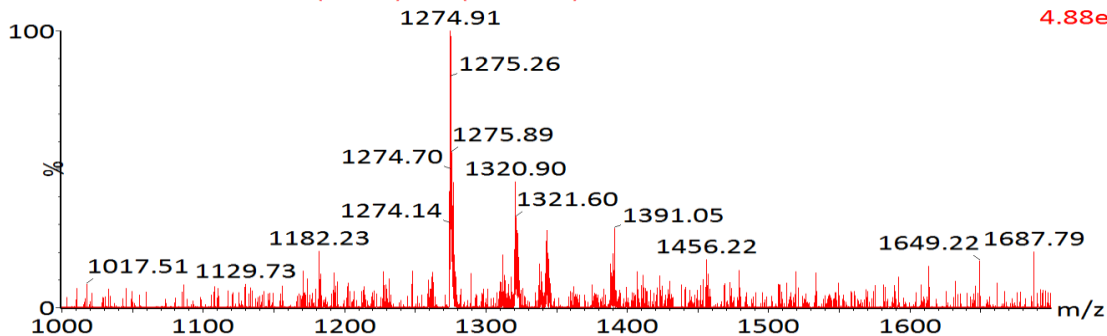
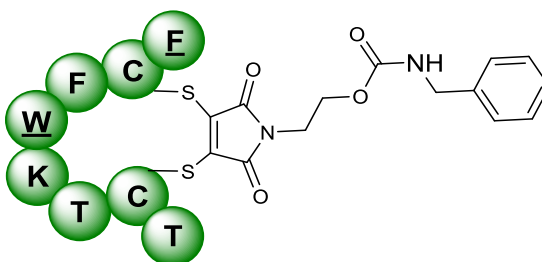


**Figure 102**  
ES negative mode spectrum of Octreotide conjugate 208<sub>c</sub>.

### Octreotide Conjugate 208<sub>d</sub>



Expected mass 1290, observed mass 1290 (ES<sup>-</sup> mode).

DR-002-45-56AP5m 350 (6.552) Cm (349:354)

2: Scan ES-  
1.30e6

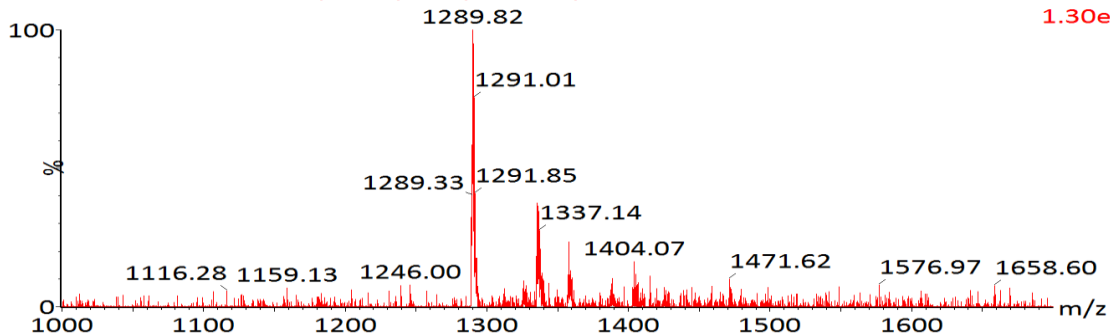
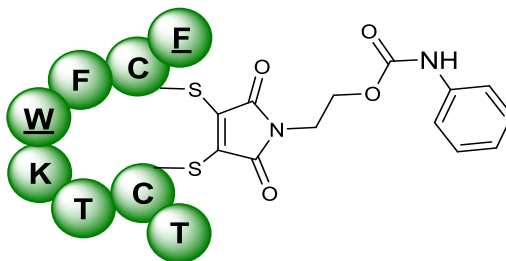


**Figure 103**  
ES negative mode spectrum of Octreotide conjugate 208<sub>d</sub>.

### Octreotide Conjugate 208<sub>e</sub>



Expected mass 1276, observed mass 1276 (ES<sup>-</sup> mode).

DR-002-47-66AP5m 351 (6.585) Cm (350:356)

2: Scan ES-  
9.67e5

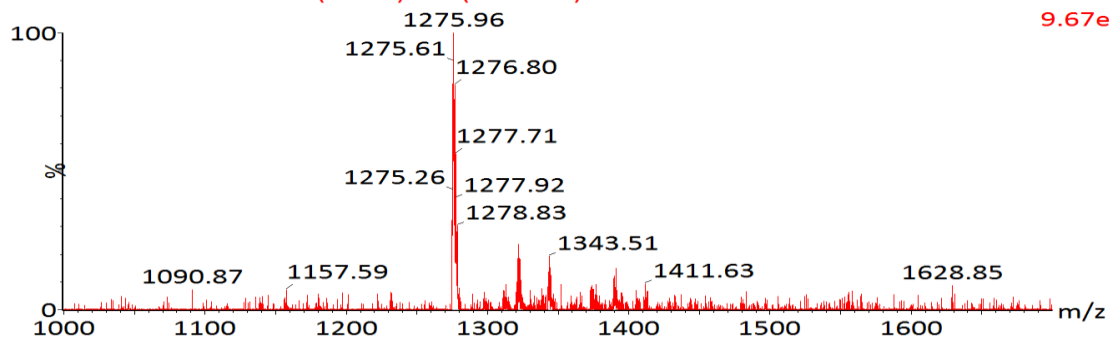
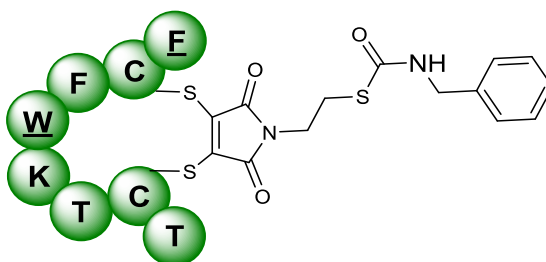


**Figure 104**  
ES negative mode spectrum of Octreotide conjugate 208<sub>e</sub>.

### Octreotide Conjugate 208<sub>f</sub>



Expected mass 1308, observed mass 1308 (ES<sup>+</sup> mode).

DR-002-45-61AP5m 364 (6.805) Cm (360:368)

1: Scan ES+  
3.81e6

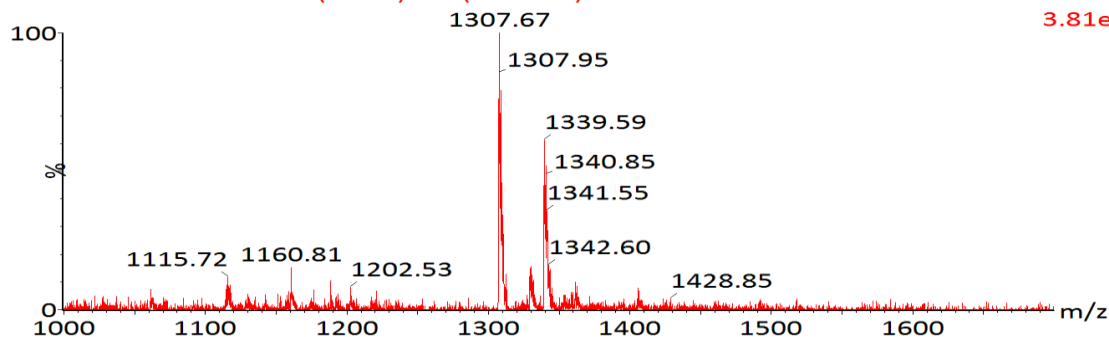
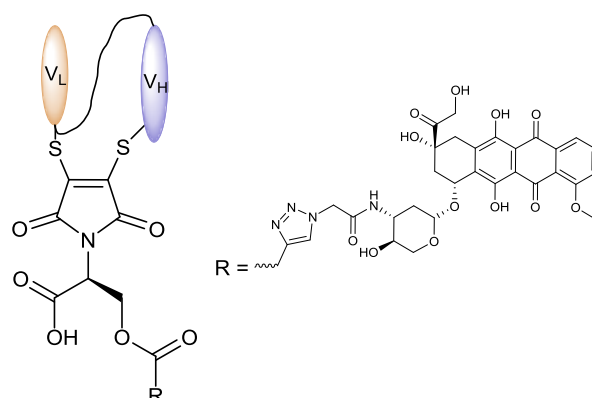


**Figure 105**  
ES negative mode spectrum of Octreotide conjugate 208<sub>f</sub>.

### 3.2.7.2: Anti-CEA scFv-Dox photocleavable ADC.

#### Modification of anti-CEA scFv 220



Anti CEA-scFv **97** (37.2  $\mu$ M in PBS pH = 7.4 + 6 mM EDTA, 200  $\mu$ l) was reacted with DTT (37.2 mM in PBS pH = 7.4, 20 equiv., 4  $\mu$ l) for one hour at room temperature. After this time the solution was purified by desalting column (GE healthcare), buffer swapped into PBS pH = 7.4, and the volume readjusted to 200  $\mu$ l. Pre-clicked dibromomaleimide-doxorubicin compound **219** (3.72 mM, 10 equiv. 20  $\mu$ l in H<sub>2</sub>O/*t*-BuOH) was added and the reaction left for 30 minutes at room temperature. After this time the solution was once again purified by desalting column, buffer swapped into PBS pH = 7.4, and the concentration adjusted to 20  $\mu$ M (205  $\mu$ l). Analysis by LCMS revealed successful reaction to produce scFv conjugate **220**. Expected mass 27626, observed mass 27624.

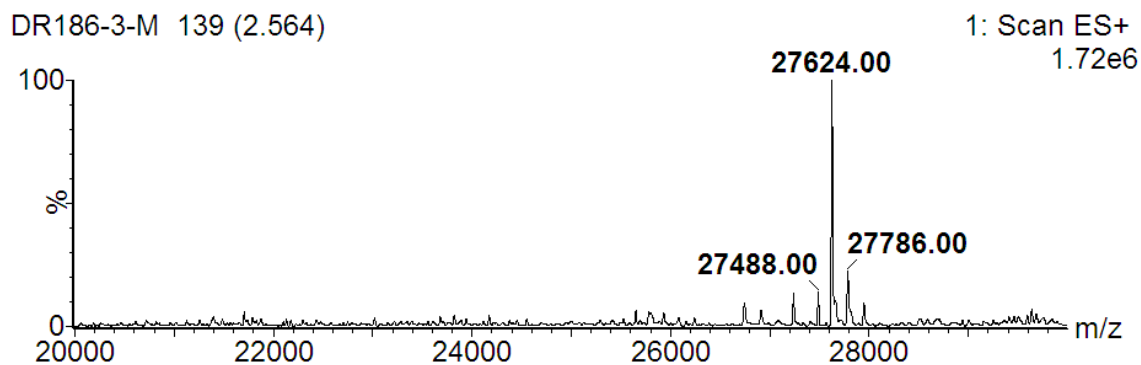
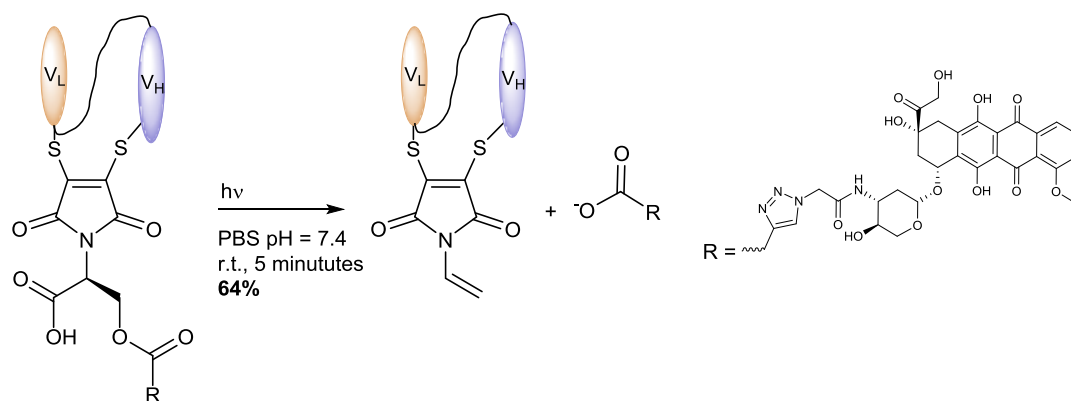


**Figure 106**  
Deconvoluted mass spectrum for scFv-Dox conjugate **220**.

### Irradiation of anti-CEA scFv-Dox 220



6 aliquots of anti-CEA scFv conjugate **220** (20  $\mu\text{M}$  in PBS pH = 7.4, 5 x 20  $\mu\text{l}$ ) were taken and individually irradiated at room temperature for one, two, three, four, five and six minutes using a 395 nm LED torch held a distance of 4 cm. The resulting samples were then analysed using HPLC monitoring at 280 and 480 nm to track the release of Dox-carboxylate **222**. See main text for details (section 2.4.6.3, page 127, Scheme 105 & Figure 52).

### 3.2.8: Cell kill assays for Doxorubicin analogues

Below is the general protocol employed by Dr Enrique Miranda Rota of the UCL Cancer Institute to test the cell toxicity of Doxorubicin. HCl **215** and Doxorubicin analogues **222** and **224**.

Capa-1, Caski and Hela cell lines expressing CEA (purchased from ATCC Cell Biology) were trypsinised and seeded in 96 well plates at a concentration of 1000 cells per well. The wells were incubated at 37 °C and 5% CO<sub>2</sub> for 24 hours to allow for attachment of the cells. The appropriate Doxorubicin analogue (**215**, **222**, and **224**) in serial dilutions (100  $\mu\text{M}$ , 33.3  $\mu\text{M}$ , 11.1,  $\mu\text{M}$ , 3.7  $\mu\text{M}$ , 1.23  $\mu\text{M}$ , 0.41  $\mu\text{M}$ , 0.14  $\mu\text{M}$ , 0.046  $\mu\text{M}$ , 0.015  $\mu\text{M}$ , and 0.005  $\mu\text{M}$ ) was added (10  $\mu\text{l}$ ) and the cells incubated at 37 °C and 5% CO<sub>2</sub> for 72 hours. The cells were emptied and washed with PBS (1 x 200  $\mu\text{l}$ ). An 10% MTS reagent (100  $\mu\text{l}$ ) was added and the wells incubated at 37 °C and 5% CO<sub>2</sub> for 1 hour. Visualisation and cell viability was calculated by recording the absorbance at 490 nm and subtracting negative controls (non-treated cells). See main text for details (section 2.4.6.4, page 129, Figure 54 & section 2.4.6.5, page 132, Figure 55).

## 4: References

- 1 H. D. Roth, *Pure Appl. Chem.*, 2001, **73**, 395–403.
- 2 H. E. Zimmerman, *J. Am. Chem. Soc.*, 1962, **84**, 4527–4540.
- 3 H. E. Zimmerman, R. D. Rieke and J. R. Scheffer, *J. Am. Chem. Soc.*, 1966, **89**, 2033–2047.
- 4 H. E. Zimmerman and G. E. Samuelson, *J. Am. Chem. Soc.*, 1967, **89**, 5973–5974.
- 5 H. E. Zimmerman and J. O. Grunewald, *J. Am. Chem. Soc.*, 1966, **89**, 5163–5172.
- 6 H. E. Zimmerman and J. W. Wilson, *J. Am. Chem. Soc.*, 1964, **86**, 4036–4042.
- 7 G. S. Hammond and W. M. Moore, *J. Am. Chem. Soc.*, 1959, **81**, 6334.
- 8 K. R. Kopecky, G. S. Hammond and P. A. Leermakers, *J. Am. Chem. Soc.*, 1961, **83**, 2397–2398.
- 9 G. S. Hammond, P. A. Leermakers and N. J. Turro, *J. Am. Chem. Soc.*, 1961, **6334**, 2395–2396.
- 10 G. S. Hammond, P. A. Leermakers and N. J. Turro, 1959, **83**, 2396–2397.
- 11 G. S. Hammond, J. Saltiel, A. A. Lamola, N. J. Turro, J. S. Bradshaw, D. O. Cowan, R. C. Counsell, V. Vogt and C. Dalton, *Mechanisms of Photochemical Reactions in Solution. XXII. Photochemical cis-trans Isomerization*, 1964, vol. 86.
- 12 G. S. Hammond, N. Turro and A. Fischer, *J. Am. Chem. Soc.*, 1961, **83**, 4674–4675.
- 13 W. M. Moore, G. S. Hammond and R. P. Foss, *J. Am. Chem. Soc.*, 1961, **1068**, 2789–2794.
- 14 G. S. Hammond, W. P. Baker and W. M. Moore, *J. Am. Chem. Soc.*, 1961, **83**, 2795–2799.
- 15 A. Jabłoński, *Nature*, 1933, **131**, 839–840.
- 16 J. Zhang, R. E. Campbell, A. Y. Ting and R. Y. Tsien, *Nat. Rev. Mol. Cell Biol.*, 2002, **3**, 906–918.
- 17 N. Hoffmann, *Chem. Rev.*, 2008, **108**, 1052–1103.
- 18 M. Di Biase, R. E. Saunders, N. Tirelli and B. Derby, *Soft Matter*, 2011, **7**, 2639.
- 19 V. Balzani, A. Credi and M. Venturi, *Photochemical conversion of solar energy*, 2008, vol. 1.
- 20 T. F. Schulze and T. W. Schmidt, *Energy Environ. Sci.*, 2014, **8**, 103–125.
- 21 S. Chatani, C. J. Kloxin and C. N. Bowman, *Polym. Chem.*, 2014, **5**, 2187.
- 22 D. Phillips, *Photochem. Photobiol. Sci.*, 2010, **9**, 1589–1596.
- 23 N. Fomina, J. Sankaranarayanan and A. Almutairi, *Adv. Drug Deliv. Rev.*, 2012, **64**,

- 1005–1020.
- 24 P. Rai, S. Mallidi, X. Zheng, R. Rahmanzadeh, Y. Mir, S. Elrington, A. Khurshid and T. Hasan, *Adv. Drug Deliv. Rev.*, 2010, **62**, 1094–1124.
- 25 Y. Wang, J. D. Byrne, M. E. Napier and J. M. DeSimone, *Adv. Drug Deliv. Rev.*, 2012, **64**, 1021–1030.
- 26 G. Ciamician and P. Silber, *Berichte der Dtsch. Chem. Gessellschaft*, 1908, **41**, 1928–1935.
- 27 G. Büchi and I. M. Goldman, *J. Am. Chem. Soc.*, 1957, **79**, 4741–4748.
- 28 S. Cristol and R. Snell, *J. Am. Chem. Soc.*, 1954, **76**, 5000.
- 29 S. Cristol and R. Snell, *J. Am. Chem. Soc.*, 1958, **80**, 1950–1952.
- 30 P. E. Eaton, 1961, **3915**, 2344–2348.
- 31 P. Eaton and T. Cole, *J. Am. Chem. Soc.*, 1964, **86**, 962–964.
- 32 P. E. Eaton and T. W. Cole Jr., *J. Am. Chem. Soc.*, 1964, **86**, 3157–3158.
- 33 P. E. Eaton, *J. Am. Chem. Soc.*, **84**, 2454–2455.
- 34 A. Gilbert and J. Baggot, *Essentials of Molecular Photochemistry*, Blackwell Scientific Publications, 1991.
- 35 E. J. Corey, J. D. Bass, R. LeMahieu and R. B. Mitra, *J. Am. Chem. Soc.*, 1964, **86**, 5570–5583.
- 36 P. de Mayo, *Acc. Chem. Res.*, 1971, **2**, 41–47.
- 37 R. O. Loutfy and P. de Mayo, *J. Am. Chem. Soc.*, 1977, **99**, 3559–3565.
- 38 N. C. Yang and M. J. Jorgenson, *Tetrahedron Lett.*, 1964, 1203–1207.
- 39 P. De Mayo, J.-P. Pete and M. Tchir, *Can. J. Chem.*, 1968, **46**, 2535–2547.
- 40 K. Fukui, T. Yonezawa and H. Shingu, *J. Chem. Phys.*, 1952, **20**, 722–725.
- 41 R. B. Woodward and R. Hoffmann, *J. Am. Chem. Soc.*, 1965, **87**, 395–397.
- 42 R. Hoffmann and R. B. Woodward, *J. Am. Chem. Soc.*, 1965, **87**, 2046–2048.
- 43 R. B. Woodward and R. Hoffmann, *Angew. Chem. Int. Ed.*, 1969, **8**, 781–853.
- 44 F. A. Carroll, *Perspectives on Structure and Mechanism in Organic Chemistry*, 1998.
- 45 E. R. Koft and A. B. Smith, *J. Am. Chem. Soc.*, 1984, **106**, 2115–2121.
- 46 E. R. Koft and A. B. Smith, *J. Am. Chem. Soc.*, 1982, **104**, 5570–5572.
- 47 M. Cavazza, G. Guella and F. Pietra, *Helv. Chim. Acta*, 1988, **71**, 1608–1615.
- 48 M. Cavazza and F. Pietra, *J. Chem. Soc. Perkin. Trans.*, 1985, 2283–2287.
- 49 U. Streit and C. G. Bochet, *Beilstein J. Org. Chem*, 2011, **7**, 525–542.

- 50 M. DellaGreca, P. Monaco, L. Previtiera, A. Zarrelli, A. Fiorentino, F. Giordano and C. A. Mattia, *J. Org. Chem.*, 2001, **66**, 2057–2060.
- 51 R. Anet, *Can. J. Chem.*, 1962, **40**, 1249–1257.
- 52 P. De Mayo and H. Takeshita, *Can. J. Chem.*, 1963, **41**, 440–448.
- 53 G. Büchi, C. G. Inman and E. S. Lipinsky, *J. Am. Chem. Soc.*, 1954, **76**, 4327–4331.
- 54 J. Iriondo-Alberdi and M. F. Greaney, *European J. Org. Chem.*, 2007, 4801–4815.
- 55 N. Sarkar, A. Nayek and S. Ghosh, *Org. Lett.*, 2004, **6**, 1903–1905.
- 56 K. C. Nicolaou, D. Sarlah and D. M. Shaw, *Angew. Chem. Int. Ed.*, 2007, **46**, 4708–4711.
- 57 I. K. Mangion and D. W. C. MacMillan, *J. Am. Chem. Soc.*, 2005, **127**, 3696–3697.
- 58 S. Hatakeyama, M. Kawamura and S. Takano, *J. Am. Chem. Soc.*, 1994, **116**, 4081–4082.
- 59 K. I. Booker-Milburn, J. K. Cowell, A. Sharpe and F. D. Jimenez, *Chem. Commun.*, 1996, 249–251.
- 60 K. I. Booker-Milburn, J. K. Cowell, F. Delgado Jiménez, A. Sharpe and A. J. White, *Tetrahedron*, 1999, **55**, 5875–5888.
- 61 K. I. Booker-Milburn, C. E. Anson, C. Clissold, N. J. Costin, R. F. Dainty, M. Murray, D. Patel and A. Sharpe, *Eur. J. Org. Chem.*, 2001, 1473–1482.
- 62 M. Conradi and T. Junkers, *J. Photochem. Photobiol. A Chem.*, 2013, **259**, 41–46.
- 63 L. Tedaldi, A. Aliev and J. R. Baker, *Chem. Commun.*, 2012, **48**, 4725–4727.
- 64 D. H. R. Barton, D. Crich and W. B. Motherwell, *J. Chem. Soc. Perkin. Trans.*, 1983, 939–941.
- 65 D. H. R. Barton, D. Crich and W. B. Motherwell, *Tetrahedron Lett.*, 1983, **24**, 4979–4982.
- 66 D. H. R. Barton, D. Crich and W. B. Motherwell, *Tetrahedron*, 1985, **41**, 3901–3924.
- 67 R. A. Sheldon and J. K. Kochi, *J. Am. Chem. Soc.*, 1968, **90**, 6688–6698.
- 68 J. K. Kochi, R. A. Sheldon and S. S. Lande, *Tetrahedron*, 1969, **25**, 1197–1207.
- 69 J. P. Ferris and P. C. Joshi, *J. Am. Chem. Soc.*, 1979, **44**, 2133–2137.
- 70 M. F. Saraiva, M. R. C. Couri, M. Le Hyaric and M. V. de Almeida, *Tetrahedron*, 2009, **65**, 3563–3572.
- 71 K. Yamaguchi, Y. Kazuta, H. Abe, A. Matsuda and S. Shuto, *J. Org. Chem.*, 2003, **68**, 9255–9262.
- 72 D. Crich and L. Quintero, *Chem. Rev.*, 1989, **89**, 1413–1432.
- 73 J. Libman, *J. Am. Chem. Soc.*, 1975, **97**, 4139–4144.

- 74 D. R. G. Brimage, R. S. Davidson and P. R. Steiner, *J. Chem. Soc. Perkin. Trans.*, 1973, 526 – 529.
- 75 Y. Kurauchi, H. Nobuhara and K. Ohga, *Bull. Chem. Soc. Jpn.*, 1986, **59**, 897–905.
- 76 K. Tsujimoto, N. Nakao and M. Ohashi, *J. Chem. Soc., Chem. Commun.*, 1992, 366–367.
- 77 Y. Kanaoka, *Acc. Chem. Res.*, 1978, **11**, 407–413.
- 78 K. Okada, K. Okamoto and M. Oda, *J. Am. Chem. Soc.*, 1988, **110**, 8736–8738.
- 79 A. G. Griesbeck, H. Mauder and I. Muller, 1993, **34**, 453–456.
- 80 A. G. Griesbeck, A. Henz, J. Hirt, V. Ptatschek, T. Engel, D. Loffler and F. W. Schneider, *Tetrahedron*, 1994, **50**, 701–714.
- 81 A. G. Griesbeck, T. Heinrich, M. Oelgemoller, A. Molis and A. Heidtmann, *Helv. Chim. Acta*, 2002, **85**, 4561–4578.
- 82 M. Sohara, T. Š. Ramljak, K. Mlinarić-majerski and N. Basarić, *Croat. Chem. Acta*, 2014, **87**, 431–446.
- 83 A. Soldevilla, R. Pérez-Ruiz, Y. Díaz Miara and A. G. Griesbeck, *Chem. Commun.*, 2010, **46**, 3747–3749.
- 84 J. A. Barltrop and P. Schofield, *Tetrahedron Lett.*, 1962, 697–699.
- 85 A. Patchornik and R. B. Woodward, *J. Am. Chem. Soc.*, 1970, **92**, 6333–6335.
- 86 D. H. R. Barton, Y. L. Chow, A. Cox and G. W. Kirby, *Tetrahedron Lett.*, 1962, **23**, 1055–1057.
- 87 J. C. Sheehan and R. M. Wilson, *J. Am. Chem. Soc.*, 1964, **86**, 5277–5281.
- 88 A. P. Pelliccioli and J. Wirz, *Photochem. Photobiol. Sci.*, 2002, **1**, 441–458.
- 89 P. Klán, C. G. Bochet, R. Givens, M. Rubina, V. Popik, A. Kostikov, J. Wirz, T. Šolomek, C. G. Bochet, A. Blanc, R. Givens, M. Rubina, V. Popik, A. Kostikov and J. Wirz, *Chem. Rev.*, 2013, **113**, 119–191.
- 90 R. S. Givens, P. G. I. Conrad, A. Yousef and J. L. Lee, *CRC Handbook of Organic Photochemistry and Photobiology, 2nd Edition*, 2004.
- 91 D. E. Falvey and C. Sundararajan, *Photochem. Photobiol. Sci.*, 2004, **3**, 831–838.
- 92 H. Zhao, E. S. Sterner, E. B. Coughlin and P. Theato, *Macromolecules*, 2012, **45**, 1723–1736.
- 93 K. Suyama and M. Shirai, *Prog. Polym. Sci.*, 2009, **34**, 194–209.
- 94 S. Tang, J.-Y. Cheng and J.-S. Zheng, *Tetrahedron Lett.*, 2015, **56**, 4582–4585.
- 95 K. Yamaguchi, T. Kitabatake, M. Izawa, T. Fujiwara, H. Nishimura and T. Futami, *Chem. Lett.*, 2000, 228–229.

- 96 H. Yu, J. Li, D. Wu, Z. Qiu and Y. Zhang, *Chem. Soc. Rev.*, 2010, **39**, 464–473.
- 97 G. C. R. Ellis-Davies, *Nat. Methods*, 2007, **4**, 619–628.
- 98 R. S. Givens, M. Rubina and J. Wirz, *Photochem. Photobiol. Sci.*, 2012, **11**, 472–488.
- 99 J. H. Kaplan, B. Forbush and J. F. Hoffman, *Biochemistry*, 1978, **17**, 1929–1935.
- 100 J. W. Walker, G. P. Reid, J. A. McCray and D. R. Trentham, *J. Am. Chem. Soc.*, 1988, **110**, 7170–7177.
- 101 H. Lusic, D. D. Young, M. O. Lively and A. Deiters, *Org. Lett.*, 2007, **9**, 1903–1906.
- 102 A. Stutz and S. Pitsch, *Synlett*, 1999, **S1**, 930–934.
- 103 Y. Mizuno, K. Baldenius and A. L. Smith, *J. Am. Chem. Soc.*, 1993, **115**, 7625–7635.
- 104 S. Ibsen, E. Zahavy, W. Wrasidlo, T. Hayashi, J. Norton, Y. Su, S. R. Adams and S. Esener, *Photochem. Photobiol.*, 2013, **89**, 698–708.
- 105 S. Ibsen, E. Zahavy, W. Wrasidlo, M. Berns, M. Chan and S. Esener, *Pharm. Res.*, 2010, **27**, 1848–1860.
- 106 E. Cabane, V. Malinova and W. Meier, *Macromol. Chem. Phys.*, 2010, **211**, 1847–1856.
- 107 C. P. McCoy, C. Rooney, C. R. Edwards, D. S. Jones and S. P. Gorman, *J. Am. Chem. Soc.*, 2007, **129**, 9572–9573.
- 108 R. P.-Y. Chen, J. J.-T. Huang, H.-L. Chen, H. Jan, M. Velusamy, C.-T. Lee, W. Fann, R. W. Larsen and S. I. Chan, *Proc. Natl. Acad. Sci. U. S. A.*, 2004, **101**, 7305–7310.
- 109 R. S. Rock, K. C. Hansen, R. W. Larsen and S. I. Chan, *Chem. Phys.*, 2004, **307**, 201–208.
- 110 R. S. Givens, P. S. Athey, L. W. Kueper, B. Matuszewski and J. Xue, *J. Am. Chem. Soc.*, 1992, **114**, 8708–8710.
- 111 K. R. Gee, L. W. Kueper, J. Barnes, G. Dudley and R. S. Givens, *J. Org. Chem.*, 1996, **61**, 1228–1233.
- 112 S. Geibel, A. Barth, S. Amslinger, A. Jung, C. Burzik, R. Clarke, R. Givens and K. Fendler, *Biophys. J.*, 2000, **79**, 1346–1357.
- 113 X. Du, H. Frei and S. Kim, *J. Biol. Chem.*, 2000, **275**, 8492–8500.
- 114 K. Stensrud, J. Noh, K. Kandler, J. Wirz, D. Heger and R. S. Givens, *J. Org. Chem.*, 2009, **74**, 5219–5227.
- 115 M. Goeldner and R. S. Givens, *Dynamic Studies in Biology*, 2006.
- 116 M. Skwarczynski, M. Noguchi, S. Hirota, Y. Sohma, T. Kimura, Y. Hayashi and Y. Kiso, *Bioorganic Med. Chem. Lett.*, 2006, **16**, 4492–4496.
- 117 J. Babin, M. Pelletier, M. Lepage, J.-F. Allard, D. Morris and Y. Zhao, *Angew. Chem. Int. Ed.*, 2009, **48**, 3329–3332.

- 118 X.-J. Yang, *Oncogene*, 2005, **24**, 1653–1662.
- 119 O. Boutureira and G. J. L. Bernardes, *Chem. Rev.*, 2015, **115**, 2174–2195.
- 120 E. Baslé, N. Joubert and M. Pucheault, *Chem. Biol.*, 2010, **17**, 213–227.
- 121 B. Leader, Q. J. Baca and D. E. Golan, *Nat. Rev. Drug Discov.*, 2008, **7**, 21–39.
- 122 R. van Vught, R. J. Pieters and E. Breukink, *Comput. Struct. Biotechnol. J.*, 2014, **9**, 1–13.
- 123 F. M. Veronese, *Biomaterials*, 2001, **22**, 405–417.
- 124 F. M. Veronese and G. Pasut, *Drug Discov. Today*, 2005, **10**, 1451–1458.
- 125 Y. Feng, Z. Zhu, W. Chen, P. Prabakaran, K. Lin and D. S. Dimitrov, *Biomedicines*, 2014, **2**, 1–13.
- 126 M. L. James and S. S. Gambhir, *Physiol. Rev.*, 2012, **92**, 897–965.
- 127 A. S. Hoffman, *Clin. Chem.*, 2000, **46**, 1478–1486.
- 128 M. Steiner and D. Neri, *Clin. Cancer Res.*, 2011, **17**, 6406–6416.
- 129 T. Oya, N. Hattori, Y. Mizuno, S. Miyata, S. Maeda, T. Osawa and K. Uchida, *J. Biol. Chem.*, 1999, **274**, 18492–18502.
- 130 T. L. Schlick, Z. Ding, E. W. Kovacs and M. B. Francis, *J. Am. Chem. Soc.*, 2005, **127**, 3718–3723.
- 131 C. D. Spicer and B. G. Davis, *Nat. Commun.*, 2014, **5**, 1–14.
- 132 G. Chen, A. Heim, D. Riether, D. Yee, Y. Milgrom, M. A. Gawinowicz and D. Sames, *J. Am. Chem. Soc.*, 2003, **125**, 8130–8133.
- 133 X. Chen, K. Muthoosamy, A. Pfisterer, B. Neumann and T. Weil, *Bioconjug. Chem.*, 2012, **23**, 500–508.
- 134 N. S. Joshi, L. R. Whitaker and M. B. Francis, *J. Am. Chem. Soc.*, 2004, **126**, 15942–15943.
- 135 A. Miseta and P. Csutora, *Mol. Biol. Evol.*, 2000, **17**, 1232–1239.
- 136 J. M. Chalker, G. J. L. Bernardes, Y. A. Lin and B. G. Davis, *Chem. - An Asian J.*, 2009, **4**, 630–640.
- 137 S. Panowski, S. Bhakta, H. Raab, P. Polakis and J. R. Junutula, *MAbs*, 2014, **6**, 34–45.
- 138 H. P. Hemantha, S. N. Bavikar, Y. Herman-Bachinsky, N. Haj-Yahya, S. Bondalapati, A. Ciechanover and A. Brik, *J. Am. Chem. Soc.*, 2014, **136**, 2665–2673.
- 139 Y. Kim, S. O. Ho, N. R. Gassman, Y. Korlann, E. V. Landorf, F. R. Collart and S. Weiss, *Bioconjug. Chem.*, 2008, **19**, 786–791.
- 140 J. M. Chalker, Y. a Lin, O. Boutureira and B. G. Davis, *Chem. Commun.*, 2009, 3714–3716.

- 141 O. Boutureira, G. J. L. Bernardes, M. Fernández-González, D. C. Anthony and B. G. Davis, *Angew. Chem. Int. Ed.*, 2012, **51**, 1432–1436.
- 142 G. J. L. Bernardes, J. M. Chalker, J. C. Errey and B. G. Davis, *J. Am. Chem. Soc.*, 2008, **130**, 5052–5053.
- 143 G. J. L. Bernardes, E. J. Grayson, S. Thompson, J. M. Chalker, J. C. Errey, F. El Oualid, T. D. W. Claridge and B. G. Davis, *Angew. Chemie Int. Ed.*, 2008, **47**, 2244–2247.
- 144 A. Maruani, M. E. B. Smith, E. Miranda, K. a. Chester, V. Chudasama and S. Caddick, *Nat. Commun.*, 2015, **6**, 6645.
- 145 L. Castañeda, Z. V. F. Wright, C. Marculescu, T. M. Tran, V. Chudasama, A. Maruani, E. a. Hull, J. P. M. Nunes, R. J. Fitzmaurice, M. E. B. Smith, L. H. Jones, S. Caddick and J. R. Baker, *Tetrahedron Lett.*, 2013, **54**, 3493–3495.
- 146 M. E. B. Smith, F. F. Schumacher, C. P. Ryan, L. M. Tedaldi, D. Papaioannou, G. Waksman, S. Caddick and J. R. Baker, *J. Am. Chem. Soc.*, 2010, **132**, 1960–1965.
- 147 M. W. Jones, R. A. Strickland, F. F. Schumacher, S. Caddick, J. R. Baker, M. I. Gibson and D. M. Haddleton, 2012, **48**, 4064–4066.
- 148 R. I. Nathani, V. Chudasama, C. P. Ryan, P. R. Moody, R. E. Morgan, R. J. Fitzmaurice, M. E. B. Smith, J. R. Baker and S. Caddick, *Org. Biomol. Chem.*, 2013, **11**, 2408–2411.
- 149 F. F. Schumacher, V. A. Sanchania, B. Tolner, Z. V. F. Wright, C. P. Ryan, M. E. B. Smith, J. M. Ward, S. Caddick, C. W. M. Kay, G. Aeppli, K. A. Chester and J. R. Baker, *Sci. Rep.*, 2013, **3**, 1–8.
- 150 E. A. Hull, M. Livanos, E. Miranda, M. E. B. Smith, K. A. Chester and J. R. Baker, *Bioconjugate Chem*, 2014, **25**, 1395–1401.
- 151 J. Youziel, A. R. Akhbar, Q. Aziz, M. E. B. Smith, S. Caddick, A. Tinker and J. R. Baker, *Org. Biomol. Chem.*, 2014, **12**, 557–560.
- 152 S. A. Fletcher, P. K. B. Sin, M. Nobles, E. Årstad, A. Tinker and J. R. Baker, *Org. Biomol. Chem.*, 2015, **13**, 9559–9563.
- 153 J. P. M. Nunes, M. Morais, V. Vassileva, E. Robinson, V. S. Rajkumar, M. E. B. Smith, R. B. Pedley, S. Caddick, J. R. Baker and V. Chudasama, *Chem. Commun.*, 2015, **51**, 10624–10627.
- 154 R. E. Morgan, V. Chudasama, P. Moody, M. E. B. Smith and S. Caddick, *Org. Biomol. Chem.*, 2015, **13**, 4165–4168.
- 155 P. Moody, M. E. B. Smith, C. P. Ryan, V. Chudasama, J. R. Baker, J. Molloy and S. Caddick, *ChemBioChem*, 2012, **13**, 39–41.
- 156 F. F. Schumacher, J. P. M. Nunes, A. Maruani, V. Chudasama, M. E. B. Smith, K. a. Chester, J. R. Baker and S. Caddick, *Org. Biomol. Chem.*, 2014, **12**, 7261–7269.
- 157 J. Rivier, P. Brazeau, W. Vale and R. Guillemin, *J. Med. Chem.*, 1975, **18**, 123–126.

- 158 J. T. Heads, R. Adams, L. E. D'Hooghe, M. J. T. Page, D. P. Humphreys, A. G. Popplewell, A. D. Lawson and A. J. Henry, *Protein Sci.*, 2012, **21**, 1315–1322.
- 159 G. Casi and D. Neri, *J. Control. Release*, 2012, **161**, 422–428.
- 160 B. A. Teicher and R. V. J. Chari, *Clin. Cancer Res.*, 2011, **17**, 6389–6397.
- 161 P. J. Carter and P. D. Senter, *Cancer J.*, 2013, **14**, 154–169.
- 162 A. Mullard, *Nat. Rev. Drug Discov.*, 2013, **12**, 483–483.
- 163 P. Agarwal and C. R. Bertozzi, *Bioconjug. Chem.*, 2015, **26**, 176–192.
- 164 H. W. Schroeder and L. Cavacini, *J. allergy Clin. Immunol.*, 2013, **125**, S41–52.
- 165 A. W. F. and A. N. Barclay, *Annu. Rev. Immunol.*, 1988, **6**, 381–405.
- 166 J. M. Woof and D. R. Burton, *Nat. Rev. Immunol.*, 2004, **4**, 89–99.
- 167 G. Vidarsson, G. Dekkers and T. Rispiens, *Front. Immunol.*, 2014, **5**, 1–16.
- 168 V. Irani, A. J. Guy, D. Andrew, J. G. Beeson, P. A. Ramsland and J. S. Richards, *Mol. Immunol.*, 2015, **67**, 171–182.
- 169 A. L. Nelson, *MAbs*, 2010, **2**, 77–83.
- 170 I. Quast, C. W. Keller, M. A. Maurer, J. P. Giddens, B. Tackenberg, L. Wang, C. Münz, F. Nimmerjahn, M. C. Dalakas and J. D. Lünemann, *J. Clin. Invest.*, 2015, **125**, 4160–4170.
- 171 M. Stern and R. Herrmann, *Crit. Rev. Oncol. Hematol.*, 2005, **54**, 11–29.
- 172 H. M. Gürcan, D. B. Keskin, J. N. H. Stern, M. A. Nitzberg, H. Shekhani and A. R. Ahmed, *Int. Immunopharmacol.*, 2009, **9**, 10–25.
- 173 A. Chan, *Ann. Oncol.*, 2007, **18**, 1152–1158.
- 174 S. L. Morrison, M. J. Johnson, L. a Herzenberg and V. T. Oi, *Proc. Natl. Acad. Sci. U. S. A.*, 1984, **81**, 6851–6855.
- 175 P. T. Hudson and C. Souriau, *Nat. Med.*, 2003, **9**, 129–134.
- 176 I. Avivi, S. Robinson and A. Goldstone, *Br. J. Cancer*, 2003, **89**, 1389–1394.
- 177 A. M. Scott, J. D. Wolchok and L. J. Old, *Nat. Rev. Cancer*, 2012, **12**, 278–287.
- 178 R. K. Jain, *Cancer Res.*, 1990, **50**, 814–819.
- 179 A. M. Wu and P. D. Senter, *Nat. Biotechnol.*, 2005, **23**, 1137–1146.
- 180 S. Girish, M. Gupta, B. Wang, D. Lu, I. E. Krop, C. L. Vogel, H. A. Burris III, P. M. LoRusso, J.-H. Yi, O. Saad, B. Tong, Y.-W. Chu, S. Holden and A. Joshi, *Cancer Chemother. Pharmacol.*, 2012, **69**, 1229–1240.
- 181 J. A. Francisco, C. G. Cerveny, D. L. Meyer, B. J. Mixan, K. Klussman, F. Chace, S. X. Rejniak, K. A. Gordon, R. Deblanc, B. E. Toki, C. Law, S. O. Doronina, C. B. Siegall, P.

- D. Senter, A. F. Wahl and D. F. Chace, *Blood*, 2003, **102**, 1458–1465.
- 182 W. Wang, E. Wang and J. Balthasar, *Clin. Pharmacol. Ther.*, 2008, **84**, 548–558.
- 183 T. Yokota, D. E. Milenic, M. Whitlow, T. Yokota, D. E. Milenic, M. Whitlow and J. Schlom, *Cancer Res.*, 1992, **52**, 3402–3408.
- 184 D. G. Covell, J. Barbet, O. D. Holton, C. D. V Black, R. J. Parker and J. N. Weinstein, *Cancer Res*, 1986, **46**, 3969–3978.
- 185 T. Olafsen and A. M. Wu, *Semin. Nucl. Med.*, 2010, **40**, 167–181.
- 186 M. S. Dennis, H. Jin, D. Dugger, R. Yang, L. McFarland, A. Ogasawara, S. Williams, M. J. Cole, S. Ross and R. Schwall, *Cancer Res.*, 2007, **67**, 254–261.
- 187 O. Almog, I. Benhar, G. Vasmatazis, M. Tordova, B. Lee, I. Pastan and G. L. Gilliland, *Proteins*, 1998, **31**, 128–138.
- 188 J. S. Huston, D. Levinson, M. Mudgett-Hunter, M. S. Tai, J. Novotný, M. N. Margolies, R. J. Ridge, R. E. Brucoleri, E. Haber, R. Crea and H. Oppermann, *Proc. Natl. Acad. Sci. U. S. A.*, 1988, **85**, 5879–5883.
- 189 R. E. Bird, K. D. Hardman, J. W. Jacobson, S. Johnson, B. M. Kaufman, S. M. Lee, T. Lee, S. H. Pope, G. S. Riordan and M. Whitlow, *Science (80-. )*, 1988, **242**, 423–426.
- 190 J.-X. Zhao, L. Yang, Z.-N. Gu, H.-Q. Chen, F.-W. Tian, Y.-Q. Chen, H. Zhang and W. Chen, *Int. J. Mol. Sci.*, 2010, **12**, 1–11.
- 191 R. H. J. Begent, M. J. Verhaar, K. A. Chester, J. L. Casey, A. J. Green, M. P. Napier, L. D. Hopstone, N. Cushen, P. A. Keep, C. J. Johnson, R. E. Hawkins, A. J. W. Hilson and L. Robson, *Nat. Med.*, 1996, **2**, 979–984.
- 192 G. P. Adams and R. Schier, *J. Immunol. Methods*, 1999, **231**, 249–260.
- 193 T. A. Afanasieva, M. Wittmer, A. Vitaliti, M. Ajmo, D. Neri and R. Klemenz, *Gene Ther.*, 2003, **10**, 1850–1859.
- 194 N. E. Weisser and J. C. Hall, *Biotechnol. Adv.*, 2009, **27**, 502–520.
- 195 K. Fosgerau and T. Hoffmann, *Drug Discov. Today*, 2014, **20**, 122–128.
- 196 C. Giordano, M. Marchiò, E. Timofeeva and G. Biagini, *Front. Neurol.*, 2014, **5**, 1–14.
- 197 S. D. Robinson, H. Safavi-Hemami, L. D. McIntosh, A. W. Purcell, R. S. Norton and A. T. Pappenfuss, *PLoS One*, 2014, **9**, e87648.
- 198 A. Padhi, M. Sengupta, S. Sengupta, K. H. Roehm and A. Sonawane, *Tuberculosis*, 2014, **94**, 363–373.
- 199 T. Uhlig, T. Kyprianou, F. G. Martinelli, C. A. Oppici, D. Heiligers, D. Hills, X. R. Calvo and P. Verhaert, *EuPA Open Proteomics*, 2014, **4**, 58–69.
- 200 A. A. Kaspar and J. M. Reichert, *Drug Discov. Today*, 2013, **18**, 807–817.

- 201 W. A. P. Breeman, M. De Jong, D. J. Kwekkeboom, R. Valkema, W. H. Bakker, P. P. Kooij, T. J. Visser and E. P. Krenning, *Eur. J. Nucl. Med.*, 2001, **28**, 1421–1429.
- 202 I. M. Modlin, M. Pavel, M. Kidd and B. I. Gustafsson, *Aliment. Pharmacol. Ther.*, 2009, **31**, 169–188.
- 203 E. M. Wolin, *Gastrointest. Cancer Res.*, 2012, **5**, 161–168.
- 204 P. Barnett, *Endocrine*, 2003, **20**, 255–264.
- 205 Y. C. Patel, *Front. Neuroendocrinol.*, 1999, **20**, 157–198.
- 206 P. Martín-Gago, E. Aragón, M. Gomez-Caminals, J. Fernández-Carneado, R. Ramón, P. Martín-Malpartida, X. Verdaguer, P. López-Ruiz, B. Colás, M. A. Cortes, B. Ponsati, M. J. Macias and A. Riera, *Molecules*, 2013, **18**, 14564–14584.
- 207 D. F. Veber, F. W. Holly, W. J. Paleveda, R. F. Nutt, S. J. Bergstrand, M. Torchiana, M. S. Glitzer, R. Saperstein and R. Hirschmann, *Proc. Natl. Acad. Sci. U. S. A.*, 1978, **75**, 2636–2640.
- 208 W. Bauer, U. Briner, W. Doepfner, R. Haller, R. Huguenin, P. Marbach, T. J. Petcher and Pless, *Life Sci.*, 1982, **31**, 1133–1140.
- 209 F. Castinetti, A. Saveanu, I. Morange and T. Brue, *Adv. Ther.*, 2009, **26**, 600–612.
- 210 K. McKeage, S. Cheer and A. J. Wagstaff, *Drugs*, 2003, **63**, 2473–2499.
- 211 R. H. Kramer, D. L. Fortin and D. Trauner, *Curr. Opin. Neurobiol.*, 2009, **19**, 544–552.
- 212 A. Specht, F. Bolze, Z. Omran, J.-F. Nicoud and M. Goeldner, *HFSP J.*, 2009, **3**, 255–264.
- 213 D. S. Lawrence, *Curr. Opin. Chem. Biol.*, 2005, **9**, 570–575.
- 214 H. S. Lee, D. R. Larson and D. S. Lawrence, *ACS Chem. Biol.*, 2009, **4**, 409–427.
- 215 C. W. Riggsbee and A. Deiters, *Trends Biotechnol.*, 2010, **28**, 468–475.
- 216 A. S. Baker and A. Deiters, *ACS Chem. Biol.*, 2014, **9**, 1398–1407.
- 217 C. Brieke, F. Rohrbach, A. Gottschalk, G. Mayer and A. Heckel, *Angew. Chemie Int. Ed.*, 2012, **51**, 8446–8476.
- 218 M. Volgraf, P. Gorostiza, R. Numano, R. H. Kramer, E. Y. Isacoff and D. Trauner, *Nat. Chem. Biol.*, 2006, **2**, 47–52.
- 219 P. Gorostiza and E. Y. Isacoff, *Science (80-. )*, 2008, **322**, 395–399.
- 220 T. Sakata, Y. Yan and G. Marriott, *Proc. Natl. Acad. Sci. U. S. A.*, 2005, **102**, 4759–4764.
- 221 H. Baruah, S. Puthenveetil, Y.-A. Choi, S. Shah and A. Y. Ting, *Angew. Chemie Int. Ed.*, 2008, **47**, 7018–7021.
- 222 G. Mayer and A. Heckel, *Angew. Chemie Int. Ed.*, 2006, **45**, 4900–4921.

- 223 G. C. R. Ellis-Davis, *Nat. Methods*, 2007, **4**, 619–628.
- 224 J. C. Miller, S. K. Silverman, P. M. England, D. A. Dougherty and H. A. Lester, *Neuron*, 1998, **20**, 619–624.
- 225 J.-Y. Kang, D. Kawaguchi, I. Coin, Z. Xiang, D. D. M. O’Leary, P. A. Slesinger and L. Wang, *Neuron*, 2013, **80**, 358–370.
- 226 P. Gorostiza and E. Isacoff, *Mol. Biosyst.*, 2007, **3**, 686–704.
- 227 M. A. Priestman and D. S. Lawrence, *Biochim. Biophys. Acta - Proteins Proteomics*, 2010, **1804**, 547–558.
- 228 N. Wu, A. Deiters, T. A. Cropp, D. King and P. G. Schultz, *J. Am. Chem. Soc.*, 2004, **126**, 14306–14307.
- 229 A. Deiters, D. Groff, Y. Ryu, J. Xie and P. G. Schultz, *Angew. Chemie Int. Ed.*, 2006, **45**, 2728–2731.
- 230 D. P. Nguyen, M. Mahesh, S. J. Elsa, S. M. Hancock, C. Uttamapinant and J. W. Chin, *J. Am. Chem. Soc.*, 2014, **136**, 2240–2243.
- 231 J. Zhao, S. Lin, Y. Huang, J. Zhao and P. R. Chen, *J. Am. Chem. Soc.*, 2013, **135**, 7410–7413.
- 232 C. Chou, D. D. Young and A. Deiters, *Angew. Chemie Int. Ed.*, 2009, **121**, 6064–6067.
- 233 R. Rakauskaitė, G. Urbanavičiūtė, A. Rukšėnaitė, Z. Liutkevičiūtė, R. Juškėnas, V. Masevičius and S. Klimaškauskas, *Chem. Commun.*, 2015, **51**, 8245–8248.
- 234 A. Gautier, A. Deiters and J. W. Chin, *J. Am. Chem. Soc.*, 2011, **133**, 2124–2127.
- 235 W. F. Edwards, D. D. Young and A. Deiters, *ACS Chem. Biol.*, 2009, **4**, 441–445.
- 236 C. Chou and A. Deiters, *Angew. Chemie Int. Ed.*, 2011, **50**, 6839–6842.
- 237 E. A. Lemke, D. Summerer, B. H. Geierstanger, S. M. Brittain and P. G. Schultz, *Nat. Chem. Biol.*, 2007, **3**, 769–772.
- 238 A. Gautier, D. P. Nguyen, H. Lusic, W. An, A. Deiters and J. W. Chin, *J. Am. Chem. Soc.*, 2010, **132**, 4086–4088.
- 239 C. H. Self and S. Thompson, *Nat. Med.*, 1996, **2**, 817–820.
- 240 S. Thompson, J. Dessi and C. H. Self, *Biochem. Biophys. Res. Commun.*, 2008, **366**, 526–531.
- 241 S. Thompson, J. Dessi and C. H. Self, *MAbs*, 2009, **1**, 348–356.
- 242 P. D. Senter, M. J. Tansey, J. M. Lambert and W. A. Blattler, *Photochem. Photobiol.*, 1985, **42**, 231–237.
- 243 C. W. Gilbert, E. B. McGowan, G. B. Seery, K. S. Black and M. D. Pegram, *J. Exp. Ther. Oncol.*, 2003, **3**, 27–35.

- 244 A. P. Gorka, R. R. Nani, J. Zhu, S. Mackem and M. J. Schnermann, *J. Am. Chem. Soc.*, 2014, **136**, 14153 – 14159.
- 245 R. R. Nani, A. P. Gorka, T. Nagaya, H. Kobayashi and M. J. Schnermann, *Angew. Chem. Int. Ed.*, 2015, **54**, 13635–13638.
- 246 D. E. J. G. J. Dolmans, D. Fukumura and R. K. Jaim, *Nat. Rev. Cancer*, 2003, **3**, 380–387.
- 247 M. Triesscheijn, P. Baas, J. H. M. Schellens and F. A. Stewart, *Oncologist*, 2006, **11**, 1034–1044.
- 248 B. Q. Spring, A. O. Abu-Yousif, A. Palanisami, I. Rizvi, X. Zheng, Z. Mai, S. Anbil, R. B. Sears, L. B. Mensah, R. Goldschmidt, S. S. Erdem, E. Oliva and T. Hasan, *Proc. Natl. Acad. Sci. U. S. A.*, 2014, **111**, E933–E942.
- 249 M. Mitsunaga, M. Ogawa, N. Kosaka, L. T. Rosenblum, P. L. Choyke and H. Kobayashi, *Nat. Med.*, 2011, **17**, 1685–1691.
- 250 W. Szymański, J. M. Beierle, H. a V Kistemaker, W. a. Velema and B. L. Feringa, *Chem. Rev.*, 2013, **113**, 6114–6178.
- 251 C. Renner and L. Moroder, *ChemBioChem*, 2006, **7**, 868–878.
- 252 L. G. Ulysse, J. Cubillos and J. Chmielewski, *J. Am. Chem. Soc.*, 1995, **117**, 8466–8467.
- 253 L. G. Ulysse and J. Chmielewski, *Chem. Biol. Drug Des.*, 2006, **67**, 127–136.
- 254 A. Cattani-scholz, C. Renner, C. Cabrele, R. Behrendt, D. Oesterhelt and L. Moroder, *Angew. Chem. Int. Ed.*, 2002, **41**, 289–292.
- 255 C. Renner, R. Behrendt, N. Heim and L. Moroder, *Biopolymers*, 2002, **63**, 382–393.
- 256 A. G. Milbradt, M. Löweneck, S. S. Krupka, M. Reif, E.-K. Sinner, L. Moroder and C. Renner, *Biopolymers*, 2005, **77**, 304–313.
- 257 C. Hoppmann, P. Schmieder, P. Domaing, G. Vogelreiter, J. Eichhorst, B. Wiesner, I. Morano, K. Rück-Braun and M. Beyermann, *Angew. Chem. Int. Ed.*, 2011, **50**, 7699–7702.
- 258 M. J. Tucker, J. R. Courter, J. Chen, O. Atasoylu, A. B. Smith and R. M. Hochstrasser, *Angew. Chem. Int. Ed.*, 2010, **49**, 3612–3616.
- 259 M. Abdo, S. P. Brown, J. R. Courter, M. J. Tucker, R. M. Hochstrasser and A. B. Smith, *Org. Lett.*, 2012, **14**, 3518–3521.
- 260 M. J. Tucker, M. Abdo, J. R. Courter, J. X. Chen, A. B. Smith, R. M. Hochstrasser and A. B. Smith III, *J. Photochem. Photobiol. A Chem.*, 2012, **234**, 156–163.
- 261 Y. Ohmuro-Matsuyama and Y. Tatsu, *Angew. Chem. Int. Ed.*, 2008, **47**, 7527–7529.
- 262 M. Wirkner, S. Weis, V. San Miguel, M. Álvarez, R. A. Gropeanu, M. Salierno, A. Sartoris, R. E. Unger, C. J. Kirkpatrick and A. del Campo, *ChemBiochem*, 2011, **12**,

- 2623–2629.
- 263 S. Bourgault, M. Letourneau and A. Fournier, *Peptides*, 2005, **26**, 1475–1480.
- 264 S. Bourgault, M. Létourneau and A. Fournier, *Peptides*, 2007, **28**, 1074–1082.
- 265 T. Kuner, Y. Li, K. R. Gee, L. F. Bonewald and G. J. Augustine, *Proc. Natl. Acad. Sci. U. S. A.*, 2008, **105**, 347–352.
- 266 M. D. Katz and B. L. Erstad, *Clin. Pharm.*, 1989, **8**, 255–273.
- 267 C. Marculescu, H. Kossen, R. E. Morgan, P. Mayer, S. A. Fletcher, B. Tolner, K. A. Chester, L. H. Jones and J. R. Baker, *Chem. Commun.*, 2014, **50**, 7139–42.
- 268 I. Palinko, P. T. Szabo, B. Torok, Z. Kele and I. Kapocsi, *Rapid Commun. Mass Spectrom.*, 1998, **12**, 1771–1776.
- 269 A. Molleman, *Wiley*, 2003, 186.
- 270 H. J. Kreienkamp, H. H. Hönck and D. Richter, *FEBS Lett.*, 1997, **419**, 92–94.
- 271 C. R. R. Grace, J. Erchegyi, M. Samant, R. Cescato, V. Piccand, R. Riek, J. C. Reubi and J. E. Rivier, *J. Med. Chem.*, 2008, **51**, 2676–2681.
- 272 A. Parra, S. Reboredo and J. Alemán, *Angew. Chem. Int. Ed.*, 2012, **51**, 9734–9736.
- 273 K. Ishihara and K. Nakano, *J. Am. Chem. Soc.*, 2007, **129**, 8930–8931.
- 274 C. Müller, A. Bauer, M. M. Maturi, M. C. Cuquerella, M. A. Miranda and T. Bach, *J. Am. Chem. Soc.*, 2011, **133**, 16689–16697.
- 275 E. A. Hull, *PhD Thesis - UCL - Antibody Conjugates via Disulfide Bridging: Towards therapeutic and diagnostic applications*, 2015.
- 276 T. Kinoshita, F. Iinuma and A. Tsuji, *Chem. Pharm. Bull.*, 1974, **22**, 2413–2420.
- 277 R. F. Chen, *Anal. Biochem.*, 1968, **25**, 412–416.
- 278 T. K. S. Kumar, B. Raman and C. H. M. Rao, *J. Biochem. Biophys. Methods*, 1995, **30**, 79–84.
- 279 R. E. Kontermann, *BioDrugs*, 2009, **23**, 93–109.
- 280 G. Proetzel, H. Ebersbach and J. M. Walker, *Methods in Molecular Biology - Antibody Methods and Protocols*, 2009, vol. 531.
- 281 J. Zempleni, S. S. K. Wijeratne and Y. I. Hassan, *BioFactors*, 2009, **35**, 36–46.
- 282 P. S. Stayton, S. Freitag, L. A. Klumb, A. Chilkoti, V. Chu, J. E. Penzotti, R. To, D. Hyre, I. Le Trong, T. P. Lybrand and R. E. Stenkamp, *Biomol. Eng.*, 1999, **16**, 39–44.
- 283 C. Marculescu, *PhD Thesis - UCL - Development of Novel Maleimide Reagents for Protei*, 2014.
- 284 A. Chung, X. Cui, W. Audeh and A. Giuliano, *Clin. Breast Cancer*, 2013, **13**, 223–232.

- 285 S. A. Hurvitz, Y. Hu, N. O'Brien and R. S. Finn, *Cancer Treat. Rev.*, 2013, **39**, 219–229.
- 286 A. G. Griesbeck, A. Henz, K. Peters, E. M. Peters and H. G. Vonschnering, *Angew. Chem. Int. Ed.*, 1995, **34**, 474–476.
- 287 A. Soldevilla and A. G. Griesbeck, *J. Am. Chem. Soc.*, 2006, **128**, 16472–16473.
- 288 M. Horvat, K. Mlinarić-Majerski, A. G. Griesbeck and N. Basarić, *Photochem. Photobiol. Sci.*, 2011, **10**, 610–617.
- 289 A. G. Griesbeck and H. Mauder, *Angew. Chem. Int. Ed.*, 1992, **31**, 73–75.
- 290 R. M. Lequin, *Clin. Chem.*, 2005, **51**, 2415–2418.
- 291 S. Arumugam and V. V Popik, *J. Am. Chem. Soc.*, 2011, **133**, 5573–5579.
- 292 W. Xi, M. Krieger, C. J. Kloxin and C. N. Bowman, *Chem. Commun.*, 2013, **49**, 4504–4506.
- 293 Y. Wang, W. Song, W. J. Hu and Q. Lin, *Angew. Chem. Int. Ed.*, 2009, **48**, 5330–5333.
- 294 Z. Yu, L. Y. Ho, Z. Wang and Q. Lin, *Bioorganic Med. Chem. Lett.*, 2011, **21**, 5033–5036.
- 295 Z. Yu, T. Y. Ohulchanskyy, P. An, P. N. Prasad and Q. Lin, *J. Am. Chem. Soc.*, 2013, **135**, 16766–16769.
- 296 C. E. Hoyle and C. N. Bowman, *Angew. Chem. Int. Ed.*, 2010, **49**, 1540–1573.
- 297 H. Gorner, M. Oelgemoller and A. G. Griesbeck, *J. Phys. Chem. A*, 2002, **106**, 1458–1464.
- 298 A. G. Griesbeck, J. Neudörfel and A. De Kiff, *Beilstein J. Org. Chem.*, 2011, **7**, 518–524.
- 299 V. M. Csizmadia, K. M. Koshy, K. C. M. Lau, R. A. McClelland, V. J. Nowlan and T. T. Tidwell, 1979, **101**, 974–979.
- 300 J. Lefranc, A. M. Fournier, G. Mingat, S. Herbert, T. Marcelli and J. Clayden, *J. Am. Chem. Soc.*, 2012, **134**, 7286–7289.
- 301 B. Husár and R. Liska, *Chem. Soc. Rev.*, 2012, **41**, 2395–2405.
- 302 S. Roy, A. J. Zych, R. J. Herr, C. Cheng and G. W. Shipp, *Tetrahedron*, 2010, **66**, 1973–1979.
- 303 C. H. Bamford, J. F. Bingham and H. Block, *Trans. Faraday Soc.*, 1970, **66**, 2612–2621.
- 304 A. Matsumoto, T. Kubota and T. Otsu, *Macromolecules*, 1990, **6**, 4508–4513.
- 305 C. Gros and B. Labouesse, *Eur. J. Biochem.*, 1969, **7**, 463–470.
- 306 I. S. Cho, H. Han, J. H. Shim, J. S. Lee, J. H. Shin, G. S. Cha and B. H. Kim, *Tetrahedron Lett.*, 2010, **51**, 2835–2839.
- 307 J. H. On, K. T. Cho, Y. Park, S. Hahm, W. Kim, J. Y. Cho, J. H. Hwang, Y. M. Jun, G. S. Cha, H. Nam and B. H. Kim, *Tetrahedron*, 2009, **65**, 1415–1423.

- 308 M. Remko and B. M. Rode, *J. Mol. Struct.*, 1995, **339**, 125–131.
- 309 V. C. Armstrong, D. W. Farlow and R. B. Moodie, *J. Chem. Soc. B*, 1968, 1099–1101.
- 310 W. Mabey and T. Mill, *J. Phys. Chem. Ref. Data*, 1978, **7**, 383–415.
- 311 C. Stock and R. Brückner, *Adv. Synth. Catal.*, 2012, **354**, 2309–2330.
- 312 J. A. Dean, *Lange's Handbook of Chemistry, 13th edition.*, 1985.
- 313 *CRC Handbook of Chemistry and Physics 84th Edition*, 2004.
- 314 F. Arcamone, G. Cassinelli, G. Faktini, A. Grein, P. Orezzi, C. Pol and C. Spalla, *Biotechnol. Bioeng.*, 1969, **11**, 1101–1110.
- 315 C. Schliemann and D. Neri, *Biochim. Biophys. Acta - Rev. Cancer*, 2007, **1776**, 175–192.
- 316 H.-P. Gerber, P. D. Senter and I. S. Grewal, *MAbs*, 2009, **1**, 247–253.
- 317 A. G. Patel and S. H. Kaufmann, *Elife*, 2012, **eLife 2012**, 1:e00387.
- 318 O. Tacar, P. Sriamornsak and C. R. Dass, *J. Pharm. Pharmacol.*, 2013, **65**, 157–170.
- 319 R. L. Momparler, M. Karon, S. E. Siegel and F. Avila, *Cancer Res.*, 1976, **36**, 2891–2895.
- 320 F. A. Fornari, J. K. Randolph, J. C. Yalowich, M. K. Ritke and D. A. Gewirtz, *Mol. Pharmacol.*, 1994, **45**, 649–56.
- 321 D. Farquhar, R. A. Newman, J. E. Zuckerman and B. S. Andersson, *J. Med. Chem.*, 1991, **34**, 561–564.
- 322 D. Farquhar, A. Cherif, E. Bakina and J. A. Nelson, *J. Med. Chem.*, 1998, **41**, 965–972.
- 323 F. Arcamone, F. Animati, M. Berettoni, M. Bigioni, G. Capranico, A. M. Casazza, C. Caserini, A. Cipollone, M. De Cesare, M. Franciotti, P. Lombardi, A. Madami, S. Manzini, E. Monteagudo, D. Polizzi, G. Pratesi, S. C. Righetti, C. Salvatore, R. Supino and F. Zunino, *J. Natl. Cancer Inst.*, 1997, **89**, 1217–1223.
- 324 S. Yu, G. Zhang, W. Zhang, H. Luo, L. Qiu, Q. Liu, D. Sun, P. G. Wang and F. Wang, *Int. J. Mol. Sci.*, 2012, **13**, 3671–3684.
- 325 L. D. Elliott, J. P. Knowles, P. J. Koovits, K. G. Maskill, M. J. Ralph, G. Lejeune, L. J. Edwards, R. I. Robinson, I. R. Clemens, B. Cox, D. D. Pascoe, G. Koch, M. Eberle, M. B. Berry and K. I. Booker-Milburn, *Chem. Eur. J.*, 2014, **20**, 15226–15232.
- 326 J. Olejnik, S. Sonar, E. Krzymańska-Olejnik and K. J. Rothschild, *Proc. Natl. Acad. Sci. USA*, 1995, **92**, 7590–7594.
- 327 C. P. Holmes and D. G. Jones, *J. Org. Chem.*, 1995, **60**, 2318–2319.
- 328 W. Li and G. Zheng, *Photochem. Photobiol. Sci.*, 2012, **11**, 460–471.
- 329 D. Muller, I. Zeltser, G. Bitan and C. Gilon, *J. Org. Chem.*, 1997, **62**, 411–416.

- 330 F. Albericio, N. K. Cordonier, S. Biancalana, L. Gera, R. I. Masada, D. Hudson and G. Barany, 1990, **55**, 3730–3743.
- 331 J. Rodríguez, R. M. Nieto, M. Blanco, F. A. Valeriote, C. Jiménez and P. Crews, *Org. Lett.*, 2014, **16**, 464–467.
- 332 N. Brabez, R. M. Lynch, L. Xu, R. J. Gillies, G. Chassaing, S. Lavielle and V. J. Hruby, *J. Med. Chem.*, 2011, **54**, 7375–7384.
- 333 J. L. Leaney, G. Milligan and A. Tinker, *J. Biol. Chem.*, 2000, **275**, 921–929.

## **5: Appendix**

The following article was published as a result of the work reported in this thesis.

D. A. Richards, S. A. Fletcher, M. Nobles, H. Kossen, L. Tedaldi, V. Chudasama, A. Tinker and J. R. Baker, *Org. Biomol. Chem.*, 2016, **14**, 455-459.